Oxides, oxides, and more oxides: high-κ oxides, ferroelectrics, ferromagnetics, and multiferroics

N. Izyumskaya, Ya. Alivov[1], and H. Morkoç

School of Engineering
Electrical and Computer Engineering Department
Virginia Commonwealth University
Richmond VA 23284-3068
[1] Present address: University of California, Irvine, Department of Radiological Sciences
School of Medicine, Medical Sciences I, B-140, Irvine, CA 92697-5000

We review and critique the recent developments on multifunctional oxide materials which are gaining a good deal of interest. Recongnizing that this is a vast area, the focus of this treatment is mainly on high-κ dielectric, ferroelectric, magnetic, and multiferroic materials. Also, we consider ferrimagnetic oxides in the context of the new, rapidly developing field of negative-index metamaterials. This review is motivated by the recent resurgence of interest in complex oxides owing to their coupling of electrical, magnetic, thermal, mechanical, and optical properties, which make them suitable for a wide variety of applications, including heat, motion, electric, and magnetic sensors; tunable and compact microwave passive components; surface acoustic wave devices; non-linear optics; non-volatile memory; and pave the way for designing multifunctional devices and unique applications in spintronics and negative refraction-index media. For most of the materials treated here, structural and physical properties, preparation methods accompanied by particulars of synthesis of thin films, devices based on them, and some projections into their future applications are discussed.

Contents

1 Introduction

Oxides comprise a wide class of materials exhibiting rich crystal structures and physical properties which make them ideal candidates for a plethora of applications.There has been a recent resurgence of interest in oxides in general and complex oxides in particular owing to their piezoelectric, ferroelectric, ferromagnetic, ferrimagnetic, and multiferroic properties as well as in many cases owing to large dielectric constants (imperative for scaled Si metal-oxide-semiconductor field effect transistors (MOSFET)). While these properties had been recognized many decades ago, the renewed interest stems from exploiting improved deposition techniques, which would potentially allow not only higher quality material but also thin films and heterstructures with new functionalities as well as composite structures with *e.g.* magnetoelectric coupling, a concept which has gotten a good deal of attention recently.

Oxide materials with large dielectric constans (so-called "high-κ dielectrics") have attracted much attention due to their potential use as gate dielectrics in MOSFETs. In the modern Si-based CMOS technology, scaling to smaller device dimensions for higher packing density, faster circuit speed, and lower power dissipation per gate requires the gate oxide thickness to be made smaller as the channel length is made shorter. When the channel length becomes of the same order of magnitude as the depletion-layer widths of the source and drain, a MOSFET device is considered to be short and the so-called short-channel effects[1] arise. To help to cope with the short channel effects, thickness of the gate oxide must be reduced. This causes a reduction in the on/off current ratios. Moreover, the reduction of oxide thicknesses results in increased gate leakage current, which is a formidable problem particularly for

large density circuits. Already, the thickness required for the venerable SiO_2 gate dielectric is comparable to tunneling distance which would cause intolerable levels of gate leakage. Consequently, high-κ dielectric materials having higher dielectric constants, which allow scaling with much larger thicknesses, are actively investigated. The benefits of high-κ dielectrics can be clearly understood from Equation 1, which represents an equivalent oxide thickness (EOT) $t|_{eq}$, a quantity used to compare performance of high-κ dielectric MOS gates with performance of SiO_2-based MOS gates. EOT is the thickness of SiO_2 gate oxide needed to obtain the same gate capacitance as that obtained with thicker high-κ dielectrics.

$$t|_{eq} = t|_{SiO_2} \frac{\varepsilon|_{high-\kappa}}{\varepsilon|_{SiO_2}} = t|_{SiO_2} \frac{\varepsilon|_{high-\kappa}}{3.9} \quad ,$$

Equation 1

where, $\varepsilon|_{high\text{-}\kappa}$ and $\varepsilon|_{SiO2}$ are dielectric constants of high-κ dielectrics and SiO_2, respectively ($\varepsilon|_{SiO2} = 3.9$). For example, a 1-nm-thick SiO_2 gate dielectric (referred to as the equivalent thickness) can be replaced with a 10 nm thick high-κ dielectric with a relative dielectric constant of 39. Thus, for a certain gate capacitance, the thickness of high-κ gate oxide can be increased by a factor of $\left(\varepsilon|_{high-\kappa}\right)/\left(\varepsilon|_{SiO_2}\right)$ as compared to that made of SiO_2. Therefore, the search is on for high-κ dielectrics that are compatible with Si and its

processing and allow retention of the gate oxide capacitance needed for reducing short channel effects, while still using sufficiently thick oxide layers to prevent current conduction through it.

Despite the fact that many dielectrics have a much higher dielectric constant (20-100), finding a material to replace SiO_2 is a formidable challenge, because of such issues as requisite high channel/dielectric interface quality, reliability, and low leakage current. To reiterate, the main criteria for a gate dielectric include band offsets that block hot charge carriers, provides chemical stability in contact with both the silicon substrate and the gate material, and low density of interface and bulk states. Attempts to introduce high-κ dielectrics into the CMOS technology began as early as in 70-80s, but was delayed because of their high defect concentrations, particularly what was perceived to be O vacancies, which resulted in charge trapping, transient threshold voltage shifts, and degradation of Si carrier mobility due to Coulombic scattering.

Different aspects of high κ dielectrics have been the subject of several excellent review papers. [2,3,4,5,6] For example, de Almeida and Baumvol[3] analyzed in details the reaction and diffusive properties of dielectric/gate and dielectric/channel interfaces. Wilk *et al.*[2] reviewed the status of the of the high-κ dielectric studies, vista 2000, which was followed by a similar review by Wallace and Wilk[4] , vista 2003, with some updates, and a very recent review by Schlom et al.,[6] vista 2008. Zhu et al.[5] provided an overview of high-resolution electron-, ion-, and photon-based techniques currently used to characterize microstructure of high-κ gate dielectrics and interfaces between high-κ dielectrics and metal gates. Since this area of research represents a large fraction of the activity in oxide

materials a succinct review of the subject matter is provided here. In concert with the stated objectives, we review only briefly the very recent progress in the field of high-κ dielectrics, while a more thorough discussion can be found in a review by Wu *et al*. [7]

Considering the broad area of oxides and their applications beyond gate dielectrics, ferroelectric and ferromagnetic oxides belong to a class of materials that exhibit spontaneous electric polarization for the former and magnetic polarization for the latter below a temperature called the Curie temperature, T_C. Both ferroelectrics and ferromagnetics show saturation and hysteresis in their polarization/magnetization characteristics *vs.* electric/magnetic field. Ferroelectrics take their name because of the similarity of their electric field dependence of electric polarization to the magnetic field dependence of magnetic polarization in ferromagnetic materials, although Fe is not involved at all. Magnetic oxides typically contain transition metals, such as Mn, Fe, etc., or a rare earth, such as Gd, etc., which forms the basis for magnetic polarization. Somewhat similarly, ferroelectric materials have an ion, such as Ti, Ta, Zr, etc., which is responsible for electric polarization. Low symmetry of a crystal, in particular non-centrosymmetric feature, is essential for the occurrence of ferroelectricity. All ferroelectric materials also exhibit piezoelectricity (ability to generate an electric potential in response to applied mechanical stress) and pyroelectricity (ability to create electric charge in response to temperature change), but the opposite does not hold.

Ferroelectric oxides are of great interest for a wide range of applications such as pyroelectric and piezoelectric sensors, capacitors, surface acoustic wave (SAW) devices, and micro-electromechanical systems (MEMS). The increased interest in these materials lately stems in part from the fact they are considered to be good candidates for non-volatile ferroelectric random-access

memory (FeRAM) devices, due to their high dielectric constant values and hysteresis in their polarization *vs.* electric field characteristics. Ferroelectrics are characterized by spontaneous polarization, the direction of which can be changed by external electric field. These two states of spontaneous polarization are used as the logic states of a memory device which does not require power backup to maintain the stored information. Thus, thin films of ferroelectric oxides can be exploited in semiconductor devices to achieve FeRAM with long endurance and high-speed access, which can overcome the barriers encountered in current semiconductor memory technologies, provided that leakage current is very low. In fact, low density embedded ferroelectric memories are being considered for implementation in commercial devices, such as cellular phones and smart cards. Various perovskite-structure oxides, including strontium bismuth tantalate $SrBi_2Ta_2O_9$ (SBT), barium strontium titanate $Ba_xSr_{1-x}TiO_3$ (BST), La-substituted bismuth titanate $Bi_{4-x}La_xTi_3O_{12}$ (BLT), and lead zirconate titanate $PbZr_{1-x}Ti_xO_3$ (PZT) have been considered as candidates for ferroelectric memory devices. Among these materials, however, only two – SBT and PZT – have been seriously attempted for penetration into the FeRAM industry.

Piezoelectric thin films have also been integrated into MEMS devices such as micro-scale accelerometers, displacement transducers, and actuators. Moreover, pyroelectric properties of thin films are used in high sensitivity IR detectors. Progress has also occurred in the application of high-dielectric-constant thin films and electro-optic thin films in the areas of high frequency devices and optical switches, respectively, for integrated optical systems. However, the relative degree of activities in those fields has not been as

large as those in the case of ferroelectric applications. In addition, ferroelectric oxides are found to be very stable to high-energy radiation, a feature which is important for space applications.[8,9]

Magnetic oxides have been exploited for many centuries. The first recognized permanent magnetic material was lodestone (naturally occurring Fe_3O_4 oxide – magnetite). Since the 1930s, ferrites, insulating ferrimagnetic oxides with a general composition $MeO{\cdot}Fe_2O_3$ (Me = divalent metal ion), have been extensively studied for their magnetic and electronic properties.[10] Ferrites find a plethora of applications in passive microwave components such as isolators, circulators, phase shifters, delay lines, switches, attenuators, and miniature antennas operating over a wide range of frequencies and as magnetic recording media, to cite a few.[11] The interest in magnetic oxides has exponentially grown, stimulated by the discovery of high-temperature superconductivity in cuprates[12,13,14,15] (which are beyond the scope of this review) and the more recent discovery of the colossal-magnetoresistance (CMR) effect in mixed-valence manganese oxides of the general formula $Re_{1-x}A_xMnO_3$ (where Re = rare earth, A = alkaline earth).[16,17] The unusual magnetoresistance behaviour of these oxides results from a unique type of a metal–insulator transition. Depending on the composition, doping, and growth conditions (temperature, pressure) the manganites exhibit a broad range of electronic and magnetic phases, ranging from low-resistance ferromagnetic metals to high-resistance insulators. Due to high spin polarization, the manganites show a great potential for applications in magnetic tunnel junctions (MTJs), which are promising candidates for non-volatile magnetic random access memory (MRAM). [18]

Besides the mixed-valence manganese oxides, diluted magnetic oxides (DMOs) have attracted considerable attention as promising materials for potential spintronic applications. Spintronics, coined from spin electronics, is an emerging technology intended for use of spin of carriers along with their charge. As compared to conventional electronic devices, spintronic devices are expected to offer some advantages, including nonvolatility, lower power consumption, higher speed of data processing, and higher packing density. At the present time, the only commercial spintronic device is MRAM exploiting MTJs made from ferromagnetic metals. Although commercial metal-based MRAM has become available recently, efforts toward semiconductor-based spintronics are motivated by the possibility to incorporate devices for information processing and non-volatile storage in a single chip.[19] Besides, spin injection across a semiconductor/metal interface can be adversely affected by the presence of defects at the interface, which results in low injection efficiency.[20] Highly efficient electrical injection of spin polarized carriers into a semiconductor active region is one of the prerequisites for realizing semiconductor-based spintronic devices such as the spin FETs, spin light-emittind diodes (LED), spin resonant tunneling device, *etc.* The spin injection may also be useful for magnetic memories, in which the magnetization reversal of bit cells could be triggered by the interaction between injected spin-polarized carriers and localized spins [21] and for semiconductor lasers that would have better mode stability and lower threshold currents. DMOs belong to a wider class of diluted magnetic semiconductors (DMSs) which are semiconducting materials in which a fraction of the host cations is substitutionally replaced by magnetic ions (transition metals (TM) with partially filled *d* states or rare-earth elements with partially filled *f* states). For practical applications in spintronic devices, a material obviously should be ferromagnetic above room temperature. Theoretical predictions that

TM-doped GaN and ZnO could have the Curie point above room temperature[22,23] and experimental findings of ferromagnetism in TM-doped TiO_2 [24] set off a flurry of extensive research, both experimental and theoretical, into TM-doped DMOs as potential materials for spintronic devices. Up to now, room-temperature ferromagnetism has been reported, with some controversy, in in various oxides, including ZnO, TiO_2, SnO_2, In_2O_3, $(In,Sn)_2O_3$ (ITO), CeO_2.

One more class of oxide materials showing great promise for spintronic applications is the so-called multiferroics.[25] By definition, a ferroic material possesses one of the ferroic properities: ferromagnetism, ferroelectricity, or ferroelasticity, while a multiferroic material exhibits two or three of the ferroic properties in the same phase.[26]

Figure 1 shows the well-known triangle used to describe the pathways between external forces, such as stress (σ) and electric (E) and magnetic (H) fields, and associated material properties, such as strain (ε), electrical polarization (P), and magnetization (M). A ferroelastic, ferroelectric, or magnetic ferroic material exhibits spontaneous strain, polarization, or magnetization which can be switched hysteretically by applied stress, electric field, or magnetic field, respectively (shown by solid arrows). In multiferroics, additional interactions also arise (dashed arrows). For example, in multiferroics which are simultaneously ferromagnetic and ferroelectric, a coupling between these two orders (magnetoelectric coupling) may arise. In these materials, called "magnetoelectric multiferroics", electric polarization can be induced by an external magnetic field, and *vice versa* meaning magnetization can be induced by an external electric field. It should be noted that not all ferromagnetic/ferroelectric multiferroics exhibit magnetoelectric coupling.[27] Figure 2 illustrates a relationship between multiferroic and magnetoelectric oxides. On the other hand, magnetoelectric

coupling may occur not only in a material with ferromagnetic and ferroelectric order, but also in any magnetically and electrically polarizable material, including ferri-, antiferro-, and paramagnets and antiferro- and paraelectrics.[27]

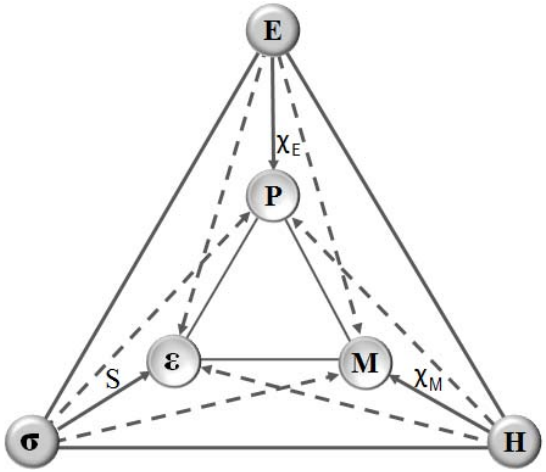

Figure 1 Diagram illustrating the interrelation between external forces (electric field E, magnetic field H, and stress σ) and material properties (electric polarization P, magnetization M, and strain ε). Also shown are coupling coefficients between the material properties and external forces, *e.g.* electric susceptibility (χ_E), magnetic susceptibility (χ_M), and compliance tensor (S).

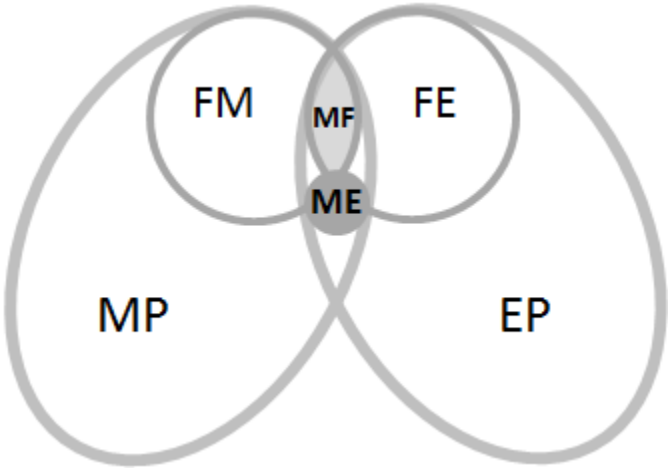

Figure 2 Diagram illustrating a relationship between multiferroic and magnetoelectric oxides. Large ovals represent magnetically polarized (MP) and electrically polarizable (EP) materials. The magnetically (electrically) polarizable materials include ferro-, ferri-, antiferro-, and paramagnets (ferro-, antiferro-, and paraelectrics). Large circles represent ferromagnetic (FM) and ferroelectric (FE) materials. Intersection of the large circle (shadowed area) represents multiferroic materials (MF). Small grey circle represents oxides exibiting magnetoelectric coupling (ME), an independent phenomenon that can, but needs not, take place in a material which is both magnetically and electrically polarizable. After Ref. 27.

The magnetoelectric effect is generally described using the Landau theory by writing the expansion of free energy F of the system in S.I. units as[27,28]

$$F(\mathbf{E},\mathbf{H}) = F_0 - P_i^S E_i - \mu_0 M_i^S H_i - \frac{1}{2}\varepsilon_0\varepsilon_{ij}E_iE_j - \frac{1}{2}\mu_0\mu_{ij}H_iH_j$$
$$-\alpha_{ij}E_iH_j - \frac{1}{2}\beta_{ijk}E_iH_jH_k - \frac{1}{2}\gamma_{ijk}H_iE_jE_k - \ldots$$

Equation 2

where F_0 is the field independent energy, P_i^S and M_i^S are the spontaneous polarization and magnetization, respectively, and ε_{ij} and μ_{ij} are the second ranked permittivity and permeability tensors, respectively. The term with the second ranked tensor α_{ij} describes the linear magnetoelectric coupling and the terms with the third ranked tensors β_{ijk} and γ_{ijk} represent the higher-order magnetoelectric effects. The polarization and the magnetization of the system may then be obtained by differentiation of **Equation 2** with respect to E_i and H_i, respectively:

$$P_i(\mathbf{E},\mathbf{H}) = -\left.\frac{\partial F(\mathbf{E},\mathbf{H})}{\partial E_i}\right|_{E_i=0} = P_i^S + \alpha_{ij}H_j + \frac{1}{2}\beta_{ijk}H_jH_k + \ldots$$

$$\mu_0 M_i(\mathbf{E},\mathbf{H}) = -\left.\frac{\partial F(\mathbf{E},\mathbf{H})}{\partial H_i}\right|_{H_i=0} = \mu_0 M_i^S + \alpha_{ij}E_j + \frac{1}{2}\gamma_{ijk}E_jE_k + \ldots$$

Equation 3

By ignoring the higher order terms in **Equation 2**, the magnetoelectric response can be shown to be limited by the geometric mean of the diagonalized permittivity and permeability tensors [29]

$$\alpha_{ij}^2 \leq \mu_0 \varepsilon_0 \mu_{ij} \varepsilon_{ij}$$

Equation 4

The tendency toward device miniaturization provides the motivation for exploring multifunctional materials, i.e. materials that can perform more than one task or that can be manipulated by several independent stimuli. Two types of multiferroic materials have already found practical use: ferroelastic ferroelectrics exhibiting both spontaneous switchable strain and polarization are widely used in piezolelectric transducers, and ferromagnetic ferroelastics exhibiting coupling between magnetization and strain are used in magnetomechanical actuators. Magnetoelectric multiferroics, combining ferroelectric and magnetic properties, also show considerable promise for applications in multifunctional devices, such as electric-field-controlled ferromagnetic resonance devices, transducers with magnetically modulated piezoelectricity, and multiple-state memory elements.[30],[31] The magnetoelectric coupling between magnetic and electrical orders in these multiferroics adds a new functionality: a possibility to control magnetic polarization by applying electric field and vice versa. This paves the way to fabrication of new type of memory devices, such as electric-field-controlled magnetic random access memory (MERAM),[32] wherein data can be written electrically and read magnetically. The use of

electric field instead of magnetic one in the writing procedure will allow drastic reduction in power consumption, increase in speed, and miniaturization of memory devices.

Unfortunately, magnetoelectric multiferroics are rare (and those exhibiting magnetoelectric effect at room temperature are extremely rare) and almost all of them are antiferromagnets or weak ferromagnets.[33] Besides, the magnetoelectric coefficient α_{ij} is usually small, since single-phase multiferroics often exhibit only weak magnetization and/or ferroelectricity. The magnetoelectric coupling may arise, however, not only directly between the two order parameters in one phase, but also indirectly via mechanical strain between two separate phases, namely ferroelectric and ferro/ferrimagnetic, combined into a multiferroic composite structure. This approach allows one to choose ferroelectric and magnetic materials with required parameters independently and to fabricate multiferroic composites with magnetoelectric response several orders of magnitude larger than that in single-phase multiferroics. These multiferroic composites have great potential for applications in multifunctional devices, such as magneticelectric transducers, actuators, sensors, and heterogeneous read/write devices.[34]

Another interesting and rapidly developing class of composite materials is the so-called negative-index (NI) metamaterials. NI metamaterials are artificial periodic structures exhibiting negative permittivity and permeability in the same frequency range, which gives rise to a negative index of refraction, a phenomenon that never occurs in natural materials. The unique properties of NI materials open possibilities for a plethora of potential applications, ranging from antennas[35],[36],[37],[38] spectrally selective filters,[39],[40] sub-wavelength waveguides, and beam steerers, to superlenses with resolution exceeding the diffraction limit,[41],[42],[43] and invisibility

cloaks.[44],[45] Generally, metamaterial structures are built up from two sets of resonators (usually an array of metal rods interspersed with an array of split ring resonators) which provide separately negative permittivity and permeability.[46] However, such structures are inconvenient for practical use: due to their resonant nature they work in a narrow frequency range, they are not tunable, and it is difficult to scale these structures to infrared and optical frequency range. This has stimulated the search for metamaterials composed partially of natural materials and drawn attention to ferrites, magnetic oxides which can provide negative permeability. NI metamaterials consisting of ferrites responsible for negative permeability and an array of conducting wires responsible for negative permittivity have been recently proposed.[47] Such structures are easier to fabricate, and they are tunable by applying magnetic field.

In this paper, we review the progress made in oxides with an emphasis on high-κ dielectric, ferroelectric, ferromagnetic, and multiferroic materials. Some attention is also paid to ferrite-based NI metamaterials. The paper is organized as follows. Section 2 is devoted to high-κ dielectric oxides. Breaf history and basic properties of ferroelectrics as well as their application and thin film growth methods are introduced in Section 3. Section 4 deals with magnetic oxides, including diluted magnetic oxides and mixed-valence manganites, which is followed by a discussion of multiferroic oxides in Section 5. The role played by oxide materials in the development of negative-index composites are discussed in Section 6. And finally, Section 7 highlights some important issues that need to be addressed in the future.

2 High-κ dielectrics

With increasing demand for higher speed and device density, the device dimensions in Si CMOS-based integration circuits are continually being scaled down, following what is termed as the Moore's law[48]. The integrated circuit fabrication based on MOSFET relies on amorphous thermally grown SiO_2 as a gate dielectric. In addition to superb electrical insulation and interfacial bonding properties, the Si/SiO_2 system offers several important advantages including a stable thermodynamic Si/SiO_2 interface, defect charge density associated with the Si/SiO_2 interface of the order of $10^{10}/cm^2$, mid-gap interface state density of about $10^{10}/cm^2eV$ or less, and hard breakdown fields in excess of 10 MV/cm. These outstanding properties clearly present a significant challenge for any alternative gate dielectric candidate. However, the reduction of gate dimensions, the cornerstone of which is the reduction of the gate and the channel length, requires that the oxide thickness be reduced in order to prevent the short channel effects or render them manageable. Thus, with scaling down of feature sizes, the thickness of the SiO_2 dielectric layer must be reduced to the point that tunneling induced leakage current becomes unacceptably large. This calls for alternative dielectrics with much higher dielectric constants. At the very minimum, in addition to compatibility with CMOS processing, the high-κ dielectric proposed to replace SiO_2 must have large band discontinuity for both the conduction and valence bands of Si (which means a large bandgap), low interface and bulk trap density, and low leakage current. There are a number of high-κ dielectrics which have been and/or are actively being pursued for replacing SiO_2. Among them are gadolinium oxide Gd_2O_3,[49] magnesium oxide MgO,[50] erbium oxide Er_2O_3,[51] neodymium oxide Nd_2O_3,[52],[53]

praseodymium oxide Pr_2O_3,[54] cerium oxide CeO_2,[55,56,57,58,59] cerium zirconate $CeZrO_4$,[60] aluminum oxide Al_2O_3, lanthanum aluminum oxide $LaAlO_3$,[54,61,62] lanthanum oxide La_2O_3,[61,63] yttrium oxide Y_2O_3,[61] tantalum pentoxide Ta_2O_5,[54,64,65,66] titanium dioxide TiO_2,[67] zirconium dioxide ZrO_2[68,69,70], zirconium silicate $ZrSiO_4$[71], hafnium oxide HfO_2,[55,72,73] HfO_2–based oxides $HfSiO_2$,[74] $HfDyO_x$,[75] $HfScO_x$,[75] hafnium silicate $HfSi_xO_y$,[76] dysprosium oxide Dy_2O_3,[77,78] strontium titanate $SrTiO_3$,[79] $LaLuO_3$,[80,81] and rare-earth scandates $LaScO_3$, $GdScO_3$, $DyScO_3$, and $SmScO_3$.[62,82,83,84,85,86] Among this variety, HfO_2 and HfO_2-based materials as well as $LaLuO_3$ and rare-earth scandates $LaScO_3$, $GdScO_3$, $DyScO_3$ are considered as the most promising candidates combining high dielectric permittivity and thermal stability with low leakage current due to a reasonably high barrier height that limits electron tunneling.[6] A list of high-κ dielectric oxides and their physical properties, such as dielectric constant, band gap, conduction band offsets relative to Si and Ge, and crystal structures is given in Table I.[49,50,51,52,54,55,58,61,80,87,88,89,90,91,92,93,94,95,96] Figure 3 presents graphical representation of the band alignments between Si and various high-κ dielectrics.

Table 1

Some physical parameters of high-κ dielectrics and heterostructures with Si and Ge.

Material	Dielectric constant (k)	Band gap E_G (eV)	Band offset ΔE_C(eV) to Si	Band offset ΔE_C(eV) to Ge	Crystal structure	Refs.
SiO_2	3.9	8.9	3.2		Amorphous	2
Si_3N_4	5.3	7	1.7	1.9	Amorphous	2,87
Al_2O_3	9	8.7	2.6	2.8	Amorphous	2,87
TiO_2	4-86	3.0 3.2 3.5	1.2		Tetragonal (rutile) Tetragonal (anatase) Amorphous	67 67 67
MgO	9.8	7.3			Cubic	50
HfO_2	~25	5.7 5.9	1.5	2.0±0.1 2.0-2.1	Monoclinic, tetragonal, cubic	2,88 91
$HfSiO_4$	13-20	6.5	2.03	2.2	Amorphous	50,87
ZrO_2	~25	5.8	1.4	1.63	Monoclinic, tetragonal, cubic	69,87
Ta_2O_5	26 25	~5 4.2	0.3 0.8		Orthorhombic Amorphous	2,64,87 54,66
CeO_2	52	3.3	0.75		Cubic	56,91,96
Er_2O_3	14.4	7.5	~3.5		Cubic	51
Nd_2O_3	12.64	5.8	2.2		Cubic	52,89
Pr_2O_3	25.4 16	4.1			Hexagonal Amorphous	54,90
Dy_2O_3	12	4.9	0.78		Cubic	77,94,95
Gd_2O_3	24	5.8	2.21	2.44 2.1	Cubic	49,87 91
La_2O_3	30	6.0	2.36	2.56	Hexagonal, cubic	2,87
Y_2O_3	15	5.6	2.36	2.56	Cubic	2,87

Sc_2O_3	~14	~6.2	2.36	2.56	Cubic	62,87,93
$SrTiO_3$	300	3.3	0.11	0.37	Cubic	87
$LaAlO_3$	26 ~13	5.7	1.53	1.72	 Amorphous	61,62,87 54
$LaLuO_3$	~32	5.2	2.1		Amorphous	80
$LaScO_3$	~22	5.7	2.0		Amorphous	62,82
$GdScO_3$	~22	5.6	2.0		Amorphous	62,82
$DyScO_3$	~22	5.7	2.0		Amorphous	62,82

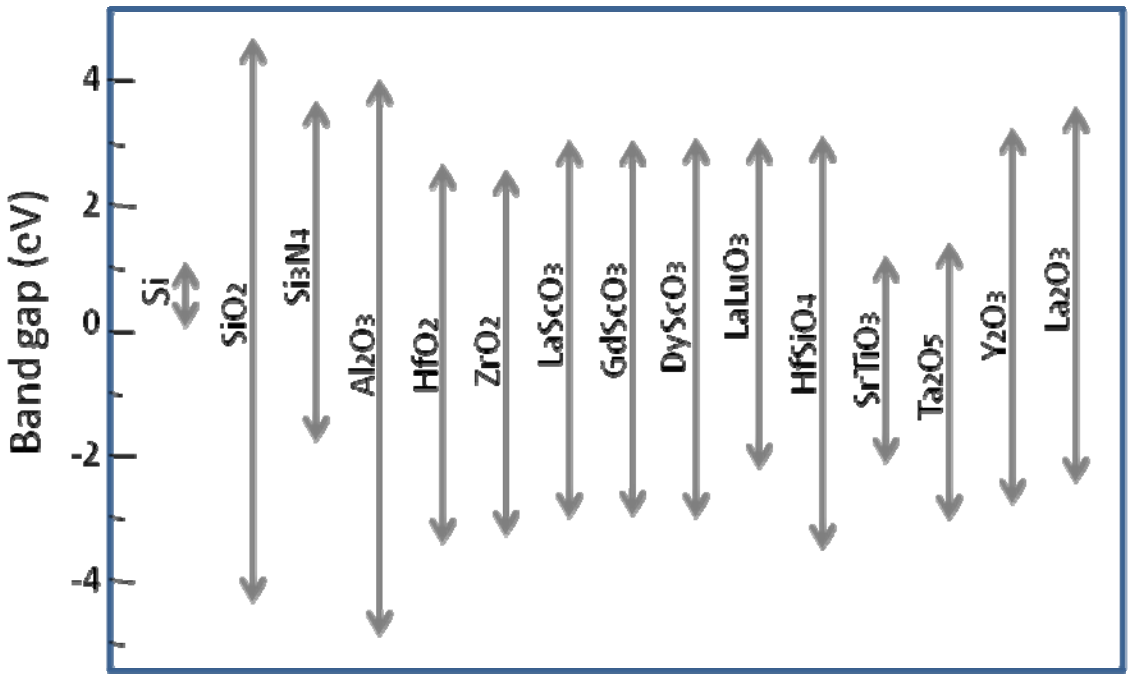

Figure 3 Bandgaps and the bandgap discontinuities between various high-κ dielectric materials and Si along with the well known SiO_2 and Si_3N_4.

The gate dielectric should also be uniform in crystalline structure and in physical properties. In polycrystalline dielectric layers, grain boundaries have a large density of electronic states, which serve as pathways for leakage current and result in non-uniform distribution of leakage which, besides being undesirable in the first place, can give rise to large statistical variations for nanometer-sized devices across the chip. Furthermore, grain boundaries serve as pathways for diffusion of Si, O, and dopant elements. For the stated reasons, polycrystalline films are not suitable for the purpose of device fabrication.

Instead, either amorphous or *extremely high quality* single crystalline (if available at all) dielectric layer should be used. There are a number of factors which favor amorphous layers: *i*) there is only a single amorphous structure for a given composition that implies uniform physical properties; *ii*) there are no dislocations or grain boundaries; *iii*) stress can be eliminated by moderate topological variations in a random network rather than through misfit dislocations; *iv*) a continuous random network tends to minimize electrically active defects.

2.1 High-κ dielectric layer growth

As discussed above, the reliable and high quality high-κ gate dielectric films are critical to scaled MOSFET. For this reason the growth of the high-κ dielectric is very important and has received much attention. Various thin film deposition techniques such as reactive thermal evaporation,[97] atomic layer deposition (ALD),[78,98,99,100,101,102,103,104,105] metal-organic chemical vapor deposition (MOCVD),[106,107] pulsed-laser deposition (PLD),[108] and molecular beam-epitaxy (MBE)[109,110] have all been employed to varying degrees to produce them. The properties of the thin films so produced have been reported to be closely dependent on the growth method. Studies to gain insight into any correlation amongst the properties of the films, the interfacial layers, and growth conditions have been undertaken.

2.1.1 Atomic Layer Deposition

ALD, a variant of CVD, is a popular technique used to deposit the ultra thin metal-oxide layers with excellent electrical characteristics and near-perfect structure

because of the layer-by-layer nature of the deposition kinetics. The growth mechanism of the ALD can be simply expressed as the surface exchange reactions between the chemisorbed metal-containing precursor fragments and adsorbed nucleophilic reactant molecules. The growth surface becomes saturated with the governing precursor so that the deposition automatically self-limits at one or two monolayers. Therefore, the growth rate in the system is independent of the precursor dose as it is surface-controlled. The ALD growth mechanism can be described as a four-step process[111], wherein a precursor gas is initially introduced followed by an inert gas to remove the unreacted species from the surface (see Figure 4).

). These first 2 steps are then followed by the introduction of the second reactive gas to the surface, which again is followed by the inert gas to remove the unreacted species. This 4-step process is repeated until a film of desired thickness is obtained. Similar to other CVD processes, there is an optimal growth condition for ALD, called the "ALD-window", which signifies the temperature range in which thin film growth proceeds by surface control in the ALD-mode.[112] Outside the ALD-window, the growth is limited by precursor condensation, decomposition, and insufficient reactivity.

Unfortunately, many of organometallic precursors commonly used for oxide growth do not exhibit a distinct ALD window. Thus, the deposition rate in these processes is dependent on the temperature, while the self-limiting feature of the ALD processes remains. Besides, ALD-grown films usually have a relatively high concentration of residual impurities due to the use of precursors, which is unfavorable for gate dielectrics. Thus, the choice of precursors providing low contamination and ability to self-limit is a critical issue for the ALD growth of high-quality oxide films. Many

precursors have been investigated in an attempt to find the optimal growth window for each of the high-κ oxide and reduce the by-product contamination. For the most promising materials, halide,[113],[114],[115] metal alkoxide,[116] and alkylamide precursors[117] have been widely used in the ALD growth. HfO_2, ZrO_2, PrO_2, $GdScO_3$, and other oxide films prepared by ALD deposition using various precursors have been reported.[118,119,120,121, 122 ,123,124 ,125,] The details will not be discussed here due to limited focus but they can be found elsewhere.[98,126 ,127]

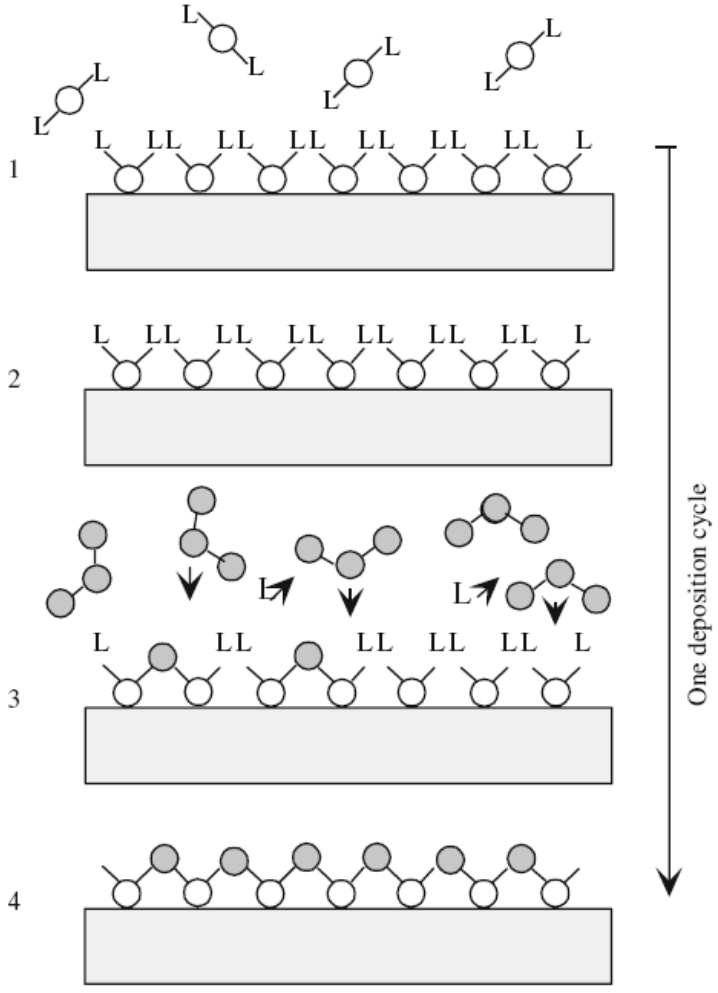

Figure 4 Schematic illustration of an ALD growth cycle (1–4) leading to the formation of an imaginary binary oxide film of metal (○) and oxygen (●). L refers to the precursor ligand. Reprinted with permission Ref. 111

2.1.1 Metal-organic chemical vapor deposition

MOCVD is a widely used technique of epitaxial growth of thin films. Recently, as the high-κ dielectric materials came under extensive investigations, MOCVD emerged as viable candidate for high-κ film deposition on Si. To be applicable to high-κ dielectrics films, however, this method should be modified. This is because many oxide precursors used for the high-κ materials have low pressure and low thermal stability, both of which are detrimental to the growth. This problem can be solved by applying liquid injection of precursors dissolved in a solvent. Even then, there remain some requirements for the precursors to meet: the precursors should be soluble and stable but not reactive to each other in the same liquid solution. In addition, it would be desirable to have precursors with nearly the same vapor pressure at conveniently attainable temperatures to avoid multiple refrigeration/heating units that house the precursor sources. These requirements place sever restrictions on the choice of precursors. Thus, as in the case of ALD, the precursor selection is of paramount importance for MOCVD growth of high-κ films.

A number of high-κ oxide films have been grown by the liquid injection MOCVD method.[77,82,128,129,130,131 132,133] For example, Bastianini et al.[132] deposited ZrO_2 thin films using $Zr(NEt_2)_4$ (NEt_2= $N(C_2H_5)_2$) as a precursor. Hendrix et al.[133] prepared $Hf_{1-x}Si_xO_2$ with compositions ranging from pure HfO_2 to pure SiO_2 using tetrakis(diethylamido)hafnium $Hf[N(C_2H_5)_2]_4$ and tetrakis(diethylamido)silicon $Si[N(CH_3)_2]_4$ liquid precursors. Marshall *et al.* [131] used metal alkoxide precursors

$[Hf(mmp)_4]$ (mmp = $OCMe_2CH_2OMe$) and $[Al(O^iPr)_3]$ to deposit hafnium aluminate $(HfO_2)_x(Al_2O_3)_{1-x}$ thin films. The layers were found to be of high purity without any detectable amount of carbon. Good control over Al incorporation was achieved by varying the gas-phase mole fraction of $[Al(O^iPr)_3]$.

It should be mentioned that both the MOCVD and ALD techniques provide high crystal quality, uniform deposition over large areas and three-dimentional structures, and are compatible with the strandard semiconductor technology. As compared to ALD, MOCVD provides much higher throughput, but typically requires higher deposition temperatures. From the standpoint of the gate dielectric application, requiring low film thicknesses and high aspect ratios, ALD seems to be the most suitable method for ultrathin high-κ film deposition due to its capability of growing highly conformal layers with atomic level accuracy in thickness.

2.1.2 Pulsed-Laser Deposition

PLD is also applied to the high-κ dielectric film growth owing to its advantages such as relative simplicity, large deposition rate, and low growth temperature.[134] Ratzke *et al.* [135] deposited HfO_2 and PrO_x films on Si substrates by the PLD method and compared their morphology, chemical composition, and crystalline structure, in particular that at the interface. Both HfO_2 and PrO_x films showed grainy structure the size of which increasing with growth temperature. The PrO_x films were found to be much more uniform than HfO_2. The interfaces were significantly different for both materials in that a silicate formation was observed for PrO_x, whereas and a rich abundance of SiO_2 and silicide was found for HfO_2. In addition to PrO_x, several other lanthanoid oxide thin films such as

$SmScO_3$,[84] Sm_2O_3, Tb_4O_7, Er_2O_3, and Yb_2O_3[136] have also been attempted with this method on Si(100) wafers. PrO_x film showed thinner equivalent oxide thickness (EOT) and a lower leakage current. The PrO_x films with EOT of 2.6 nm and a leakage current density of 2×10^{-3} A/cm^2 at -1 V have been achieved after annealing at 600°C. Some films grown by PLD turn out to be amorphous, among which are zirconium silicate films on n-Si (100) substrates.[137] The amorphous Zr-rich Zr silicate films showed excellent thermal stability: they remained amorphous even after rapid thermal annealing (RTA) at 800°C. Silicon oxynitride (SiO_xN_y) thin films have also been grown by combining the PLD plume containing silicon species in an oxygen background with a remote plasma-based atomic nitrogen source (ANS).[138]

2.1.3 Molecular beam epitaxy

MBE is a powerful and sophisticated technique due to its precise control over growth parameters at the atomic scale. Despite these strengths, MBE is not very popular for the high-κ dielectric deposition. In order to meet the high-κ materials growth requirements, MBE systems must be modified due to the corrosive oxygen environment, oxygen reaction with the source material in cells, and difficulties associated with production of reactive oxygen sources. Against this background, various high-κ dielectric oxides have been successfully grown by MBE.[49,51,55,55,57,81,139,140,141,142,143,144] For expamle, Lin et al.[143] grown Gd_2O_3 epitaxial thin films on nearly lattice-matched (111)Si substrates by MBE. Detailed structural studies have revealed excellent crystallinity of the layers and atomically sharp interfaces. Vellianitis et al.[144] have grown perovskite-like $LaAlO_3$ and pyrochlore $La_2Hf_2O_7$ on the SiO_2/Si substrates. The values of EOT of 1.1 nm and leakage

current of 2×10^{-3} A/cm^2 at 1V for the $LaAlO_3$, and EOT of 1.14 nm, and leakage current of 4×10^{-5} A/cm^2 at 1V for $La_2Hf_2O_7$ were achieved. Triyoso et al.[81] reported MBE growth of $LaLuO_3$ films. The oxide film was formed by co-deposition of elemental La, Lu in the presence of molecular oxygen. Post deposition anneals were performed in either nitrogen or oxygen at 700 °C environment, or nitrogen at 900°C. Cross-sectional transmission electron microscopy (TEM) revealed that the as-deposited layers were amorphous, and the $LaLuO_3$/Si interface was quite sharp with an extremely thin interfacial layer. TEM studies indicated also good thermal stability of the films: they remained mostly amorphous after post-growth annealings, although secondary ion mass spectrometry (SIMS) data indicated Si interdiffusion into $LaLuO_3$, likely forming $LaLuO_3$-silicate, and an increase in the thickness of the SiO_2 interfacial layer upon annealing.

Laser molecular beam epitaxy (LMBE), combining the merits of both PLD and conventional MBE for depositing films with atomic scale thickness control, was used to grow the HfO_2 film in an oxygen ambient.[145] It was found that the growth of the interfacial layer depends strongly on the oxygen partial pressure. Another variant of MBE is metalorganic molecular beam epitaxy (MOMBE). Due to source evaporation at a well-controlled rate under ultra high vacuum condition, this technique allows obtaining abrupt interfaces and good thickness control. MOMBE has been applied for the growth of HfO_2[146] and ZrO_2[147] films. MOMBE-grown HfO_2 films were found to have a dielectric constant of 20–22 and low leakage current density of ~10^{-8} A/cm^2. Electrical characteristics and surface morphology of the HfO_2 films showed a strong dependence on the O_2/Ar gas flow ratio. As the O_2/Ar gas ratio increased, the density of interface states

and negative fixed charges in the films decreased and the surface morphology improved.[146]

2.2 Doping of high κ dielectrics

Beyond the preparation of the high-quality high-κ films, the critical issue is their stability and processing compatibility with the standard CMOS processing steps. Various dopant atoms are added to the dielectrics in order to enhance the stability of the high-κ films, especially the stability of the high-κ/Si interface, and decrease the gate current leakage. Among them, nitrogen incorporation has been shown to reduce the leakage current efficiently.[148] Nitrogen doping can also suppress crystallization during high-temperature treatment, reduce penetration of boron (from B-doped bulk Si and poly-Si gate, where B concentration is continually increased to combat the short channel effects), and increase the dielectric constant of the high-κ films. Furthermore, accumulation of N at the SiO_2/Si interface can improve hot carrier resistance, and the use of oxynitrides can also suppress B diffusion from a poly-Si gate to SiO_2. There have been several reports on the incorporation of nitrogen into binary metal oxides aimed at increasing crystallization temperature through high-temperature annealing in oxygen-free N_2 plasma,[149,150,151] and NH_3 ambient.[152] However, nitridization of high-κ dielectric materials in NH_3 results in increased interface trap density and deterioration of the interfacial carrier mobility. At the atomic level, N atoms act to couple favorably with oxygen vacancies (V_O) in HfO_2 and extract electrons from V_O and elevate the V_O energy level.[153] Consequently, N incorporation removes the electron leakage paths mediated by V_O-related gap states by

deactivating the V_O-related gap states. This leakage path elimination mechanism is schematically depicted in **Figure 5**.

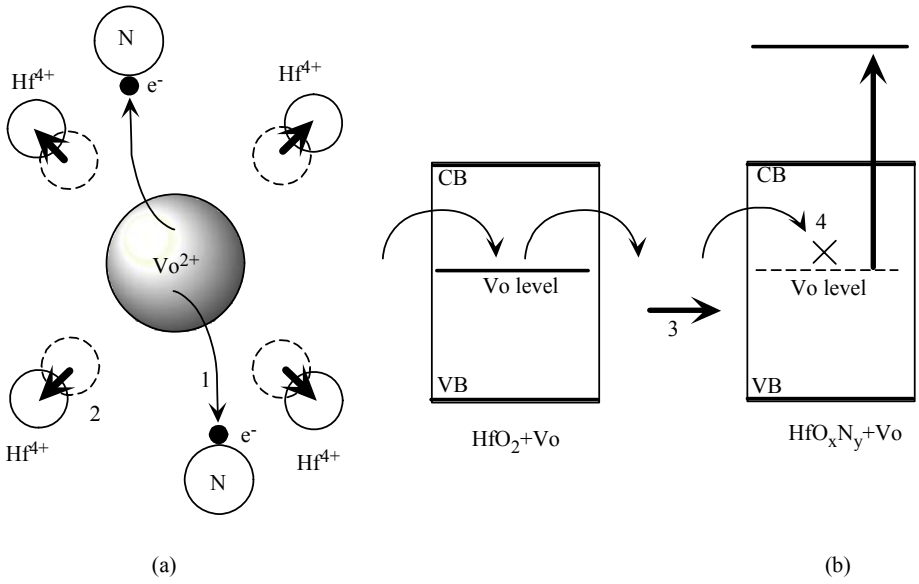

Figure 5 Schematic illustration of N incorporation effects: (a) N-induced atomistic relaxation around V_O. (1) Electron transfer from V_O to N atoms; (2) outward movement of Hf^{4+} ions due to the increase in Hf^{4+}–Hf^{4+} Coulomb repulsion; (b) N-induced elimination of leakage paths; (3) drastic V_O level elevation due to the decrease in attractive Coulomb interaction with Hf^{4+} ions around V_O; (4) removal of leakage paths oewing to the elimination of a V_O level. Reprinted with permission Ref. 153.

Another impurity that has been studied for high-κ dielectric doping is fluorine (F). When incorporated, F atoms act as an effective passivant for reducing the trap density in the high-κ films, because it is the only element that is more electronegative than O but with comparable bond length.[154] The F atoms substitute for O vacancies (F_O) in gate oxides and reduce the charge trap density and lower the pFET threshold voltage.[155] Furthermore, F incorporation can reduce the CV hysteresis and improve the device reliability.[156,157] However, the gate leakage increases due to the EOT reduction caused by F incorporation.

Other impurity atoms that have been studied in this context are Al and Si, which, when incorporated, have been shown to enhance the thermal stability of high-κ films. One drawback of HfO_2 is that it crystallizes at a relatively low temperature of about 400°C. However, in the standard Si-based CMOS processing relatively higher temperature annealing steps are frequently used, which causes at least partial crystallization of the otherwise amorphous HfO_2 dielectric layer. By adding about 30 % Al, the crystallization temperature of HfO_2 can be increased by 400 °C–500 °C above that of pure HfO_2.[72] The downside is that introduction of Al atoms into HfO_2 lowers its dielectric constant. Furthermore, the negative fixed oxide charge due to Al accumulation at the HfAlO/Si interface results in mobility degradation.[158] The fixed charge acts as scattering centers and degrades the channel carrier transport. Compared with Al, addition of 20% Si makes the HfO_2 dielectric layer withstand a 5-s long rapid annealing at 1000°C without any extensive HfO_2 crystal formation in the layer.[159] Detailed structural analyses indicated that the major part of HfSiO remained amorphous but a small fraction crystallized into the tetragonal or orthorhombic phase. The caveat is that HfSiO can fully phase separate into HfO_2 and SiO_2 via spinodal decomposition after 900°C O_2 RTA treatment.[160]

As an alternative to Al and Si dopants, which deteriorate the dielectric constant, introduction of La and Y into HfO_2 has been studied.[161,162,163] By adding La atoms, the crystallization temperature of HfO_2 can be raised to 900ºC, without compromising on the dielectric constant (κ = 20 can be achieved). Doping with Y was found to increase the dielectric permittivity of HfO_2: κ as high as 27 was obtained by 4 at. % Y doping.[162] The increase in permittivity was explained by a change in crystal structure of the oxide

induced by the introduction of Y, despite Y. Indeed, under annealing at 600 ºC, pure HfO_2 crystallized in a monoclinic phase, while Y-doped HfO_2 films prepared by co-sputtering of HfO_2 and Y_2O_3 had a cubic structure which, as predicted theoretically,[164] should have much larger dielectric response than the monoclinic phase.

2.3 Remaining challenges

Electrical properties of high-κ dielectric films and their integration with the conventional CMOS processing are the main topics of research now. In the context of compatibility with the Si MOSFET technology, the high-κ oxides present many challenges, among them are incompatibility with annealing temperatures used for activating poly-Si gates, relatively poor quality which causes charge trapping and makes the Si MOSFET gate unstable, channel mobility degradation, and threshold voltage shift induced by high-κ material.

In addition to the compatibility of the gate dielectric stack with Si and the processing steps, the suitability of the gate electrode for the particular high-κ oxide stack is also critical. Poly-Si has been the dominant gate electrode until recently. However, annealing above 1000°C for the poly-Si activation is harmful to high-κ films. To reiterate, annealing of HfO_2 gate dielectric at high temperatures causes the crystallization of amorphous HfO_2 into the monoclinic polycrystal which is not insulating.[165] In addition, a 5-10Å layer of SiO_2 is formed at the interface, which eliminates in part the benefits to be gained from high-κ dielectric.[166] As discussed earlier, Si, N, or Al is added to the gate oxide material to increase its crystallization temperature.[72,167]

Another approach to this problem is the use of metal electrodes instead of conventional poly-Si. When incorporating a new metal electrode, complications related to channel mobility and threshold voltage shift arise. A relative disadvantage of the metal electrodes is that, unlike the poly-Si gate electrodes, they cannot be used for both *n*- and *p*-MOS simply by adding different dopants. There is no such versatility when a metal gate with a fixed work function is used. Two methods are usually implemented for employing metal electrodes. The first is the so-called "midgap metals", such as TiN,[168] which causes the Fermi level to be at the midgap of Si, as shown in Figure 6a.[2] The advantage of this method is symmetrical threshold voltage (V_T) values for both *n*-MOS and *p*-MOS, because the Fermi level being at the midgap would allow for the same energy difference between the metal Fermi level and the conduction and valence bands of Si. This approach allows a simpler CMOS processing scheme, where only one mask and one metal would be required for the gate electrode, and no ion implantation step would be needed. A severe drawback of this method is too high threshold voltage (~0.5 V for both *n*-MOS and *p*-MOS), while typical threshold voltages for sub-0.13 mm CMOS devices are desired to be lower, ~ 0.2–0.3 V.[2]

The second approach involves the use of two different metals for *n*- and *p*-MOS, as shown in Figure 6b.[2] The possible choices of metal electrodes, however, are limited by their thermal stability. Most of the low-work-function metals are reactive and not stable at high temperatures used in the conventional Si MOSFET processing, whereas most of the mid-bandgap metals are stable under these kinds of processing.

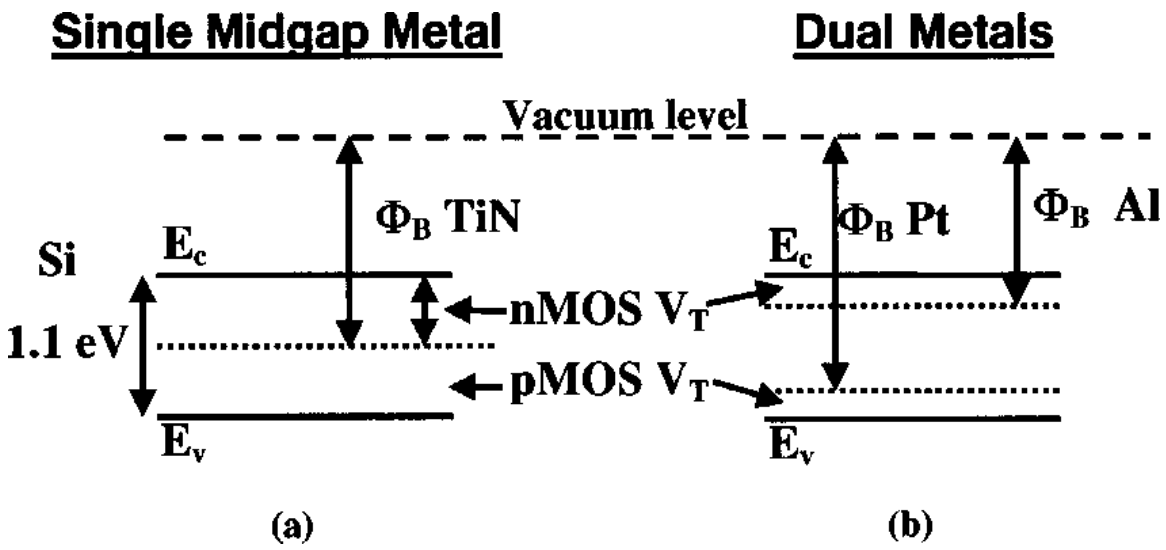

Figure 6 Energy diagrams of threshold voltages for *n*-MOS and *p*-MOS devices using (a) midgap metal gates and (b) dual metal gates. Reprinted with permission Ref. 2.

Reduction of carrier mobility in the inversion layer of Si MOSFETs is another important issue in considering high-κ dielectric gate oxides. Unlike SiO_2, the high-κ dielectrics have soft optical phonons, and the long-range dipole field associated with the interface excitations resulting from these phonon modes and from their coupling with surface plasmons causes degradation of the effective electron mobility in the inversion layer.[169] Figure 7 compares values of the effective electron mobility in the inversion layer at the interface between Si and an infinitely thick film of several insulators.[169] Figure 8 shows the effects of all the scattering and degradation mechanisms on the inversion channel carrier mobility summarized by Yang *et al.*[170] An effort was made to improve mobility values by doping. It was found that addition of Si into the HfO_2 enhances the mobility due to the reduction of the remote phonon scattering.[171] As for the N incorporation, the mobility is usually reduced, because N incorporation induces fixed

charge in the high-κ layer and the resulting Coulomb scattering by the fixed charge reduces the carrier mobility.[172]

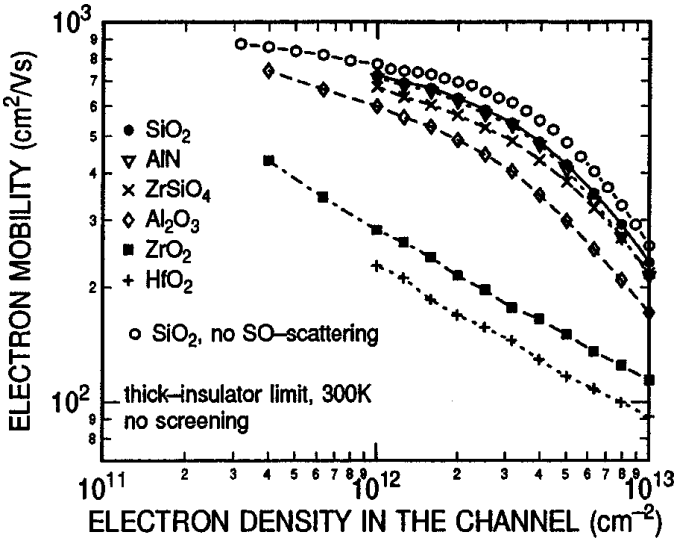

Figure 7. Effective electron mobility in Si inversion layers of MOS systems with the insulators indicated. A triangular well approximation has been used to model the subband structure of the inversion layer. Reprinted with permission Ref. 169

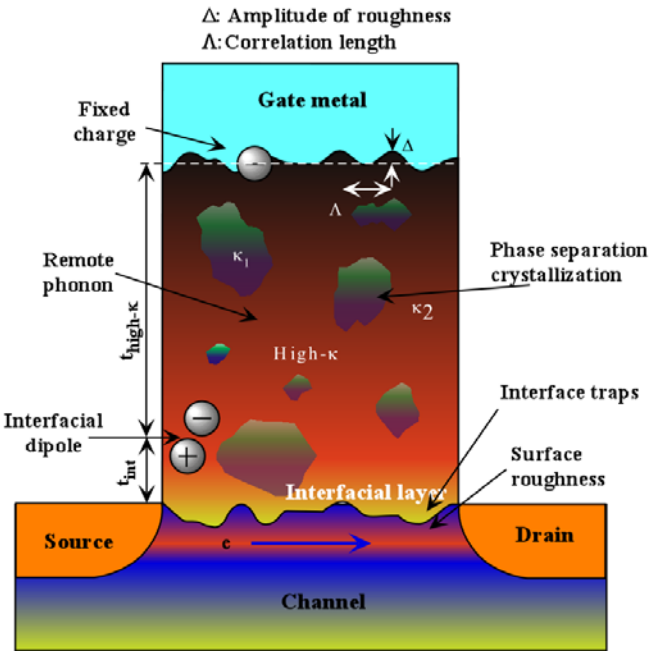

Figure 8 Schematic representation of factors contributing to carrier mobility degradation in a high-κ oxide layer. Reprinted with permission Ref. 170

The last issue that we will discuss here is the threshold voltage shift of the poly-Si/ high-κ dielectric stack. Hobbs et al. [173],[174] explained the shift by the Fermi-level pinning at the interface, which in turn was attributed interfacial Si–Hf and Si–O–Al bonds for HfO_2 and Al_2O_3, respectively. Oxygen vacancies at poly-Si/HfO_2 interfaces also lead to Fermi pinning. The interface states partially screen the electric field from the gate electrode, preventing it from modulating the channel completely. An efficient method to reduce the threshold voltage shift is to add a layer of Al_2O_3 on top of the oxide layer. Kim *et al.*[175] reported the Fermi-level effect free HfO_2 gate stack by depositing an Al_2O_3 capping layer onto $HfSiO_x$. The *p*-MOS gate threshold shift was only 0.2 V. It is likely that the negative fixed charge is introduced into the oxide layer when Al_2O_3 is added. Frank *et al.*[176] used an AlN capping layer to prevent the threshold voltage shift and also obtained shift values as low as 0.2 V. Besides the Al_2O_3 cap layer, other oxides have been applied to prevent the threshold voltage shift. For example, Alshareef et al.[177] used La_2O_3 to passivate $HfSiO_x$ on N-MOSFET. A reduction of the threshold voltage by as much as 0.25 V was achieved. Passivation of HfSiO dielectric with a 0.5-2 nm thick Dy_2O_3 cap layer resulted in a threshold voltage of 0.2 eV.[178]

Clearly, the high-κ dielectric materials and related techniques are crucial for continuing the Si-based scaling engineering. Although many investigations have been devoted to different aspects of the preparation and properties of high-κ dielectrics and their integration with conventional Si devices, there are still many obstacles that need to be conquered. In terms of the deposition aspects, the precursors and growth conditions

for the high-κ films should be honed in and/or optimized further. The thermal stability issue should be addressed with the aim to increase the crystallization temperature of the high-κ oxides to prevent the crystallization of amorphous dielectric films during subsequent high temperature processing. The gate electrodes suitable for the high-κ oxide stack and processing integration compatibility also need further research and development. A search for new high-κ dielectric materials is now in progress. Some multicomponent oxides, such as $LaLuO_3$ and rare-earth scandates $LaScO_3$,' $GdScO_3$, $DyScO_3$, and $SmScO_3$, exhibit high dielectric constants (similar to or exceeding that of HfO_2), wide band gaps, and large band offsets of ≥2 eV to both the valence and conduction bands of Si (see Table 1), low leakage current, and superior thermal stability of amorphous phase. [85,179,180] These oxides are now under intensive investigations for potential high-κ applications,[62,80,82,83,84,85,86,118,77,] and, in the future, could compete with Hf-based oxides as gate dielectrics for Si-based MOSFETs.

3 Ferroelectric Oxides

3.1 Brief history of ferroelectrics

The birth of ferroelectrics can probably be traced back to 1921 when Valashek [[181]] observed nonlinear electrical properties of potassium sodium tartrate tetrahydrate ($KNaC_4H_4O_6{\cdot}4H_2O$), a material which was known for more than two centuries due to Pier Seignette from La Rochelle, France, who first prepared it in 1672. In this compound, also known as Rochelle salt, Pierre and Jacques Curie discovered piezoelectricity in 1880, some 40 years before the observations of Valashek. However, the discovery of Valasek did not become a subject of interest among the scientists for the first decade, particularly

because the Rochelle salt was the only compound at that time showing such interesting properties. In addition, very small deviations of the composition from the chemical stoichiometry destroyed the phenomenon completely. First theoretical interpretation of ferroelectricity was done by Kurchatov in 1933.[182] In 1935, Busch and Scherrer[183] produced another ferroelectric crystal, potassium dihydrogen phosphate (KH_2PO_4, abbreviated as KDP). KDP exhibited good piezoelectric properties above Curie point and was successfully used as underwater transducer and detector during World War II.

Ten years later, in 1945, a new type of ferroelectric - barium titanate $BaTiO_3$ - was discovered,[184] although some reports go as far back as 1927.[185] Having phase transition at 120 °C, $BaTiO_3$ was a very important discovery since it was the first ferroelectric structure without hydrogen bonds and had more than one ferroelectric phase. The same year, Ginsburg developed a phenomenological theory of $BaTiO_3$ based on Landau's general theory of phase transitions.[186] Several years later a number of ferroelectrics began to increase rapidly. New representatives of perovskite-type crystals were discovered: potassium niobate ($KNbO_3$) in 1949, lead titanate ($PbTiO_3$) in 1950, and antiferroelectric lead zirconate ($PbZrO_3$) in 1951. These compounds were followed by guanidine aluminum sulphate hexahydrate $C(NH_2)_3Al(SO_4)_2{\cdot}6H_2O$ (abbreviated as GASH) in 1955 and tryglicine sulphate in 1955. In 1959, Smolensky and Agranovskaya[187] discovered ferroelectric properties of $PbBi_2Nb_2O_9$, a representative compound of a large family of Bi-layer structured ferroelectrics. Then, Smolensky et al.[188] and Subbarao[189] confirmed ferroelectric properties for a large number of Bi-layer materials with a general formula $(Bi_2O_2)^{2+}(A_{m-1}B_mO_{3m+1})^{2-}$, where m is an integer number, A can be one-, two-, or tree-valence ions, and B represents Ti^{4+}, Nb^{5+}, Ta^{5+} or a

combination of them. From the very beginning, it was realized that the layered structure of these compounds, where perovskite blocks are interleaved with Bi_2O_2 layers, should lead to high dielectric, ferroelectric, and piezoelectric anisotropy due to the predominantly two-dimensional character of ferroelectric switching. At the end of the 1960s, Cummins and Cross[190] could demonstrate highly anisotropic optical and electrical properties of $Bi_4Ti_3O_{12}$, one of the most popular Bi-layer structured ferroelectrics, which will be discussed in more details below. The strong anisotropy is a major limiting factor in piezoelectric applications of the Bi-layer structured ceramics and single crystals. Renewed interest in Bi-layer structured ferroelectrics came in the mid-1990s, when it was understood that, along with the high switching polarization and sufficiently low coercive field, some of these materials, namely $SrBi_2Ta_2O_9$ and $SrBi_2Nb_2O_9$, are resistive to polarization fatigue.[191], [192] Paz de Araujo et al.[192] showed that capacitors made of $SrBi_2Ta_2O_9$, $SrBi_2NbTaO_9$ and $SrBi_4Ta_4O_{15}$ do not show significant fatigue after 10^{12} switching cycles, and they exhibited good retention characteristics and low leakage currents even with films less than 100 nm thick. The unique peroperties of these materials made them very perspective for FeRAMs.[193],[194]

Today there are about known 1000 ferroelectrics. A list of some ferroelectrics, year of their discovery and some important properties are given in Table 2. Further information beyond Table 2 about these compounds can be found in books.[183,195,196,197]

Table 2 A list of ferroelectrics materials and their pertinent properties.

Compound	Chemical formula	Year discovered	Symmetry at room temp.	Curie point, T_c, K	Remanent polarization, P_s, $\mu K \cdot cm^{-2}$
Rochelle salt	$KNaC_4H_4O_6 \cdot 4H_2O$	1921	Monoclinic between the Curie points Orthorhombic at other temperatures	255 and 297	0.25
Barium titanate	$BaTiO_3$	1945	tetragonal	398	25
Lithium niobate	$LiNbO_3$	1949	Trigonal	1415	10-30
Potassium niobate	$KNbO_3$	1949	Orthorhombic	400	20-40
Guanidine aluminum sulphite hexahydrate	$C(NH_2)_3Al(SO_4)_2 \cdot 6H_2O$	1955	Trigonal	473	0.5
Potassium dihydrogen phosphate	KH_2PO_4	1935	Orthorhombic	123	6.1
Lead titanate	$PbTiO_3$	1950	tetragonal	763	20-96.5
Lead zirconate	$PbZrO_3$	1951	Orthorhombic	503	20-50
Lead zirconate titanate	$PbZr_{1-x}Ti_xO_3$	1949	Tetragonal for Ti-rich and Rhombohedral for Zr-rich	Depends on composition	20-97
Strontium bismute tantalate	$SrBi_2Ta_2O_9$	1960	Orthorhombic	600	30-70
Barium strontium titanate	$Ba_{0.73}Sr_{0.27}TiO_3$	1960	Tetragonal	298	10-30
Bismute titanate	$Bi_4Ti_3O_{12}$	1961	Orthorhombic	953	10-30

3.2 Basic properties of ferroelectrics

Ferroelectrics belong to a wider class of materials called pyroelectrics, which in turn belong to a piezoelectric class. Pyroelectricity is the phenomenon that electric charge is created in certain materials as a result of temperature change, and piezoelectricity is the ability to generate an electric potential in response to applied mechanical stress (and vice versa). All pyroelectric materials are also piezoelectric, but the opposite is not true. For example, quartz is piezoelectric, but not pyroelectric. All ferroelectric materials also exhibit piezoelectricity and pyroelectricity, but not vice versa. For example, the wide bandgap materials such as GaN, AlN, and ZnO are not ferroelectric materials although they are both piezoelectric and pyroelectric. Ferroelectrics are a class of materials exhibiting spontaneous polarization below the ferroelectric Curie temperature (T_C), and the polarization direction can be changed by applied electric field. At temperatures above T_C, the crystals are non-polar and no longer ferroelectric and behave like normal dielectrics. Generally there may exist more than one Curie temperature, although most of the ferroelectrics have one Curie point. The Rochelle salt $KNaC_4H_4O_6{\cdot}4H_2O$, for example, has two Curie points, one at 24°C and one at -18°C, so that the ferroelectric state exists in the temperature range from -18 to +24°C. The polar ferroelectric phase is monoclinic, while paraelectric phase outside the temperature region of -18°C – +24°C is orthorhombic. There are also ferroelectric materials, for example guanidine aluminum sulphate hexahydrate $C(NH_2)_3Al(SO_4)_2{\cdot}6H_2O$ (GASH) which does not exhibit a Curie point because the material begins to decompose before the Curie temperature is reached.

The dielectric constants of ferroelectric materials are extremely high, especially near the Curie temperature.

A ferroelectric crystal consists of domains, i.e. regions with uniform spontaneous polarization. The boundary of two neighboring domains is called a domain wall. In the absence of electrical field, the domains are randomly oriented that results in near complete compensation of polarization. When an external electric field is applied, the domains become oriented along the field causing polarization of the material. The switching of domain orientation proceeds through domain-wall motion. Domain dynamics and a domain's contribution to dielectric, piezoelectric, pyroelectric, and ferroelectric properties has been identified as the key physical phenomenon in ferroelectrics, and hence a subject of extensive scientific research.[198],[199] The most prominent feature of a ferroelectric material is the reversibility of permanent polarization, which results in a hysteresis loop in the dependence of polarization *P* on electric field *E,* analogous to magnetization curves in ferromagnetic materials. A typical view of hysteresis P-E loop is shown in Figure 9. The hysteresis loop is characterized by saturation polarization P_s, remanent polarization P_r, and coercive field E_c. Saturation polarization is the maximum polarization that can be reached, remanent polarization is the polarization present when no electric field is applied, and coercive field is a value of electric filed which is required to bring the polarization to zero. The P-E hysteresis loop results from the domain structure of the ferroelectric which is formed below the Curie temperature in an effort to minimize the depolarization field.

In short, the most distinguishing features of ferroelectrics are: spontaneous polarization below Curie temperature T_C, nonlinear dependence of polarization on

electric field, presence of domain structure below T_C, high values of dielectric constants (up to $2x10^4$), and high values of piezoelectric and pyroelectric constants.

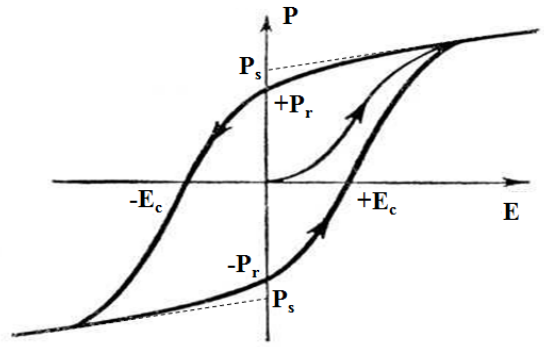

Figure 9 Typical polarization vs. electric field (P-E) hysteresis loop of ferroelectrics.

Ferroelectric oxides have attracted great attention for device applications, one of which is ferroelectric RAM, because of their ability to retain two stable polarization states. To obtain long-term operation (consistent polarization switching over many cycles of applied electric field, more than 10^{12} is desirable), which is a critical issue to realize FeRAM, it is imperative to overcome the reliability problems, such as fatigue, retention, and imprint. Conventional ferroelectric capacitors based on $Pb(Zr,Ti)O_3$ films on Si wafers coupled with Pt top/bottom electrodes show strong loss of switchable polarization with repeated cycling, known as fatigue. Factors affecting fatigue include intrinsic properties of ferroelectric oxides (crystal quality, microstructure, crystallographic orientation, defects, domain structure, film thickness) as well as extrinsic factors (interactions between film and substrate, temperature, and pressure). Excellent reviews of the physical and chemical mechanisms of the fatigue phenomenon in ferroelectric ceramics and various fatigue models can be found in the reports by Lupascu[200] and Lupascu and Roedel.[201] The suggested mechanisms of fatigue so far consider inhibition

of nucleation and growth of oppositely polarized domains, polarization pinning, development of interfacial passive layers, appearance of 90◦ domains, and so on. Several mechanisms of fatigue can be operative simultaneously.

Another important failure mechanism in ferroelectric thin films for FeRAM applications is imprint, which is basically the preference of one polarization state over the other and is essentially caused by asymmetric behavior of polarization states. The imprint behavior is believed to be closely related to oxygen vacancies, defect-dipole complexes, and trapping of free charges.[202,203,204,205] Retention, the ability of maintaining a given logic state of polarization (stored information), is another important characteristic for FeRAM applications. Retention loss reduces the difference between switched (P^*) and nonswitched ($P^\wedge$) polarizations (i.e., $\Delta P = P^* - P^\wedge$ = sensing margin of FeRAM). The larger is the margin, the easier is to distinguish between the two logical states in a binary system. Small margins lead to an inability to distinguish between the two logic states. In general, retention loss is related to the imprint, which originates from the presence of internal electric field acting as a depolarizing internal field against the externally applied electric filed.[206]

Let us now discuss briefly crystal structure of the most important ferroelectric materials, such as $BaTiO_3$ (BT), $Ba_xSr_{1-x}TiO_3$ (BST), $Pb(Zr,Ti)O_3$ (PZT), $SrBi_2Ta_2O_9$ (SBT), $Bi_4Ti_3O_{12}$ (BIT), $Bi_{4-x}La_xTi_3O_{12}$ (BLT) and $Bi_{4-x}Nd_xTi_3O_{12}$ (BNT).

3.2.1 $BaTiO_3$ (BT)

$BaTiO_3$ (abbreviated as BT) has tetragonaslly distorted perovskite structure, which belongs to ABO_3 family of perovskite mineral $CaTiO_3$. In this perovskite crystal

structure, A and B are metal ions, the total charge of which is +6. The A and B ions must be of different radii, and the smaller ion must be of larger charge in order to exhibit ferroelectric behavior. In $BaTiO_3$, for example, the radius of Ba^{2+} is 1.35 Å, and the radius of Ti^{4+} is 0.68 Å. The crystal structure of ABO_3 type perovskite structure is shown in Figure 10.[207] As seen from Figure 10, the structure can be described also as a set of BO_6 octahedra arranged in a simple cubic pattern, with A atoms located in spaces between the octahedra. Above the Curie temperature, BT has the cubic perovskite structure and is paraelectric. Below the Curie temperature, a structural distortion takes place, leading to lower symmetry and off-center shift of the Ti^{4+} cation. As a result, spontaneous polarization appears in BT. Various dopants are used to modify the properties of pure BT. For example, Zr and Hf, substituting for Ti in the $BaTiO_3$ lattice, are utilized to increase chemical stability and decrease dielectric loss of the material.[208,209,210]

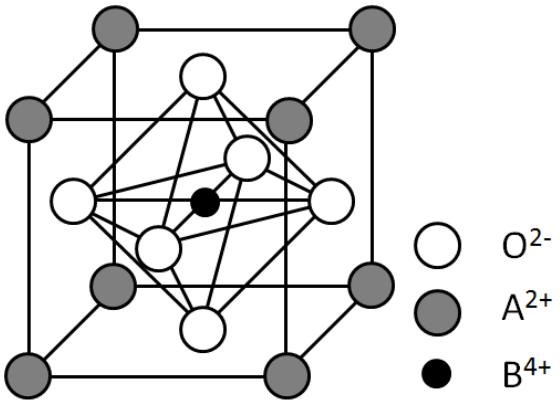

Figure 10 ABO_3 cubic perovskite structure Reprinted with permission Ref. 207.

3.2.2 $Ba_xSr_{1-x}TiO_3$ (BST)

Barium strontium titanate, $Ba_xSr_{1-x}TiO_3$ (BST), is a solid solution of $BaTiO_3$ and $SrTiO_3$. $BaTiO_3$ and Ba-rich $Ba_xSr_{1-x}TiO_3$ compounds have tetragonal lattice and are ferroelectric, while $SrTiO_3$ and Sr-rich $Ba_xSr_{1-x}TiO_3$ compounds are cubic and paraelectric at room temperature (see Figure 11, Figure 12).[211] Substituting Ba with Sr results in the decrease of the Curie temperature (Figure 12) and the increase of the dielectric constant of the material.[212] The phase diagram of the $BaTiO_3$ - $SrTiO_3$ system has been studied by several groups. [213,214.215,216,217,218] Figure 13 shows the phase diagram in the entire conentration range obtained by Menoret et al.[213] based on neutron (powder diffraction and single crystal inelastic scattering) and high-resolution powder x-ray data. The critical concentration $x_c \approx 0.094$ separates the phase diagram in two regions. The low-temperature structure of $Ba_xSr_{1-x}TiO_3$ compounds with $x < x_c$ is tetragonal with a ferroelastic nonferroelectric 14/mcm space group. The compounds with $x > x_c$ show a succession of three ferroelectric phases - *P*4*mm* (tetragonal), *Amm*2 (orthorhombic), and *R*3*m* (rhombohedral) as temperature decreases.

Exceptionally high values of the dielectric constants have been reported for bulk BST ceramics (2500)[219] and epitaxial films (2000–6000).[220] The high dielectric constant of ferroelectric BST arises from an ionic displacement upon applied electric field, in contrast to materials with lower dielectric constants, such as SiO_2, which experience only an electronic displacement. One more important property of BST is the ability to change the dielectric constant and dielectric-loss tangent near the ferroelectric Curie temperature by an externally applied field, which makes this material ideally suited for electrically

tunable microwave devices, such as resonators, filters, and phase shifters.[221,222,223,224,225,226]

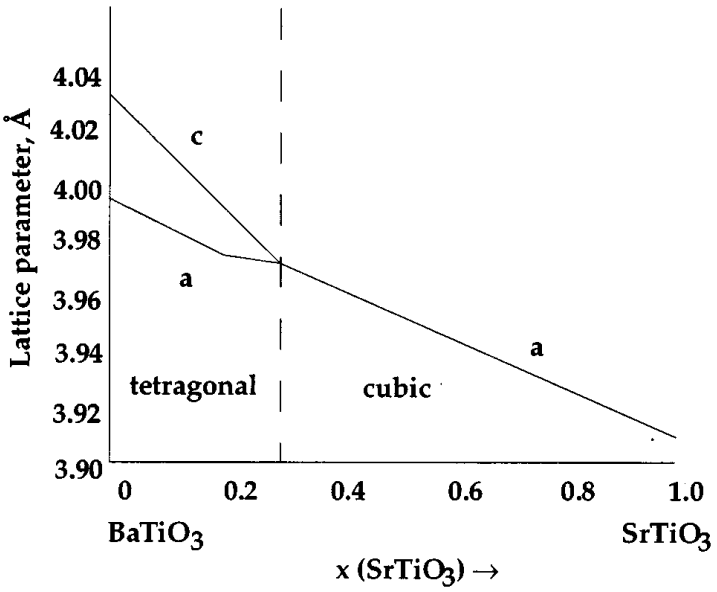

Figure 11 Lattice parameter of $Ba_{1-x}Sr_xTiO_3$ versus composition. Reprinted with permission Ref. 211

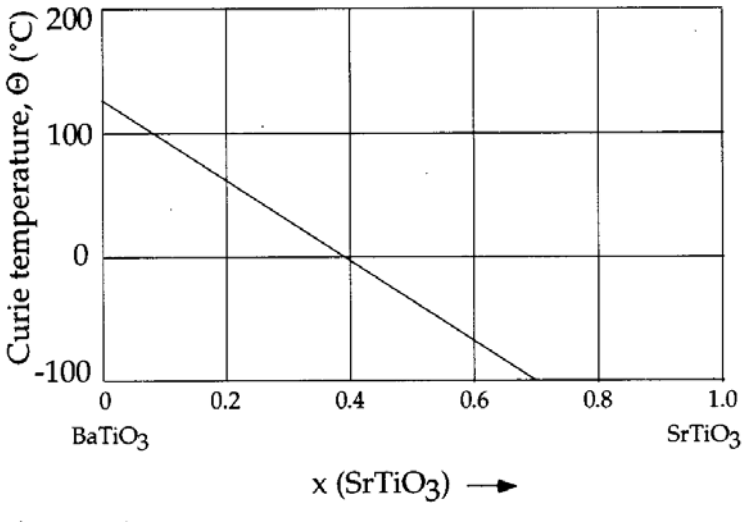

Figure 12 Curie temperature of $Ba_{1-x}Sr_xTiO_3$ versus composition. Reprinted with permission Ref. 211.

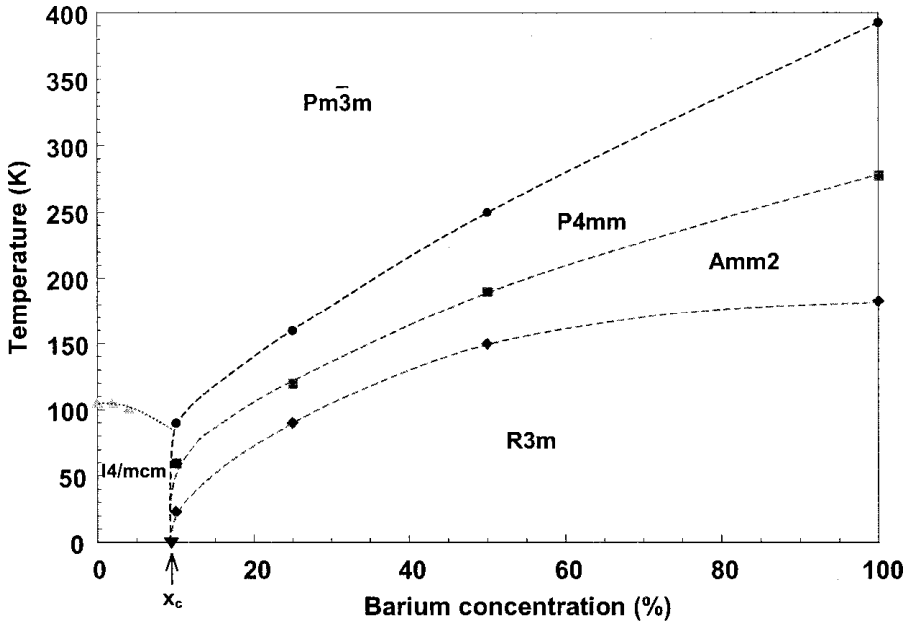

Figure 13 Critical temperature *vs.* concentration phase diagram of $Ba_xSr_{1-x}TiO_3$. Reprinted with permission Ref. 213.

3.2.3 $PbZr_{1-x}Ti_xO_3$ (PZT)

Lead zirconate titanate, $PbZr_{1-x}Ti_xO_3$ (abbreviated as PZT), is a solid solution of $PbTiO_3$ and $PbZrO_3$ compounds. As many other ferroelectric materials, it has an ABO_3 type perovskite structure, where A is a metal ion with a +2 valence (Pb) and B is a metal ion with a +4 valence (Ti, Zr). In the case of PZT, the A positions (corners of the cube) are occupied by Pb^{2+} ions, B positions (body center) by Zr^{4+} or Ti^{4+} ions, and O^{-2} ions occupy the face centers. $PbTiO_3$ has a Curie temperature of 490 °C, at which it undergoes a first-order phase transition from cubic paraelectric phase to tetragonal ferroelectric

phase with lattice parameters c=4.153Å and a=3.899Å.[227] In contrast, $PbZrO_3$ (*a*=5.886 Å, *b*=11.749 Å, *c*=8.248 Å[228]) is an antiferroelectric material at room temperature with a Curie point equal to 230 ^oC, where a transition from cubic paraelectric to orthorhombic antiferroelectric phase occurs. Above the Curie temperature, PZT is cubic over the whole range of compositions.

The properties of $PbZr_{1-x}Ti_xO_3$ depend the fraction of $PbTiO_3$ (that is, *x*) and temperature, according to a $PbTiO_3$-$PbZrO_3$ phase diagram. Figure 14 shows the phase diagram obtained by Woodward et al.[229] The most prominent feature of this diagram is the existence of a "morphotropic phase boundary" (MPB), which divides the ferroelectric region into two parts: a tetragonal Ti-rich region with space group symmetry *P4mm* and a rhombohedral Zr-rich region, containing high- and low-temperature phases with symmetries *R3m* and *R3c*, respectively. There is also another particular region at the phase diagram close to $PbZrO_3$, where the rhombohedral ferroelectric phase changes into an antiferroelectric orthorhombic phase. The MPB occurs at x≈0.47, and PZT solid solutions of this composition exhibits superior ferroelectric and piezoelectric properties. It was believed for a long time that the increased ferroelectric sensitivity of PZT at MPB was due to coexistence of tetragonal and rhombohedral phases at MPB. However, more recent structural studies of PZT revealed a monoclinic phase in the vicinity of what was previously regarded as the boundary separating the rhombohedral and tetragonal regions of the PZT phase diagram.[230,231] One can see a narrow region of monoclinic phases with *Cm* and *Cc* symmetries at compositions corresponding to the MPB. Now it is believed that the monoclinic phase is responsible for the unusually high piezoelectric response of

PZT. The existence of the monoclinic phase, however, is not irrefutable, and the phase composition at MPB is still open for debate.[232]

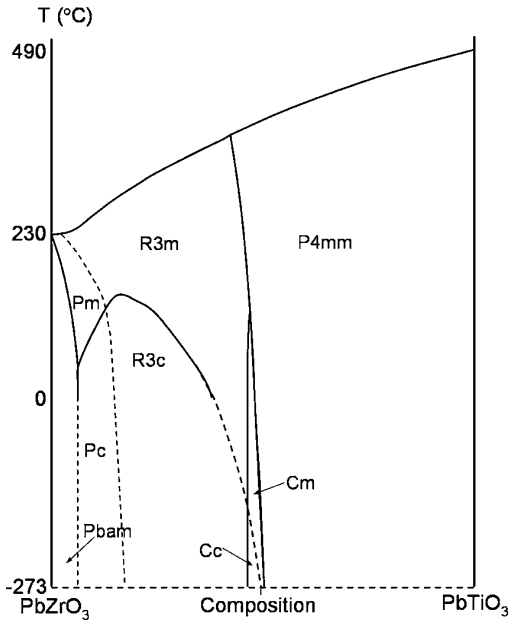

Figure 14 $PbZrO_3$-$PbTiO_3$ phase diagram according to Woodward et al. Reprinted with permission Ref. 229.

3.2.4 $SrBi_2Ta_2O_9$ (SBT)

Another important ferroelectric material is $SrBi_2Ta_2O_9$ (SBT), thanks to its many desirable properties such as fatigue-free characteristics even after 10^{12} switching cycles, good retention characteristics, low switching fields, and low leakage currents.[192] The ferroelectricity of SBT was discovered in early 1960s by Smolenskii et al.,[233] a decade after Aurivillius[234] reported on mixed bismuth oxides with layer lattices in the year 1949. The Curie temperature was determined to be 335 ˚C with a dielectric constant of 180 at

room temperature.[189] SBT belongs to the family of Aurivillius compounds with a general formula $(Bi_2O_2)^{2+}(A_{m-1}B_mO_{3m+1})^{2-}$, consisting of perovskite units sandwiched between bismuth oxide layers, where *A* is Na, Sr, Ca, Ba, Pb, or Bi and B is Ti, Ta, or Nb, and *m* can be an integer or ½ integer, with *m*=2 for SBT. The crystal structure of SBT is shown in Figure 15. The *A* ion, Sr^{2+}, is surrounded by 12 oxygen ions as in the perovskite structure, and the *B* ion, Ta^{5+}, is octahedrally coordinated by 6 oxygen ions. At three of the four distinct oxygen sites, O(1) and O(2) are bonded to two Ta ions, as in perovskites, while O(3) is bonded to one Ta. Bi and O(4) form a rippled BiO layer in which Bi ions lie alternatively above and below the O(4) plane. The Bi sites are asymmetric, forming four short bonds to O(4) sites and four longer bonds to O(3) sites. The room-temperature structure is orthorhombic, and the primitive cell contains 28 atoms. The lattice parameters of the conventional unit cell are *a*=5.531 Å, *b*=5.534 Å, and *c*=24.984 Å.

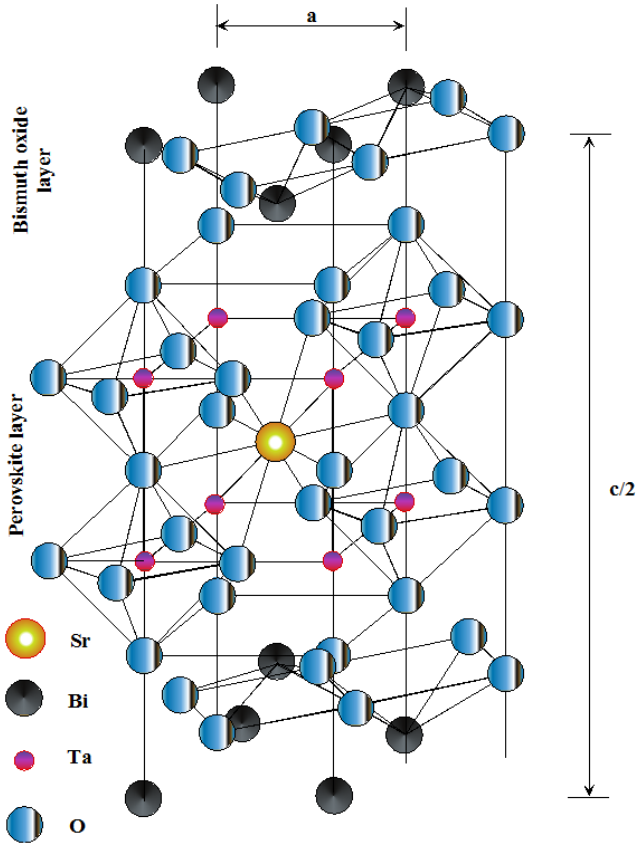

Figure 15 Crystal structure of $SrBi_2Ta_2O_9$ (SBT).

As a result of the layered structure of SBT, its properties exhibit a high degree of anisotropy. Figure 16a shows a temperature dependence of the relative permittivity measured upon cooling in the *ab* plane (along the [110] direction) and along the *c* axis of single-crystal SBT. [235] In both cases, the maximum of dielectric permittivity corresponding to the ferro–paraelectric phase transition is clearly observed at T_C = 355 °C, in agreement with other reports. [236,237,238] The maximum permittivity of SBT in the *ab* plane (~1500) is about an order of magnitude greater than that along the *c* axis (~135), consistent with the results obtained by Irie et al. [239] The anisotropy of dielectric permittivity, i.e., the ratio between the average permittivity in the *ab* plane and along *c* axis is about 10 at T_C and decreases to ~2 at room temperature. The values of the permittivity in the *ab* plane of single crystal SBT exceed significantly those of bulk ceramics.[240] Figure 16b compares the temperature behavior of the dielectric losses (tanδ) measured at 1 MHz in the *ab* plane and along the *c* axis.[235] The losses at low temperatures are essentially higher in the *ab* plane, which is indicative of a large contribution from domain wall motion. The *P*–*E* hysteresis loops measured both along the *c* axis and in the *ab* plane (parallel to the [110] direction) of single-crystal SBT are shown in Figure 17.[235] The hysteresis loop for the *ab* plane is well-saturated, whereas only a linear *P*–*E* behavior with vanishing remanent polarization is observed for measurements along the *c* axis due to the anisotropy of single-crystal SBT and the fact that the P_S vector in the SBT structure lies entirely in the *ab* plane and no polarization can be obtained perpendicular to the bismuth oxide layer.

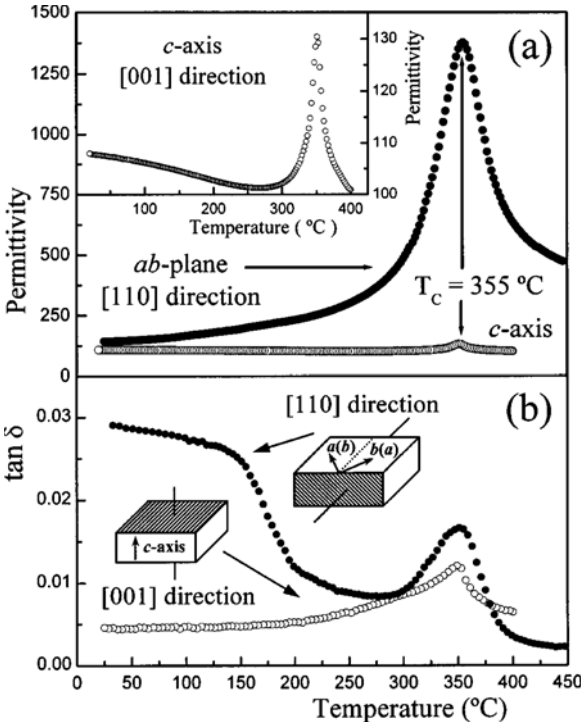

Figure 16 Temperature dependence of the (a) dielectric permittivity and (b) dielectric losses at 1 MHz along the [110] (*ab*-plane) and the [001] (*c*-axis) directions in the $SrBi_2Ta_2O_9$ single crystal. Reprinted with permission Ref. 235.

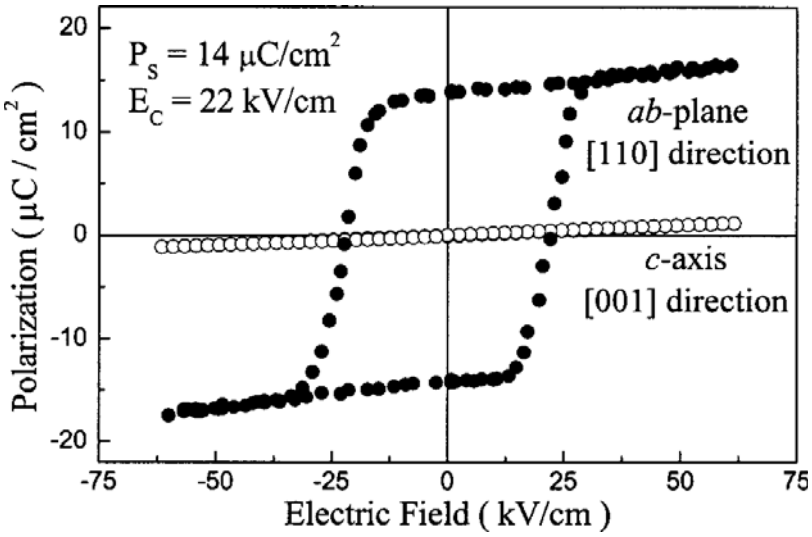

Figure 17 *P–E* hysteresis loops along the [110] (*ab*-plane) and the [001] (*c*-axis) directions in the $SrBi_2Ta_2O_9$ single crystal. Reprinted with permission Ref. 235.

The fatigue-free behavior of SBT is considered to be due to the Bi-containing layered perovskite structure with double layers of Ta–O octahedra sandwiched between $(Bi_2O_2)^{2+}$ layers. Since the $(Bi_2O_2)^{2+}$ layers have net electrical charge, their positioning in the lattice is self-regulated to compensate for space charge.[241]

3.2.5 $Bi_4Ti_3O_{12}$ (BIT)

Due to its small coercive field[242] and fatigue-free behavior,[243] bismuth titanate $Bi_4Ti_3O_{12}$ (BIT) is another lead-free candidate for FeRAM applications. The Curie temperature of BIT is 675 ◦C,[244] which makes it a suitable candidate for high-temperature piezoelectric devices. As SBT, BIT belongs to the family of the Aurivillius compounds.[234] The crystal structure of BIT consists of $(Bi_2O_2)^{2+}$ sheets alternating with $(Bi_2Ti_3O_{10})^{2-}$ layers along the pseudotetragonal *c*-axis, as shown in Figure 18.[244] In the $Bi_2Ti_3O_{10}$ units, Ti ions are enclosed by oxygen octahedra, which are linked through corners forming the O-Ti-O linear chains. Bi ions occupy the spaces in the framework of TiO_6 octahedra. The $Bi_2Ti_3O_{10}$ units exhibit a remarkable similarity to the perovskite structure. As established by Aurivillius,[234] BIT has orthorhombic symmetry with room-temperature lattice parameters are a=5.410, b=5.448, and c=32.84 Å. Similar to SBT, BIT exhibits highly anisotropic properties due to the layered structure, with maximum electrical conductivity in the same plane as polarization.[245]

It is interesting that BIT shows relatively worse fatigue properties.[246] although it has the layered perovskite structure with $(Bi_2O_2)^{2+}$ layers similar to that of SBT, The origin of the fatigue behavior of BIT and SBT thin films was studied by Park et al.[247],[248]

They concluded that oxygen ions near the Bi ions are less stable than those near Sr ions due to the volatility of Bi, and therefore oxygen vacancies in SBT are located only in the $(Bi_2O_2)^{2+}$ layers. In BIT, however, oxygen vacancies can be induced both in the $(Bi_2O_2)^{2+}$ layers and in the TiO_6 octahedra layers. Thus, it was deduced that the difference in stability of the metal–oxygen octahedra is responsible for different fatigue behaviors of SBT and BIT. Therefore, the fatigue characteristics of BIT could be improved by substituting of Bi ions near the Ti–O octahedra with other elements which make oxygen ions stable. Doping of $Bi_4Ti_3O_{12}$ with La or Nd, substituting into the Bi site yields the materials named bismuth lanthanum titanate ($Bi_{4-x}La_xTi_3O_{12}$, abbreviated as BLT) and bismuth neodymium titanate ($Bi_{4-x}Nd_xTi_3O_{12}$, abbreviated as BNT). This doping allows one to improve fatigue characteristics, increase the remanent polarization, and decrease the process temperature of the material, albeit at the expense of an increased coercive field.[247] Piezoelectric properties of BIT in relation to their structural and microstructural features are well described in review,[249] and comparison of ferroelectric properties of PZT and BIT epitaxial thin films from the standpoint of their FeRAM applications can be found in Ref. 243.

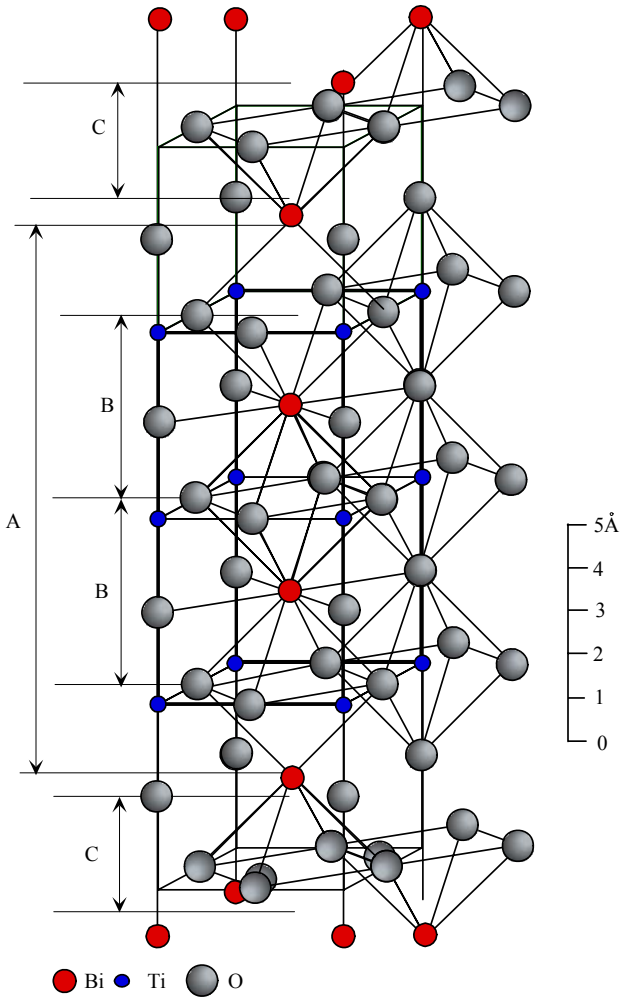

Figure 18 One half of the pseudotetragonal unit cell of $Bi_4Ti_3O_{12}$. A denotes the perovskite layer $(Bi_2Ti_3O_{10})^{2-}$, C denotes $(Bi_2O_2)^{2+}$ layers, and B denotes a unit cell of hypothetical perovskite structure $BiTiO_3$. Patterned after permission Ref. 244. He we can say that it is patterned after Ref. 244.

3.3 Growth of ferroelectric thin films

Ferroelectric films with highly oriented microstructures are preferable for many applications such as high density FeRAMs,[250],[251] electro-optic or acousto-optic waveguide devices,[252],[253] and SAW filters.[254] The fabrication of high-quality single-crystal epitaxial films with good ferroelectric properties also makes possible down scaling of ferroelectric device dimensions and integration of ferroelectric oxides with

semiconductor technologies. A great number of research efforts on the growth of high quality ferroelectric thin films have been undertaken using a variety of deposition techniques including rf magnetron sputtering, pulsed laser deposition (PLD), molecular beam epitaxy (MBE), metal-organic chemical vapor deposition (MOCVD), hydrothermal synthesis, and chemical solution deposition (CSD and also sol-gel). While the sol-gel technique is employed in low-density FeRAM applications, MOCVD (at least based on the results obtained so far) is a preferred method for high-density FeRAM applications due to its high deposition rate, uniformity, and high degree of step coverage over the complex device topographies of ultra-large scale integrated (ULSI) circuits. MBE has been a workhorse of epitaxial growth of various compound semiconductors such as SiGe, III-V, and II-VI compounds, at least in research and development phases, due to low defect density and precise control of composition in grown films. However, MBE is just beginning to be considered for attaining ferroelectric oxides, while other physical vapor deposition techniques, such as PLD and sputtering have been extensively employed for ferroelectric oxide growth. In all these growth methods, the emphasis is placed on the interface control to promote high quality film growth and on identification of optimum deposition parameters. In this vein, various deposition techniques for the growth of ferroelectric thin films will be briefly discussed.

3.3.1 Deposition of ferroelectric films by sol-gel technique

The chemical solution deposition (CSD) or sol-gel technique has been extensively used to synthesize a wide range of ferroelectric oxides[255,256,257,258,259,260,261,262,263,264] because of its numerous advantages, including simplicity, low cost, excellent thickness

and compositional control, short fabrication cycle, and uniformity over large areas. A conventional sol–gel process includes the preparation of stable solution of metal oxide precursors in a suitable solvent with other chemical additives to control the solution properties. This is an important step for sol–gel processing, and many complicated chemical reactions such as hydrolysis, condensation, and chelation proceed during the solution preparation. The solution is partially hydrolyzed to form a stable sol, and then the sol is polymerized to form a gel. Afterwards, it is dried and fired to remove the organic components and form an oxide powder, which can be sintered to make ceramics. To fabricate thin films, the sol-gel solution is spin-coated on a flat substrate, and then the resulting film undergoes a low-temperature heat treatment (pyrolysis) to remove organic components. Most organic materials from precursor solutions are decomposed and removed from the films during the pyrolysis step. The thickness of the deposited layer is usually very low, of the order 50 nm, and preparation of films with thicknesses of 0.5-1 μm requires repeated deposition steps. Finally, the as-pyrolized amorphous film is subjected to high-temperature annealing to form a dense crystalline layer of the desired phase composition and thickness. More information about precursor characteristics as well as various chemical, physical, and technological aspects of the sol-gel process can be found in Refs. 265,266,267,268,269,270. Structural and, therefore, physical properties of sol-gel films depend strongly on such processing conditions as temperature of pyrolysis and final heat-treatment, heat treatment atmosphere and duration, solution composition, and seeding layer.[271,272,273,274,275,276,277,278,279]

It should be mentioned that although the sol-gel technique is studied and successfully used for many years, it still has some significant drawbacks. One of them is

the formation of cracks during the drying process of a sol-gel film. As the solvent evaporates from the film, its volume decreases and the film shrinks, which results in biaxial tensile stress relieved by developing cracks.[280,281] Delamination of the film due to the difference in thermal expansion coefficient between a film and a bottom electrode is one more unresolved problem.[281] Among other limitations of this technique are poor step coverage and residual organic impurities in the films.[282]

In the case of perovskite-type ferroelectrics, such as PZT, one of the major drawbacks of the sol-gel technique is that it does not yield the desired perovskite phase directly. The formation of perovskite phase upon final annealing is preceded by the undesirable nonferroelectric pyrochlore phase. It was found that distribution of the nearest neighbor and next nearest neighbor ions in the pyrochlore phase is similar to those in the amorphous phase.[271] Therefore, although perovskite is the thermodynamically stable phase in the temperature range used in sol-gel fabrication, the transformation from amorphous to pyrochlore phase is kinetically more favorable than a straight transformation to the perovskite phase.

3.3.2 Deposition of ferroelectric films by hydrothermal method

In hydrothermal technique, chemical reactions in aqueous solutions are used to synthesize ferroelectric materials in both powder [283,284,285,286,287,288,289,290,291,292,293,294] and thin film form [295, 296, 297, 298, 299, 300, 301, 302, 303, 304, 305, 306] The main advantage of the hydrothermal technique is low synthesis temperature (typically 100-200°C) and environmentally friendly processing conditions. Due to the low process temperature, such problems as cracking due to residual thermal stresses and interdiffusion and chemical reaction between the film and the substrate are suppressed. Other advantages of this

technique are automatically aligned polarization, possibility of deposition on non-flat surfaces and preparation of very thick films (up to tens of microns) at a relatively low cost. A drawback of this technique is that monitoring of the growth process is impossible and concentrations of precursors are not controlled during the synthesis. It should be mentioned, however, that Ohba et al.[307] designed a continuous-supply autoclave system, which allowed them to control the chemical composition of the solution during the reaction phase.

3.3.3 Deposition of ferroelectric films by sputtering

The sputtering technique is widely used for the deposition of ferroelectric thin films [308,309,310,311,312,313,314,315,316,317,318,319,320,321,322] for its relatively simple fabrication processes, compatibility with standard device fabrication technology, high deposition rates, uniformity of film thickness and composition over a large area, and low concentration of residual impurities. As for the disadvantages, we should mention poor step coverage and somewhat inferior quality as well as the difficulty in composition control of compounds containing volatile elements, such as Pb and Bi. To compensate for the Pb or Bi loss, targets with excess Pb or Bi content or multiple targets are typically used.[318,323,324,325,326] Depending on the type of targets, two types of sputtering methods – dc and rf sputtering – can be applied for ferroelectric film deposition. When an insulating ceramic target is used as a source of material, rf magnetron sputtering is employed. The dc sputtering is utilized for deposition from metallic (conductive) targets. The growth is typically carried out in the deposition chamber with a mixed O_2 + Ar atmosphere. O_2 acts as the reactive gas and Ar serves to enhance sputtering from the target. To grow doped

films, an appropriate dopant element is added during the target preparation. Structural and ferroelectric properties, growth rate, phase composition, and stoichiometry of the grown films depend on a number of sputtering parameters, among which are substrate temperature,[318,319] gas pressure and composition,[315,317,320,321,322] sputter power,[317,322] target-to-substrate distance, and target composition.[314]

3.3.4 Pulsed laser deposition of ferroelectric films

PLD has been regarded as one of the most suitable methods for most oxide thin film growth. It is widely used for ferroelectric film growth.[327,328,329,330,331,332,333,334,335,336,337,338,339,340] Physical processes in PLD are very complex and interrelated, and depend on the laser pulse parameters and the properties of the target material. As in the case of sputtering, PLD uses composite ceramic targets as source material for growth. Unlike sputtering, however, short and intense laser (generally excimer) pulses are used to evaporate and ablate the target material. An intense laser stream passes through an optical window of a vacuum deposition chamber and is focused onto a target where it is partially absorbed. As a result, a supersonic jet of plume is generated and directed normal to the target surface. The plume expands away from the target with a strong forward directed velocity distribution of different particles. Significant material removal in the form of a plume occurs above a certain power density. The threshold power density needed to produce such a plume depends on the target material, its morphology, and the laser pulse wavelength and duration. Material from the plume is then re-condensed on the substrate, where the film growth occurs. As in the case of sputtering, targets with excess Pb or Bi content are typically used to compensate for

the loss of the volatile components (Pb or Bi) during growth.[330,334,335] The growth process may be supplemented by a passive or reactive gas or ion source, which may affect the ablation plume species in the gas phase or the surface reaction, which is referred to as reactive PLD.

Laser ablation for thin film growth has many advantages compared to other methods. In particular, the energy source (laser) is outside the deposition chamber which allows much greater flexibility in materials used and geometrical arrangements; almost any kind of condensed matter material can be ablated; film growth rates may be controlled to any desired value because of the pulsed nature of the laser beam; the evaporating source material is localized only where the laser beam is incident; under optimal conditions the ratios of the elemental components of the bulk and film are the same regardless of the chemical complexity of the systems. At the same time, PLD also has some drawbacks: production of macroscopic particles during the ablation process, defects caused in the growing film through bombardment by high kinetic energy particles, and inhomogeneous flux and angular energy distributions within the ablation plume, which makes this technique not easily adaptable to for large-area substrates and hence for industrial production.

Numerous deposition parameters - ambient gas pressure, substrate type and temperature, substrate-to-target distance and target-substrate geometry, target composition, laser spot size, fluence, wavelength, repetition rate - have a pronounced effect on the deposition rate, stoichiometry, phase composition, and crystalline quality of ferroelectric films.[327,333,334,336,337,338,339,340]

3.3.5 Metal-organic chemical vapor deposition of ferroelectric films

MOCVD is a well-established method based on decomposition of gaseous precursors on a hot substrate to form a film of desired composition. MOCVD is one of the most promising methods for FeRAM applications because of its high deposition rate, high crystal quality of the films, good step coverage and conformal deposition on three-dimensional surfaces, uniformity of film composition and thickness over a large area, and compatibility with semiconductor technologies. In addition, reevaporation of highly volatile elements, such as Pb and Bi, which are constituents of some ferroelectric materials (PZT, SBT, BIT), can be prevented owing to the relatively high gas pressure. Film composition can be easily controlled by varying the molar ratio of the precursors fed into the growth chamber. One of the key advantages of MOCVD growth of ferroelectric films for FeRAM applications is the possibility to decrease the growth temperature down to 370-570 °C,[327, 341 , 342 , 343 , 344 , 345 , 346 , 347 , 348 , 349 , 350] which is essential to prevent interdiffusion between ferroelectric thin films and electrodes. For example, SBT and PZT films having good ferroelectricity were obtained at 415 and 570 °C, respectively.[344] The possibility to decrease the growth temperature has been achieved due to a pulsed MOCVD process, wherein short growth periods are interspersed with intervals of no precursor supply.[327,344,345,346,349] This effect was explained by the acceleration of decomposition of source gases and migration of adsorbed species as well as by reevaporation of the excess Pb and Bi from the surface during the interval time. In the case of PZT growth, it has been also demonstrated that $PbTiO_3$ seeds are very useful not only to improve the PZT crystal quality and surface morphology, but also to decrease the epitaxial growth temperature.[343,345,347] The films grown on $PbTiO_3$, which has a structure

similar to that of perovskite PZT and the relatively small lattice mismatch, exhibit better crystallinity even at lower substrate temperatures due to the templating effect. Various aspects of MOCVD growth of ferroelectric films, including consideration of reactors and precursors, are reviewed in details in Refs. [266,327,351,352,353,354,355]

3.3.6 Molecular beam epitaxy of ferroelectric films

MBE played a pivotal role in epitaxial growth of various compound semiconductors such as SiGe, III-V, and II-VI compound due to its precise control over growth parameters and composition of grown films. However, the growth of oxides by MBE is a very difficult task, because of oxidation of materials in effusion cells, which necessitates use of oxygen tolerant materials for MBE component fabrication such as effusion cells and substrate heater. Therefore, MBE has not yet been widely applied to the growth of ferroelectric oxides unlike the other growth techniques discussed earlier. In spite of the foregoing shortcomings, there have been some reports on epitaxial growth of ferroelectric oxides using MBE including $LiNbO_3$,[356,357] $LiTaO_3$,[358] $BaTiO_3$,[359,360,361,362] (Ba, Sr)TiO_3, [363],[364] $Bi_4Ti_3O_{12}$,[365,366] and $PbTiO_3$.[367,368,369] Very recently the growth of high quality PZT films on $SrTiO_3$ substrates has been reported.[370,371]

In conclusion, it should be mentioned that structural, piezoelectric, dielectric, and ferroelectric properties as well as fatigue, retention, and imprint characteristics of ferroelectric thin films can differ substantially from those of bulk ceramic samples.[372,373,374,375,376,377,378] The growth method applied and a myriad of growth parameters determine stoichiometry, phase composition, and crystalline quality of the

layers, and, therefore, have a strong influence on their ferroelectric characteristics. Domain/grain structure, crystallographic orientation, defects, strain, substrate clamping effect, film thickness, film/substrate interface, and composition are critically important factors affecting the film properties. More detailed discussion of the factors affecting ferroelectric thin film characteristics can be found in reviews [327,379,380,381] and references therein.

3.4 Applications of ferroelectric oxides

Ferroelectrics are of great interest for a wide range of applications. Pyroelectric properties of ferroelectric thin films are used for high sensitivity IR detectors. Piezoelectric thin films have also been integrated into MEMS devices such as micro-scale accelerometers, displacement transducers, and actuators. Excellent piezoelectric properties of perovskite oxides can be exploited in SAW devices used as filters, phase shifters, and phase delay lines. Currently, typical piezoelectric materials for SAW filters are single-crystal $LiNbO_3$, $LiTaO_3$, AlN, and ZnO, which have SAW phase velocities in the range of 2500–6000 m/s and resulting device central frequencies are in the GHz range. Reports on SAW properties or devices made of perovskite ferroelectric thin films are relatively few in number,[382,383,384,385] although PZT at its morphotropic phase boundary may exhibit a high electromechanical coupling coefficient. As for sensors, it should be noted that most of them operate in complex environments, where various parameters such as temperature, pressure, humidity, radiation, gas concentration, and so on, change simultaneously. In this vein, novel sensor designs capable of providing the same output and/or linear characteristics as functions of a variety of environmental perturbations, i.e.

multifunctional sensors, are in high demand. So far, only a limited number of reports are available on humidity and temperature sensors.[386,387,388] For example, thick films of $Ba_{1-x}Sr_xTiO_3$ exhibit a change in the dielectric constant in response to temperature variations, while the electrical conductivity of $Ba_{1-x}Sr_xTiO_3$ is a function of humidity. Hence, the temperature and humidity can be simultaneously detected by measuring the film capacitance and the film resistance, respectively, without incurring crosstalk. The response times of the thick-film sensors to humidity and temperature are 30 seconds and 60 seconds, respectively. [387]

Progress has been made also in the application of ferroelectric thin films in the field of high-frequency devices and optical switches for integrated optical systems. Today, $LiNbO_3$ single crystals are the most widely used electro-optic material for telecommunication devices. However, $LiNbO_3$ has some drawbacks, such as low electro-optic effect and strong temperature dependence. Perovskite oxides $(Pb,La)(Zr,Ti)O_3$ (PLZT) and $Pb(Mg_{1/3}Nb_{2/3})O_3$-$PbTiO_3$ (PMN-PT) feature high electro-optic effect, good transparency, ruggedness, and low cost,[389] which makes them good candidates for electro-optic devices. [390, 391, 392] Such materials as $Pb(Zr,Ti)O_3$,[393],[394] $Sr_{1-x}Ba_xNb_2O_6$ (SBN),[395, 396] and $BaTiO_3$[397] also can be used for electro-optic applications. For example, using spectroscopic ellipsometry Kang et al.[393] observed a large linear electro-optic effect in PZT films grown epitaxially on Nb-doped $SrTiO_3$(001) substrates by RF magnetron sputtering. However, the relative degree of activities in those fields has not been as extensive as those in the case of ferroelectric applications.

Ferroelectric oxides have been extensively studied also for tunable microwave passive components, such as resonators, filters, and phase shifters. Among ferroelectric

materials, BST is the most promising candidate as a medium for tunable microwave passive components due to its large dielectric tunability, i.e., the large change in dielectric constant with applied voltage, and low dielectric loss at microwave frequencies.[221,398] The relative tunability n is defined as the relative change of the permittivity between zero bias and bias in a field E with respect to the zero-bias value:[221]

$$n = \frac{\varepsilon(0) - \varepsilon(E)}{\varepsilon(0)} . \qquad \text{Equation 5}$$

The loss tangent, tan δ, is given by the ratio of the imaginary ε'' and real ε' parts of the permittivity:

$$\tan\delta(E) = \frac{\varepsilon''(E)}{\varepsilon'(E)} . \qquad \text{Equation 6}$$

Both the tunability and the dielectric constant peak near the ferroelectric Curie temperature. The composition dependence of T_C (see Figure 12) makes possible for one to tailor the dielectric properties of BST by tuning its composition. Unfortunately, the dielectric-loss tangent is also large just below the Curie temperature. Therefore, a tradeoff between a high dielectric tunability and large dielectric loss tangent is required.

Most of studies aimed at microwave applications of BST are focused on thin films because of their low cost, low leakage current, and possibile integration with standard semiconductor technologies (see Ref. 221 and references therein). As compared to the bulk material, strain in BST thin films is an additional factor affecting the Curie temperature and the dielectric properties. [399,400,401,402] Therefore, tailoring the strain provides an alternative approach (referred to as strain engineering) to varying the barium-to-strontium ratio. Compressive or tensile strain in BST films was found to shift the Curie

temperature, thus affecting the dielectric constant and tunability values.[399,400] Thermal stability of the dielectric properties is another critical characteristic of a material for tunable microwave devices. The permittivity of BST is very sensitive to temperature near the ferroelectric transition temperature, which is a potential drawback from the standpoint of device applications, because the strong temperature dependence of ε leads to the change in device characteristics as the temperature changes. As a solution of this problem, compositionally graded BST films have been proposed. [403,404,405,406] A compositionally graded film is composed of several layers with different compositions and thus different ferroelectric transition temperatures. Such compositionally graded films have been shown to have weak temperature dependence and high permittivity and tunability.[403,404,405,406] It should be mentioned that a weak temperature dependence of permittivity was also observed for BST films under compressive strain.[399,400]

As mentioned already, the increased interest in ferroelectric oxides stems also from the fact they are considered to be good candidates for non-volatile FeRAM devices. Various perovskite-structure materials as $SrBi_2Ta_2O_9$ (SBT), $Ba_xSr_{1-x}TiO_3$ (BST), $Bi_4Ti_3O_{12}$ (BIT), $Bi_{4-x}La_xTi_3O_{12}$ (BLT), $BaMgF_4$, $Pb_5Ge_3O_{11}$, and $Pb(Zr,Ti)O_3$ (PZT) have been considered as candidates for FeRAM, among which SBT and PZT are considered to be most suitable materials for FeRAM development. PZT exhibits superior ferroelectric properties such as higher dielectric constants, lower coercive field, and higher Curie temperature as compared to BST. However, PZT suffers from the fatigue problem which proved to be somewhat intractable, at least up to now. Typically, Pt/PZT/PT capacitors lose more than 50% of their polarization after 10^9-10^{10} cycles which is not acceptable for IC technology while a fatigue lifetime more that 10^{14} cycles is

considered acceptable for commercial applications. Fatigue properties associated with PZT have been improved significantly by using conductive oxide electrodes,[407,408,409,410,411,412] albeit further improvements are still called for.

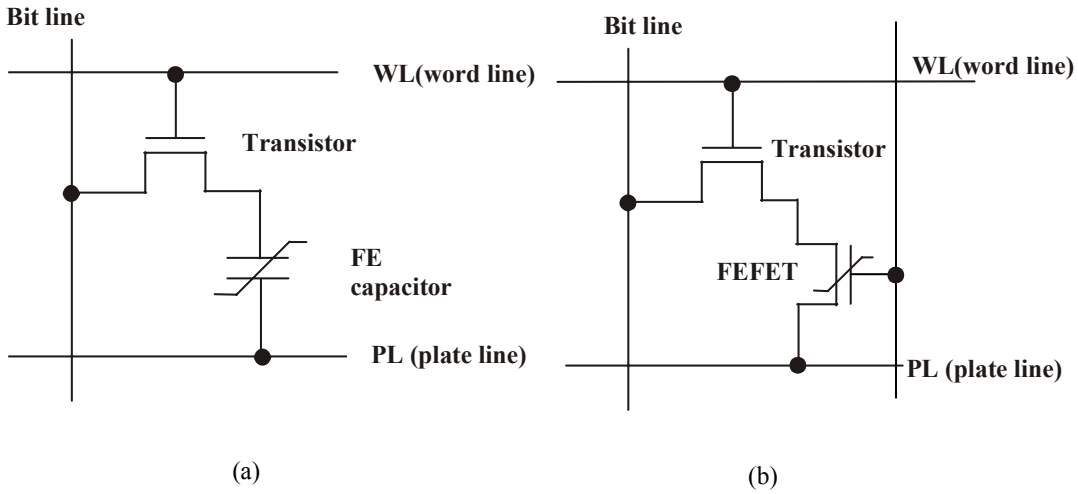

Figure 19 Circuit configuration of ferroelectric random access memories. (a) capacitor type (destructive readout type) and (b) MFSFET type (nondestructive readout type).

There are two types of memory cell structures in FeRAMs. A cell of the first type consists of a transistor (MOSFET) and a ferroelectric capacitor (1T/1C structure), as shown in Figure 19a. A memory cell of the second type includes one transistor and a metal-ferroelectric-semiconductor field effect transistor (MFSFET, or FeFET) instead of the ferroelectric capacitor (Figure 19b). FeFET is essentially a conventional FET with a gate dielectric replaced by a thin ferroelectric layer. In this device, the channel conductance is regulated by the polarization state of the ferroelectric, so that when "0" or "1" data are written in the ferroelectric film as the direction of polarization, they can be read as a difference of the drain current of the FET and does not require switching of the

polarization in order to read the memory cell. This feature is called non-destructive readout.

The structure of the capacitor-type cell shown in Figure 19a is essentially the same as that of DRAM, except for a plate line. In the "write" operation, the polarity of the ferroelectric capacitor is directed either upward or downward by applying a positive or negative voltage pulse between the bit and plate lines and by switching-on the FET in the cell. While in the "read" operation, a voltage pulse to align the polarization upward, for example, is given to a selected cell and the response current of the capacitor is measured. In this operation, if the initial polarization of the ferroelectric film is downward, the polarity reversal current flows as well as the usual displacement current. Since the stored data are destroyed through this operation, it is necessary to rewrite the data after each "read" operation. The fabrication process of this type of FeRAM is, however, easier than that of the FET-type FeRAM, and all products so far commercialized belong to this type. At present, a prototype FeRAM device with a capacity of 128 Mbits has been recently presented by Toshiba.[413] Thorough discussion on current status and future perspectives of nonvolatile ferroelectric memory can be found in Refs. 379,351,414,415,416,417.

More detailed considerations of ferroelectric materials can be found in several excellent reviews.[207,249,379,380 ,418,419,420,421] Shaw et al. [418] reviewed the size effects in ferroelectric materials. Technology of ferroelectric ceramics has been the topic of discussion by Haertling.[419] Reports by Ishwara[420] and Scott[421] are devoted to problems in ferroelectric FET memory developments. Setter et al.[379] extensively discussed properties and applications of ferroelectric thin films. Review by Izyumskaya et al.[380] encompasses

film growth technology, characterization, processing, and device fabrication with regard to $Pb(Zr,Ti)O_3$, while the treatise by Maeder et al.[249] is devoted to Pb-free piezoelectric materials.

4 Magnetic Oxides

For practical device applications, magnetic materials obviously should exhibit a Curie point above room temperature. A variety of oxides, including mixed-valence manganites, diluted magnetic oxides, spinels,[422] ferrites,[11] and double perovskites[423] have been studied for high Curie temperature ferromagnetism. In this section, we will focus on diluted magnetic oxides and mixed-valence manganese oxides of the general formula $Re_{1-x}A_xMnO_3$ (Re = trivalent rare earth element, A = divalent alkaline earth element), which are considered as magnetic materials for potential spintronic and magnetic memory applications.

4.1 Diluted magnetic oxides

Diluted magnetic oxides (DMOs) are transparent, wide-band-gap materials in which a small fraction of the host cations is substituted with magnetic ions.

Transition metals (TM) with partially filled *d* states (Sc, Ti, V, Cr, Mn, Fe, Co, Ni as well as Cu which has a completely filled *d* shell, but acts as magnetic impurity when in Cu^{2+} charge state) and rare earth elements with partially filled *f* states (Eu, Gd, Er) can be used as magnetic ions in DMOs. The concept is expanded to include diluted magnetic semiconductors (DMS), such as (Ga,Mn)As and TM-doped GaN, ZnSe, ZnS, ZnTe, CdTe, CdSe, CdS. These materials have attracted considerable attention due to their

potential spintronic applications, where the spin of carriers is exploited along with their charge. For practical applications in spintronics devices, the DMO materials must exhibit a Curie temperature above room temperature, which is naturally deemed to be the bottleneck issue.

4.1.1 Experimental findings

Intensive search for diluted magnetic semiconductors, including dilute magnetic oxides, showing room-temperature or above ferromagnetism started after 2000, when Dietl *et al.*[22] and Sato and Katayama-Yoshida[23] predicted theoretically that ZnO could exhibit ferromagnetism above room temperature upon doping with transition elements such as Mn, V, Cr, Fe, Co and Ni. In 2001, Matsumoto *et al.* [24,424] reported on the discovery of ferromagnetism in the Co-doped anatase TiO_2 thin films. Later, high-temperature ferromagnetism was observed for various oxides, including TiO_2 doped with Co,[24,425,426,427] Fe,[426,428,429] V,[426,430] Cr,[426,431] Ni,[426,432] Mn,[433] and Cu;[434] ZnO doped with Cr,[435,436,437] V,[438,439,440] Mn,[441,442,443,444] Co,[440,442,444,445,446] Ni,[440,447,448] Ti,[440] Fe,[440,449] Sc,[440] Cu,[450,451] and Fe+Cu;[452] SnO_2 doped with Co,[453,454] Fe,[454,455,456] Cr,[454,457] Ni,[435,454,458] Mn,[454] and V ;[459] In_2O_3 doped with Ni,[460] Cr,[461] Fe+Mn,[462] Fe+Cu,[463,464,465,466,467] and Fe+Cr;[468] $(In,Sn)_2O_3$ (ITO) doped with Mn,[469] Cr,[470] Ni,[460] and Cu+Fe;[463] CeO_2 doped with Co;[471] and surprisingly in oxides doped with non-magnetic impurities, such as C-doped ZnO[472] as well as in undoped HfO_2,[473,474,475] TiO_2,[475,476,477] and In_2O_3.[475] Table 3 lists magnetic and transport properties of various DMOs.

Despite the large number of studies in this field, the origin of ferromagnetism in DMOs still remains somewhat unclear. First of all, observed magnetic properties could in fact be due to, at least in some cases, the formation of metallic clusters (Fe, Co, Mn) or

magnetic secondary phases and precipitates, such as CoO, Co_3O_4, CuO, FeO, Fe_3O_4, (Zn, Fe)$_3O_4$, MnO, MnO_2, Mn_2O_3, in the DMO matrix. [478],[479],[480],[481],[482] Moreover, trace amounts of magnetic contamination coming from stainless steel tools, such as tweezers and substrate holders, also can provide a sufficiently large signal detectible by superconducting quantum interference devices (SQUIDs) and magnetometers. [483],[484],[485],[486],[487] For example, Abraham et al.[486] reported that they observed ferromagnetism only in HfO_2 samples handled with stainless steel tweezers; therefore, ferromagnetism in this oxide is not intrinsic, but is related to sample contamination. It should be also noted that DMOs frequently exhibit ferromagnetic properties when prepared in the form of poor-crystalized thin films or nanoparticles, while their bulk counterparts or well-crystallized films usually show no evidence of ferromagnetism. [488],[489],[490],[491],[492] In addition, reported properties of DMOs depend strongly on the preparation technique and growth conditions, and they significantly vary from research group to group, which makes the interpretation of experimental data extremely complicated.

4.1.2 The origin of ferromagnetism in DMOs

The mechanism of intrinsic ferromagnetic in DMOs is a matter of debate.[22,23,493,494] Early attempts to explain the magnetic behavior of DMSs are based on carrier-mediated mechanisms implying that moments of magnetic ions are coupled via double-exchange and Ruderman-Kittel-Kasuya-Yoshida (RKKY) type interactions.[22,23,495] In the double exchange mechanism originally proposed by Zener, [496,497] magnetic ions in different charge states couple ferromagnetically by virtual hopping of an 'extra' electron from one ion to the other through interaction with *p*-orbitals. In

Section 4.2.1, we will consider the double-exchange mechanism in more details. The main idea behind the RKKY interaction is the exchange coupling between magnetic ions and free electrons. An electron is magnetized in the vicinity of a magnetic ion, with the polarization decaying with distance from the magnetic ion in an oscillatory fashion. This oscillation causes an indirect superexchange interaction (RKKY interaction) between the two magnetic ions on the nearest or the next nearest magnetic neighbor sites. This coupling may result in a parallel (ferromagnetic) or an anti-parallel (antiferromagnetic) setting of the moments depending on the separation between the interacting atoms. The mean-field Zener model proposed by Dietl *et al*.[22] is based on the original model of Zener and the RKKY interaction. As compared to the RKKY interaction, the mean-field Zener model takes into account the anisotropy of the carrier-mediated exchange interaction associated with the spin-orbit coupling in the host material. In the process, it reveals the important effect of the spin-orbit coupling in the valence band in determining the magnitude of the T_C and the direction of the easy axis in *p*-type ferromagnetic semiconductors. Based on this model, it was predicted that TM-doped *p*-type ZnO is one of the most promising candidates for ferromagnetic DMS with a high Curie temperature.[22] However, this prediction has been made assuming hole concentrations of above 10^{20} cm^{-3}, which in fact may never be attainable. Based on first principles calculations of the electronic structures of TM-doped ZnO, Sato and Katayama-Yoshida[23,495] have suggested that the ferromagnetism in DMSs is a consequence of a competition between the ferromagnetic double-exchange interaction and the anti-ferromagnetic super-exchange interactions, and the magnetic properties of DMS materials can be controlled by changing the carrier (electrons or holes) density.

The mechanisms based on carrier-mediated interactions, such as RKKY and double-exchange, however, require high concentrations of free carriers, electrons or holes, which is not always the case in DMOs. In addition, ferromagnetic order in the oxides doped with only a few percents of TM is hard to explain in terms of superexchange or double exchange interaction, since the fraction of TM ions are far below the percolation threshold, x_p, associated with nearest-neighbour cation coupling. The value of x_p is ~2/Z, where Z is the cation coordination number. For oxides, Z = 6 or 8, thus x_p is typically 25-30%.[498] Coey *et al.*[493] have developed a theoretical model which is applicable to low-doped (few percent) and insulating DMOs. The model suggests that ferromagnetic exchange in TM-doped oxides is mediated by localized donor electrons in the impurity band, which couple with 3*d* moments of TM ions to form bound magnetic polarons (BMPs).[499,500] An electron associated with a donor defect (oxygen vacancy for example) is confined in a hydrogenic orbital of radius $r_H = \varepsilon(m/m^*)a_0$, where ε is the high-frequency dielectric constant, m is the electron mass, m^* is the effective mass of the donor electrons, and a_0 is the Bohr radius. As the defect concentration increases, the 1*s* orbitals overlap to form an impurity band. The hydrogenic electrons associated with defects interact with TM ions within their orbits and align dopant spins, which results in ferromagnetic exchange coupling between the ions, as illustrated in Figure 20.[493] As the defect density increases, the hydrogenic orbitals overlap, and, as the polaron percolation threshold is reached, the material becomes ferromagnetic. High Curie temperatures were explained by hybridization and charge transfer from a donor-derived impurity band to unoccupied 3d states of TM ions at the Fermi level.[493]

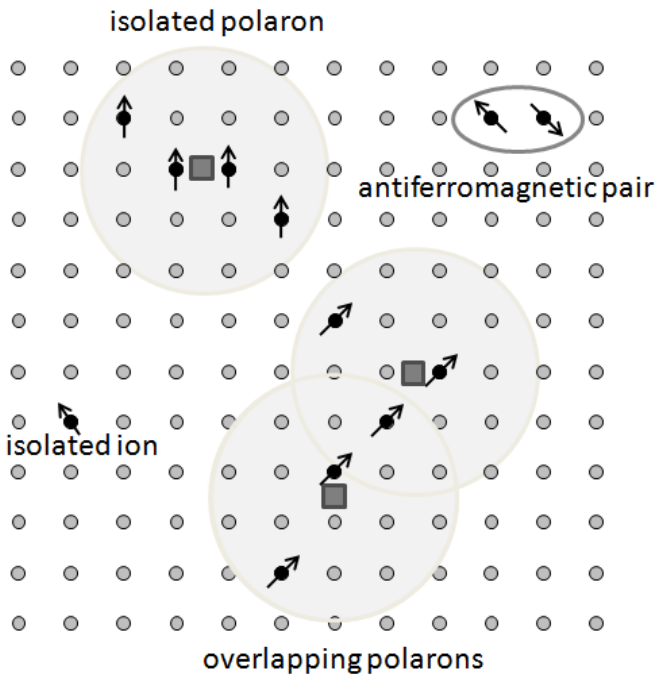

Figure 20 Magnetic polarons in DMO. Small circles represent cation sites; small black circles, TM ions; and squares, oxygen vacancies. Oxygen sites are not shown. A donor electron in its hydrogenic orbit (large circles) couples with its spin antiparallel to impurities with a 3*d* shell that is half-full or more than half-full. After Coey *et al.* [493]

As mentioned above, ferromagnetism was observed also in some oxides containing no impurity ions with partially filled *d* or *f* shells. [434,440,472,473,474,475,476,477] The origin of this phenomenon, which has received the name d^0 ferromagnetism,[501] is most likely related to lattice defects,[473,501, 502] leaving aside the possibility of sample contamination.[483,484,485,486,487] To account for the mysterious d^0 ferromagnetism, Coey *et al.*[498,503,504] have developed a general model of charge-transfer ferromagnetism, which explains also the ferromagnetic behavior of TM-doped DMOs. The model suggests that the ferromagnetic order in MDOs is not due to the spins of 3*d* dopant electrons, but is related to itinerant electrons associated with structural defects (point or planar defects distributed throughout a film or defects at surfaces and interfaces). These defects create

states in the band gap to form an impurity band, which need not even be occupied, but must be close to the Fermi level. The density of states in the tight-binding model depends on the number of nearest neighbors. This number is reduced at the surface or in the vicinity of defects, resulting in the increase of the local density of states associated with them, leading to some sort of structure of the density of states, as shown in Figure 21, which illustrates schematically the charge-transfer model.[503] Another essential feature of this model is the presence of an electron reservoir, from which electrons can be transferred to the defect states. Ions coexisting in different valence states could serve as such a reservoir. If the density of states is sufficiently large, spontaneous Stoner spin splitting of the impurity band may occur.[501] Generally, the Fermi level does not coincide with a sharp maximum in the density of states. However, electron transfer from the reservoir to the defect states could raise the Fermi level up to the point where the spontaneous Stoner splitting of the impurity band occurs, provided that the energy gain from spin splitting exceeds the energy cost of the charge transfer, and spontaneous ferromagnetic order of the defect-related electrons appears (see Figure 21). In TM-doped oxides, the charge transfer in doped oxides can be produced by mixed-valence TM ions. Note that in this model the enabling feature of the TM ions is not that they carry a magnetic moment, but it is their ability to feed electrons into the local density of states (or to accept charge from it) that explains the dopant cation's ability to promote ferromagnetism. This general theory is able to explain a wide range of experimental observations, but needs solid experimental proof.

.

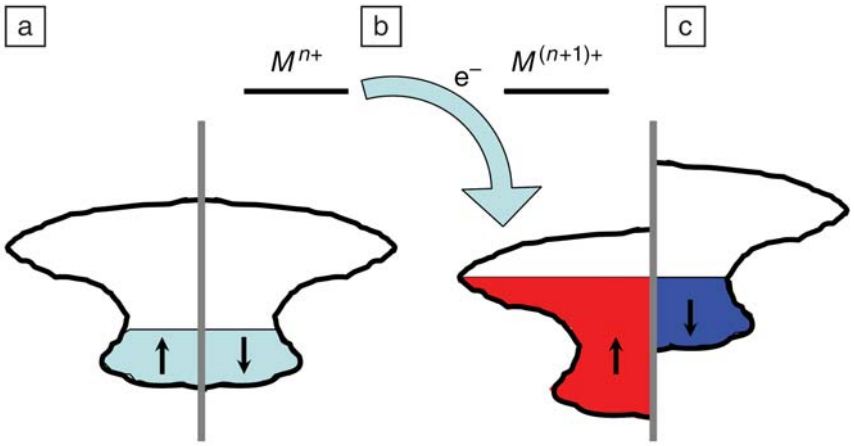

Figure 21 Charge-transfer ferromagnetism. (a) A defect-related density of states is (b) linked to an electron reservoir. (c) By electron transfer to or from the defects, the Fermi level can be shifted to a position where spontaneous ferromagnetic splitting of the defectrelated density of states occurs. Reprinted with permission Ref. 503.

Up to now, there is no decisive evidence in support of one or another mechanism responsible for ferromagnetic order in DMOs. Numerous theoretical[434,476,502,504,505,506,507] and experimental [433, 434,435, 445,474,491, 508,509,510,511,512, 513,514,515, 516,517] data indicate that ferromagnetism in DMOs is associated with structural defects. For example, Liu *et al.*[514] observed the increase of magnetization of Co-doped ZnO films upon annealing in vacuum, which is known to result in the creation of oxygen vacancies. Annealing in air, which caused oxygen to diffuse into the film thus decreasing concentration of oxygen vacancies, was found to decrease the magnetization value.[514] Applying annealing in different oxidation atmospheres and in the presence or absence of Zn vapor, Khare et al.[513] have demonstrated that Zn interstitials play a crucial role in the origin of ferromagnetism of Co-doped ZnO films. They also have found that magnetization of the films is not correlated with free-carrier concentration, which supports the bound polaron

model.[513] In addition, several groups have reported that there is no correlation between the carrier concentration and ferromagnetism in DMOs.[433,445,513,517] On the other hand, there are experimental results[438 ,518,519,520,521] indicating that the increase in free carrier concentration favors ferromagnetic ordering in DMO, which speaks in favor of the carrier-mediated exchange mechanisms.

Summarizing, it is obvious that much remains to be done both experimentally and theoretically to reveal the origin of ferromagnetism in DMOs. It is still not sufficiently clear what is responsible for the observed magnetic hysteresis in magnetization measurements: uniformly doped hosts, secondary phases, magnetic contaminations, or lattice defects. To make conclusive judgment about the intrinsic nature of ferromagnetism revealed by SQUID measurements, optical and magneto-transport techniques sensitive to ferromagnetic order of the semiconductor matrix should be used. Magneto-optic spectroscopy, which probes the magnetooptical signal as a function of photon energy, can be used to verify the intrinsic nature of ferromagnetism in DMOs. The magneto-optical effect in DMOs is directly related to the interaction between the *d*-electrons of the TM ions and the *s,p* electrons of the host semiconductor. Magneto-optic spectroscopy is particularly useful for thin film studies because the effect of substrate on the spectrum is negligible contrary to magnetization measurement. Recently, intrinsic room-temperature ferromagnetism has been confirmed by magneto-optic measurements in highly conductive ($n \sim 10^{20}$ cm^{-3}) ZnO films doped with Ti, Co, and V, while the ferromagnetic order in semiconducting (Zn,Mn)O samples was found to be of extrinsic origin.[522] The authors claim that the observed strong *s-d* exchange interaction points to the presence of carrier-mediated exchange which is very desirable for spintronics devices.

Later, the same group[523] has reported the observations of intrinsic ferromagnetism in semi-insulating ZnO samples doped with Mn and Co, which likely supports the model of magnetic polarons developed by Coey *et al.*[493]

As for theoretic studies, the results from different theoretical approaches do not agree well with experimental data. Most likely, no single model is capable of explaining the properties of a wide class of TM-doped DMOs. As an example, Behan *et al.*[523] have demonstrated that two mechanisms – bound magnetic polarons and carrier-mediated exchange – can be operative in ZnO, depending on the density of charge carriers.

Table 3 magnetic and transport properties of various magnetic oxides.

Oxide	**Dopant**	**Dopant concentration**	**T_C (K)**	**Magnetization**	**Resistivity or carrier concentration**	**Reference**
ZnO	Mn	2% Mn+1%Al	>300	4.36 μ_B /Mn	6.3×10^{20} cm^{-3} n-type	442
	Cr	1.1	>395	~0.7 μ_B /Cr		436
	V	15	>350	0.5 μ_B /V	$1x10^{18}$ cm^{-3} n-type	438
	Co	~2	>300	5.9 μ_B /Co	≥200 Ω cm	446
	Co	4	790	6.1 μ_B /Co		445
	Ni	1	>300	0.37 μ_B /Ni	10^{17} - 6×10^{18} cm^{-3} n-type	448
	Ti	5	>300	0.5 μ_B /Ti		440
	Fe	4	400	0.15 μ_B /Fe		449
	Cu	2	350	1.8 μ_B /Cu	10^{18} cm^{-3} n-type	450
	Fe+Cu	5%Fe+1%Cu	550	0.75 μ_B /Fe	4.2×10^{17} cm^{-3} 0.1 Ω cm n-type	452
	C	~1	>400	2.0-3.0 μ_B /C	2.1×10^{18} cm^{-3} 0.195 Ω cm n-type	472

TiO_2	Co	1	~700	~1.4 μ_B /Co	~2.8×10^{18} cm^{-3} n-type	425
	Cr	8	400-700	~0.5 μ_B /Cr	1.5×10^{19} cm^{-3} n-type	431
	Cr	5	>400	~2.6 μ_B /Cr		426
	V	4	>400	4.23 μ_B /V		426
	Ni		>400	~2.9 μ_B /Ni		426
	Fe	2	300	2.4 μ_B /Fe	~10^{22} cm^{-3} 0.0015 Ω cm p-type	428
In_2O_3	Ni	5	>300	0.03–0.06 μ_B /Ni	~2 Ω cm	460
	Cr	2	850–930	1.5 μ_B /Cr	3×10^{20} cm^{-3} n-type	461
	Fe+Mn	Fe0.1−xMnx 0<x<0.1	>300	0.35 μ_B / _Fe+Mn_		462
	Fe+Cu	20% Fe+2%Cu	750	1.45 μ_B /Fe	~6×10^{-3} Ω cm n-type	466,467
	Fe+Cu	15%Fe+ 5%Cu	>300	0.502 μ_B/Fe	3.99×10^{18} cm^{-3} n-type	463
	Fe	15	>300	0.838 μ_B/Fe	3.60×10^{18} cm^{-3} n-type	463
	Fe+Cr	10%Fe+10%Cr	>300	0.35 emug/g	62 Ω cm	468
$(In,Sn)_2O_3$	Ni	5	>300	0.03–0.06 μB /Ni	~2×10^{-2} Ω cm	460
	Mn	5	>300	0.8 μ_B/Mn	~2.5×10^{19} cm^{-3} n-type	469
	Fe	15	>300	0.291 μ_B/Fe	2.38×10^{19} cm^{-3} n-type	463
	Fe+Cu	15%Fe+ 5%Cu	>300	0.132 μ_B/Fe	7.35×10^{19} cm^{-3} n-type	463
SnO_2	Co	5	650	7.5 μ_B/Co	~4.45×10^{18} cm^{-3} 0.4 Ω cm n-type	453
	Fe	5	610	1.8 μ_B/Fe	n-type	455
	Cr	5	>400	6 μ_B/Cr		457
	V	~7	~400	3 μ_B/V		459
CeO_2	Co	3	740–875	8.2 μ_B/Co	n-type	471
HfO_2	undoped	0	>500	~0.15 μ_B/ HfO_2 formula unit	n-type	473
TiO_2	undoped	0	600 (Ne´el	~0.15 μ_B/Ti	~3×10^{17} cm^{-3} n-type	476,477

			transition at 880K)			

4.2 Mixed-Valence Manganites

Before we commence discussing properties of mixed-valence manganites, let us introduce a term of magnetoresistence (MR) and consider types of MR existing in nature. A simple definition of MR is a change of electrical resistance of a material when exposed to an applied magnetic field. There are several different types of magnetoresistance depending on the underlying physical mechanisms.

Conventional (ordinary) magnetoresistance is a change of electrical resistance of a material under applied magnetic field. Ordinary magnetoresistance arises from the field dependence of the mean-free path of charge carriers. This effect is measurable only in metals with a large mean free path in zero magnetic field, where an applied magnetic field reduces the mean free path by inducing the electrons to move in orbits. Even then, the change in resistivity is usually limited to a few percent in best samples tested in practical magnetic fields.

Colossal magnetoresistance (CMR)[16,17,524] is a huge (orders of magnitude) change of electrical resistivity of a material under an applied magnetic field, which is observed mostly in manganese-based perovskite oxides near the Curie temperature in high magnetic fields. Due to the CMR effect resulting from a unique type of a metal–insulator transition, these oxides are considered as promising candidates for technological applications in magnetic devices. The CMR effect is also observed in the layered perovskites (Ruddlesden-Popper phases)[525] and some pyrochlore-type oxides.[526]

Giant magnetoresistance (GMR) represents a large (a few tens of percent) change in electrical resistance in response to an applied magnetic field. This quantum mechanical effect is observed in artificial structures, such as stacks of alternating nonmagnetic and antiferromagnetically coupled magnetic layers [527], [528] and granular systems. [529], [530] Electrical resistance of the nonmagnetic layers depends on the relative orientation of magnetic moments in the magnetic layers: the resistance is maximum for anti-parallel and minimum for parallel alignment of the magnetizations due to spin-dependent scattering of charge cariers. In zero field, the magnetic layers are coupled antiferromagnetically, and the resistance is high. Under applied magnetic field, magnetic moments of the adjacent magnetic layers become parallel, which results in lowering electrical resistance of the nonmagnetic layers. This phenomenon paved the way for realizing non-volatile magnetoresistive random access memory devices, [531] which use magnetic moment direction for information storage and the resultant MR difference for sensing.

Tunneling magnetoresistance (TMR) is observed in structures called magnetic tunnel junctions (MTJs).[532,533] An MTJ consists of at least two magnetic layers separated by an ultra-thin insulating layer, which serves as a tunneling barrier. The tunneling current is measured perpendicular to the barrier. The tunneling resistance depends on the relative orientation of the magnetization of the two magnetic layers: it is minimum for parallel and maximum for antiparallel orientation. In addition, the resistance depends exponentially on the insulating barrier thickness.

A large negative magnetoresistance is observed also in polycrystalline samples due to spin-polarized tunneling between grains. [534,535,536] In contrast to the CMR effect requiring large applied magnetic fields (typically a few Teslas), this effect is observed in

very low fields (< 0.5T) and is named as low field negative magnetoresistance (LFMR). Enhanced LFMR response was observed in many manganite-based two-phase composites, containing insulating oxides, [537,538,539,540,541,542,543,544,545,546,547] hard ferromagnetic materials, [548] soft magnetic materials, [549] metals, [550] or other CMR oxides [551] as a second phase. The presence of the secondary phases impedes the magnetic homogeneity near the grain boundary, increasing the height of the tunnel barrier between the neighboring ferromagnetic grains and thus influencing the tunneling process. In most cases, this strategy was applied to bulk ceramics or screen-printed thick films, but there are also reports on the LFMR effect in thin films. For example, Koster et al. [538] successfully adopted this approach to $La_{0.7}Ca_{0.3}MnO_3$-MgO composite thin films, consisting of $La_{0.7}Ca_{0.3}MnO_3$ columnar grains grown perpendicularly to the substrate surface and MgO located at the grain boundaries, acting as a tunneling barrier and enhancing spin polarized tunneling similar to a system with vertical artificial tunnel junctions. Liu et al.[552] also reported enhanced LFMR effect on laser-ablated $La_{0.5}Sr_{0.5}MnO_3$ thin films with amorphous $La_{1-x}Sr_xMnO_3$ as insulating matrix. Since the LFMR effect is observed at low magnetic fields and in a rather wide temperature range, the LFMR composites are considered to be well suited for device applications.[534,538]

4.2.1 Physical properties and crystal structure of manganites

Manganese oxides have the general formula $Re_{1-x}A_xMnO_3$, where Re is a trivalent rare earth element (Re = La^{3+}, Pr^{3+}, Nd^{3+}, Sm^{3+}, Eu^{3+}, etc.), and A is a divalent alkaline earth element (A = Ba^{2+}, Sr^{2+}, Ca^{2+}, etc.). In these compounds, when divalent alkaline-earth ions substitute trivalent rare-earth ions at the *A* sites, part of Mn^{3+} cations convert

into Mn^{4+} valence state to maintain the charge neutrality of the system. In stoichiometric oxides, the fractions of Mn^{3+} and Mn^{4+} ions correspond to 1-x and x, respectively.

The $Re_{1-x}A_xMnO_3$ manganites crystallize into the perovskite structure (see Figure 10), where the large rare earth and alkaline earth ions fill the A sites with 12-fold oxygen coordination, and small Mn^{3+} and Mn^{4+} ions occupy the B sites located at the center of the oxygen octahedra. A Mn atom has an electronic configuration $1s^22s^22p^63s^23p^63d^54s^2$ with the incomplete *d*-shell. In the $Re_{1-x}A_xMnO_3$ lattice, Mn ions are in octahedral oxygen coordination, and the five-fold orbital degeneracy of the 3d levels of Mn is split by the octahedral crystal field into the lower-lying triply degenerate t_{2g} states and the higher-lying doubly degenerate e_g states (see Figure 22). According to the Hund's first rule (maximum S), the d-electrons have the same spin orientation. An Mn^{3+} ion has an electronic configuration $3d^4$ with three electrons at the t_{2g} levels and one electron at the e_g level (S =2). A Mn^{4+} ion with the $3d^3$ electron configuration has three t_{2g} electrons and no electron at the e_g level (S = 3/2). The degeneracy of the t_{2g} and e_g levels can be further removed as a result of the Jahn–Teller distortion: a crystal field with symmetry lower than octahedral (which takes place, for example, when the oxygen octahedron is axially elongated) lifts the degeneracy of the t_{2g} and e_g levels, as shown on the right side of Figure 22 . One can see that the energy of the Mn^{4+} ion having no e_g electrons remains unchanged, whereas the energy of the e_g occupied state of the Mn^{3+} ion is lowered due to the Jahn–Teller distortion at a cost of the lattice energy. Therefore, Mn^{3+} ions have a great tendency to the Jahn–Teller distortion of their octahedral environment. In the manganites with high concentration of Mn^{3+} ions, cooperative Jahn–Teller distortions take place, leading to lowering of the lattice symmetry. For example, the compound

$LaMnO_3$ containing Mn in the 3+ state has the orthorhombically distorted perovskite lattice.

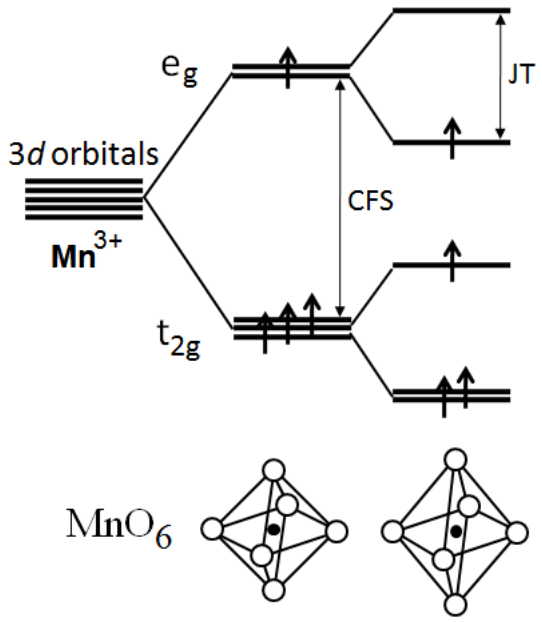

Figure 22 Crystal-field splitting (CFS) of the five-fold degenerate atomic 3d levels into lower t_{2g} (triply degenerate) and higher e_g (doubly degenerate) levels (in the middle). The Jahn–Teller (JT) distortion of the MnO_6 octahedron further lifts each degeneracy. Splitting of the t_{2g} and e_g levels and distortion of the MnO_6 octahedron due to the Jahn–Teller effect is shown on the right side.

Depending on composition, $Re_{1-x}A_xMnO_3$ compounds exhibit a wide range of electronic and magnetic phases, ranging from low-resistance ferromagnetic metals to high-resistance insulators. At high temperatures, these materials are paramagnetic and semiconducting or insulating. When the temperature is decreased, a transition from the paramagnetic to ferromagnetic metallic state occurs at the Curie temperature, the value of which depends both on the doping level x and the average ionic radius r_A of the cation in

the A position. The correlation between the electrical conduction and ferromagnetism in certain perovskite manganites were first studied by van Santen and Jonker[553,554] in the 1950's. They revealed a striking correlation between the magnetic Curie temperature, saturation magnetization, and electrical conductivity in $La_{1-x}A_xMnO_3$ (A = Ca^{2+}, Sr^{2+}, or Ba^{2+}) compounds, when measured as a function of *x*. It was found that the Curie temperature T_C and magnetoresistance M_S reach optimum values at x ~ 0.3, i.e. when about 30% of Mn^{+3} ions are converted to the Mn^{+4} state.[524,554] For example, for polycrystalline $La_{0.7}Sr_{0.3}MnO_3$ samples, $T_{C,max}$ = 370 K, $M_{S,max}$ ~ 90 G/g, and the electrical conductivity, σ_{max} = 300 $\Omega^{-1}cm^{-1}$. Santen and Jonker[553,554] also have found other basic properties of manganites, which were confirmed by careful examination of their results in many experiments. These are listed below:

- The maximum Curie temperature, minimum electrical resistivity, and linear relationship between the magnetoresistance and magnetization of the specimens, is observed when $x \approx 0.3$;
- Both divalent element content and oxygen stoichiometry can transform part of Mn^{3+} ions to Mn^{4+} ions;
- The relevant parameter determining T_C is not the distance between Mn atoms, but the angle of the Mn-O-Mn bond.

The magnetic properties of the manganites are governed by indirect exchange interactions between magnetic moments of Mn ions. A striking correlation between the magnetic and transport properties revealed first by van Santen and Jonker[553,554,555] was

explained theoretically by the double-exchange mechanism proposed by Zener[496,497] and further elaborated on by Anderson and Hasegawa,[556] de Gennes,[557] and Goodenough.[558] Zener[496,497] presumed that ferromagnetism of the doped manganites arises from an indirect coupling between the *d*-shells of Mn^{3+} and Mn^{4+} ions separated by an oxygen atom. As described above, in the doped manganites Mn exists in two states: Mn^{3+} with one electron at the e_g level and Mn^{4+} having no electrons at the e_g level. An e_{2g}-electron localized at a Mn^{3+} ion can hop on the vacant place of a neighboring Mn^{4+} ion (which corresponds to the movement of a hole in the opposite direction). The transfer of a charge carrier occurs simultaneously from Mn^{3+} to O^{2-} and from O^{2-} to Mn^{4+}. Since Hund's rule coupling is strong, the carriers can hop from one Mn ion to another only if the the core spins of the two ions are parallel.

This double-exchange mechanism is the basic mechanism of electrical transport and explains the observed simultaneous occurrence of metallic conductivity and ferromagnetism in the manganites. Since the same e_g electons are responsible for electrical transport and ferromagnetic interaction, the paramagnetic-to-ferromagnetic transition in the doped manganites is accompanied with insulator–to-metal transition around the ferromagnetic Curie temperature. An external magnetic field applied at temperatures around T_C promotes alignement of the local spins and hence reduces the randomness of the electron hopping, which increases the electrical conductivity markedly, giving rise to the CMR effect. It should be noted that the double exchange takes place between Mn ions with different valence states and is always ferromagnetic, unlike the super-exchange interaction which occurs between two next-to-nearest neighbor Mn ions of the same valence separated by an oxygen atom and is frequently

antiferromagnetic. [558, 559, 560] The competition between the exchange mechanisms is apparently responsible for the comlex phase diagrams of the $Re_{1-x}A_xMnO_3$ compounds.

Anderson and Hasegawa[556] derived the dependence of the probability of carrier transfer between the Mn ions on the angle between their spins:

$$\tau = \tau_0 \cos(\theta/2), \qquad \text{Equation 7}$$

where τ is the transfer integral, τ_0 is the normal transfer integral which depends on the spatial wavefunctions, and θ is the angle between the two spin directions. The transfer probability varies from 1 at $\theta = 0$ to zero at $\theta = 180^{\circ}$. This $\cos(\theta/2)$ angular dependence is quite different from the $\cos(\theta)$ dependence for the usual exchange interaction.

Considering the case of low-doped $LaMnO_3$, where mobile "Zener" electrons exist in the antiferromagnetic matrix, de Gennes[557] has found that the coexistence of the ferromagnetic double-exchange and antiferromagnetic superexchange interactions results in a spin-canted state. It should be mentioned, however, that more recent theoretical investigations revealed that phase separation into ferro- and antiferromagnetic regions rather than the canted state takes place at low doping levels.[561] In addition, de Gennes considered localization of charge carriers in the vicinity of a divalent A-site ion. The bound charge carrier interacts with spins on neighbouring B sites and produces a local distortion of the spin lattice, which is the concept of the bound magnetic polaron.

The double-exchange theory allowed qualitative explanation of the transport properties of the manganites, but was inconsistent with a number of experimental results. It predicted wrong values of resistivity and the Curie temperature, too slow doping dependence, an incorrect behavior for $T<T_C$ or under an applied field, and failed to explain the huge magnitude of the CMR effect. This discrepancy was resolved by Millis

et al. [562,563,564,565,566] who proposed that, in addition to the double-exchange interaction, a strong electron–phonon coupling due to the dynamic Jahn-Teller distortion is responsible for the manganite properties. The electron-phonon coupling arises from the Jahn-Teller splitting of the *d* level of Mn^{3+} (see Figure 22). The e_g electron occupying the lowest-energy e_g level together with the surrounding locally distorted lattice forms a self-trapped state called a Jahn–Teller polaron. According to Millis,[566] the transport in the manganites is governed by a competition between the self-trapping and delocalization due to the ferromagnetic ordering. The strength of the electron–phonon coupling is characterized by a dimensionless quantity λ, which is defined as[566]

$$\lambda = E_{latt} / t_{eff}, \qquad \text{Equation 8}$$

where E_{latt} is the energy gained from the electron–phonon coupling in the absence of hybridization and t_{eff} is 'bare' electron kinetic energy. At high temperatures (above the Curie temperature), t_{eff} is sufficiently small, and λ is so large that the electron–phonon interaction localizes the electrons, leading to the observed activated resistivity behavior in the paramagnetic phase. As the temperature decreases through Tc, the growing ferromagnetic order increases t_{eff}, thus decreasing λ, which allows delocalization of the e_g electrons and results in metallic behavior. The theory by Millis *et al.*[562] predicts more correct T_c values and explains the insulating behavior above T_c and the huge value of the CMR effect. More thorough consideration of physics in the mixed-valence manganites can be found in other reviews. [567,568,569,570,571]

4.2.1.1 Half metallicity

The charge transfer in the ferromagnetic manganites is provided by spin-polarized electrons. Such ferromagnets having only one type of conduction

electrons are called “half-metallic”. This class of materials was discovered by de Groot et al.[572] in 1983. The half-metallic ferromagnets exhibit an energy gap between valence and conduction bands for electrons of one spin direction and continuouis bands for the electrons of the other spin direction, so that the minority electrons (spins antiparallel to magnetization) are semiconducting, whereas the majority electrons (spins parallel to magnetization) show metallic behavior. As a result, the conduction electrons at the Fermi level are 100% spin polarized.[572] This unique property distinguishes them from usual ferromagnetic metals, in which spins of conduction electrons have both directions. Figure 23 compares conduction bands of a typical ferromagnetic metal (Ni) and half-metallic $La_{2/3}Sr_{1/3}MnO_3$.[534] The wide conduction band of Ni is split into minority and majority carrier bands offset by a small exchange energy (~0.6 eV), which results in a partial (~11%) electron polarization. To the contrary, in $La_{2/3}Sr_{1/3}MnO_3$ the narrow majority and minority bands are completely separated by large Hund’s energy, as well as an exchange energy (~2.5 eV), which leads to complete polarization of the carriers. Thus, the electronic density of states is completely spin-polarized at the Fermi level, and the conductivity is provided by spin-polarized electrons, which makes this class of materials very promising for spintronics applications.

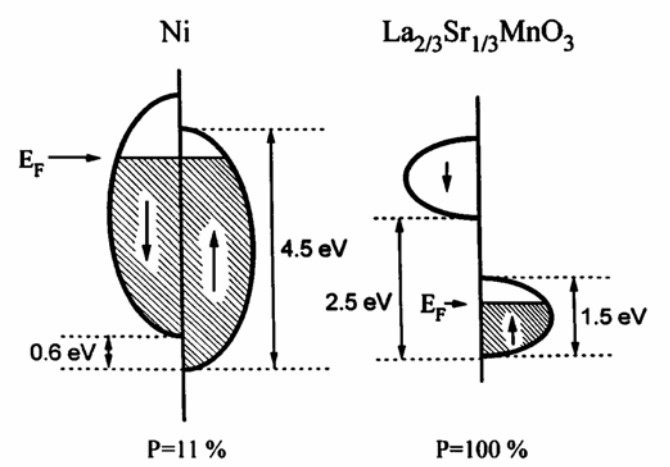

Figure 23 Energy level diagram comparing the conduction band of Ni with $La_{2/3}Sr_{1/3}MnO_3$. Reprinted with permission Ref. 534 Numerical values are from Refs. 573,574,575,576. This is so generic that we can produce our own. However, we would still cite the reference in the text*.

The half-metallic nature of the doped manganites is, however, still under debate. Theoretical and experimental values of the spin polarization obtained by different techniques vary over a wide range.[577, 578, 579, 580, 581, 582, 583, 584] Local spin-density approximation (LSDA) band calculation for $La_{0.67}Ca_{0.33}MnO_3$ predicted a spin polarization of only 36% at the Fermi level.[577] At the same time, Park et al.[580] reported pure half-metallic behavior of $La_{0.7}Sr_{0.3}MnO_3$ well below the Curie temperature. From spin-resolved photoemission spectroscopy data, the authors concluded that the spin polarization in $La_{0.7}Sr_{0.3}MnO_3$ was 100%. Spin-resolved tunneling experiments[578,578,] revealed an incomplete spin polarization for $La_{0.67}Sr_{0.33}MnO_3$ (54% and 81%, respectively). Worlege and Geballe[581] also reported an incomplete spin polarization of only 72% in this compound. Spin polarized tunnelling transport studies performed by Bowen et al.[583] on $La_{2/3}Sr_{1/3}MnO_3/SrTiO_3$ heterostructures have demonstrated a spin

polarization value of up to 99%. Nadgorny et al.[582] studied the spin polarization in bulk $La_{0.7}Sr_{0.3}MnO_3$ using the point-contact Andreev reflection technique. Their results strongly suggest that this material does have minority spin states at the Fermi level and thus is not a true half-metal. At the same time, the authors revealed a high degree of current spin polarization P ($58\% < P < 92\%$) in $La_{0.7}Sr_{0.3}MnO_3$. The origin of this high current spin polarization was attributed to a large difference in mobility of the spin-up and spin-down electrons rather than their density of states, so that the minority electons do exist at the Fermi level, but do not contribute to the conduction due to their much lower mobility relative to majority electrons. For this reason, Nadgorny et al.[582] called $La_{0.7}Sr_{0.3}MnO_3$ a "*transport* half-metal".

4.2.1.2 **Tolerance factor**

In the ideal perovskite structure (see Figure 10), the ratio between the A-O and B-O bond lengths should be equal to $\sqrt{2}$. In reality, the crystal structure of the doped manganites is usually distorted due to the difference in size between the rare-earth and alkaline-earth cations and due to the Jahn-Teller effect. The lattice distortion in the perovskites is characterized by Goldschmidt's tolerance factor *t*,[585] which is a geometric parameter that measures the deviation from perfect cubic structure. It is defined as

$$t = d_{A-O} / \sqrt{2} d_{B-O} \qquad \text{Equation 9}$$

or, since the bond lengths are mainly determined by the ionic radii

$$t = (r_A + r_O) / \sqrt{2}(r_B + r_O) \qquad \text{Equation 10}$$

where $d_{A\text{-}O}$ ($d_{B\text{-}O}$) is the the distances between the A (B) site and the nearest O ion, and r_A, r_B, and r_O are the average ionic sizes of A, B, and oxygen ions, respectively. For the

perfect closely packed cubic structure t is equal to 1, but the perovskite structure is stable in the range $0.89 < t < 1.02$. As t (i.e. r_A) decreases, the lattice structure transforms from cubic to the rhombohedrally distorted $R3^{-}c^{-}$ structure ($0.96 < t < 1$) due to a cooperative rotation of the BO_6 octahedra around the cubic [111] axis, and then to the orthorhombic *Pbnm* structure of the $GdFeO_3$ type ($t < 0.96$) due to a buckling of the network of octahedra corresponding to cooperative rotation about the [110] axis. As a result of this lattice distortion, the Mn–O–Mn bond angle (which is 180° for the cubic perovskite structure) decreases with decreasing the tolerance factor [567,586,587, 588,589]

The tolerance factor (i.e. r_A) have a profound influence on the properties of the doped $Re_{1-x}A_xMnO_3$ manganites. Hwang *et al.* [590] performed a detailed study of the relationship between the Curie temperature and the tolerance factor for doped $LaMnO_3$ compounds. In their study, the the average ionic radius of the cation at the A site r_A was varied by substituting different rare-earth ions for La, and the hole concentration was fixed at 0.3 by keeping the concentration of a divalent alkaline earth element constant. Figure 24 shows the resulting T_c- r_A diagram. Three principal regions are observed in the diagram: a paramagnetic insulator (PMI) at high temperatures, a ferromagnetic metal (FMM) at low temperatures and large r_A, and a ferromagnetic insulator (FMI) at low temperatures and small r_A. The Curie temperature is maximum (~365K) at r_A = 1.24Å (t = 0.93) and decreases with decreasing r_A . As mentioned above, the reduction of r_A leads to bending of the Mn–O–Mn bond, which disturbs the exchange interaction between the Mn^{3+} and Mn^{4+} ion spins and decreases the carrier mobility. As a result, the temperature range of ferromagnetic ordering becomes narrower with decreasing r_A and an insulating phase appears for small r_A (Figure 24).

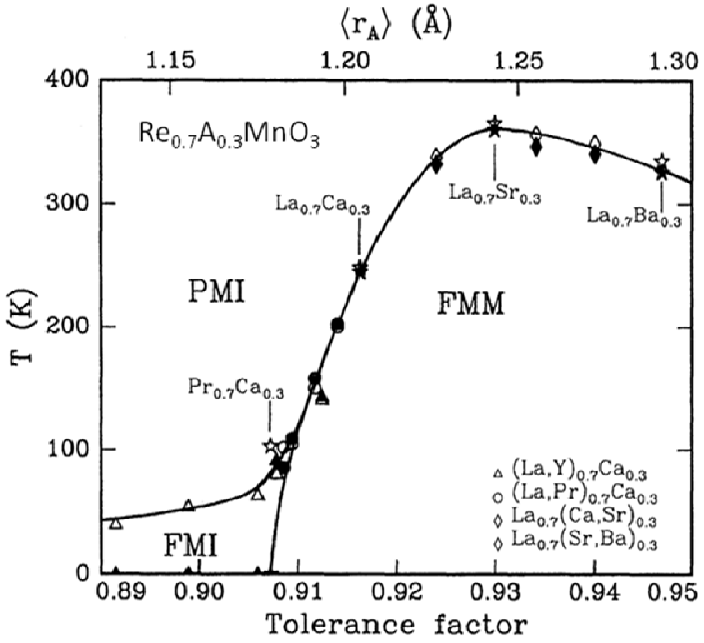

Figure 24. Temperature versus tolerance factor and average radius of cation at A site for the system $Re_{0.7}A_{0.3}MnO_3$. Reprinted with permission Ref. 590.

4.2.1.3 Charge and Orbital Ordering

Charge ordering is a phenomenon observed in the doped manganites when cations with different oxidation states are located on specific lattice sites, forming a long-range ordered structure.[591,592,593] This phenomenon arises from interactions between the charge carriers and phonons and takes place at low temperatures, when mobile electrons can be localized on certain Mn ions to form a regular lattice. Charge ordering is driven by interatomic Coulomb interactions and most likely occurs in the $Re_{1-x}A_xMnO_3$ compounds when proportions of Mn^{3+} and Mn^{4+} ions are rational fractions, e.g., when x=⅛, ½, or ¾. In a charge-ordered lattice, electrons are localized due to the ordering of Mn^{3+} and Mn^{4+}

cations on specific lattice sites, as shown in Figure 25(*a*).[588] Thus, charge ordering promotes insulating and atriferromatnetic behavior of a material.[593]

In addition to the charge ordering, the Mn^{3+} e_g orbitals and the associated lattice distortions can exhibit long-range ordering, called orbital ordering (see Figure 25(*b*).[588] The driving force is electrostatic repulsion of the charge clouds, and coupled Jahn-Teller distortions of adjacent octahedra stabilize the effect. Figure 25(c) illustrates the coupled charge and orbital order.[588]

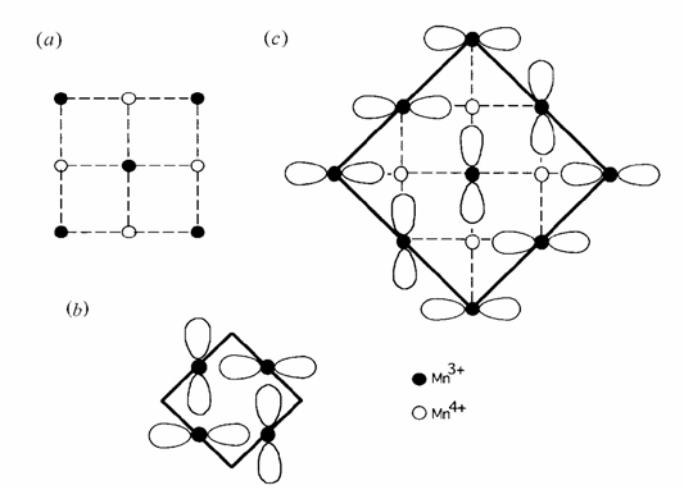

Figure 25
(a) Charge ordering of Mn^{3+} and Mn^{4+} in a mixed crystal with x = 0.5. (b) Orbital ordering of the d_z^2 orbitals of Mn^{3+} when x = 0. (c) Combined charge and orbital ordering when x = 0.5. Reprinted with permission Ref. 588

4.2.1.4 Oxygen stoichiometry

Oxygen content is another important parameter determining the magnetic and transport properties due to its influence on the Mn^{4+}/Mn^{3+} ratio and the Mn–O–Mn bond angles.[594,595,596,597,598,599,600] Taking into account the valent states of all constituencies, we can write the chemical formula of mixed-valence manganites as $Re^{3+}_{1-x}A^{2+}_{x}Mn^{3+}_{1-z}Mn^{4+}_{z}O^{2-}_{3-\delta}$. One can see that a deviation of the oxygen content from the stoichiometric value, δ,

inevitably changes the concentration of Mn^{4+} ions, z, to satisfy the neutrality condition. Thus, oxygen deficiency in the mixed-valence manganites results in the decrease of hole concentration and, consequently, in weaker double-exchange interaction, lower conductivity, lower magnetization, and the lower Curie temperature.

4.2.2 Phase diagrams

The phase diagrams of $Re_{1-x}A_xMnO_3$ manganites have a complex dependence on the doping level, *x*, that comes from the competition between the ferromagnetic double-exchange interaction, antiferromagnetic superexchange interaction, charge/orbital-ordering, and effects of the Jahn-Teller distortion. There have been a number of reports on the phase diagram of manganites, particularly for $La_{1-x}Sr_xMnO_3$,[553,554,601,602,603] $La_{1-x}Ca_xMnO_3$,[554, 604 , 605 , 606 , 607] $Pr_{1-x}Ca_xMnO_3$,[608 , 609 , 610] $Pr_{1-x}Sr_xMnO_3$,[610, 611 , 612] $Nd_{1-x}Sr_xMnO_3$,[612, 613] $Sm_{1-x}Sr_xMnO_3$,[610] and $Sm_{1-x}Ca_xMnO_3$.[610] A thorough analysis of the phase diagrams of the mixed-valence manganites can be found in Refs.[567,614,615,616,617] In this paper, we consider the phase diagram of the most popular compounds, namely $La_{1-x}Sr_xMnO_3$ and $La_{1-x}Ca_xMnO_3$.

4.2.2.1 $La_{1-x}Ca_xMnO_3$ phase diagram

$La_xCa_{1-x}MnO_3$ (LCMO) may be considered as a solid solution of $LaMnO_3$ and $CaMnO_3$. The complete phase diagram of $La_{1-x}Ca_xMnO_3$ was first reported by Schiffer et al.[604] who carried out magnetization and resistivity measurements over a broad range of temperatures and doping levels as well. A more detailed phase diagram was constructed

later by Cheong and Hwang.[605] The phase diagram of $La_{1-x}Ca_xMnO_3$is shown in Figure 26. The parent compounds, $LaMnO_3$ and $CaMnO_3$, are antiferromagnetic at low temperatures and insulating at all temperatures. At high temperatures, LCMO is a paramagnetic insulator over the whole composition range. At low temperatures, Ca doping leads to a series of phase transitions. At low dopant level (x< 0.175), canted antiferromagnetic and then ferromagnetic insulating and charge-ordered phases are observed (Figure 26). In the Ca concentration range from 0.175 to 0.50, LCMO is a ferromagnetic metal. The CMR effect occurs in the aforementioned composition range. Near x = 0.50, the ground state of the material changes from a ferromagnetic conductor to a charge-ordered antiferromagnetic insulator. At high doping level (x>0.87), LCMO becomes a canted antiferromagnetic insulator again. Note that some peculiar features appear in the diagram at commensurate Ca concentrations, indicating the importance of electron–lattice coupling:[605] the Curie temperature reaches its maximum at x = ⅜ (0.375), and the charge-ordering temperatures peak at x=⅛ (0.125) and x=⅝ (0.625). At x = 4/8 (0.5), the phase boundary between the ferromagnetic and charge-ordered antiferromagnetic states takes place; and there is another phase boundary at x = 7/8 (0.875).

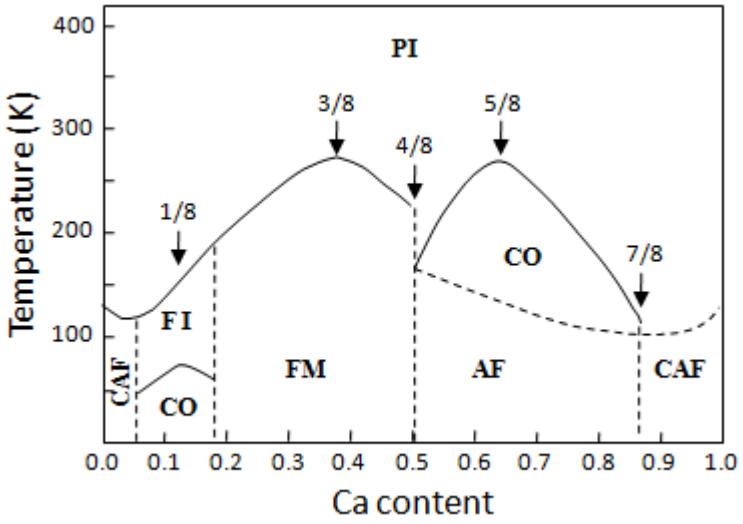

Figure 26 Phase diagram of $La_{1-x}Ca_xMnO_3$. Solid curve represents a boundary between the insulating paramagnetic state and spin-ordered states, dashed lines indicate boundaries between different ground states. PI denotes paramagnetic insulator; CAF, canted antiferromagnet; FI, ferromagnetic insulator; CO, charge/orbital order; FM, ferromagnetic metal; AF, antiferromagnetic phase. After Cheong and Hwang. [605]

.

4.2.2.2 $La_{1-x}Sr_xMnO_3$ phase diagram

The rich and complex phase diagram of $La_{1-x}Sr_xMnO_3$ (LSMO), a solid solution of $LaMnO_3$ and $SrMnO_3$, has been studied by many groups.[553,554,602,603,618,619,620,621,622] The first phase diagram of LSMO was reported as early as 1950 by Jonker and van Santen [553,554] and result is very close those obtained recently by Paraskevopoulos et al.[602] and by Hemberger et al.[603] Paraskevopoulos et al.[602] performed detailed studies of susceptibility, magnetization, and magnetoresistance of $La_{1-x}Sr_xMnO_3$ for $x \leqslant 0.2$, and constructed a phase diagram which showed a ferromagnetic and insulating ground state for $0.1 \leqslant x \leqslant 0.15$, followed by a canted antiferromagnetic phase at higher temperatures. The ferromagnetic transition was stated to be strongly coupled to a structural transition from a Jahn–Teller distorted phase to a pseudocubic orthorhombic phase and accompanied by

the appearance of large positive magnetoresistance effects. The observations were interpreted by the authors by means of orbital ordering, due to interplay between superexchange interaction and Jahn–Teller distortion.

Figure 27 shows the phase diagram of LSMO for the entire concentration range ($0<x<1$) constructed by Hemberger et al.[603] with the use of the results by Paraskevopoulos et al.[602] for $0<x<0.3$. The phase diagram shows a pronounced asymmetry between the hole-doped ($x<0.5$) and the electron-doped ($x>0.5$) regions, originating mostly from geometrical constraints via the tolerance factor, which increases from 0.89 to 1.01 as x rises from 0 to 1, i.e. buckling of the MnO_6 octahedra in LSMO decreases with increasing Sr concentration. In addition, this asymmetry is driven by the increasing importance of orbital degeneracy with increasing concentration. Near $x=0$, the strong Jahn-Teller distortions provide orbital order that determines the antiferromagnetic *A*-type spin structure. For higher doping levels, orbital degeneracy plays an important role yielding completely different spin ground states.[603] When x is increased, a ferromagnetic component evolves in addition to the anti-ferromagnetic order of subsequent planes. As the concentration increases to $x>0.17$, LSMO becomes a ferromagnetic metal with a rhombohedral structure and exhibits the CMR effect. Near $x\sim0.5$, a ferromagnetic metallic phase with a tetragonal structure appears, which undergoes a transition into a monoclinic antiferromagnetic phase with decreasing temperature, but still exhibits metallic behavior. At x~0.6, a two-dimensional metallic antiferromagnetic phase with a monoclinic structure evolves. For $x>0.75$, LSMO is in a purely antiferromagnetic and insulating, and has a nearly cubic structure.

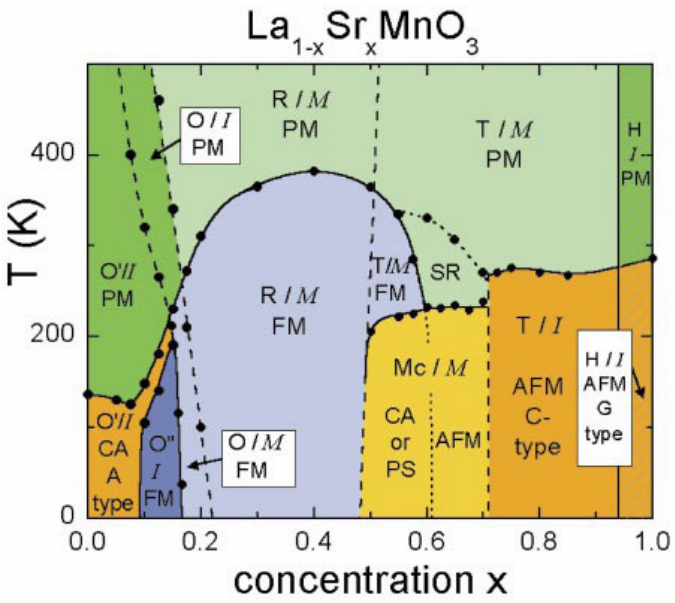

Figure 27 Phase diagram of $La_{1-x}Sr_xMnO_3$ for the whole concentration range. The crystal structures (Jahn-Teller distorted orthorhombic: O', orthorhombic O; orbital-ordered orthorhombic: O", rhombohedral: R, tetragonal: T, monoclinic: Mc, and hexagonal: H) are indicated as well as the magnetic structures (paramagnetic: PM, short-range order (SR), canted (CA), *A*-type antiferromagnetic structure: AFM, ferromagnetic: FM, phase separated (PS), and AFM *C*-type structure) and the electronic state (insulating: *I*, metallic: *M)*. Reprinted with permission Ref. 603

4.2.3 Doping on Mn site

Doping of $A_xB_{1-x}MnO_3$ with various 3d transition metal ions substituting the Mn site (Ni,[623,624] Bi,[625] Cu,[626,627] Cr,[628] Zn,[629] Ga,[630,631] Al,[632,633] Mg,[634] Nb,[634] Ti,[633,634,635] Ta,[636] Sb,[637,638] Fe,[639,640,641] Zr,[641] Hf,[641] Ru[642,643,644,645,646,647]) has a great of influence on the double exchange interaction and conduction mechanisms and allows tailoring the material characteristics for specific device applications. Most of the impurities substituting Mn decrease the Curie temperature (and the associated metal-insulator transition temperature), which has been explained by weakening of the ferromagnetic

orderig due to the interruption of the double exchange interaction between Mn^{4+} and Mn^{3+} ions. [624,625,629,627,630,631,632,633,635,636,640,641] The only exeption is Ru doping, which can increase the Curie temperature and induce metallic behavior and ferromagnetism in some antiferromagnetic materials.[642,644,645, 646,647] It was argued[642,645,647] that Ru favors the double-exchange interaction because it can exist in the mixed valence state with *d*3 and *d*4 electronic configurations similar to those of Mn^{4+} and Mn^{3+}, which makes possible ferromagnetic interaction between the Mn^{3+} and $Ru^{5+/4+}$ ions.

4.2.4 Growth of manganite thin films

For most device applications, a material should be in the form of thin films and preferably with superior quality which necessitates growing epitaxial thin films. Single-crystal layers of the $Re_{1-x}A_xMnO_3$ compounds have been grown by various techniques, including pulsed laser deposition,[648,649,650,651,652,653,654,655] metal-organic chemical vapor deposition, [656, 657, 658, 659, 660, 661, 662, 663] atomic layer deposition,[664] sputter deposition, [665,666,667,668,669,670,671,672] molecular beam epitaxy, [673,674 675, 676,677] and the sol-gel method. [678,679,680,681,682,683,684] A comprehensive treatment of various aspects of manganite film growth and properties can be found in the reviews by Haghiri-Gosnet,[524] Prellier,[685] and Van Tendeloo.[686] Here, we overview briefly the methods currently used for the growth of manganite thin films and the effects of growth conditions and substrate clamping on film properties.

4.2.4.1 Pulsed laser deposition of manganite thin films

PLD is a simple and straightforward method for the growth of thin films of complex compounds. In PLD, films are deposited by ablating a target of a desired

composition with a laser in oxygen ambient. As discussed in Section 3.3.4, the mechanism of PLD growth is rather complex. Oxygen pressure in the chamber, substrate temperature, and the target-to-substrate distance are the main parameters determining structural, transport, and magnetic properties of PLD produced films.

Studying the effect PLD parameters on structural and physical properties of $La_{0.7}Sr_{0.3}MnO_3$ films grown on (100)$SrTiO_3$ substrates, Koubaa et al. [650] uncovered a strong dependence of microstructure, surface morphology, the Curie temperature, saturation magnetization value, and low-temperature resistivity of the layers on the substrate–to-target distance D (see Figure 28*)*. For each set of growth parameters, the optimal distance $D = L_0$ can be calculated using the P–D scaling law[687] obtained from the ‘‘wave blast’’ model[688]

PD^3 =constant, **Equation 11**

where P is growth pressure, and L_0 is a so-called ‘‘plume range”, the particular target-to-substrate distance, for which all the species are thermalized in the plume.[689] In the D– P diagram shown in Figure 28a, L_0 defines two distinct regions for the morphology and the microstructure. When $D<L_0$, the films exhibit a dense, smooth, and large grain morphology due to the bombardment of the film surface by a nonthermalized directive energetic particles. These films are perfectly epitaxial, single-phase, and not relaxed. When $D>>L_0$, very rough films with columnar structure were obtained.[650]

The films with best magnetic and electrical properties were grown in a sharp transition window between these two regions. As seen from Figure 28b, at a substrate temperature of 570 °C and an oxygen pressure of 350 mTorr, the optimal substrate-to–target distance is 5 cm. The films deposited at D = 5 cm exhibited properties very similar

to those of bulk samples, with a sharp decrease of magnetization at T_C, the highest saturation moment of ~2.9 μB per formula unit, and the lowest resistivity of 125 mVcm.[650] Such a strong distance dependence of the film properties was explained as follows. L_0 is the transition distance at which the energetic species start to be sharply thermalized. At high pressures, this transition region in the plasma is spatially very sharp.[690] Thus, the growth parameters providing films with optimized structural, magnetic, and electrical properties should be chosen in this very sharp window that corresponds to the plume range L_0. Armed with the above knowledge, Koubaa et al.[650] have demonstrated that LSMO films with a low roughness, dense morphology, and good magnetic and electrical properties can be grown in a very narrow window of PLD parameters.

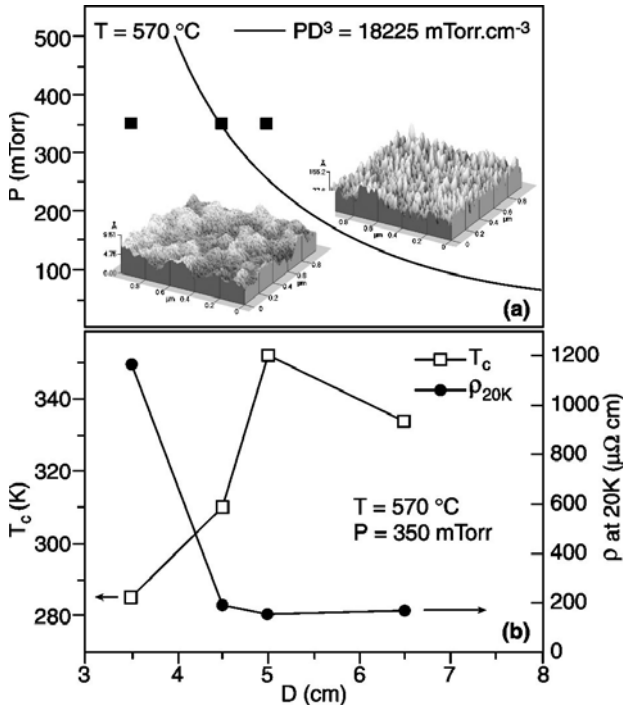

Figure 28
Variation of the Curie temperature T_C and the resistivity at 20 K as a function

of the target-to-substrate distance *D* (lower panel) in accordance with the *P–D* diagram for morphology evolution (upper panel). Reprinted with permission Ref. 650

The influence of growth and annealing temperatures on the resistivity and magnetoresistance behavior of $Nd_{0.7}Sr_{0.3}MnO_{3-\delta}$ and $La_{0.67}Ba_{0.33}MnO_{3-\delta}$ PLD films was studied by Xiong et al.[691] It was found that the deposition at a high temperature and annealing at a high temperature have opposite effects on the resistivity of the films. At a fixed gas pressure (300 mTorr N_2O), the layers grown at a higher substrate temperature (600–850 °C) showed a larger resistivity maximum and a lower conductor-insulator transition temperature. To the contrary, high-temperature (900 °C) annealing in oxygen atmosphere reduced the resistivity maximum and increased the transition temperature. The decrease in the film resistivity and the increase in the temperature of semiconductor–metal transition upon high-temperature annealing in oxygen has been reported also for MOCVD films.[663] These results were attributed to the variation of oxygen content in the films during deposition and subsequent heat treatment. The growth at a high substrate temperature can result in oxygen deficiency, while heat treatment in oxygen atmosphere can refill oxygen into oxygen-deficient films. The variation in the oxygen content leads to the variation in the Mn^{3+}/Mn^{4+} ratio in $Nd_{0.7}Sr_{0.3}MnO_{3-\delta}$ and $La_{0.67}Ba_{0.33}MnO_{3-\delta}$, and thus influences the resistivity and magnetoresistance behavior of the films. In addition to the oxygen content, annealing can affect the defect and vacancy motion and recombination, thus affecting the resistivity and the GMR ratio. These findings led the authors to the conclusion that oxygen stoichiometry and diffusion are important factors determining the magnetoresistance behavior of doped manganites.

4.2.4.2 Metal Organic Chemical Vapor Deposition of manganite thin films

MOCVD offers many advantages, including high deposition rates, easy control over film composition, excellent crystallinity, good step coverage and capability of coating complex shapes, uniformity of film composition and thickness over a large area, and compatibility with the standard semiconductor technology. A great disadvantage of this technique for doped manganite growth is the poor volatility and thermal stability of Ba, Sr and other rare-earth based oxide precursors.[662] Several solutions have been proposed to overcome this problem. [662,663,692,693,694,695] For example, a pulsed liquid injection delivery scheme alowing the generation of a stable gas phase from unstable precursors was developed.[692] Abrutis et al.[663] used this technique to grow high-quality LSMO films. The deposition was carried out in a vertical hot wall injection CVD reactor, shown in Figure 29**.** The reactor has three evaporators, each connecting one injector. The latter injects microdoses of a solution containing a dissolved mixture of organo-metallic precursors. After injecting, the droplet immediately evaporates and the resulting vapor is transported by an Ar-O_2 carrier gas towards the substrate. The pulse width determines the volume of each droplet, and the injection frequency keeps the amount of reactants at a certain level during growth. The injector is a computer-controlled high-speed precision electromagnetic valve. Several injectors can be used simultaneously in one system whose settings can be changed during growth. This technique allows also the growth of superlattices with with ultrathin films of a few monolayers. Dubourdieu et al.[661] reported the deposition of $La_{0.7}Sr_{0.3}MnO_3$ /$SrTiO_3$ superlattices consisting of 15 bilayers by pulsed liquid-injection MOCVD. The thickness of each layer was precisely controlled by adjusting injection parameters.

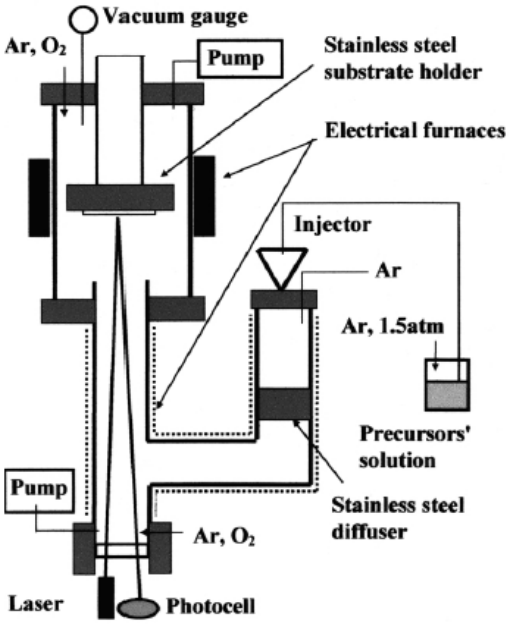

.

Figure 29 Schematic representation of injection MOCVD reactor. Reprinted with permission Ref**.** 663.

Electrical and magnetic properties of MOCVD grown films are strongly dependent on their composition, crystal perfection, stoichiometry, strain, oxygen content and therefore are very sensitive to growth conditions. Abrutis et al.[663] have reported that the most important factors are the deposition temperature, solution composition, and the ratio of oxygen flow rate to solvent and precursor vapor flow rate. They found that an increase in the deposition temperature led to an increase in the temperature coefficient of resistance (TCR), magnetoresistance ratio (MR), and the semiconductor–metal transition temperature T_ρ. But T_ρ was less sensitive to the deposition temperature when a solution more rich in Mn was used. Abrutis et al.[663] explained this finding by the influence of the substrate temperature on the decomposition reaction of precursors (and, consequently, on the film stoichiometry), and presumed that this influence is stronger for the Mn precursor.

Thus, the authors suggested that the deposition temperature determined the degree of deviation from the stoichiometric Mn concentration in the films. This explanation was supported by the fact that similar behavior (TCR and MR increased together with T_ρ) was observed for a series of films deposited at the same temperature from solutions with a variable Mn content. The best films were deposited at 825ºC on $LaAlO_3$ substrates from solutions with the composition $La_{0.6}Sr_{0.4}Mn_{0.63}$. These films exhibited T_ρ = 320K, TCR of ~4.5% (300 K), and MR of ~43% (1.5 T, 300 K). The peak resistivity of the films was about 10 mΩ cm, and the resistivity at 100 K was about 130 μΩ cm.

Figure 30 a and b illustrate the effects of oxygen partial pressure and injection frequency (i.e. solvent + precursor vapor flow rate) on the properties of LSMO films, respectively. One can see that the increase in the oxygen pressure and the decrease in the injection frequency have the same effect: T_ρ decreases, while the values of TCR and MR increases. Figure 30c shows the film properties vs. the ratio of oxygen and solvent + precursor vapor flow rates V_{O2}/V_{vapor} (calculated from the data of Figure 30 a and b). The dependencies presented in Figure 30c were obtained in two series of measurements, one with variable oxygen partial pressure and the other with variable injection frequency. One can see that both dependencies are very similar, evidencing that the factor influencing the film properties is excess oxygen with respect to the vapor concentration. The authors have suggested that the variation in the oxygen concentration influences the yields of precursor decomposition reactions and, consequently, the film composition, most probably, the Sr content, since the behavior of T_ρ, TCR, and MR are similar to that caused by the variation in the Sr content.[663]

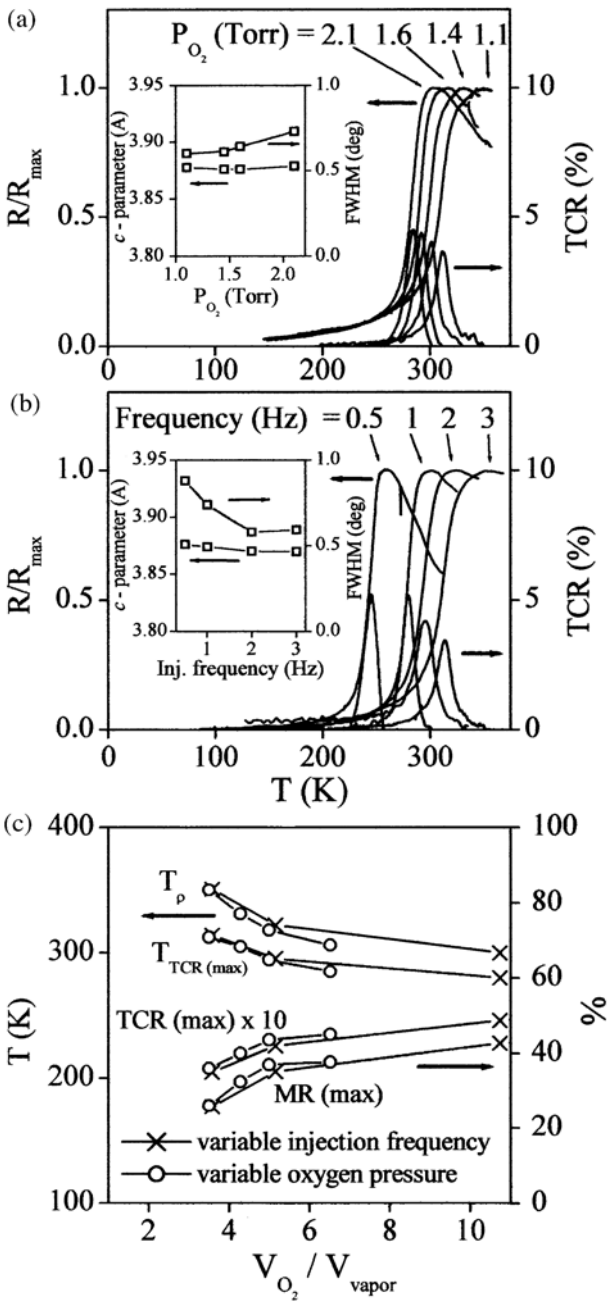

Figure 30 Effect of oxygen partial pressure (a) and injection frequency (b) on electrical properties of LSMO films deposited on $LaAlO_3$ substrates at 825 C, (c) electrical properties of films vs.the ratio of oxygen and vapor flow rates (calculated from the data of a and b). R/R_{max} is resistance normalized to maximum value. Solution composition is $La_{0.6}Sr_{0.4}Mn_{0.63}$. Insets in a and b show the variation of *c*-parameter of LSMO lattice and FWHM of rocking curve for LSMO (200) reflection. Reprinted with permission Ref. 663.

4.2.4.3 Deposition of manganite thin films by sputtering

As mentioned in Section 3.3.3, sputter deposition is a simple tool for growing complex oxide films. Both dc[665,666,666] and rf[667,668670,672] sputtering techniques are used for the growth of manganite films. Sputter deposition provides high deposition rates, uniformity of thickness and composition over a large area, and is compatible with the standard microelectronics technology. However, difference in sputtering yield of different target materials can lead to poor control over film composition. In addition, as-sputtered manganite films usually have been suggested to be oxygen deficient, which deteriorates their crystalline quality as well as electrical and magnetic properties. Therefore, post-growth annealing in oxygen atmosphere, which is a common procedure fore many oxide film growth techniques, is especially important for sputtered manganite films.[665,666,667,670,672] For example, Li et al.[670] found that the Curie temperature and saturation magnetization of sputtered LSMO films increased, and coercivity dramatically decreaced upon post-growth annealing in oxygen. The increase in conductivity, the Curie temperature, metal–insulator transition temperature, magnetoresistance, and saturation magnetization of LSMO upon annealing was reported by Sahu et al.[666] The improvement of the magnetic properties of manganite films after annealing in oxygen is generally attributed to the increase in Mn^{4+}/Mn^{3+} ratio due to oxygen incorporation into the lattice.[666,670, 672]

The growth of high-quality epitaxial manganite films was demonstrated by Casanove et al.,[667] who deposited the LSMO layers on (001)MgO and (001)$SrTiO_3$ substrates by rf magnetron sputtering. The crystal structure of the films was examined by x-ray diffraction and transmission electron microscopy. The LSMO layers were found to

be single-crystal, (001) cube-on-cube epitaxial with in-plane orientational relationship [100]LSMO//[100]substrate. The best magnetic properties were obtained for fully relaxed films. For the layers grown on MgO, relaxation of epitaxial strain was observed at the very first stage of the growth due to the large lattice mismatsh (~8%), while full strain relaxation in the films grown on $SrTiO_3$ (misfit ~0.89%) was found to be favored by annealing and slow growth rate at high temperature.

RF magnetron sputtering has also been successfully employed for the growth of an $La_{0.7}Sr_{0.3}MnO_3/SrTiO_3$ superlattice with atomically flat interfaces. [668] The superlattice was grown on a (001)$LaAlO_3$ substrate with a 60-nm-thick $SrTiO_3$ buffer layer. The growth was carried out at a temperature of 720 °C and pressure of 300 mTorr which was followed by annealing in oxygen. The final structure consisted of 12 pairs of alternating $La_{0.7}Sr_{0.3}MnO_3$ (76nm) and $SrTiO_3$ (56 nm) layers with very sharp (<1 nm) interfaces between them. The high-resolution TEM image shown in Figure 31 demonstrates perfect epitaxial growth comparable to similar structures grown by PLD.[696]

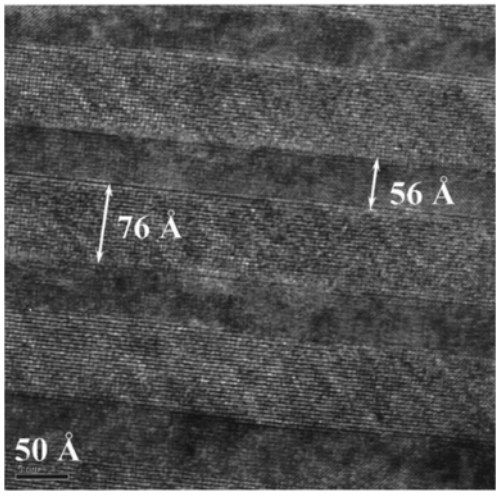

Figure 31 High-resolution cross-sectional TEM lattice image of a LSMO/$SrTiO_3$ superlattice. Reprinted with permission Ref. 668.

4.2.4.4 Molecular beam epitaxy of manganite thin films

MBE is one of the best methods for growing high-quality thin films of complex compositions. In this techinque, pure components of a compound are evaporated individually from effusion cells and then condense on a heated substrate surface, where they react with each other to form an epitaxial film of a desired composition. In contrast to the PLD and sputtering techniques, where the target composition is fixed, the flux of each component in MBE is controlled independently, which allows a fine control over the film composition. Due to low pressure in the growth chamber, MBE allows surface in-situ characterization by high-energy electron diffraction (RHEED) and sometimes Auger electron spectroscopy (AES). In addition, oxide films grown by MBE ususally do not require post-growth annealing in oxygen despite a low oxygen pressure during the growth.[675] However, MBE growth of oxide films is a challenge, because of oxidation of materials in effusion cells, as already mentioned in Section 3.3.6. Therefore, in spite of the numerous advantage of this technique, MBE is not widely applied to the growth of manganite oxides and the data in the literature are rare.[673,674,675,676] Mercone et al.[675] reported MBE growth of LSMO films on different substrates. In their work, Sr and Mn were everporated from effusive cells, while La was delivered from an e-beam evaporation source due to its high melting point. A mixture of oxygen+5% ozone was used as an oxidizing agent. Atomic layer-by-layer molecular beam epitaxy (ALL-MBE) developed by Eckstein and Bozovic[697] for high-temperature superconductors and other complex oxides has been applied to the growth of LSMO[673,677] and LCMO[674,676] thin films as well. With this method, layers with atomically flat surfaces and abrupt interfaces can be produced by deposition of one atomic layer at a time.

4.2.4.5 Deposition of manganite thin films by sol-gel technique

As mentioned in Section 3.3.1, the sol-gel process is an attractive method for depositing complex oxide thin films, due to its simplicity, excellent composition and thickness control, low cost, short fabrication cycle, and uniformity over large areas. Although widely used for the preparation of ferroelectric thin films, this method was found to be less desirable for manganites apparently due to inferior quality of sol-gel films compared to those grown by other techniques. The layers prepared by the sol-gel route are usually polycrystalline with the magnetotransport properties dominated by tunneling of spin-polarized carriers between grain boundaries and showing strong grain size dependence.[679,681,683] For example, Yan et al.[683] found that the resistivity of nanocrystalline $La_{0.7}Sr_{0.3}MnO_3$ films on Si(100) substrates fabricated by the sol-gel method is three-orders larger than that of an $La_{0.67}Sr_{0.33}MnO_3$ film grown by MOCVD.[698] The high resistivity of the sol-gel layers was explained by the presence of grain boundaries acting as transport barriers. The temperature of the metal-to-insulator transition for the sol-gel films was found to be about 220 K, while the Curie temperature was about 365 K. The large difference between these temperatures (which are usually close for epitaxial films or single crystals) was also attributed to grain boundary effects. Low-field magnetoresistance due to tunneling of spin-polarized carriers between grain boundaries was observed in these films as well.[683]

The data on epitaxial growth of manganite films by the sol-gel method are very few.[678,679] Bae and Wang[678] reported on the epitaxial growth of $La_{0.67}Ca_{0.33}MnO_3$ films on (001) MgO and (100) $LaAlO_3$ substrates by the sol-gel route. The stock solution was prepared by dissolving La, Ca, and Mn acetates with molar ratios La:Ca:Mn =

0.67:0.33:1 in 2-methoxymethanol followed by refluxing at 80ºC for 24 hours after adding H_2O. Xerogel was finally obtained after aging the solution for several days followed by distillation and drying. To fabricate thin films, the sol-gel solution was spin-coated on MgO and $LaAlO_3$ substrates and immediately pyrolyzed at 400ºC after each coating. The spin-coating was repeated several times to achieve film thickness of 700–1000 Å. Then the layers were annealed in oxygen at a temperature between 700 and 1000ºC for 12 hours. The resulting $La_{0.67}Ca_{0.33}MnO_3$ films exhibited a magnetoresistance ratio of ~ 900%, a semiconductor to metal transition temperature of 225 K, and the Curie temperature of 228K.[678]

4.2.4.6 Influence of Substrates

Structural, electrical, and magnetic properties of manganite thin films may be considerably different from those of bulk manganites. The main factor determining crystallinity of thin films is lattice mismatch between a film and a substrate, which is usually defined as $(a_s - a_f)/a_s$, where a_s and a_f are in-plane lattice constants of the deposited film and the substrate, respectively. When $a_s > a_f$ (positive mismatch), the film is under tensile strain. In the case when $a_s < a_f$ (negative mismatch) the film is under compressive strain. When manganite thin films are deposited on the substrates providing low lattice mismatch, the films grow epitaxially, and their transport propreties and magnetoresistance behavior are similar to those of bulk single crystals. The films deposited on highly mismatched substrates are usually polycrystalline, and exhibit different transport behavior due to the grain boundary effects.[671,699 700] For example, studing the effect of crystallinity on magnetoresistance in epitaxial and polycrystalline

$La_{2/3}Ba_{1/3}MnO_3$ and $La_{2/3}Ca_{1/3}MnO_3$ thin films, Shreekala et al.[699] found that magnetoresistance in epitaxial films exhibited field and temperature dependences similar to those for bulk single crystals and ceramics, with a magnetoresistance peak close to the Curie temperature. In contrast, the polycrystalline films showed either a monotonic increase or saturation of magnetoresistance with decreasing temperature. The field dependence in the polycrystalline films was also remarkably different. The anomalous behavior of the magnetoresistance in polycrystalline films was attributed to the spin-polarized transport across grain boundaries.

The properties of single-crystal, epitaxial films are strongly influenced by the choice of substrate due strain arising from the lattice mismatch between the film and the substrate as well as due to the diffecrence in thermal expansion coefficients. Tensile or compressive strain distorts the perovskite lattice, thus affecting the orbitals responsible for the carrier transport in the mixed-valence manganites. The lattice distortion due to the mismatch strain can also result in phase transformation in thin films.[701] The srain effects in manganite films has been widely studied, both experimentally [685,702,703,704,705,706,707,708,709, 710,711,712,713,714,715,716,717,718,719,720,721] and theoretically.[722,723] The most common single crystal substrates used to grow manganite thin films and their properties are presented in Table 4.[234,702,724,725,726] The most popular substrates for epitaxial growth of LSMO films are $SrTiO_3$ and $LaAlO_3$, due to their commercial availability and low lattice mismatch with LSMO. The best quality epitaxial LSMO layers reported in the literature were grown on the aforementioned substrates. [663,667,671, 700,727, 728,729]

Table 4. Substrates most commonly used for growth of manganite thin films

Material	CrystalStructure	Lattice parameter (Å)	Thermal expansion coefficient ($\times 10^{-6}$/K)	Ref.
$Bi_4Ti_3O_{12}$	orthorhombic	*a*=5.410 *b*=5.448, *c*=32.84 Å.	~11	234,726
$SrTiO_3$	cubic perovskite	3.905	10.4	724
$LaAlO_3$	rhombohedral	*a*=3.788, α = 90°4'	11	724
Si	cubic	5.43	~3	725
YSZ	cubic	5.14	~10	726
$NdGaO_3$	orthorhombic	*a* = 5.426Å, *b* = 5.502Å, *c* = 7.706Å		702
MgO	cubic rocksalt type	4.216	10.5	724

A series of papers have been devoted to comparison of manganite films grown on various substrates.[663,664,667,671,699, 700,728, 730,731,732] Yang et al. [671] compared characteristics of $La_{0.7}Sr_{0.3}MnO_3$ films deposited on various substrates: single crystal $LaAlO_3$(001), $SrTiO_3$(001), MgO(001), SiO_2/Si(001), and amorphous quartz. The 300-nm-thick films were grown by off-axis magnetron dc sputtering at temperatures 700- 800ºC, depending on the substrate, all other conditions of the deposition and post-annealing being the same. XRD θ-*2*θ scans shown in Figure 32 illustrate the dependence of the film cristallinity on the lattice mismatch. The XRD patterns for the LSMO grown on $SrTiO_3$ and $LaAlO_3$ substrates (Figure 32 a, b) contain only (00n) peaks, indicating that the films are c-axis oriented due to the low lattice mismatch. For films grown on MgO (Figure 32c), (011) and (111) peaks in addition to (00n) peaks appeared revealing that the film is less textured and polycrystalline. The preference for the {011} orientation was attributed to the smaller lattice mismatch between the {011} LSMO plane and {001} MgO (1%) as

compared to that for the {001} plane (7.8%). For SiO_2/Si(0 0 1), the lattice mismatch of the {001} LSMO plane is further increased and the lattice mismatch of the {011} LSMO plane is further reduced. As a result, the (011) peak dominates the XRD pattern shown in Figure 32d. The film grown on the amorphous quartz substrate is polycrystalline, and all LSMO planes diffract (Figure 32 e).

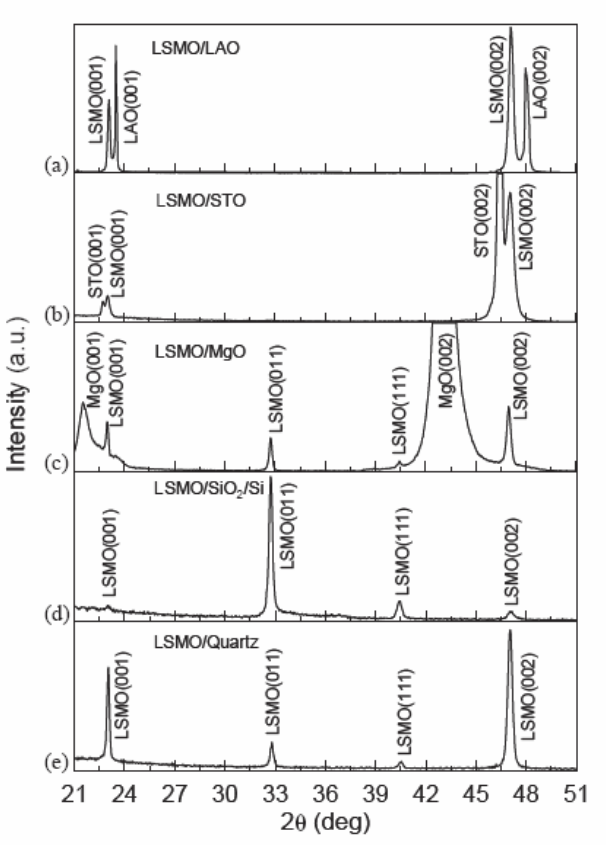

Figure 32
θ–2θ XRD patterns of the LSMO films deposited on single crystals of (a) $LaAlO_3$(0 0 1), (b) $SrTiO_3$(0 0 1), (c) MgO(0 0 1), (d) SiO_2/Si(0 0 1), and (e) amorphous quartz plate. Reprinted with permission Ref. 671.

Abrutis et al.[663] compared properties of $La_{1-x}Sr_xMnO_3$ thin films deposited on perovskite ($LaAlO_3$, $SrTiO_3$, $NdGaO_3$) and non-perovskite (yittria stabilized zirconia YSZ(001), MgO(001), r-plane sapphire) substrates by MOCVD. The films grown on the

non-perovskite substrates were found to have a broader semiconductor–metal transition and lower T_ρ values (~270, ~240, and ~210 K for films on YSZ, MgO, and sapphire, respectively, as compared to ~320 K for films on $LaAlO_3$). The inferior quality of the films on the non-perovskite substrates was attributed to incomplete epitaxy of the films on these more mismatched substrates rather than to strain effects, because the determined lattice c-parameter (~3.87 A˚) did not indicate the presence of biaxial strain in the films.

Integration of the perovskite manganites with technologically important Si substrates remains a challenging task for potential integrated device/systems applications such as information processing and data storage. In addition to the lattice and thermal mismatch, chemical reaction with Si substrates has to be taken into account. Various buffer layers have been used to to compensate for thermal and lattice mismatch and avoid interfacial reactions.[726,733,734, 735] For example, Pradhan et al.[734] achieved epitaxial growth of $La_{0.7}Ba_{0.3}MnO_3$ and $La_{0.7}Sr_{0.3}MnO_3$ films on Si(100) and Si(111) substrates using $SrTiO_3$ buffer layers. Gao and Hu[733] reported the fabrication of *p*-$La_{0.9}Ba_{0.1}MnO_3$(LMBO)/*n*-Si heterojunctions, with ultrathin $SrTiO_3$ buffer layers inserted between $La_{0.9}Ba_{0.1}MnO_3$ and Si to avoid oxidation of the silicon surface. The obtained $La_{0.9}Ba_{0.1}MnO_3$ films, however, were not epitaxial, but were consisted of (110) and (111)-oriented grains. $Bi_4Ti_3O_{12}$ layers can be used as templates for deposition of $La_{0.7}Sr_{0.3}MnO_3$ on Si, because $Bi_4Ti_3O_{12}$ is ideally lattice matched to $La_{0.7}Sr_{0.3}MnO_3$[726] and shows high affinity for c-axis oriented growth on any substrates. [736] Trajanovic, et al.[726] reported on the growth of high quality $La_{0.67}Sr_{0.33}MnO_3$ films on $Bi_4Ti_3O_{12}$/YSZ-buffered (001)Si substrates. From relative ~45° shift of ϕ -scan peaks of the $La_{0.67}Sr_{0.33}MnO_3$ and $Bi_4Ti_3O_{12}$, the authors found that $La_{0.67}Sr_{0.33}MnO_3$ grew along the

diagonal of the underlying $Bi_4Ti_3O_{12}$ lattice, thus minimizing the lattice mismatch and allowing for almost strain free growth of the manganite film. The same group reported PLD deposition of $La_{0.7}Sr_{0.3}MnO_3$ layers on SiO_2/Si (100) substrates using $Bi_4Ti_3O_{12}$ as a template.[735] In this case, both $Bi_4Ti_3O_{12}$ and $La_{0.7}Sr_{0.3}MnO_3$ layers were found to be *c*-axis oriented, but without any alignment in the *a*-*b* plane, in contrast to the in-plane aligned LSMO films on $Bi_4Ti_3O_{12}$/YSZ(001)Si templates.[726] These films exhibited a Curie temperature of 360 K which is comparable to that of an epitaxial LSMO film on $LaAlO_3$ substrates. However, the insulator-metal transition temperature was much lower (T_ρ = 220K), and the resistivity was several orders of magnitude higher than that for the epitaxial LSMO films. The difference in the transport properties between the textured $La_{0.7}Sr_{0.3}MnO_3$ films grown on the $Bi_4Ti_3O_{12}/SiO_2$/Si templates and the epitaxial films grown on $LaAlO_3$ substrates was attributed to spin tunneling through highly resistive grain boundaries present in the textured layers.

4.2.4.7 Influence of Layer thickness

Thickness is an important factor governing the electrical and magnetic properties of manganite films, because the mismatch stress induced by the clamping effect of the substrate is a strong function of the thickness. In general, the stress in epitaxial films increases with thickness and, after it reaches a critical value determined by film and substrate materials and growth temperature, strain relaxation proceeds in the films via introduction of defects at the interface. The effect of thickness on the manganite film properties has received much attention.[655,663,710,703,704,719,721,728,729, 737 , 738 , 739 , , 740 , 741 , 742,743,744,745,746,747] The effect of thickness on magnetoresistance,[663,704,719,721] insulator-to-

metal transition temperature,[663,719,721] the Curie temperature,[729,741,746] and coercive field [710,741] have been revealed. As an example, the relation between film thickness and film properties was studied by Abrutis et al.[663] for epitaxial $La_{1-x}Sr_xMnO_3$ thin films deposited on $LaAlO_3$, $SrTiO_3$ and $NdGaO_3$ substrates by MOCVD. The film thickness was varied from 8 to 300 nm. The LSMO films on $SrTiO_3$ substrates were under tensile strain, and those on $LaAlO_3$ and $NdGaO_3$ substrates were under compressive strain. From thickness dependences of the *c*-lattice parameter (Figure 33a), it was found that considerable strain present influenced properties only in very thin films (<60 nm). The films of thicknesses above ~100nm were completely relaxed. The semiconductor–metal transition temperature T_ρ and magnetoresistance for the films on three different substrates showed pronounced thickness dependences in the thickness range from 0 to 60 nm, and were saturated in the range from 60 to 300 nm (Figure 33c and d).

Similar results were obtained by Wang et al.,[721] who studied the strain effects on the structural and magnetotransport properties of $Pr_{0.67}Sr_{0.33}MnO_3$ films epitaxially grown on $LaAlO_3$(001), $SrTiO_3$(001), and $NdGaO_3$(110) substrates that induced biaxial compressive, tensile, and almost no strain, respectively. The film thickness was varied from 4 to 400 nm. Wang et al.[721] revealed two distinct thickness ranges with different thickness dependences of the magnetotransport properties. For thicknesses below 20 nm, the zero-field resistance peak temperature T_ρ and the high-field magnetoresistance (HFMR) were found to be critically dependent on the thickness and the substrate due to the substrate-induced strain. For thicknesses above 20 nm, T_ρ and the HFMR ratio showed weak thickness dependences. Okawa et al.[729] reported that thick (200 nm) $La_{1-x}Sr_xMnO_3$ (x = 0.3 and 0.4) films showed metallic and ferromagnetic properties simillar

to those of a bulk material with the Curie temperature T_C = 370 K, whereas thin (20 nm) films exhibit lower T_C and insulator properties due to epitaxial strain appearing in the thinner layers.

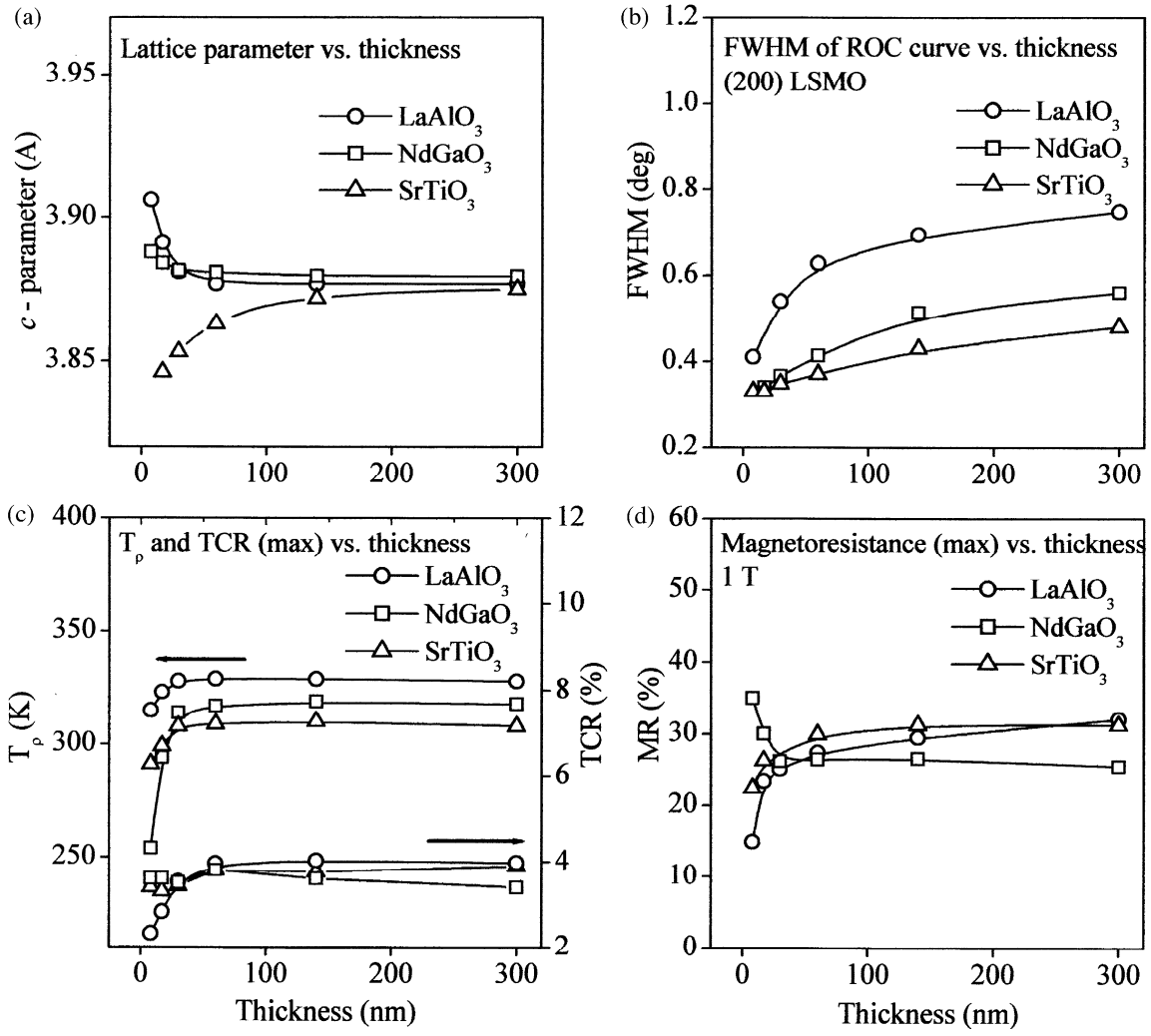

Figure 33
Effect of film thickness on the properties of LSMO films deposited on perovskite substrates at 825 C. Reprinted with permission Ref. 663.

4.3 Device applications of mixed-valence manganites

The unique correlation between the structure, electronic, transport, and magnetic properties of the mixed-valence manganites makes them promising candidates for magnetoresistive read heads, magnetoresistive random access memory, spintronic devices, magnetic-field sensors, and infrared detectors operating at ambient temperature. Due to their high temperature coefficient of resistance (TCR), the mixed-valence manganites are promising for bolometric detectors.[748,749,750] A bolometer is a device for detecting and measuring the energy of incident radiation. Therefore, a material for bolometric applications should possess high TCR, which allows small temperature variations caused by absorbed IR radiation to generate a significant voltage drop across the bolometer. Typical values of TCR of the manganites are 10%–15% over a temperature interval of ~10 K in the vicinity of the resistivity peak,[750] which is better than that for VO_x, a material commonly used for bolometer fabrication. Moreover, the manganite composition can be tuned so that the resistivity peak becomes closer to room temperature, which provides the possibility for ambient temperature operation.

In terms of other applications, hybrid structures consisting of high-temperature superconductor (HTSC) and mixed-valence manganite layers have been studied as potential candidates for use in spin-injection devices.[751,752,753,754,755] These HTSC-CMR structures take advantages of the perfect structural and lattice match between superconducting and CMR perovskite oxides and the half-metallic nature of the manganites, yielding better spin polarization than typical metallic ferromagnets.

In the last decade, MTJs have been extensively studied as potential candidates for memory element and magnetic-field sensor applications.[756, 757, 758] Employing half-metallic perovskite manganites in MTJs as electrodes makes such devices very promising.

Due to the high spin polarization of carriers, spin dependent tunneling between two ferromagnetic manganite electrodes across a thin insulating barrier should produce a very large MR response. For ideal half-metallic materials with 100% spin polarization, conductance is zero at T = 0 K in the antiparallel configuration and hence an infinite TMR is expected. A large TMR effect have been observed in LCMO-,[759,760,761] LSMO,-[583,762,763,764,765,766,767,768,769,770] and $La_{2/3}Ba_{1/3}MnO_3$−based MTJs.[771] Table 5 compares the values of TMR and polarization for TMJs based on the manganites and few other ferromagnetic materials.[772,773,774] As an illustration, Figure 34 shows the junction resistance *vs.* applied magnetic field for an $La_{0.7}Ca_{0.3}MnO_3/NdGaO_3/La_{0.7}Ca_{0.3}MnO_3$ junction obtained by Jo et al.[759] The measurements were carried out on a 6x6 μm^2 mesa at 77 K. The value of TMR, defined as $(R_{high}-R_{low})/R_{high}$ was found to be 86% with extremely sharp switching, where R_{high} and R_{low} are the high and low resistance states corresponding to antiparallel and parallel alignment of the magnetization of the two LCMO electrodes. Very large tunneling magnetoresistance up to 1200% was observed for $La_{2/3}Ba_{1/3}MnO_3/SrTiO_3/La_{2/3}Ba_{1/3}MnO_3$ trilayer structures grown on (001)$SrTiO_3$ substrates.[771] However, the most promising results were obtained for LSMO electrodes. Bowen *et al.*[762] performed magnetotransport measurements on $La_{2/3}Sr_{1/3}MnO_3/SrTiO_3/La_{2/3}Sr_{1/3}MnO_3$ magnetic tunnel junctions. A magnetoresistance ratio of more than 1800% is obtained at 4 K, from which a spin polarization in LSMO of at least 95% was deduced.

The main drawback of manganite electrodes from the standpoint of device application is that the large TMR effect observed at low temperatures vanishes even well below room temperature, which is definitely below T_C of LSMO (360 K).[583,760,762,770]

Figure 25 shows the temperature dependence of the TMR measured for an LSMO/STO/LSMO structure by Bowen *et al.*[762] One can see that the value of TMR drops drastically with decreasing temperature and completely vanishes at about 280 K. At 250 K, the TMR ratio was found to be 30% (Figure 35c), and at 270 K the TMR ratio was only 12%. [762] This decay in TMR is generally attributed to loss of the spin polarization at electrode/barrier interaces.[583,760,762,770] Indeed, deterioration of magnetic properties (lower T_C, smaller magnetization, reduction of the metallic character) is observed in manganites within a few nanometers from the manganite/insulator interface [775], [776] or the manganite surface. [777], [778] Such factors as separation into ferromagnetic metallic and nonmagnetic regions,[775,776] distortion of the Mn-O-Mn bonds,[770] spin canting in LSMO at the interface,[779] and the loss of cubic symmetry at the surface[778] have been considered as possible sources of weakening of ferromagnetism.

The large spin polarization of carriers, and consequently large TMR ratios, in the mixed-valence manganites makes them very attractive material for spintronics. Up to present, LSMO-based MTJs show the best figure of merit among the manganite-based tunneling structures. Unfortunalely, the TMR ratio of these MTJs decays rapidly with temperature, vanishing completely well below T_C. For real applications, however, the high polarization should persist at room temperature. Therefore, there is a need for further search for half-metallic materials with higher Curie temperatures as well as improved quality of manganite/insulator interfaces.

Table 5 Tunneling magnetoresistance (TMR) and spin polarization (P) for various ferromagnetic heterostructures

Magnetic material	Heterostructure	TMR (%)	P (%)	T (K)	Refs.
NiFe, CoFe	$Co/Al_2O_3/Ni_{0.8}Fe_{0.2}$ $Co/Al_2O_3/Co_{0.5}Fe_{0.5}$	<24	< 33	77	772
Co, Fe, Ni	Co, Fe, Ni foil & film		42 ~ 46.5	4	768
NiFe	$Ni_{0.8}Fe_{0.2}$ film		37 ± 5	4	768
NiMnSb			58 ± 2.3	4	768
CrO2			90 ± 3.6	4	768
$Co_{20}Fe_{60}B_{20}$	$Co_{20}Fe_{60}B_{20}/MgO/ Co_{20}Fe_{60}B_{20}$	472 804		RT 5	773
Co_2MnSi	Co_2MnSi/ amorphous Al oxide/ Co_2MnSi	570	83-89	6	774
LSMO	LSMO film		78 ± 4.0	4	768
LSMO	LSMO/STO/LSMO		81	4	579
LSMO	LSMO/STO/LSMO	400-450	> 82	4	769
LSMO	LSMO/ $PrBa_3Cu_{2.8}Ga_{0.2}O_7$ /LSMO	400-450	> 82	4	769
LSMO	LSMO/CeO_2/LSMO	400-450	> 82	4	769
LSMO	LSMO/STO/LSMO	1,850	> 95	4	762
LSMO	LSMO/STO/LSMO	540	92	4	770
LSMO	LSMO/TiO_2/LSMO	140	64	4	770
LSMO	LSMO/ $LaAlO_3$ (LAO)/LSMO	301	77.5	4	770
$La_{2/3}Ba_{1/3}MnO_3$	$La_{2/3}Ba_{1/3}MnO_3/SrTiO_3/$ $La_{2/3}Ba_{1/3}MnO_3$	1200		7	771
LCMO	$La_{0.7}Ca_{0.3}MnO_3$ /$NdGaO_3$ / $La_{0.7}Ca_{0.3}MnO_3$	86	86	77	759,760

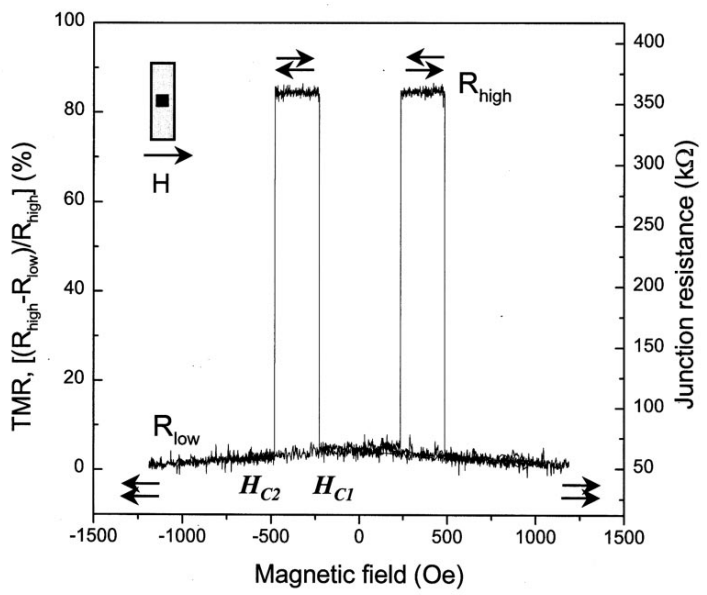

Figure 34 Tunneling junction resistance versus applied magnetic field for $La_{0.7}Ca_{0.3}MnO_3$ /$NdGaO_3$ /$La_{0.7}Ca_{0.3}MnO_3$ junction. Reprinted with permission Ref. 759.

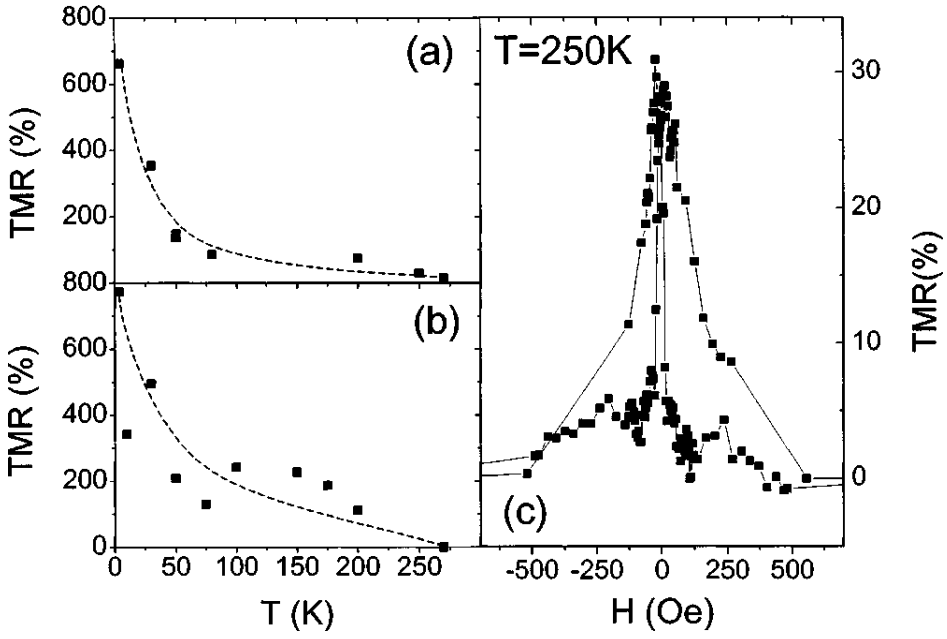

Figure 35 Temperature dependence of the TMR for two junctions: (a) 2x6 μm^2 and (b) 1.4x4.2 μm^2 . Dashed lines are guides to the eye. (c) $R(H)$ loop at T = 250 K showing 30% TMR. Reprinted with permission Ref. 762.

5 Multiferroics

As discussed in the Introduction Section, magnetoelectric multiferroic materials exhibit magnetic and ferroelectric ordering (and coupling between them) in a single phase. Due to their unusual physical properties and fascinating underlying physics, the magnetoelectric multiferroics have attracted extraoridinary scientific interest. In addition, the combination of magnetism and ferroelectricity makes them promising materials for multifunctional devices, and the magnetoelectric effect (i.e., a magnetic moment produced by an externally applied electric field or an electric moment produced by an externally applied magnetic field) provide additional degree of freedom in design of new devices such as tunable microwave passive components.

.

5.1 Brief history and basic properties of multiferroic materials

The first theoretical prediction of magnetoelectric effect in antiferromagnetic Cr_2O_3 is due to Dzyaloshinskii [780] in 1959, which was shortly followed by the experimental observations of this effect, both electrically and magnetically induced.[781,782,783,784,785] However, the magnetoelectric coupling coefficient of Cr_2O_3 has been found to be only $\alpha_M = \mu_0 \delta M / \delta E = 4.13$ ps/m, which is really very small for any practical application. The discouraging results in Cr_2O_3 led to a search for alternative single phase compounds. Subsequently, the magnetoelectric effect in compounds such as boracites $Ni_3B_7O_{13}I$, [786] $FeB_7O_{13}Cl$, and $Mn_3B_7O_{13}Cl$, [787] Ti_2O_3, [788] $GaFeO_3$, [789] Gd_2CuO_4, Sm_2CuO_4, $KNiPO_4$, $LiCoPO_4$, [790] $LiNiPO_4$, [791] garnets such as YIG [792] and $(YBiPrLu)_3(FeGa)_5O_{12}$, [793] $BaMnF_4$, [794] solid solutions such as $PbFe_{0.5}Ta_{0.5}O_3$ and $PbFe_{0.5}Nb_{0.5}O_3$, [795] , [796]

orthorhombic manganites $GdMn_2O_5$,[797] molybdate $Tb(MO_4)_3$, [798] $LiNiPO_4$,[799] hexagonal perovskite $YMnO_3$,[800] monoclinic perovskite $BiMnO_3$,[801,802] rhombohedral perovskite $BiFeO_3$, [803,804] $TbMn_2O_5$ and $TbMnO_3$,[805] hexaferrite $Ba_{0.5}Sr_{1.5}Zn_2Fe_{12}O_{22}$,[806] spinel $CdCrS_4$,[807] has been observed. Relatively large magnetoelectric coefficients were measured for $LiCoPO_4$ (30.6 ps m^{-1} at 4.2 K),[808] YIG films (30 ps m^{-1} at very low temperatures),[809] and $TbPO_4$ (36.7 ps m^{-1} at 1.92 K).[810] The first synthetic antiferromagnetic ferroelectric material $Pb(Fe_{2/3}W_{1/3})O_3$ and its solid solutions (1-*x*)$Pb(Fe_{2/3}W_{1/3})O_3$ - *x*$Pb(Mg_{1/2}W_{1/2})O_3$ was produced by Smolensky et al. in 1961.[811] In this compound, diamagnetic Mg^{2+} and W^{6+} ions provide ferroelectricity, while d^5 Fe^{3+} ion provides magnetic ordering. Since then, the number of newly synthesized magnetoelectric materials significantly increased to the point where there are some sixty members of such materials. It is interesting to note that almost all multiferroics are artificially synthesized materials except two of them – congolite $Fe_3B_7O_{13}Cl$ [812,813] and chambersite $Mn_3B_7O_{13}Cl$ [814].

Multiferroic materials have various crystal structures. Smolenskii and Chupis [815] divided them into four major multiferroic groups, although there are also some multiferroics with crystal structures not falling into these four groups.

(1) Compounds with perovskite crystal structure ABO_3, in which the B position is fully or partially occupied by magnetic ions. This group is the largest family, and the celebrated member of this family is bismuth ferrite $BiFeO_3$, which is considered perhaps the most promising multiferroic material due to high ferroelectric and ferromagnetic Curie temperatures. This class involves also

complex perovskite-like layered compounds with a general formula $A_{m+1}B_mO_{3m+3}$ where A=Bi, Ca, Sr, Ba, and B=Fe, Ti, Mo, Ni.

(2) Hexagonal-structure rare-earth manganites $RMnO_3$, where R= Ho, Er, Tm, Yb, Lu, as well as Y and Sc, which are good ferroelectrics with antiferromagnetic or weak ferromagnetic properties. Most studied member of this group is $YMnO_3$.

(3) Boracites, compounds of chemical formula $M_3B_7O_{13}X$, where M is a bivalent metal ion (M = Cr, Mn, Fe, Co, Cu, Ni) and X=Cl, Br, I, which are, as a rule, ferroelectrics and antiferromagnetics/weak ferromagnetics.

(4) Compounds with a general formula $BaMF_4$, where M=Mn, Fe, Co, Ni, Mg, Zn. This compounds exhibit pyro- or ferroelectric properties and are antiferromagnetic/weak ferromagnetic at rather low temperatures.

Some physical properties of known multiferroic materials at the time were summarized by Smolenski and Chupis in a review paper**.** [815] Table 6 lists the most studied multiferroic materials with most recent physical properties.[786, 787,801,806,816,817, 818,819,820,821, 822,823,824, 825, 826,827,828,829,830,831,832,833, 834, 835, 836, 837,838,839,840,841] As seen from this table, most of the multiferroics reported so far are antiferromagnets without spontaneous magnetization, and most of the compounds have their Néel or Curie temperature far below room temperature. For now, only a few multiferroics are known to have magnetic and ferroelectric ordering above room temperature, one of which is bismuth ferrite $BiFeO_3$ with ferroelectric and magnetic ordering below 1100 K and 643 K, respectively. Although the mutual control of electric and magnetic properties is an attractive possibility,

the number of candidate materials is, therefore, limited, and the effects are typically too small to be useful in real applications.

Table 6 Multiferroic materials along with their physical properties

Multiferroics	Space group	Crystal structure	Magnetic ordering	Electrical ordering	$T_{N,M}$, K	T_C, K	Ref.
$YMnO_3$	$P6_3cm$	hexagonal	AFM	FE	70 -80	914	816,817
$YbMnO_3$	$P6_3cm$	hexagonal	AFM	FE	87	983-993	787,818
$HoMnO_3$	$P6_3cm$	hexagonal	AFM	FE	72 (~49[819])	875	820
$TmMnO_3$	$P6_3cm$	hexagonal	AFM	FE	86	>573 (348[821])	787,818
$TbMnO_3$	Pbnm	orthorombic	AFM	FE	41	28	822,841
$DyMnO_3$	Pbnm	orthorombic	AFM	FE	~40	~19	823
$LaMnO_3$	Pbnm	orthorombic	AFM		140		819
$BiMnO_3$	C2	monoclinic	FM	AFE	105	723	801,824, 825
$BiFeO_3$	R3c	rhombohedral	AFM	FE	643	1100	826,827, 828
$BiCrO_3$	C2/c	monoclinic	AFM	AFE	109	420	829,830
$HoMn_2O_5$	Pbam	orthorombic	AFM	FE	~45	~39	831,832
$ErMn_2O_5$	Pbam	orthorombic	AFM	FE	~45	~39	831,832, 833
$TmMn_2O_5$	Pbam	orthorombic	AFM	FE	~45	~36	832,833
$TbMn_2O_5$	Pbam	orthorombic	AFM	FE	~45	~38	832,833
$DyMn_2O_5$	Pbam	orthorombic	AFM	FE	~42	~38	832,833, 834
YMn_2O_5	Pbam	orthorombic	AFM	FE	~45	~41	832,833
$BiMn_2O_5$	Pbam	orthorombic	AFM	FE	39	~38	832,833, 835
$Ni_3B_7O_{13}I$	$F\bar{4}3c$ (77 K) $Pca2_1$ (<62K)	cubic orthorhombic	AFM	FE	~120	<64	786,836
$Ba_{0.5}Sr_{1.5}Zn_2Fe_{12}O_{22}$	$R\bar{3}m$	hexagonal	noncollinear helical spin structure	FE under applied magnetic field	326	~130	806,837
Bi_2FeCrO_6	R3	rhombohedral	ferrimagnetic		between 600 and 800	above RT	838,839840

There has been some degree of debate regarding the origin of magnetoelectric coupling in multiferroic materials, because the notion implies coexistence of the

ferroelectricity and magnetic ordering in the same material, even though the physical mechanisms underlying these two phenomena are different and tend to exclude one another.[33,842,843,844,845,846] From first-principles calculations, Filippetti and Hill[843] have found the fundamental role of *d* orbital occupation in preventing or favoring the simultaneous presence of magnetic and electric polarization. In ferroelectric materials, spontaneous polarization is achieved by the small transition-metal cation at the center of the octahedron of oxygen anions being moved off the center position through distortion. In order for the distortion to occur, the *d* orbitals in the direction of the electric polarization must be empty (so called d^0-ness). On the other hand, the magnetic spin polarization is achieved by the presence of partially filled *d* states. Spin-polarization is meant to show the presence of any kind of local moments ordered either ferro- or antiferromagnetically. Therefore, the existence of ferroelectricity, requiring empty *d* orbitals, is inconsistent with the occurrence of spin polarization which requires partially filled *d* orbitals. It was concluded that some additional electronic or structural driving force would have to be present for magnetism and ferroelectricity to occur simultaneously in the same material.[33,844] For this to take place, the d^0 rule must be broken which can occur if the particulars of the chemistry or structure create an asymmetric potential with a double potential well, in spite of the *d* occupation of the magnetic cation, *i.e.* a new mechanism for ferroelectricity takes place.[33,844] For example, in the hexagonal yttrium and rare-earth manganites, polarization originates from the buckling of the MnO_5 polyhedra accompanied by a displacements of *R* ions.[33,844,846,847] In $BiMnO_3$ and $BiFeO_3$, the asymmetry is caused by the Bi-O hybridization.[33, 845,848,849] It should be noted, hovewer, that the detailed mechanisms of the magnetoelectric effect are

not yet completely understood and warrant further theoretical and experimental investigations.

Next in this section we will consider the properties of some of the most studied and most promising magnetoelectric multiferroic materials.

5.2 Bi-based perovskite oxides

5.2.1 $BiFeO_3$

As stated earlier, $BiFeO_3$ (BFO) is one of the single phase multiferroic materials with high ferroelectric Curie (Tc=830 °C) and antiferromagnetic Néel (T_N =370 °C) temperatures that makes it attractive for magnetoelectric applications. For this reason there have been extensive studies of the structure and properties of bulk and thin film BFO. Bulk BFO has a rhombohedrally distorted perovskite structure (a_{rh}=5.6343 Å and α_{rh}=59.348°) with space group $R3c$.[827,850,851] Figure 36 shows the structure of a primitive unit cell of BFO, which contains two formula units (ten atoms), arising from counter rotations of neighboring O octahedra about the [111] axis.[851] The displacement of Bi, Fe, and O ions from their ideal positions along the [111] axis results in spontaneous polarization along [111].[851] BFO exhibits a G-type antiferromagnetic ordering, where the Fe magnetic moments are aligned ferromagnetically within the (111) planes and antiferromagnetically between the adjacent (111) planes. Bulk BFO exhibits also a spiral spin structure, where the antiferromagnetic axis rotates through the crystal with a long-wavelength period, superimposed on the antiferromagnetic ordering, of 620 Å, whichcancels macroscopic magnetization leading to an extremely small saturation magnetization.[852,853]

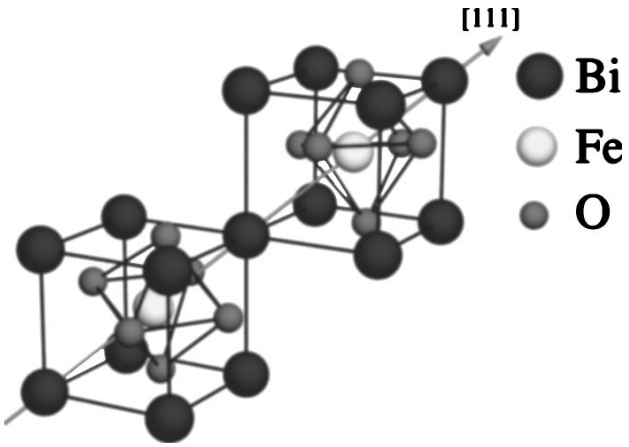

Figure 36 Structure of R3c $BiFeO_3$. Notice the position of the oxygen octahedra relative to the Bi framework; in the ideal cubic perovskite structure the oxygen ions would occupy the facecentered sites. Reprinted with permission Ref. 851.

Today, there are several challenges facing BFO that must be overcome before this material can be considered suitable for practical applications. These challenges are *i*) high leakage current, *ii*) small remanent polarization, *iii*) high coercive field, and *iv*) inhomogeneous magnetic spin structure. Of these challenges, large leakage current is the most serious factor limiting the applications of BFO. The large leakage current is usually attributed to deviation from oxygen stoichiometry, which leads to the change in oxidation state of Fe ions (from Fe^{3+} to Fe^{2+}) in order to compensate for the charge of oxygen vacancies. The coexistence of Fe^{3+} and Fe^{2+} causes electron hopping between Fe^{3+} and Fe^{2+} ions, oxygen vacancies acting as a bridge between them, which increases the leakage current.[854, 855, 856, 857] The inhomogeneous spin structure results from the spatially modulated, cycloidal spin structure with the periodicity of about 620 Å, which is incommensurate with the crystallographic lattice parameters. Several approaches have been proposed to overcome the spiral spin structure, among which are doping and

formation of $BiFeO_3$-based solid solutions [858,859,860,861] and application of high magnetic field [858, 862] and strain. [863],[864]

Until recently, the value of polarization in bulk BFO was considered to be small, with spontaneous polarization on the order of a few $\mu C/cm^2$ and non-saturated hysteresis loops.[828] However, epitaxial BFO films have attracted significant interest when strong multiferroic behavior together with large values of magnetization and electric polarization were reported by Wang et al. [863] in 2003. For BFO films epitaxially grown on $SrTiO_3$ substrates, they found very high spontaneous polarization up to 50-60 $\mu C/cm^2$, some one order of magnitude higher than that for bulk BFO, and a saturation magnetization of 150 emu/cm^3. The magnetization was stated to be dependent on the film thickness. The huge difference in the properties of the BFO films from the bulk material was attributed to the difference in the crystal structure of the thin films under investigation caused by the mismatch strain. It should be noted however that, although large polarization values for BFO films were also reported by other groups,[865,866,867,868,869,870] Wang et al.[863] is the only group so far who reported such high values of magnetization, and the accuracy of the data as well as the mechanism of the enhancement of magnetization and polarization is still under discussion.[871],[872]

BFO layers were grown by all the conventional growth methods such as PLD, [863,865,866,867, 873] MOCVD, [874] , [875] chemical solution deposition (CSD), [876] , [877] RF sputtering,[878,879] and sol-gel.[880,881] Epitaxial BFO films show much higher polarization values that bulk samples[865,866,867,868,870] which is consistent with theoretical considerations [851,869] and can be explained by improved crystal quality and stoichiometry, different structural modifications stabilized in the thin films,[867,870] or within the modern theory of

polarization.[851, 882,883,884] Structural and physical properties of epitaxially grown BFO films were found to depend on ambient oxygen pressure during PLD growth.[865,867,885] For example, Yun et al.[867] have found that the crystal structure and lattice constant of BFO films depend strongly on the oxygen pressure. In this study, the BFO films deposited at various oxygen pressures were single phase with a tetragonally destorted perovskite structure, in spite of the fact that bulk BFO is known to be a rhombohedrally distorted perovskite. The c/a ratio of the films decreased from 1.032 to 1.014 as the oxygen pressure decreased from 0.15 to 0.005 Torr. The tetragonal distortion in epitaxial BFO films is attributed generally to the mismatch strain, and the dependence of the *c*/*a* ratio on the oxygen pressure was attributed by the authors to both the lattice strain and oxygen stoichiometry in the films.[867]

Fujino et al. [885] deposited BFO thin films by ablating a $Bi_{1.1}FeO_3$ target with a KrF excimer laser ($\lambda = 248$ nm) at a typical fluence of 2 J/cm^2. The oxygen pressure during deposition was varied in the range from 10^{-4} to 10^{-1} Torr, and the substrate temperature was kept constant at 600 °C. Epitaxial BFO films with (001) orientation were obtained at oxygen pressures above 1×10^{-3} Torr. Figure 37 shows the phase composition of the BFO films as a function of oxygen pressure. At low pressures ($< 2 \times 10^{-2}$ Torr), the Fe_2O_3 phase was found in the BFO films, and the portion of the Fe_2O_3 increasing as the oxygen pressure decreased. Pure BFO phase was identified by XRD for a pressusre range from 5×10^{-3} Torr to 5×10^{-2} Torr. At high oxygen pressures ($> 5 \times 10^{-2}$ Torr), the Bi_2O_3 phase was observed, and the Bi_2O_3 content in the films increased with pressure.

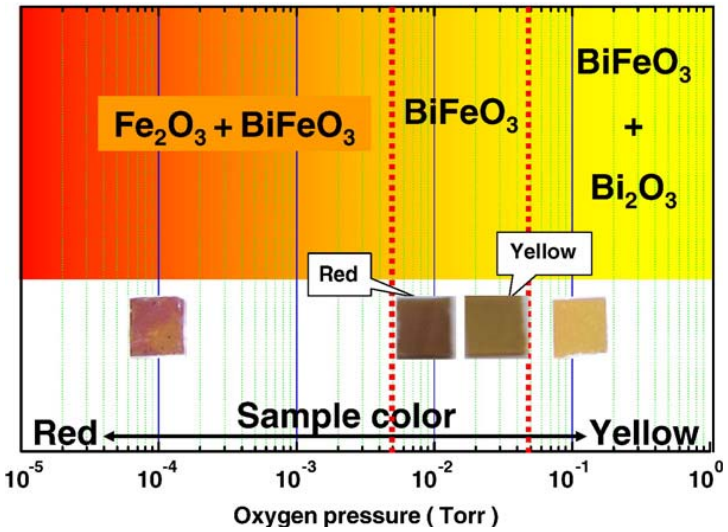

Figure 37 Summary of phases present in BFO films as a function of oxygen deposition pressure as determined by XRD analysis. The sample color changes from yellow to red. Reprinted with permission Ref. 885.

Li *et al*.[870] investigated the effect of the orientation of epitaxial BFO films on their remanent polarization. For this investigation, the (001)-, (101)-, and (111)-oriented films were grown by PLD on (001), (110) and (111) $SrTiO_3$ substrates, respectively. The BFO films grown on (111) substrates had a rhombohedral structure, identical to that of bulk single crystals; whereas the films grown on (101) or (001) substrates were monoclinically distorted from the rhombohedral structure due to the epitaxial constraint. The remanent polarization P was found to be ~55, ~80, and ~100 $\mu C/cm^2$ for the (001)-, (101)-, and (111)-oriented films, respectively. Figure 38 shows the values of $\sqrt{3}P_{(001)}$, $\sqrt{2}P_{(101)}$, and $P_{(111)}$ *vs.* electric field for the oriented films with different orientations. One can see, that the values of the projected polarizations are nearly equivalent, indicating that the axis of spontaneous polarization lies close to (111) for all orientations, and that the values measured along (101) and (001) are simply projections onto these orientations.

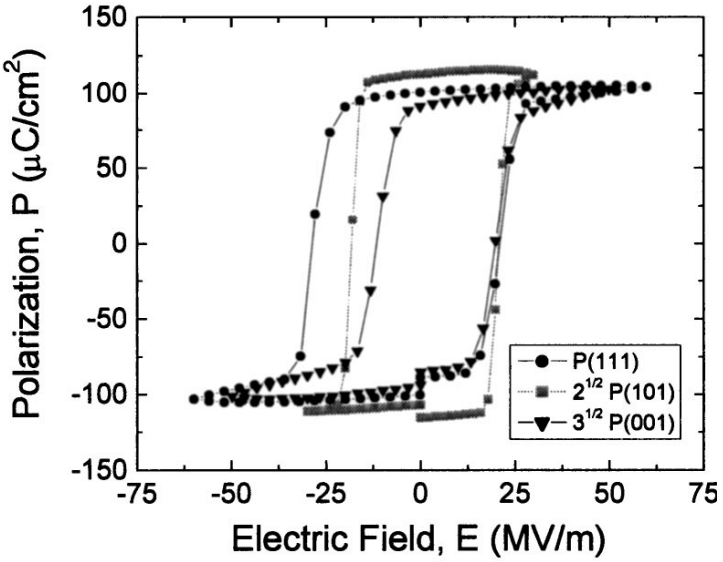

Figure 38 *P–E* curve (001), (101), (111) BiFeO3 films projected onto (111). Reprinted with permission Ref. 870

As mentioned above, one of the major problems limiting device applications of BFO is the large leakage current caused by coexistence of Fe^{3+} and Fe^{2+} ions, which in turn results from charge compensation of oxygen vacancies.[854,855,856] According to the defect chemistry theory, doping of BFO with aliovalent ions should change the oxidation state of iron and the concentration of oxygen vacancies, paving the way for control over the leakage current in BFO. Qi et al.[886] proposed to dope BFO with aliovalent Ti^{4+} and Ni^{2+} ions, which substitute for the Fe^{3+} ions and are similar in size with Fe^{3+}. The authots have suggested that the charge compensation in the 4+ cation-doped material can be achieved by one or more of the following mechanisms: filling of oxygen vacancies, decrease of cation valence by formation of Fe^{2+}, and creation of cation vacancies. On the other hand, charge compensation in BFO doped with 2+ charged ions can be realized by creating oxygen vacancies or increasing cation valence by transformation of Fe^{2+} to Fe^{3+}. Doping with Ti^{4+} hence is expected to eliminate oxygen vacancies and possibly to

increase Fe^{2+} content, whereas doping with Ni^{2+} is expected to introduce more oxygen vacancies and to prevent the formation of Fe^{2+}. The performed experiments showed that, indeed, doping of BFO thin films with 2 % Ti^{4+} resulted in the increase in resistivity by more than three orders of magnitude. In contrast, doping with Ni^{2+} reduced the resistivity by two orders of magnitude. Analysis of the *I–V* characteristics indicated that the main conduction mechanism for pure and Ni^{2+} doped BFO was space-charge limited, which was associated with free carriers trapped by the oxygen vacancies, while the field-assisted ionic conduction was dominant in the Ti^{4+} doped samples. The lower resistivity of the Ni^{2+} doped films was attributed to the higher concentration of oxygen vacancies and, consequently, higher density of free carriers. This have led authors to the conclusion that oxygen vacancies rather than Fe^{2+} ions are responcible for the high conductivity of BFO.[886]

The above mentioned approach was used by Chung et al.[877] to study the influence of Mn and Nb doping on the electrical properties of BFO films grown by the CSD method. They found that doping with Nb^{5+} resulted in the increase of BFO film resistivity, while doping with Mn, which was partially in Mn^{2+} state, resulted in the opposite effect, that is a decrease of resistivity, in agreement with previous results.[886] Increase of the electrical resistivity of BFO ceramics by approximately six orders of magnitude due to Nb doping was reported by Jun et al.[887] Singh and Ishiwara[888] have found a similar effect with Mn doping on BFO film resistivity. In their experiments, the leakage current density increased steadily with increase of the Mn concentration in the films. However, the breakdown characteristic of the films containing 3%–5% Mn was considerably improved so that at electric fields > 0.6 MV/cm the leakage current density for the doped films was

much lower than that for the undoped BFO. As a result, the BFO films doped with 5% Mn showed well saturated polarization hysteresis loops with a remanent polarization of 100 μC/cm^2 at the measurement frequency of 1 kHz.

In order to improve the ferroelectric properties of BFO thin films grown by chemical solution deposition, Kim et al.[889] doped the films with Cr, which substituted for Fe in BFO. It was found that doping with 3% Cr considerably improved P-E hysteresis characteristics and reduced the leakage current by approximately four orders of magnitude. A large room temperature remanent polarization of 61 μC/cm^2 was observed for the Cr-doped films. The authors presumed that Cr in BFO thin film suppresses the formation of oxygen vacancies, thus decreasing conductivity of the films.

Doping with Ba also was proposed for improving magnetic properties of BFO. Wang et al.[890] studied Ba-doped single-phase BFO ceramics with Ba content up to 25%. These samples exhibited ferromagnetism and ferroelectricity simultaneously at room temperature. The origin of spontaneous magnetization was explained by two possible reasons. One possibility is that Ba distorts the structure of BFO, changing the Fe–O–Fe bond angle, which results in the magnetization of $Bi_{1-x}Ba_xFeO_3$. Another possible explanation is that adding Ba^{2+} ions in BFO requires charge compensation, which can be achieved by formation of Fe^{4+} or oxygen vacancies. If Fe^{3+} and Fe^{4+} ions coexist in the lattice, their statistical distribution in the octahedral may also lead to net magnetization and ferromagnetism.[858] Magnetoelectricl coupling in $Bi_{1-x}Ba_xFeO_3$ was evidenced by the increase of the dielectric constant ε_r with the applied magnetic field, as shown in Figure 39. Here, the magnetoelectric effect is defined as $[\varepsilon_r(H)- \varepsilon_r(0)]/\varepsilon_r(0)$. One can see that the dielectric constant increases with an increase of magnetic field, and the positive values of

the magnetoelectric effect are temperature dependent. At 300 K and H=8 kOe, the values of magnetoelectric effect are 0.8% and 1% for x=0.15 and 0.25, respectively. At 80 K, these values are 1.5% and 1.7% for x=0.15 and 0.25, respectively. The increase in the values of the magnetoelectric effect at low temperature was attributed to the increase of magnetic ordering, which strengthened the sublattice interaction.[890]

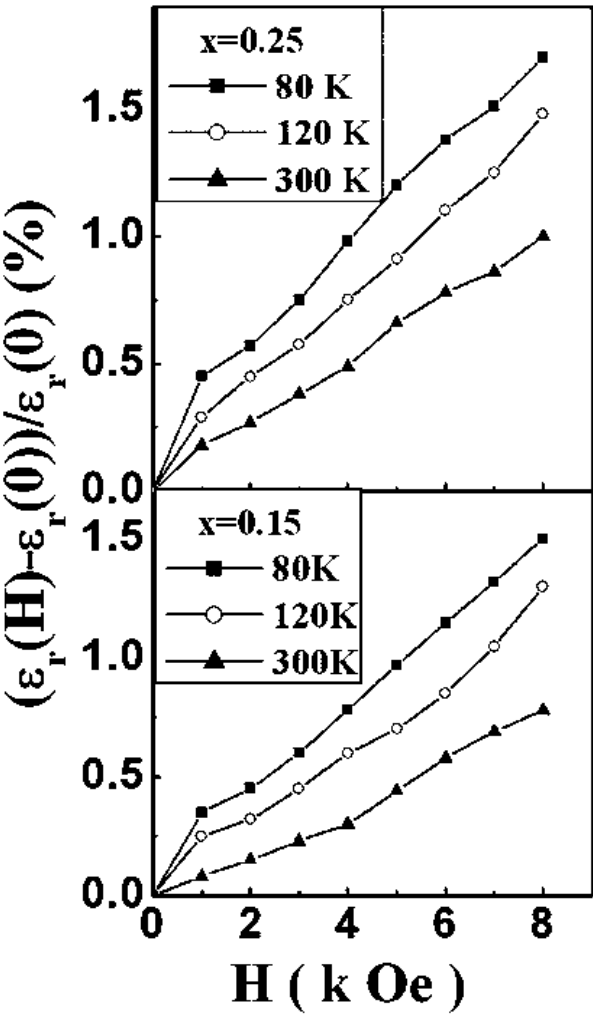

Figure 39 Magnetic field-induced change in dielectric constant of $Bi_{1-x}Ba_xFeO_3$ (x=0.15,0.25) measured at 80, 120, and 300 K. Reprinted with permission Ref. 890.

Doping of BFO with rare-earth ions substituting for Bi sites, such as La^{3+} and Nd^{3+}, is also of great interest. As indicated earlier in Section 3.2.4, doping of $Bi_4Ti_3O_{12}$

with La^{3+} and Nd^{3+} cations suppresses the formation of oxygen vacancies due to the substitution of volatile Bi with the rare-earth cations, which enhances the ferroelectric properties of this material.[247] In La-doped BFO ($Bi_{1-x}La_xFeO_3$), substitution of Bi with La could also suppress the inhomogeneity of magnetic spin structure, stabilizing macroscopic magnetization of BFO, because orthorhombic $LaFeO_3$, the other endpoint of the$BiFeO_3$–$LaFeO_3$ solid solution, exhibits homogeneous antiferromagnetic order (T_N=740 °C). [891,892] These ideas spawned a number of investigations on the influence of La and Nd doping on polarization switching, ferroelectric reliability, and multiferroic properties of BFO films. [893,894,895,896]

Zhang et al.[895] performed La doping of BFO ceramics in the concentration range from 5 to 40 % and found a transition from rhombohedral to orthorhombic phase near x=0.30. This phase transition was found to destruct the spin cycloid of BFO that resulted in enhanced magnetoelectric interaction and improved multiferroic properties of the $Bi_{0.7}La_{0.3}FeO_3$ ceramics with remanent polarization $2P_r$ = 22.4 μC/cm^2 and magnetization $2M_r$ = 0.041 emu/g. An increase of saturation magnetization with La concentration (varying between 0 and 15%) was observed also for La-doped BFO epitaxial films on $SrRuO_3$-buffered $SrTiO_3$ (001) substrates.[894] Capacitors fabricated in this work showed fatigue-free ferroelectric switching characteristics up to 4×10^{10} read/write cycles at a frequency of 1 MHz. Similar effect of La doping on magnetization was reported by Lee et al.[893] for thin films grown on $BaPbO_3$/Pt/TiO_x/SiO_2/Si templates by rf-magnetron sputtering. Remanent polarization and dielectric constant of the La-doped BFO films were increased and polarization switching and the fatigue behavior of the BFO films were significantly improved due to La doping.

Different results were reported by Uchida et al.,[896] who observed continuous crystal anisotropy and Curie temperature degradation with increasing contents of La^{3+} or Nd^{3+} cations of BFO films. La- and Nd-substituted BFO films with chemical compositions of $(Bi_{1-x}M_x)Fe_{1.0}O_3$ (x=0–0.15, M=La or Nd) were fabricated on (111)Pt/TiO_2/SiO_2/(100)Si substrates using a chemical solution deposition technique. Polarization (P)-electrical field (E) hysteresis loop measured at 10 K revealed that the intrinsic remanent polarization of La^{3+}- and Nd^{3+}-substituted BFO films with x=0.05 were 44 and 51 $\mu C/cm^2$, respectively, smaller than that of an undoped BFO film (79 $\mu C/cm^2$), which was ascribed to the degradation of crystal anisotropy and the Curie temperature of the BFO crystals. However, in agreement with previous reports, the leakage current density of the BFO films at room temperature lowered due to the doping from approximately 10^{-3} down to 10^{-6} A/cm^2.

5.2.2 $BiMnO_3$

$BiMnO_3$ is one of the few magnetoelectrics with ferromagnetic ordering [897,898,899] (see Table 6). From the powder neutron-diffraction data collected at 20 K, dos Santos et al. [900] revealed a collinear ferromagnetic structure with the spin direction along [010] and a magnetic moment of 3.2 μB. The ferromagnetism in $BiMnO_3$ was attributed to the orbital ordering that produces three-dimensional ferromagnetic super-exchange interaction. $BiMnO_3$ has a monoclinic structure with unit-cell parameters a=59.5317(7) Å, b=55.6047(4) Å, c=59.8492(7) Å, and β=5110.60(1)°.[900] The monoclinic structure of $BiMnO_3$ can be considered as a distorted perovskite structure, achieved by distorting and rotating the MnO_6 octahedra in the simple cubic perovskite structure. [824] As for electric properties, $BiMnO_3$ is an insulator and ferroelectric below the ferroelectric Curie

temperature of 720–770 K.[801, 901] Dos Santos *et al.*[801] demonstrated ferroelectric hysteresis loops at room temperature and below, but the value of polarization was found to be rather small (0.13 and 0.043 μC cm^{-2} at 87 and 200 K, respectively). The coupling between the ferroelectric and ferromagnetic orders in $BiMnO_3$ was confirmed experimentally: Kimura et al.[902] observed pronounced changes in the dielectric constant induced by the magnetic ordering as well as a strong magnetic field dependence of the dielectric constant near the ferromagnetic transition temperature.

The origin of ferroelectricity in $BiMnO_3$ is, however, still under discussion. Until recently, this compound was believed to have non-centrocymmetric lattice structure with space group C2, which allows the existence of ferroelectricity.[900, 903] The off-center distortion responsible for the polar structure of $BiMnO_3$ was attributed to stereochemical activity of the $6s^2$ lone pairs of electrons on the Bi^{3+} ions.[848,900] Hovewer, several groups have reported theoretical and experimental studies indicating that $BiMnO_3$ might crystallize rather in the centrosymmetric C2/c than in the noncentrosymmetric C2 structure, which is incompatible with ferroelectricity.[904,905 906,907] Ferroelectricity in the centrosymmetric $BiMnO_3$ structure was proposed to arise from local non-centrosymmetry[908] or oxygen-deficient superlattice.[905] Very recently, Yokosawa et al.[824] have performed thorough selected-area electron diffraction (SAED) studies to gain further information on the symmetry of the $BiMnO_3$ structure. In the SAED patterns, they observed *h*0*l* (*l*=2*n*+1) and *h*0*l* (*h*=2*n*+1) reflections, indicating the noncentrosymmetric long-range (space group C2) and short-range (P2 or $P2_1$) ordered structures, respectively. These reflections were not detected in structurally related $BiScO_3$ and $BiCrO_3$, indicating that these compounds belong to centrosymmetric *C*2/*c*. The authors concluded that the

noncentrosymmetric long-range ordered structure (*C*2) of $BiMnO_3$ is attributed not only to Bi^{3+} ions with lone electron pair, but also to Mn^{3+} ions, that is, to correlation between Bi^{3+} and Mn^{3+} ions.

As was sited above, Kimura et al.[902] observed the negative magnetodielectric effect in the vicinity of the magnetic transition in $BiMnO_3$. The effect was rather weak however, maximum 0.6% at 9 T. More recently, Yang et al.[909] have suggested that the magnetoelectric coupling in multiferroic materials exhibiting a large difference in the ferroelectric and magnetic transition temperatures would be enhanced if one can bring the electric and magnetic transitions into the same temperature region. In $BiMnO_3$, as an example, magnetism and ferroelectricity originates from different sourses: the ferromagnetic order is due to Mn ions, whereas the ferroelectricity is due to $6s^2$ lone pairs of Bi^{3+} ions. For this reason, $BiMnO_3$ exhibits a large gap between the ferroelectric and ferromagnetic transition temperatures. In order to bring the ferroelectric transition temerature of $BiMnO_3$ close to the magnetic one, Yang et al.[909] randomly replaced Bi ions with La ions. A $Bi_{0.8}La_{0.2}MnO_3$ thin film was deposited on a conducting (111) $SrTiO_3$ substrate by pulsed laser deposition. The $Bi_{0.8}La_{0.2}MnO_3$ film showed a broad ferroelectric transition below 150 K and ferromagnetic ordering below 110 K. The magnetization value for these films reaches ~230 emu/cm^3 (1.6 μB per Mn ion), which is much lower than that for bulk $BiMnO_3$ (3.6 μB per Mn[801]). It is interesting that La substituting for Bi ions has an effect on the magnetic state of $BiMnO_3$ despite the fact that the replacement occurs in nonmagnetic ions. On the contrary, the value of polarization is much higher than that for the bulk material: 12 μC/cm^2 for the $Bi_{0.8}La_{0.2}MnO_3$ film as compared to 0.13 μC/cm^2 at 87 K for bulk $BiMnO_3$.[801] The enhancement polarization in

$Bi_{0.8}La_{0.2}MnO_3$ was believed to come from uncanceled dipole moments in the vicinity of La ions and/or from strain in the film. The temperature dependence of polarization of the films shows two abrupt features: as the temperature decreases, the polarization increases sharply at ~150 K, slows down below 110 K, then again rises rapidly, and finally saturates. The increase in polarization at ~150 K obviously indicates the onset of ferroelectric ordering, while the second the abrupt increase is most likely related to the onset of magnetic ordering, since it occurs in the range of the rapid increase in magnetization. A correlation between the magnetic and ferroelectric degrees of freedom in $Bi_{0.8}La_{0.2}MnO_3$ is further confirmed by the magnetic field dependence of pyroelectric current.

5.2.3 $BiCrO_3$

As compared to its neighbors $BiMnO_3$ and $BiFeO_3$, little is known about $BiCrO_3$.[829,830, 910,911,912] Bismuth chromite was first synthesized by Sugawara et al.[913] in 1968 and was reported to be antiferromagnetic below 123 K with a weak parasitic ferromagnetic moment. **A**ccurate structural parameters of polycrystalline $BiCrO_3$ have been determined recently by Belik et al.[829] from neutron diffraction data measured in a wide temperature range. It was found that above 420 K $BiCrO_3$ crystallizes in the orthorhombic system (space group *Pnma*) in the $GdFeO_3$-type structure. In the temperature range from 420 to 7 K, $BiCrO_3$ has a highly distorted perovskite-type structure of monoclinic symmetry (space group *C*2/*c),* with the lattice parameters *a*= 9.4641(4) Å, *b* = 5.4790(2) Å, *c* = 9.5850(4) Å, and β = 108.568(3)°at 7 K.

From first-principles density functional calculations, $BiCrO_3$ was predicted to have a G-type antiferromagnetic ordering (in which each Cr^{3+} ion is surrounded by

neighbors of the opposite spin).[910] This prediction was confirmed experimentally based on neutron diffraction data.[829] Figure 40 illustrates the magnetic structure of $BiCrO_3$. Below the transition temperature, magnetic moments of Cr^{3+} ions are coupled antiferromagnetically in all directions, forming the so-called G-type antiferromagnetic structure. Four anomalies of magnetic origin were found near 40, 75, 109, and 111 K in BiCrO3.[912]

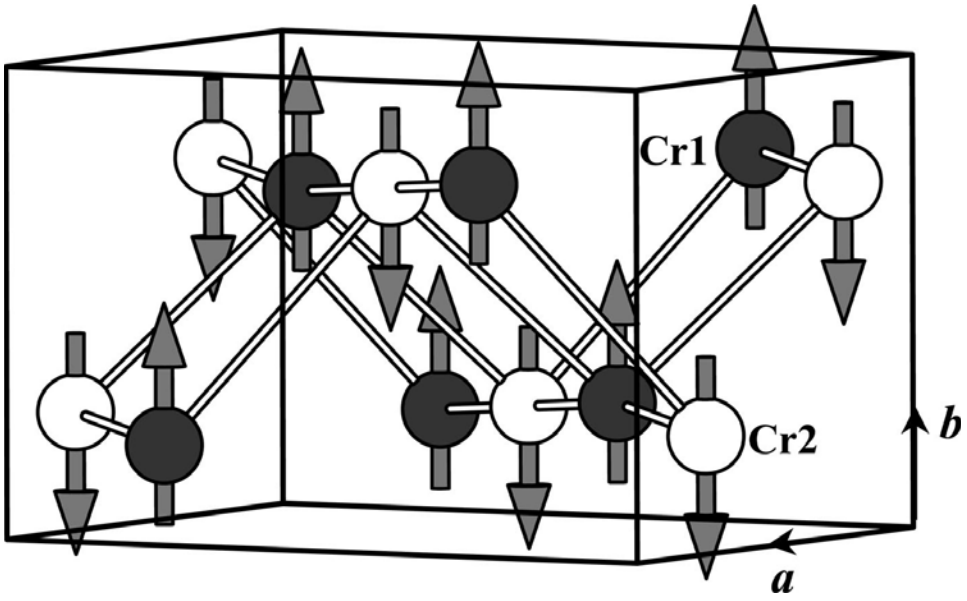

Figure 40 Magnetic structure of $BiCrO_3$ with solid lines displaying the unit (chemical and magnetic) cell. Arrows show the direction of the magnetic moments below T_N. Reprinted with permission Ref. 829.

As for electric properties of $BiCrO_3$, antiferroelectric ordering was predicted theoretically[910] and later observed experimentally on $BiCrO_3$ thin films.[830] The first-principles density functional calculations performed by Hill et al.[910] predicted a G-type antiferromagnetic ground state of $BiCrO_3$, with an antiferrodistortive or antiferroelectric structural distortion, similar to that in $PbZrO_3$. It was found that, like $BiMnO_3$ and

$BiFeO_3$, $BiCrO_3$ is unstable in the ideal cubic perovskite phase, and the structural instability is driven by the stereochemical activity of the Bi lone pair. Cr^{3+} ions, however, resist the off-center displacement and prefer to retain in the ideal octahedral environment.[910] To study ferroelectric properties of $BiCrO_3$ experimentally, Kim et al.[830] grew epitaxial $BiCrO_3$ films on $SrTiO_3$ (001) substrates with $SrRuO_3$ bottom electrodes by pulsed laser deposition. Figure 41a presents the electric field dependence of dielectric constant ε_r for a $BiCrO_3$ film measured at 10 kHz by decreasing and increasing the dc bias. The dependences show two distinct maxima around ±150 kV cm^{-1} with a clear hysteretic behavior. The electric field dependence of polarization also reveals double hysteresis loop (Figure 41b). The polarization value for the $BiCrO_3$ film is relatively small, ~12 $\mu C/cm^2$ at a maximum applied field of 700 kV/cm. The small remanent polarizations at zero field was attributed to a small leakage current of the capacitor. The double hysteresis loops in the electric field dependences of the dielectric constant and polarization is a clear indication of antiferroelectric ordering in the $BiCrO_3$ film. The lack of off-center displacement of the Cr^{3+} ions, as predicted by Hill et al.,[910] was suggested to be responcible for the antiferroelectric rather than ferroelectric order in $BiCrO_3$.

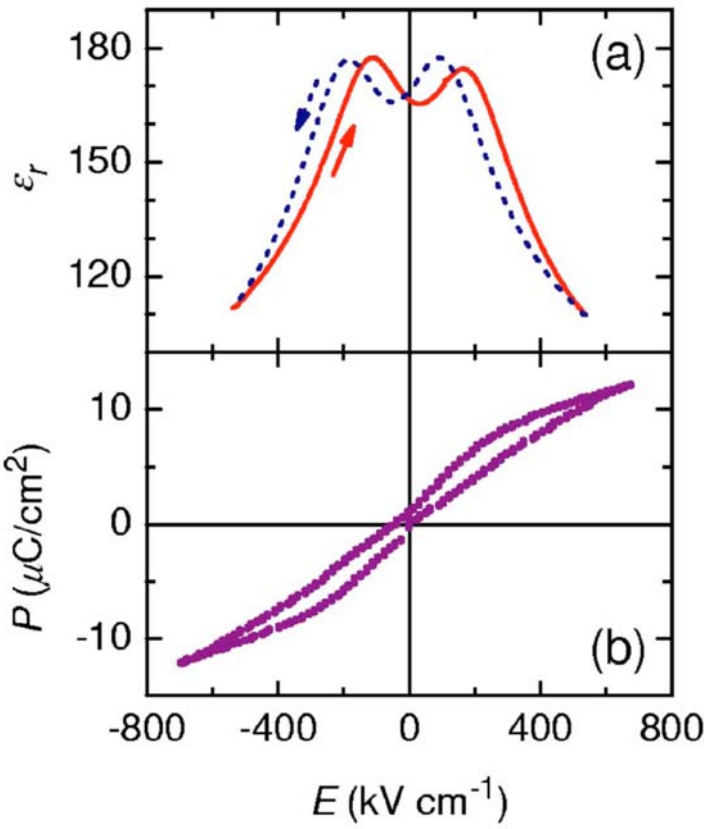

Figure 41 (a) ε_r and (b) P vs electric field loops of a $BiCrO_3$ film capacitor measured at a temperature of 10 K (15 K) and a frequency of 10 kHz (1 kHz). The solid and dotted lines in Figure (b) are measured with increasing and decreasing the electric fields, respectively. Reprinted with permission Ref. 830.

5.2.4 Bi_2FeCrO_6

Baettig et al.[838,839] have predicted theoretically that the ordered perovskite compound Bi_2FeCrO_6 will exhibit properties far exceeding the properties of any known multiferroic material: a polarization of 80 $\mu C/cm^2$ along the [111] direction, a piezoelectric coefficient of 283 $\mu C/cm^2$, and a magnetization of 160 emu/cm^3 (2 μ_B per formula unit). Ferroelectric polarization in Bi_2FeCrO_6 is driven by the Bi lone pair, like in its parent compounds $BiFeO_3$ and $BiCrO_3$, and ferrimagnetism with a net magnetic

moment of 2 μ_B per an Fe–Cr pair originates from the antiferromagnetic exchange interaction between d^3 Cr^{3+} and d^5 Fe^{3+} (with 5 μ_B per Fe^{3+} and 3 μ_B per Cr^{3+} in opposite directions). The structure of this material is very similar to that of $BiFeO_3$ with the *R*3*c* symmetry, except that the Fe^{3+} ions are replaced by Cr^{3+} ions in every second (111) plane, which corresponds to a rocksalt ordering of the Fe and Cr octahedrals and reduces the symmetry to the space group *R*3. A number of attempts were made to prepare both a random $BiFeCrO_3$ solid solution [914, 915] and an ordered Bi_2FeCrO_6 compound experimentally.[840, 916, 917, 918, 919] Kim et al.[915] grew epitaxial films of disordered $BiFe_{0.5}Cr_{0.5}O_3$ solid solution on (001)$SrTiO_3$ substrates with $SrRuO_3$ bottom electrodes by pulsed laser deposition. The films films were found to be ferroelectric with 77-K remanent polarization as high as 60±1 $\mu C/cm^2$ along the pseudocubic [001] direction. The magnetic ordering in the solid solution was however antiferromagnetic, in contrast with the expectations for the system with ordered Fe and Cr cations, where ferrimagnetism was anticipated. For epitaxial films of ordered Bi_2FeCrO_6, Nechache *et al.* [916,917] reported ferroelectric and magnetic hysteresis at room temperature with a polarization of 2.8 $\mu C/cm^2$ and a saturated magnetization of 0.26 μ_B per unit cell. More recently, the same group has reported that the ordered Bi_2FeCrO_6 films undergo a magnetic phase transition between 600 and 800 K.[840] The experimental value of saturated magnetization is low as compared to the expected theoretical value of 2 μ_B per an Fe–Cr pair.[838,839] Such value of magnetization can be explained by several reasons: (i) only partial ordering of Fe and Cr cations in the lattice, (ii) partial chemical disorder that generates an antiferromagnetic antisite contribution (Fe-Fe, Cr-Cr), and/or (iii) partial strain relaxation in the film resulting in a more distorted structure. Further investigations of structural, magnetic, and

electric properties of ordered Bi_2FeCrO_6 are needed; however, the results obtained so far clearly indicate that this compound is one of the rare high-temperature multiferroics.

5.3 Yttrium and rare-earth manganites *R*MnO_3

Rare-earth manganites with a general formula *R*MnO_3 (*R* is a trivalent cation) crystallize in two structures, depending on the size of the R^{3+} cation: hexagonal (*P63cm*) for *R*=Ho, Er, Tm, Yb, Lu, Sc, and Y, which have small ionic radii *r* ($r_R^{3+} < r_{Dy}$), and orthorhombic (*Pbnm*) for *R*=La, Ce, Pr, Nd, Sm, Eu, Gd, Tb, and Dy, which have larger ionic radii ($r_R^{3+} \geq r_{Dy}$).[817,920] The Mn-O-Mn angle in *R*MnO_3 is approximately 180° which facilitates magnetic ordering via an indirect exchange interaction between the Mn^{3+} ions through O ions.[920] All *R*MnO_3 compounds exhibit antiferromagnetic ordering with the paraelectric-antiferroelectric transition temperatures ranging from 40 to 140 K.[819,921,922,923,924] For the hexagonal perovskite manganites *R*MnO_3 (*R*=Ho, Tm, Lu, and Y), the ferroelectric Curie temperatures well above room temperature (T_C =570-990 K) with saturated polarization > 5.6 $\mu C/cm^2$ and the Néel temperatures in the range 73– 124 K are reported.[816,818,925,926,927] To the contrary, the orthorhombic manganites have the ferroelectric Curie temperature lower than the Néel temperature and very low remanent polarization (<0.2 $\mu C/cm^2$).[823,841, 928] The existence of ferroelectricity in these orthorhombic compounds was attributed to lattice modulation accompanied by the antiferromagnetic order.[823,841]

Figure 42 shows a polyhedral representation of the high-temperature centrosymmetric (left panel) and the low-temperature ferroelectric (right panel) structure

of hexagonal RMnO$_3$.[845] The structure consists of close-packed layers of MnO_5 trigonal bipyramids linked by corners in the (001) planes. Each Mn^{3+} ($3d^4$) ion is located in the center of the oxygen polyhedral and is surrounded by three in-plane and two apical oxygen ions. Along the hexagonal *c*-axis, the MnO_5 layers are separated by layers of R^{3+} ions. Below the ferroelectric Curie temperature, the MnO_5 bipyramids undergo a collective rotation that leads to unit cell tripling, as shown in the right panel in Figure 42. The cooperative rotation of the MnO_5 bipyramids displaces the R^{3+} ions along the *c* axis, giving rise to ferroelectricity in the material with polarization direction along the c-axis.[846] Below the Néel temperature, the magnetic moments of Mn^{3+} are aligned on the *ab* plane with a 120˚ structure, forming a triangular, geometrically frustrated network of antiferromagneticaly coupled spins. Systematic studies of magnetic point symmetry of the RMnO$_3$compounds were carried out by Fibig *et al*.:[927]

The structure of orthorhombic RMnO$_3$ compounds can be considered as an orthorhombically distorted cubic perovskite structure.[929] The distortion from the ideal cubic structure arises from two sources.[924,930] The first is the mismatch of the *R*-O and Mn-O equilibrium bond lengths which is adjusted by cooperative rotation of the MnO_6 octahedra. The rotation increases with decreasing *R* ion radius. The second reason for the lattice distortion is a deformation of the MnO_6 octahedra due to the orbital ordering characteristic of the Jahn-Teller effect of Mn^{3+} cations. The degree of orbital ordering slightly increases from La to Tb and then remains almost unchanged for the last terms of the series. Details of orbital and magnetic ordering in a series of orthorhombic RMnO$_3$ compounds have been studied by Tachibana et al.[924] and Kimura et al.[819] as a function of the *R* ionic radius.

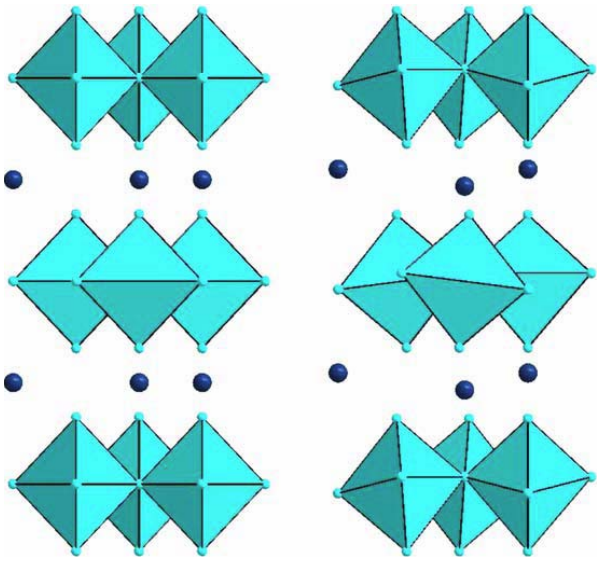

Figure 42
High-temperature centrosymmetric (left) and low-temperature ferroelectric structure (right) of hexagonal $RMnO_3$. In the low-temperature structure the oxygen polyhedra undergo a collective rotation that leads to a unit cell tripling. This unit cell tripling is accompanied by displacements of the R cations (spheres) along the (0001) directions which lead to an electric dipole moment. Reprinted with permission Ref. 845.

It should be mentioned that pressure, strain, or special synthesis conditions can convert the hexagonal structure to the denser orthorhombic perovskite phase and, vise versa hexagonal structure can be stabilized under certain conditions.[924, 929,931,932,933,934,935] Since the hexagonal RMnO$_3$ compounds exhibit ferroelectricity at room temperature, realization of a metastable hexagonal phase for orthorhombic RMnO$_3$ (R=Ho, Tb, Dy, Gd, Sm, Eu) has been the subject of many papers.[935,936,937,938,939,940] The difference between the formation energies of the orthorhombic and the hexagonal RMnO$_3$ phases is sufficiently small that allows the growth of thin films of the orthorhombic manganites in a metastable hexagonal phase, which does not exist in the bulk form. Epitaxial stabilization of some metastable compounds was realized using various substrates,

including MgO,[936] yttria-stabilized zirconia (YSZ),[937,938,939] Pt(111)/Al_2O_3(0001),[928] and $YMnO_3$,[939] whose surface atomic arrangements ensured the hexagonal symmetry of epitaxially grown films. Balasubramaniam et al. [939] have grown single-phase hexagonal *R*MnO_3 (R=Dy, Gd, Sm) films on (110)-oriented of single-crystal hexagonal $YMnO_3$ using PLD. The films were stable against back transformation to the perovskite structure up to a thickness of at least 50 nm. Lee et al. [928] also demonstrated 50-nm-thick hexagonal $DyMnO_3$ films grown epitaxially on Pt(111), Al_2O_3(0001), and (111) YSZ substrates, which have in-plane hexagonal symmetry. The ferroelectric properties of these films were significantly enhanced compared to those of the bulk orthorhombic $DyMnO_3$. The polarization hysteresis loop revealed the existence of ferroelectricity below 70 K (compared to 28 K for orthorhombic $DyMnO_3$), with remanent polarization of 2.2 $\mu C/cm^2$ at 25 K, which was an order of magnitude higher than the value for the bulk orthorhombic material. In addition, the hexagonal $DyMnO_3$ films also revealed an antiferroelectric-like signature above 70 K and spin-glass-like magnetic behavior, which was likely to arise from the geometric frustration of antiferromagnetically coupled Mn spins with an edge-sharing triangular lattice. The antiferromagnetic Néel temperature of the hexagonal $DyMnO_3$ films was found to be around 60 K, while the temperature of spin reorientation transition to be around 40 K.

5.3.1 $YMnO_3$

Being originally considered as a promising ferroelectric, $YMnO_3$ is the most studied member of the hexagonal *R*MnO_3 group. $YMnO_3$ has been the main subject of theoretical first-principles studies of the fundamental physical properties the *R*MnO_3 compounds, since the empty 4*f* shell of the Y^{3+} ion makes $YMnO_3$ a convenient system

for application of the pseudopotential-based methods.[33,845] In addition to being fundamentally important, $YMnO_3$ has attracted a good deal of interest as a multiferroic material for applications in magnetic storage media and spintronics, since the electrical and magnetic orders in $YMnO_3$ were shown to be coupled.[800,817,941] The coupling was found to originate from an interaction between magnetic and electric domain walls. [800] $YMnO_3$ has an antiferromagnetic Néel temperature of 80 K and a ferroelectric Curie temperature of 914 K.[817,920] As discussed above, the $RMnO_3$ compounds can crystallize either in orthorhombic or in hexagonal structure, depending on the *R* ionic radius. Y has the intermediate ionic radius and is hexagonal under ambient conditions,[942] but the orthorhombic structure can be stabilized by low-temperature,[932] high-pressure synthesis conditions,[933,934] or under compressive epitaxial strain in thin films.[931,943,944,945]

A number of studies have been devoted to doping $YMnO_3$ with the aim to modify its structural, electric and magnetic properties properties. [847,946,947,948,949,950,951,952,953] Katsufuji et al.[847] investigated the effects of Zr doping into the *R* site in the hexagonal $RMnO_3$ compounds (*R*=Y, Lu, Sc) and found that Zr doping drastically suppresses both the ferroelectric distortion and magnetic ordering. Substitution of Fe at the Mn sites was found to increase the Néel temperature of the compound.[817,946,947] Ga doping of the hexagonal $RMnO_3$ (*R*=Y and Ho) compounds was demonstrated to increase the ferrielectric Curie temperature while decreasing the Néel temperature.[949] Iliev et al.[951] studied the structural, magnetic and electrical properties of orthorhombic $Y_{1-x}Ca_xMnO_3$ ($0 \leq x \leq 0.5$) depending of the Ca concentration, *x*. The structure of this compound remained orthorhombic in the entire substitutional range. It was found that the average magnetic exchange interaction changed from antiferromagnetic for $x < 0.08$ to

ferromagnetic for x > 0.08. In order to reduce the growth temperature of $YMnO_3$ films and suppress the interfacial reactions and interdiffusion, Choi *et al.* [953] doped $YMnO_3$ with Bi at Y sites. They have found that Bi doping leads to formation of a very thin Bi oxide layer at the surface of growing films which results in enhanced surface mobility of adatoms and thereby reduced growth temperature by more than 150 °C from the typical growth temperature of $YMnO_3$ films (>800 °C).

For device applications, preparation of $YMnO_3$ in the form of thin films is required. A number of reports have been devoted to the growth of $YMnO_3$ films by various techniques, such as MBE,[954,955] PLD, [956,957,958,959,960,961,962] sputtering,[963,964,965] and chemical deposition.[966, 967, 968] Various substrates have been used to achive epitaxial growth of $YMnO_3$. Single-crystal hexahonal films were grown on (111) MgO,[969] ZnO:Al/(0001) sapphire,[969] (111)Pt/(0 0 0 1) sapphire,[955,959,962] (111)Y_2O_3/(111)Si,[955,959] (111)Y-stabilized ZrO_2, [970] and wurtzite GaN/AlN/6H-SiC(001).[961] However, as mentioned above, compressive stress can bring $YMnO_3$ into the undesirable non-ferroelectric orthorhombic phase. For example, $YMnO_3$ films epitaxially grown on $SrTiO_3$ substrates were found to be orthorhombic due to large in-plane compressive strain in the films. [945, 970]

Multiferroic behavior of $YMnO_3$ films has been recently demonstrated.[960,962, 971 , 972] Dho and Blamire[960] investigated the dual ferroelectric-antiferromagnetic functionality of $YMnO_3$ films grown on (111)Si with a native oxide and found that ferroelectric and magnetic properties depended on the $YMnO_3$ crystal orientation. The PLD-grown $YMnO_3$ films obtained in this work exhibited a single-phase

hexagonal structure, with the film texture being strongly dependant on the oxygen pressure during the deposition. $YMnO_3$ films grown at 10 mTorr were predominantly (0001) oriented, while those grown at 0.1 mTorr were $(11\bar{2}1)$ oriented. The (0001)-oriented $YMnO_3$ films displayed small coercivity and zero exchange bias, while the $(11\bar{2}1)$-oriented $YMnO_3$ layers exhibited relatively large values of coercivity and exchange bias. Such a large variation in exchange bias with orientation was attributed to the difference in the Mn–Mn spin coupling strength with direction in the hexagonal structured $YMnO_3$. The Mn–Mn distance along the *c*-axis direction (~6.07 Å) is much longer than that in the *ab* plane (~3.55 Å).[800, 942] This implies that the interplane Mn–Mn spin coupling is much smaller than the intra-plane Mn–Mn spin coupling. Thus, the (0001)-oriented $YMnO_3$ films were found to be optimal for ferroelectric applications but unfavorable for magnetic applications. This result indicates that simultaneous utilization of the dual functionality of $YMnO_3$ may indeed be very challenging.[960]

5.4 RMn_2O_5

RMn_2O_5 (R = rare earth or La, Y, Bi) compounds have attracted great interest after the multiferroic properties[805] and colossal magnetoresistance effect[834, 973] had been discovered in these materials. At room temperature, all members of this family exhibit the orthorhombic structure, space group *Pbam*.[974] Mn in RMn_2O_5 exists in two oxidation states, Mn^{3+} and Mn^{4+} each of which occupies different crystallographic sites. Each Mn^{3+} is coordinated to five oxygen ions located at the apexes of a distorted square-base pyramid, while each Mn^{4+} ion has octahedral oxygen coordination. Each R^{3+} ion is surrounded by eight oxygen atoms. The size of all three kinds of coordination polyhedron

decreases gradually as R radius dercreases.[975] Figure 43 presents a polyhedral representationof the RMn_2O_5 structure,[832,835] which can be considered as consisting of infinite chains of $Mn^{4+}O_6$ octahedra which shares edges along the *c* axis and linked together by $Mn^{3+}O_5$ and RO_8 units.

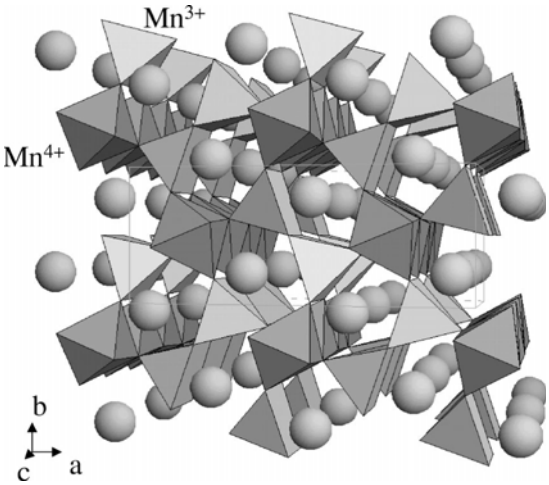

Figure 43 Projection of the RMn_2O_5 structure, approximately along the *c* axis. Octahedra and tetragonal pyramids correspond to MnO_6 and Mn_2O_5 units, respectively. The structure is orthorhombic (space group *Pbam*). Reprinted with permission Ref. 835.

According to neutron diffraction studies,[976,977,978] RMn_2O_5 compounds have a complex antiferromagnetic structure with magnetic moments of Mn^{3+} and Mn^{4+} ions forming a helical magnetic ordering below the Néel temperature. The specific lattice geometry of the Mn sublattices and competing magnetic interactions between Mn^{3+} and Mn^{4+} as well as R^{3+} magnetic moments leads to complex magnetic structure characterized by a highly frustrated spin system.[979,980,981] The helical spin ordering was noted to break the inversion symmetry and stabilize ferroelectric order in the lattice.[982] As a result, ferroelectric order in RMn_2O_5 is very sensitive to an applied magnetic field.[805,841] At room temperature, these compounds are paramagnetic and paraelectric, and they undergo multiple magnetic and ferroelectric phase transitions upon cooling.[983] First, long-range

incommensurate magnetic ordering occurs at T_{N1}=40–43 K. At T_{C1}≈ 38–40 K, a lock-in transition of the magnetic ordering into a commensurate type takes place, which coincides with the onset of ferroelectric polarization along the *b* axis.[805,984] At T_{C2}≈ 13–18 K, another sharp change in the polarization is observed which coincides with the unlocking of the commensurate order into another incommensurate magnetic order. This low-temperature phase was attributed also to a new excitation referred to as electromagnons.[985] And finally, ordering of rare-earth spins below 10 K takes place. Figure 44 shows the electric and magnetic phase transitions in the RMn_2O_5 compounds summarized by Kimura et al.[833] As before, PE, FE, and X (X') stand for paraelectric, ferroelectric, and unidentified dielectric phases, respectively. Note that although the phase diagrams vary from one to another RMn_2O_5 compound, ferroelectricity is observed only in commensurate magnetic phases, indicating close relation between the magnetic-structure periodicity and the spontaneous electric polarization.[833]

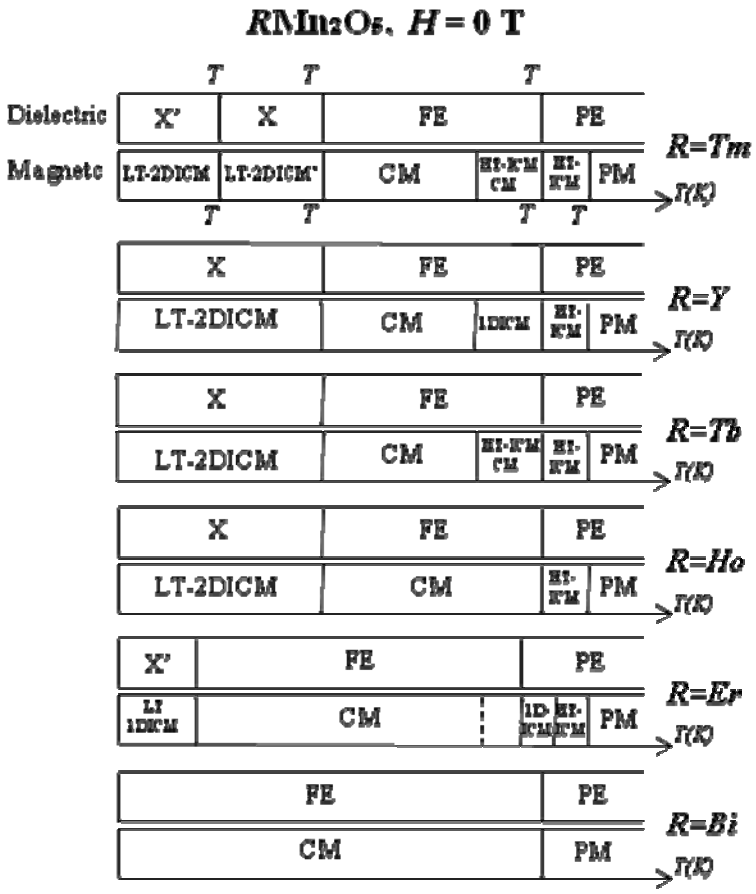

Figure 44 Dielectric and magnetic phase diagrams as a function of temperature for RMn$_2$O$_5$ compounds, which contain PE (ParaElectric), FE (FerroElectric), X (undidentified), and X' (unidentified, but different from X) phases, and also contain PM (ParaMagnetic), HT-ICM (High Temperature-Incommensurate Magnetic), 1DICM (1 Dimensionally modulated Incommensurate Magnetic), CM (Commensurate Magnetic), LT-2DICM/LT-2DICM' (Low Temperature-2Dimensionally modulated Incommensurate Magnetic), and LT-1DICM (Low Temperature 1Dimensionally modulated Incommensurate Magnetic) phases for the magnetic phase. After Ref. 833.

The most complex phase diagram was observed for DyMn$_2$O$_5$ with five subsequent transitions upon decreasing temperature in zero magnetic field.[986,987] All phase transitions were signified by distinct changes in termperature dependences of the dielectric constant $\varepsilon(T)$ and/or the ferroelectric polarization $P(T)$ (Figure 45). The

difference between the cooling and warming data in Figure 45 indicates that several phase transitions exhibit thermal hysteresis. As seen from the figure, below T_{N1}=43 K the antiferromagnetic order of the Mn spins sets in (*M* phase with incommensurate magnetic order). At T_{C1}=39.6 K a magnetic lock-in transition into an antiferromagnetic phase takes place, and the ferroelectric polarization arises. At T_{N2}=27 K a sharp increase in $\varepsilon(T)$ and a change of the $P(T)$ curve slope is observed. Such a sharp increase of $\varepsilon(T)$ and a significant drop of $P(T)$ at T_{C2}=14 K (18 K upon heating) are indicative of the unlocking of the commensurate order and transitioning it into an incommensurate phase. At T_{C3} = 6 K (8 K upon heating), the $\varepsilon(T)$ dependence show a step-like decrease and the polarization drops to zero due to a re-entrant transition into a low-temperature paraelectric phase with the appearance of the commensurate order of Dy-moments.

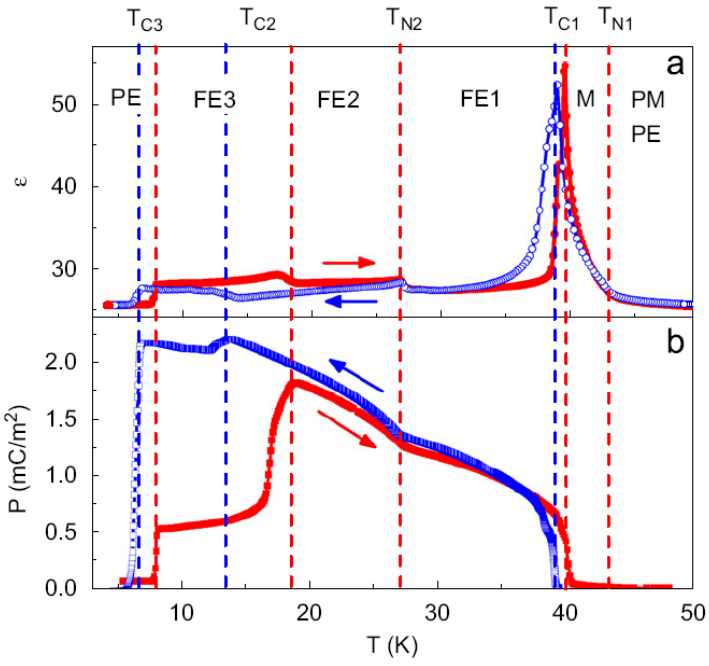

Figure 45 Cascade of phase transitions in $DyMn_2O_5$ determined by measurements of the dielectric constant (a) and the ferroelectric polarization (b). Large temperature hysteresis was observed below TC_2. Cooling and heating data are shown by open and closed symbols, respectively. Reprinted with permission Ref. 987.

As seen from Figure 45, the magnetic phase transitions in the multiferroic material manifest themselves as distinct anomalies of the dielectric constant (magnetodielectric effect) which is a clear indication of strong magnetoelectric coupling due to significant spin–lattice coupling.[834,981] For some materials, the relative change of the dielectric constant $\Delta\varepsilon/\varepsilon_0$ can reach considerably large values such as tens and even hunders of percent. For example, Hur et al. [834] discovered the colossal magnetodielectric (CMD) effect in $TbMn_2O_5$, $DyMn_2O_5$, and $HoMn_2O_5$ single crystals. The values of $\Delta\varepsilon/\varepsilon_0$ were found to be 22% and 40% near T_N for $TbMn_2O_5$ and $HoMn_2O_5$ respectively, while this value for $DyMn_2O_5$ was as high as 109% at 3 K. For $DyMnO_3$[823] and $CdCr_2S_4$, [988] giant values of $\Delta\varepsilon/\varepsilon_0$ up to 500% were reported.

A dramatic enhancement of the electric polarization under pressure was reported by dela Cruz et al.[983] for $R$$Mn_2O_5$ (R=Tb, Dy, Ho) compounds. It is interesting to note that application of pressure was found to have the same effect on the ferroelectric phase stability as magnetic field along the easy magnetization axis. It was argued that, while the magnetic field changes the magnetic structure by aligning spins with applied field, pressure directly changes the interatomic distances and bond angles in the lattice, thus affecting the exchange coupling constant. Complete p-T phase diagrams were constructed for $R$$Mn_2O_5$ (R=Tb, Dy, Ho); however, further experimental and theoretical studies are needed for a deeper understanding of the pressure effect on the phase transitions in $R$$Mn_2O_5$ multiferroics.

Another member of the $R$$Mn_2O_5$ family is $BiMn_2O_5$. Detailed studies of the structural, magnetic, and magnetoelastic properties of this compound have been recently

performed. [835,989,990] The main peculiarity of the $BiMn_2O_5$ structure is that the BiO_8 units are much more distorted than the RO_8 units in other RMn_2O_5 compounds due to the presence of an electronic lone pair on Bi^{3+}.[835] $BiMn_2O_5$ is magnetically ordered below T_N=39 K. The magnetic structure of this compound is also different: $BiMn_2O_5$ is the only member of the RMn_2O_5 family that exhibits no transitions to incommensurate magnetic order and therefore is ferroelectric in the whole temperature range below T_N. The $BiMn_2O_5$ magnetic structure is defined by the commensurate propagation vector **k**(1/2,0,1/2), whereas the magnetic structure is incommensurate along the *c* axis, with **k**(1/2,0,τ) for the other RMn_2O_5 compounds. Figure 46 shows the component of the magnetic propagation vector along the *c* axis, k_z, as a function of the ionic radius.[835] The values of k_z are low for the smaller rare-earth ions, because the smaller the R^{3+} cation is, the shorter the Mn^{4+}-O distance is, and, therefore, the stronger the direct antiferromagnetic interaction is between the Mn^{4+} planes along the chains of $Mn^{4+}O_6$ octahedra. In $BiMn_2O_5$, the Mn^{4+}-O distance is larger than in any other RMn_2O_5 compounds, which results in a weaker direct antiferromagnetic coupling along the chains. Thus, the indirect Mn^{4+}-O-Mn^{3+}-O-Mn^{4+} interaction (i.e., the coupling between Mn^{4+} neighbors via bridging Mn^{3+} cations) predominates in $BiMn_2O_5$ in such a way that the final coupling between the Mn^{4+} planes separated by the Mn^{3+} planes is purely ferromagnetic. The commensurability of the structure is directly related to this pure ferromagnetic interaction. In other RMn_2O_5 compounds, the moments of the Mn^{4+} couples form a certain non-zero angle, implying the incommensurability of the magnetic structure. [835]

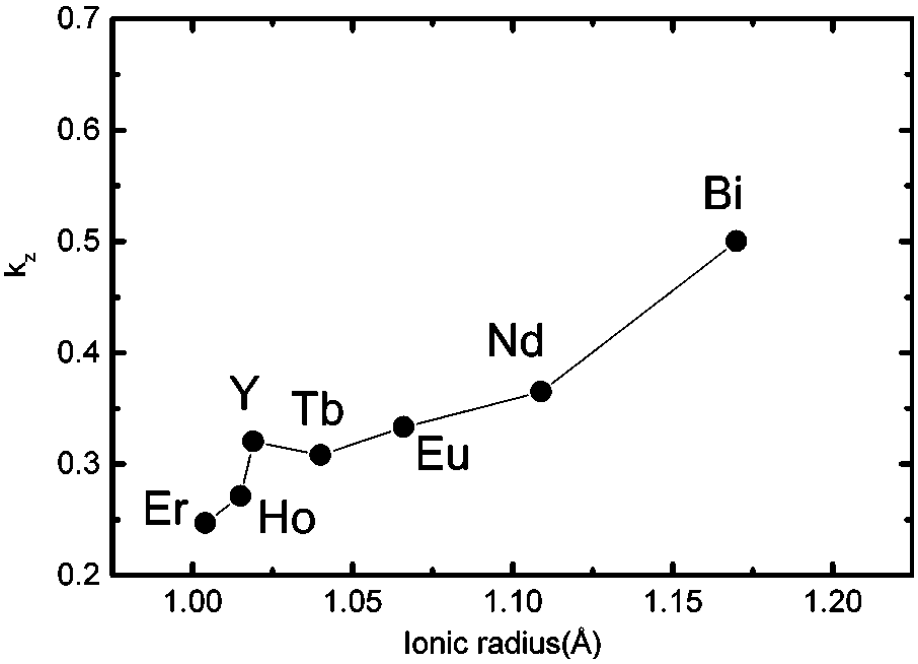

Figure 46
Evolution of the k_z component of the propagation vector **k**(1/2,0,k_z) as a function of the R^{3+} ionic radius (in eightfold coordination) for the RMn$_2$O$_5$ family. Reprinted with permission Ref. 835 Ionic radii are taken from Ref. 991 and k_z from Refs. 976,977,978,992.

Since the magnetoelectric coupling in RMn$_2$O$_5$ takes place at very low temperatures, efforts have been made to improve the multiferroic properties of these materials by doping. [993,994,995,996,997,998] For example, Munoz et al.[993] synthesized a new oxide material YFeMnO$_5$ by substituting Fe ions into Mn sites in the parent YMn$_2$O$_5$ compound. YFeMnO$_5$ was found to be isostructural with RMn$_2$O$_5$ oxides, containing infinite chains of $Mn^{4+}O_6$ octahedra sharing edges, which were linked together by $Fe^{3+}O_5$ pyramids and YO$_8$ units. A certain level of disorder was found between the Mn and Fe metallic positions in that about 5% of Mn cations were replaced by Fe and vice versa. It has been demonstrated that YFeMnO$_5$ exhibits ferrimagnetic order below 165 K. Substitution of Ce for Bi ions in BiMn$_2$O$_5$ was found to result in transformation of the

antiferromagnetic phase of $BiMn_2O_5$ with a Néel temperature of about 42 K to ferromagnetic phase of $Bi_{0.9}Ce_{0.1}Mn_2O_5$ with a Curie temperature of about 46 K. [995] Besides, the permittivity of $Bi_{0.9}Ce_{0.1}Mn_2O_5$ was found to be much higher than that of $BiMn_2O_5$. The authors proposed the following mechanism for the change of the magnetic ordering from the antiferromagnetic to the ferromagnetic one. When Ce is introduced into the lattice, Ce^{4+} ions occupy a portion of the Bi^{3+} sites, the excess electrons make some Mn ions change the electronic state from $t_{2g}^3e_g^0$ Mn^{4+} into a $t_{2g}^3e_g^1$ Mn^{3+} and induce a partially filled electron band, which weakens the direct Mn^{4+}–O–Mn^{4+} super exchange interaction and, therefore, the antiferromagnetic coupling between Mn^{4+} ions. In addition, the double exchange interaction of the bridge Mn^{3+}–O–Mn^4 could be activated, thus making $Bi_{0.9}Ce_{0.1}Mn_2O_5$ ferromagnetic.[995] Shim et al.[997] prepared $YMn_{2-x}(Fe,Co)_xO_{5-\delta}$ ($0.0 \leq x \leq 1.0$) compounds via the sol-gel process and studied their structural, electrical, and magnetic properties. They found that the substitution of Fe and Co at the Mn sites led to a drastical increase in the magnetic and ferroelectric transition temperatures. The $YMn_{1.8}Fe_{0.2}O_{5-\delta}$ and $YMn_{1.8}Co_{0.2}O_{5-\delta}$ compounds exhibited spontaneous polarization and ferromagnetic ordering at room temperature, which obviously could pave the way to their practical applications.

5.5 Two-phase multiferroics

As mentioned in the Introduction, the realizable magnetoelectric coefficient in single-phase multiferroics is very small (see Table 7) and not sufficient for practical applications. The weaknesses of the single-phase materials have their genesis in the limitation set by Equation 4. Moreover, magnetoelectric effect in most of the single-phase

multiferroics is observed only at low temperatures, because either ferromagnetic (or antiferromagnetic) or ferroelectric transition temperature is very low. An alternative approach to realization of the magnetoelectric effect is the fabrication of multiferroic composites, which makes use of indirect coupling via mechanical strain between two different materials, namely ferroelectric and ferromagnetic. Generally, the composites may consist of particles of one phase embedded into another phase matrix (Figure 47a), alternating layers of two phases (Figure 47b), and rodes of one phase surrounded by another phase matrix (Figure 47c).[34] With the possibility of independent optimization of the two different phases for room temperature operation, the limiting condition described in Equation 4 is lifted. As a result, the magnetoelectric effect in the composites may be more than several orders of magnitude higher than that in single-phase materials. Depending on the composition and preparation conditions, magnetoelectric coefficients of the composites vary from about 10 to 100 mV/cm Oe at low-frequencies, reaching up to V/cm Oe orders of magnitude at resonance (see Ref. 34 and references therein). As an illustration, Table 7 lists the magnetoelectric coupling coefficients measured for various multiferroic single-phase materials as well as the values for some two-phase systems.[999,1000,1001,1002,1003,1004] A detailed discussion of composite materials is beyond the scope of this review. However, recent activities in the field of magnetoelectric composites are reviewed in detail in Ref. 34.

Table 7. Magnetoelectric coupling coefficients measured for various multiferroic single phase materials. Some two-phase systems are also included for comparison.

Material	**magnetoelectric coefficient**		
	$\alpha_M = \mu_0 \delta M / \delta E$ (ps/m)	$\alpha_E = \delta E / \delta H$ (mV/cm Oe)	**Ref.**

Cr_2O_3		20	1000
$TbMn_2O_5$	21 (at 28 K)		805
$LiCoPO_4$	30.6 (at 4.2 K)		808
$LiNiPO_4$	1.7 (at 20 K)		791
YIG	30 (at very low T)		809
$TbPO_4$	36.7 (at 1.9 K)		810
$BiFeO_3$		0.3 (at 20 K)	803,804
$La_{0.7}Sr_{0.3}MnO_3$/PMN-PT (001) bilayer	60000 (at 300 K)		999
$La_{0.7}Sr_{0.3}MnO_3$/PZT laminated composite		32 (at 300 K)	1000
$NiFe_2O_4$/PZT laminated composite		1500 (at 300 K)	1001
LSMO/PZT laminated composite		60	1002
$0.3NiFe_2O_4/0.7$PZT ceramic composites		20-30	1003
$BaTiO_3/CoFe_2O_4$ ceramic composite		up to 2540	1004

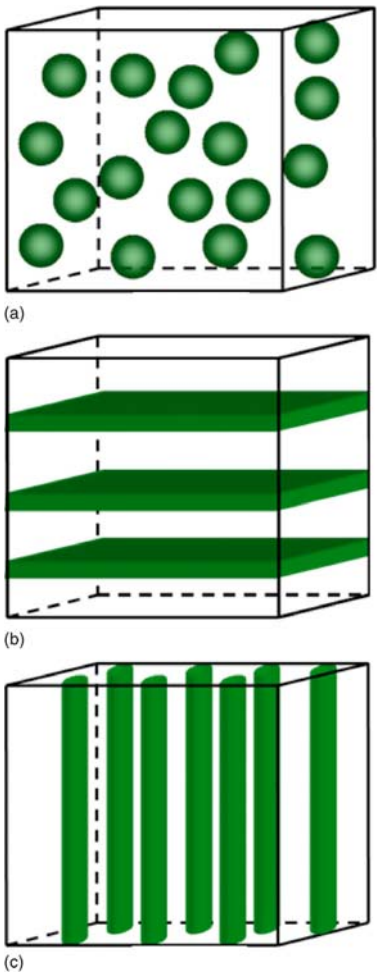

Figure 47 Schematic illustration of three types of composites: (a) particles embedded into matrix of another phase, (b) laminate/layered composite, and (c) fiber/rod composite. Reprinted with permission Ref. 34.

6 Metamaterials

In this Section, we will consider oxides, namely ferrites, as a constituent of the so-called metamaterials, new artificial media which have unusual electrical and magnetic properties due to their structure. Unlike naturally occurring materials, metamaterials exhibit negative values of the main parameters determining the material response to

electromagnetic waves: electrical permittivity ε, magnetic permeability μ, and, as a result, the index of refraction $n = \pm\sqrt{\varepsilon\mu}$. Metamaterials are also called negative index (NI) or left handed (LH) materials, since the vectors of electric field **E**, magnetic field **H,** and phase vector **k** form a left-handed system in this case. A theoretical concept of the LH media has been developed as early as in 1967 by Veselago,[1005] who has pointed out that unusual physical phenomena arising from the sign change of the group velocity would be observed in such materials. To cite them, the phase velocity direction would be opposite to that of the energy flow, the Doppler shift would be reversed, a moving charge would emit Cherenkov radiation in the backward direction, radiation pressure would be reversed to radiation tension, converging lenses would become diverging lenses and vice versa. In 1996, Pendry *et al.*[1006] have demonstrated that an artificial material composed of very thin metallic wires arranged in a simple cubic lattice exhibits negative electrical permittivity. Later, the same group [1007] designed a periodic array of split ring resonators (SRRs) that exhibit negative magnetic permeability in a certain microwave frequency range. And finally in 2000, Smith *et al.*[46,1008] fabricated an NI medium in which both the effective permittivity and the effective permeability were simultaneously less than zero over a finite frequency band. In 2001, Shelby *et al.*[1009] demonstrated negative refraction in a Snell's Law experiment with a prism-shaped LH-material sample. This artificial medium consisted of two sets of resonators - an array of metal posts interspersed with an array of SRRs - which were separately responsible for the negative ε and μ. Figure 48 shows an example of such a metamaterial.[1010] The size of the constructing elements and the spacing between them are much smaller than the radiation wavelength, and thus the composite medium can be considered pseudo-homogeneous at the wavelengths of

interest. Just as the permittivity and permeability of natural materials derive from the response of constituent atoms to applied fields, ε and μ of metamaterials are determined by the response of their constituent elements.

Figure 49 shows a schematic of an NI metamaterial and its building blocks, SRRs and metallic rods. [1011] A single split-ring resonator consists of two nonmagnetic conducting concentric split rings facing in opposite directions (Figure 49a). An SRR can be considered as an *LC* circuit consisting of inductive (rings) and capacitive (slits and the gap between the rings) elements with a resonance frequency $\omega_0 \sim \sqrt{1/LC}$. The gaps allow the SRR to be resonant at wavelengths much larger than its physical dimensions. The combination of SRRs to form a periodic structure with a strong magnetic coupling between the resonators creates a medium with an effective magnetic permeability $\mu_{eff}(\omega)$. A time-varying magnetic field applied normal to the ring plane induces circulating currents, which in turn produce an opposing magnetic field in the loop due to Lenz's law. At frequencies below ω_0, currents in SRR can keep up with the driving force produced by the applied magnetic field and a positive response is achieved. At frequencies exceeding ω_0, the response is out of phase with the driving magnetic field and negative values of the real part of the permeability are attained. The general form of the frequency dependence of the permeability of an SRR can be written as[46]

$$\mu_{eff} = 1 - \frac{F\omega^2}{\omega^2 - \omega_0^2 + i\omega\Gamma},$$

where ω is the frequency of incident radiation, F is the area of the unit cell occupied by the interior of the split ring, and Γ is the dissipation factor. Figure 50 shows the frequency dependence of the real and imaginary parts of the permeability of a metamaterial

composed of SRRs. If the resonance is strong enough and the losses depicted by μ_i are small enough, the SRR can yield a negative magnetic response.

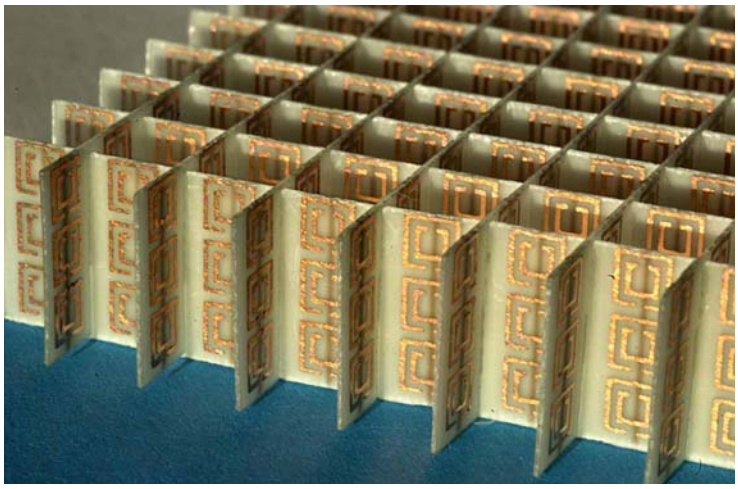

Figure 48. A photograph of a SSR etched into copper circuit board plus copper wires to give negative μ and negative ε. Reprinted with permission Ref. 1010.

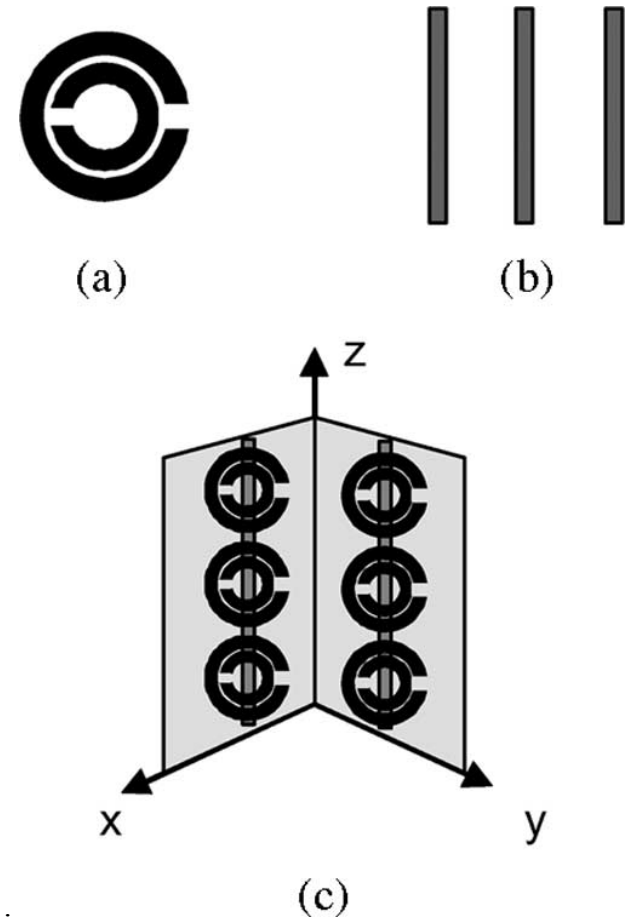

Figure 49 (a) Magnetically resonant ($\mu < 0$) metal structure: a single split-ring resonator (SRR) consisiting of two counterfacing split rings of subwavelength dimensions. (b) Electrically resonant ($\varepsilon < 0$) metallic structure: metal rods. (c) Combination of both structures results in a negative-index metamaterial $n < 0$. Reprinted with permission Ref. 1011.

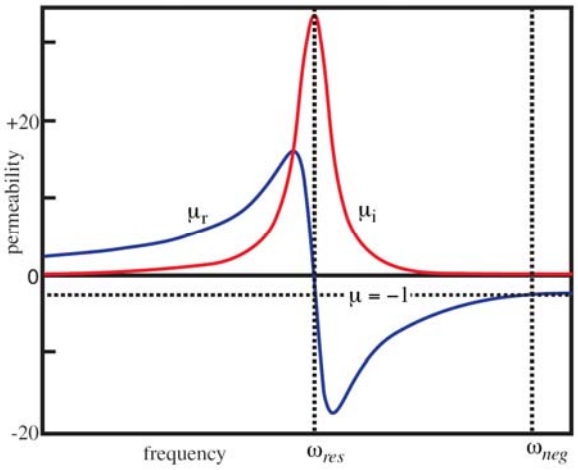

Figure 50 Schematic permeability of a magnetic metamaterial consisting of SRRs manufactured in layers which are then stacked to form an array of resonant columns. Reprinted with permission Ref. 1010.

It should be mentioned that materials having negative values of electrical permittivity also occur naturally. For example, at frequencies below the plasma frequency ω_p, all metals yield negative response to the electric component of electromagnetic radiation due to screening of the radiation by free electrons. As mentioned above, negative electric response is also found for periodic structures composed of a regular array of thin conducting wires or a grating on a conductor. Figure 51 shows an example of an artificial medium concstructed from thin infinite wires arranged in a simple cubic lattice. Such a structure simulates the properties of low-density plasma having a dielectric response of the form[1010]

$$\varepsilon(\omega) = 1 - \frac{\omega_p^2}{\omega^2} \ .$$

As illustrated in Figure 52, the permittivity of the material is negative for $\omega < \omega_p$. The plasma frequency is a function of carrier density n and effective electron mass m^* through:

$$\omega_p^2 = 4\pi \frac{ne^2}{m^*},$$

where e is the charge of an electron. For metals, ω_p is typically in the ultraviolet region.[1010] As compared to naturally occurring materials, the artificial negative electric response media have an advantage in that their plasma frequency can be easily tuned by varying the size and geometry of the building blocks. Indeed, the effective electron density in the wire structure shown in Figure 51 is considerably reduced relative to solid metal and can be tuned by varying the wire size and wire-to-wire spacing, thus allowing a change of the operation frequency.[1010] Moreover, inductance of the wires contributes to the electron effective mass. For structures with a typical wire radius of a few micrometers and wire-to-wire spacing of a few millimeters, the effective electron mass is of the same order as that of a nitrogen atom. As a result, the value of ω_p is lowered to the GHz frequency range.[1006, 1010] Thus, the plasma frequency (and the region of negative electric response) of metamaterials can be modified by changing the geometry of the artificial materials.

Due to the unique physical properties of metamaterials, new kinds of devices could be imagined, including super lenses providing resolution exceeding the diffraction limit,[41,42,43] miniaturized antennas[35,36,37,38] beam steerers, modulators, band-pass filters, as well as coatings making an object 'invisible' to electromagnetic radiation.[44,45,1012] More detailed information on the NI metamaterials can be found in recent reviews.[1010,1013, 1014, 1015, 1016, 1017]

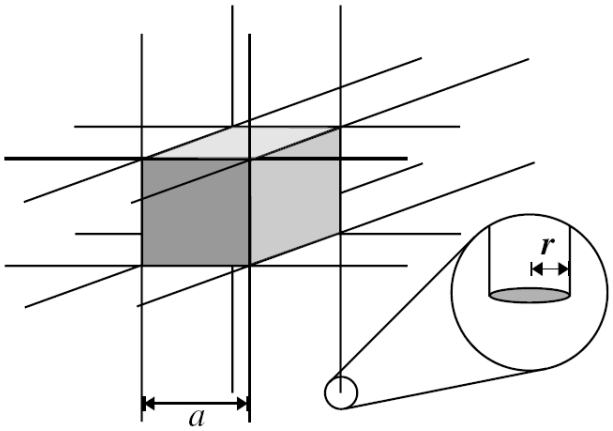

Figure 51 A metamaterial with ε<0: a periodic structure composed of thin infinite wires arranged in a simple cubic. Reprinted with permission Ref. 1010.

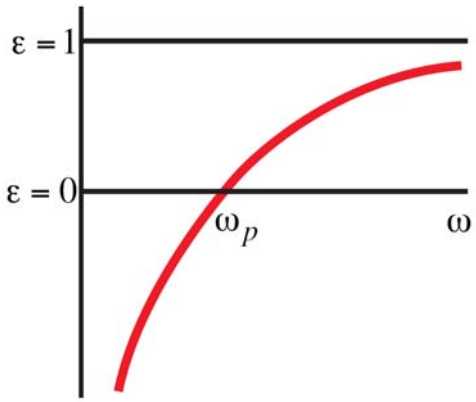

Figure 52 The schematic of permittivity, ε, of a plasma. Below the plasma frequency, ω_p, ε is negative. Reprinted with permission Ref. 1010.

The "classical" NI metamaterials consisting of SRR and conducting wire arrays have, however, some disadvantages. First of all, these structures work in a fixed and rather narrow frequency band determined by the size and periodicity of their constituent blocks and thus are not tunable once built. In addition, it is difficult to manufacture such metamaterials operating in the IR and optical frequency range, because the dimensions of the constituent elements should be smaller than the wavelength. One more issue is that commonly used metals, such as copper, gold, silver, and aluminum, which are highly conductive at RF and microwave frequencies, do not exhibit conductivity at optical

frequencies, but instead exhibit plasmonic resonance (coupling of electromagnetic wave with collective oscillation of conduction electrons at metal surfaces). Besides, some natural materials (e.g. ferrites[11,1018]) are known to exhibit negative μ in the microwave range, so the SRR array can be replaced with a natural material.

For these reasons, other types of NI composite materials, which are tunable by applying electric or magnetic field, composed partially of natural materials, and easier to manufacture on an industrial scale, have been investigated both theoretically[1019,1020,1021,1022,1023,1024,1025,1026] and experimentally.[1027,1028,1029,1030] Examples of such metamaterials are metallic magnetic nanoparticles embedded into an insulating matrix,[1020,1031] superlattices consisting of natural materials,[1021, 1023,1027] and combination of ferrite and metallic wires.[1022,1028,1029,1030] It is interesting to note that, although it is generally believed that NI materials do not naturally occur, the negative refraction index has been obtained recently in the colossal magnetoresistance oxide $La_{2/3}Ca_{1/3}MnO_3$ in the gigahertz frequency range.[1032] Moreover, Pimenov et al.[1032] claim that conditions for negative refraction can be expected in any ferromagnetic metal such as iron, provided the existence of narrow ferromagnetic resonance.

The efforts to construct NI media from natural materials have drawn attention to ferrites due to their capability to provide negative permeability.[47,1018,1019,1021,1022,1028,1029,1030,1033] Ferrites are insulating ferrimagnetic oxides possessing high permeability and moderate permittivity and low microwave losses. Since ferrites are dielectrics, electromagnetic waves are able to penetrate the materials, thereby permitting an interaction between the electromagnetic radiation and magnetization within the ferrite material. This interaction makes possible a plethora of applications in passive

microwave components such as isolators, circulators, phase shifters, tunable filters, and miniature antennas.[11,1018,1034]

Ferrites crystallize in spinel, garnet, and magnetoplumbite-type structures. In all ferrite structures, metallic cations are located on the interstices of a close-packed lattice of oxygen anions. The ferrites with the cubic spinel structure have the general formula AB_2O_4, where A is a divalent metallic ion, and B is Fe^{3+}. In spinels, metallic cations can occupy two types of lattice sites: tetrahedral A sites having 4 oxygen neighbors and octahedral B sites having 6 oxygen neighbors. In each unit cell, there are 8 A sites and 16 B sites occupied by cations. The antiferromagnetic superexchange interaction between cations on the A and B sites aligns their spins to be antiparallel, therefore the net magnetization M of the material is difference in magnetic moment between A and B sites:

$$M = M_B - M_A. \qquad \text{Equation 12}$$

The partial cancellation of magnetic moments is the reason of lower magnetization of ferrites as compared to that of metallic ferromagnets with parallel alignment of spins. As obvious from Equation 12, the magnetization of spinel ferrites can be increased by decreasing M_A. This approach is realized via doping with non-magnetic cations which exhibit a strong preference for occupation of the A sites, e.g. Zn^{2+}. To reiterate, partial substitution of magnetic ions on the A sites by non-magnetic ions leads to decrease in M_A and, consequently, increase in net magnetization. It should be, however, remembered that the spontaneous alignment of moments on B sites arises from their coupling to moments on the A sites. Therefore, as the concentration of magnetic ions on the A sites further decreases, the aligning forces on the B-site moments also decrease, resulting in a decrease in M_B and the net magnetization.

Garnet ferrites have orthorhombic crystal structure with the general formula $Me_3Fe_5O_{12}$, where Me is a trivalent rare-earth ion. In this structure, Me cations occupy dodecahedral sites (8 oxygen neighbors), while Fe cations reside on the tetrahedral and octahedral sites.[1035] The most important member of this group is yttrium iron garnet $Y_3Fe_5O_{12}$ (YIG) owing to its narrow ferromagnetic resonance (FMR) linewidth (0.6 Oe[1036]) and very low microwave loss.

Magnetoplumbite-type ferrites have a very comlex hexagonal structure (and therefore are referred to to as hexaferrites). These materials exhibit large magnetic uniaxial anisotropy, with the crystallographic *c*-axis being the magnetic easy axis. There are a number of hexaferrites, such as M, U, X, Y Z, and W-type hexaferrites. The best known member of this group is M-type barium hexaferrite $BaFe_{12}O_{19}$.[1037] The large anisotropy field of ~17000 Oe makes this material attractive for self-biased microwave circulators. [1038] A detailed consideration of structures, physical properties, and applications of ferrites can be found in review by Özgür et al. [11]

Lets us now turn our attention back to the NI metamaterials. Dewar[47] proposed an NI material consisting of an array of small metallic strips embedded into a non-conducting ferro- or ferrimagnetic matrix (for example, YIG). In this metamaterial, the array of strips provides $\varepsilon<0$, and the host medium gives rise to $\mu<0$. The frequency range where μ is negative can be tuned via a static magnetic field applied parallel to the plane of the structure. This structure has a negative index of refraction for electromagnetic waves polarized so that electric field is parallel to the plane of the structure and magnetic field is normal to this plane and to the tuning magnetic field. Another variant of such a metamaterial proposed by Dewar[47] is a square array of parallel wires embedded into the

ferromagnetic host medium. Wu[1021] theoretically analyzed a periodic metal–ferrite–metal film composite (as shown in Figure 53). He demonstrated that at some microwave frequencies this composite may have negative ε and negative μ simultaneously, i.e., have a negative effective refraction index. Based on a theoretical analysis using the transfer function matrix technique, He *et al.* [1022] have demonstrated that a metamaterial composite consisting of Cu wires and yttrium iron garnet (YIG) slabs exhibits negative index of refraction and provides a means to fabricate a low-loss, tunable NI metamaterials.

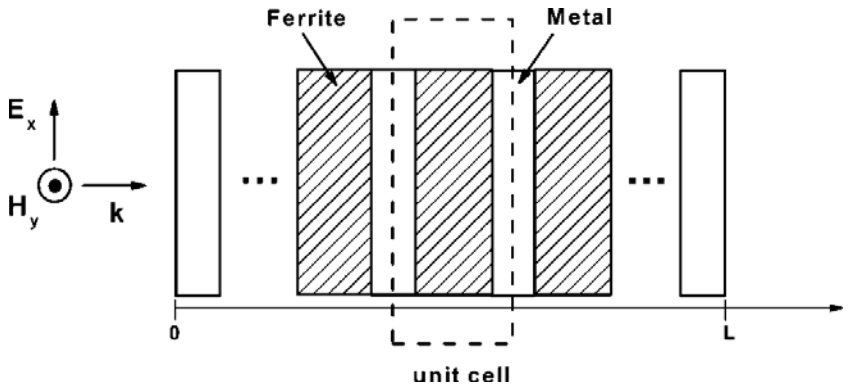

Figure 53 Schematic diagram for the periodic metal–ferrite–metal layered composite. The incident radiation is a linearly polarized plane wave normally incident on the surface of the composite. Reprinted with permission Ref. 1021.

Hea *et al.* [1030] have constructed a NI metamaterial from yttrium iron garnet (YIG) films and an array of copper wires. Figure 54 shows a schematic sketch of this NI metamaterial inserted into a K-band waveguide. The composite consists of eight Cu wires 25 mm in thickness and 100 mm in width, spaced 1mm apart and a 400-μm-thick multilayered YIG film deposited by liquid phase epitaxy on both sides of a gadolinium gallium garnet (GGG) substrate. An air gap is maintained between the periodic array of the wires and the YIG slab in order to reduce the coupling between them. Figure 55

displays a frequency dependence of the refraction index calculated from experimental data. The major downward peak of real part of *n* centered at 23GHz represents the negative refraction index region. To demonstrate the tunability of the ferrite/wire metamaterial, Hea *et al.* [1030] measured the transmission coefficient S_{21} under different external magnetic fields applied along the *x*-axis. Figure 56 shows the shift of the region of negative index with applied field. As the field increased from 5.8 to 7.0 kOe, the S_{21} peak shifted from 18 to 23 GHz. Thus, the NI metamaterial was demonstrated to be magnetic field tunable in the frequency range form 18 to 23GHz with a figure of merit of 4.2 GHz/kOe.

In addition, a left-handed metamaterial composed of SRRs and slabs of ferroelectric oxide ceramics ($0.8Pb(Ni_{1/3}Nb_{2/3})O_3$-$0.2PbTiO_3$) was experimentally realized by Bai et al.[1039] In this metamaterial, negative permeability was provided by an array of SRR, while the negative permittivity originated directly from intrinsic dielectric resonance in the ferroelectric material. Experimental results obtained by Bai et al. indicate left-handed behavior of the SRR/ferroelectric metamaterial in the microwave frequency range.

Bichurin *et al.*[1040] proposed an NI metamaterial based on bi- and multilayered ferrite-ferroelectric composites with strong magnetoelectric interactions. A schematic of the proposed structure is presented in Figure 57a. The structure consists of ferrite-ferroelectric composite disks arranged in a three-dimentional lattice. A constant magnetic field applied for tuning the resonance frequency is directed normal to the disk plane. As shown in Figure 57b, metal electrodes are deposited on both surfaces of the disks, with the electrode thickness far smaller than the skin depth. The calculations performed by Bichurin *et al.*[1040] have found that the permeability and permittivity of this metamaterial

take negative values in a certain frequency range determined by physical properties of the composite and electrode materials, disk dimentions, array parameters, as well as by applied electric and magnetic fields. Due to the strong magnetoelectric interaction in the ferrite-ferroelectric composites, the composite-based NI metamaterials would have a unique possibility for tuning by means of both electric and magnetic fields, which paves the way for design of new devices.

In conclusion, it was proved that SRR arrays responsible for negative permeability of NI metamaterials can be replaced with natural materials, such as ferrites, while negative permittivity can be provided by metallic wire arrays. Such ferrit-metallic wire metamaterial composites are tunable by applying of electrical or magnetic field and are much more conducive for fabrication on industrial scale. Now, the magnetic and electric responses of the man-made metamaterials can be controlled over a broad frequency range, from RF to IR [1041,1042,1043,1044,1045] and even zero frequency.[1046,1047]

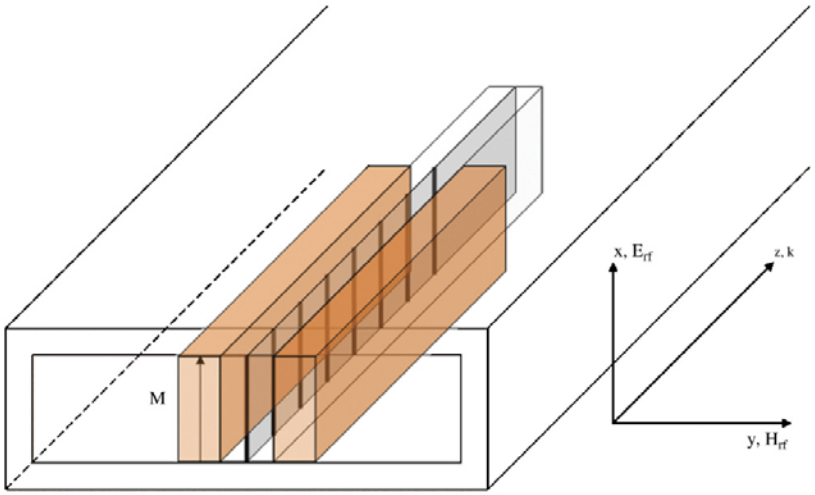

Figure 54 Schematic diagram of the experimental setup showing the NIM composite inserted in a K-band waveguide (inside dimensions: 1.07 cm by 0.43 cm). The composite structure consisted of eight copper wires spaced 1 mm apart and multilayered YIG films with a total thickness of 400 μm. The shaded regions are YIG layers whereas the black lines represent copper wires. Note that each ferrite material is separated from the wires by a nonmagnetic dielectric material. Reprinted with permission Ref. 1030.

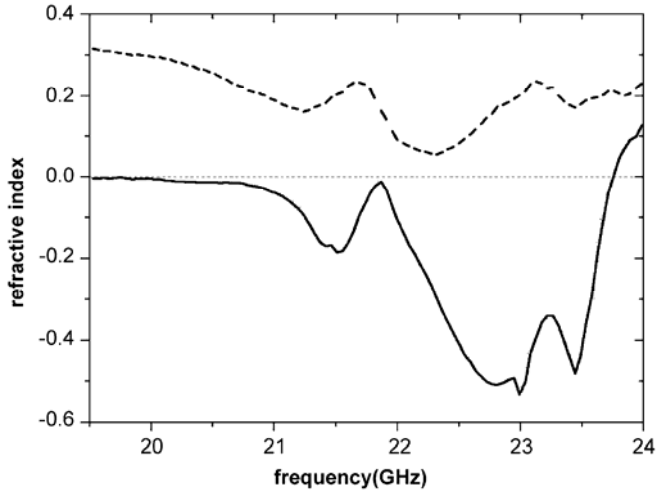

Figure 55 Real (solid line) and imaginary (dashed line) parts of the index of refraction deduced from experimental data for the structure shown in Figure 54. The salient downward feature of real part of *n* centered at 23GHz represents the negative refraction index region. Reprinted with permission Ref.1030.

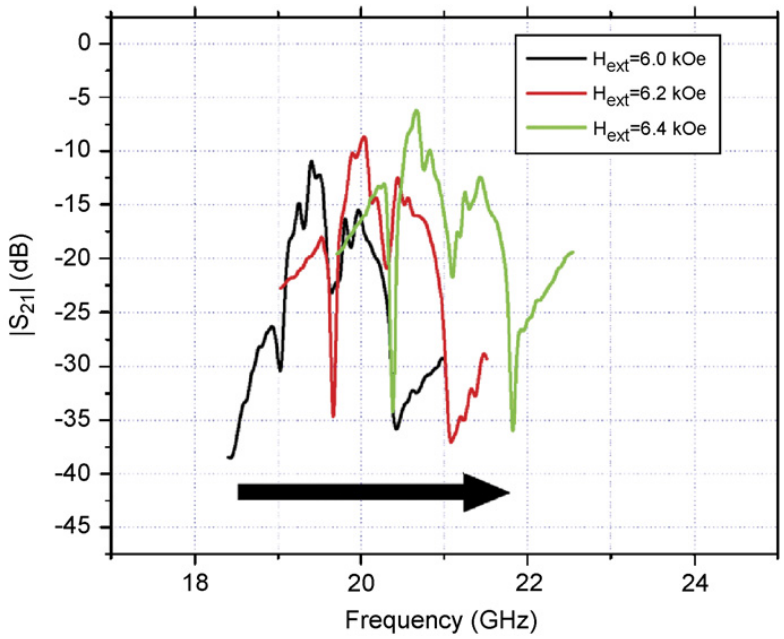

Figure 56 Demonstration of electronic tunability of a ferrite/wire metamaterial using external field. The large arrow at the bottom denotes the direction of frequency shift with increasing magnetic field. Reprinted with permission Ref. 1030.

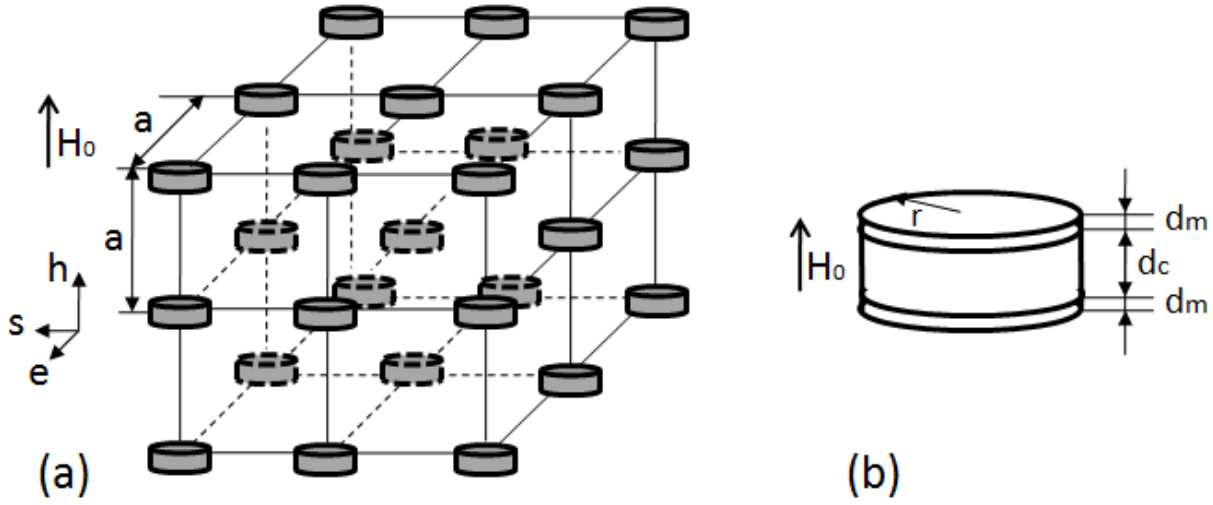

Figure 57 (a) Array of composite disks with negative permeability and permittivity. (b) Element of array: r and d_c are radius and thickness of composite disks, d_m is thickness of the metal disk electrode ($d_m << d_c$). After Ref. 1040.

7 Concluding remarks

A comprehensive and critical review of technologically important oxide materials, with an emphasis on high-κ dielectric, ferroelectric, ferromagnetic, and multiferroic oxides, as well as oxides found use in the new developing field of metamaterials, has been given. There has been a resurgence of interest in oxides in general and complex oxides in particular owing to their piezoelectric, ferroelectric, ferromagnetic, ferrimagnetic, and multiferroics (particularly, magnetoelectric coupling in one material) properties. Although these properties had been recognized many decades ago, the interest in oxide materials has been renewed due to the natural tendency toward device miniaturization and increasing perceived need in multifunctional materials, as well as considerable imrpovment of deposition techniques, which would potentially allow not only higher quality material but also thin films and heterstructures with new functionalities, e.g. multiferroic composite structures with magnetoelectric coupling.

As clearly delineated by the Si industry roadmap, scaling is imperative for increasing speed of Si-based integrated circuits. With down scaling of the channel length and associated gate dielectric thickness reduction, the gate current leakage becomes increasingly intolerable, which has awakened interest in high-κ dielectric oxides. A large variety of high-κ oxides has been proposed for replacing SiO_2 as a gate dielectric, among them HfO_2 and HfO_2-based materials have been found to be the most promising candidates combining compatibility with Si technology, high dielectric permittivity and thermal stability with low leakage current due to a reasonably high barrier height that

limits electron tunneling. Alternative candidates for high-κ dielectric applications are multicomponent oxides, such as $LaScO_3$, $GdScO_3$, $DyScO_3$, and $LaLuO_3$, which exhibit figures of merit similar to or exceeding that of HfO_2 and thus could be quite competitive with the Hf-based oxides in the nearfuture. A variety of deposition methods has been used for the high-κ oxide film deposition. It appears that ALD is the most widely used technique due to its precise thickness, composition control, and excellent step coverage, the last of which is very crucial for high-aspect device structures. However, the choice of a precursor for the ALD growth is one of the most crucial issues as impurities and defects are introduced by the precursors. In the context of compatibility of high-κ dielectrics with the Si MOSFET technology, some problems need to be solved, among them incompatibility with annealing temperatures used for activating poly-Si gates, the relatively poor quality (as compared to SiO_2), which causes charge trapping and makes the Si MOSFET gate unstable, channel mobility degradation, and threshold voltage shift induced by high-κ materials. Nevertheless, great strides have been made in Hf-based gate oxides and carried forward to production. For example, Hf-based high-κ materials have already been implemented in commercial products such as the Intel 45 nm Penryn processors based on high-κ/dual metal gate CMOS technology.[1048] Additionaly, NEC is marketing a poly-Si/Hf-based high-κ low-power technology. As always, other companies are following suite by announcing high-κ products for the near future. In the upcoming years, a plethora of techniques will be undoubtedly explored at the research level, which will be following by insertion by the industry in Si CMOS circuits making the devices smaller, faster and less expensive.

The increasing demand in non-volatile random-access memory fuels interest in ferroelectric and ferro-/ferromagnetic oxides, due to their reversible spontaneous polarization and magnetization which can be used to write information in FeRAM and MRAM. In addition, a high degree of carrier polarization in magnetic oxides, such as mixed-valence manganites and DMOs, makes them promising candidates for spintronic applications. Despite a large volume of research carried out in these fields, many problems remain to be resolved. To improve characteristics of FeRAM devices, the reliability problems such as fatigue, retention, and imprint should be further addressed. As for magnetic oxides, much remains to be done both experimentally and theoretically to clarify the origin of magnetic order in DMOs. Numerous experimental data do not agree well with different theoretical approaches. Presumably, there is no single model capable of explaining the properties of a wide class of DMOs. Some data point to the existence of different types of ferromagnetic ordering in the same material depending on free carrier concentration. An important issue that must be resolved theoretically and confirmed experimentally is the existence of carrier-mediated ferromagnetic exchange in DMOs, which is the most desirable exchange mechanism for devices exploiting spin polarized carriers. One more important issue is the need for conclusive demonstration of injection of spin-polarized carriers into a semiconductor active region, which is an imperative step towards spintronic device applications.

Magnetoelectric multiferroics, the materials combining ferroelectric and magnetic properties in a single phase, were demonstrated to be promising candidates for multifunctional and spintronic devices. The candidates however are very few in number. In addition, magnetoelectric coupling in these materials is too weak and/or takes place at

temperatures to low to be practically useful. Much work is warranted on the search for single-phase materials suitable for real device applications. There is also room for theoretical studies aimed at better understanding of the underlying physics of multiferroic phenomena. From the standpoint of device applications, two-phase multiferroic composites making use of indirect coupling via mechanical strain between the ferroelectric and magnetic phases are much more appealing, at least at the present time. The possibility of independent selection of ferroelectric and magnetic components with required characteristics results in magnetoelectric coefficients several orders of magnitude higher than those in single-phase multiferroics. Among various types of multiferroic composites, epitaxial thin-film heterostructures and self-assembled nanostructures look very attractive due to the perfect contact between the two phases at epitaxial interfaces and resulting efficient strain transfer. Besides, epitaxial composites are well suitable for integration in microelectronic devices.

In the field of negative-index metamaterials, the use of ferrite oxides providing negative permeability has been proposed as an alternative to split ring resonators. Ferrite-based NI media allow designing tunable, low-loss NI structures and expanding the operating frequency band to IR and visible range. In addition, they are much simplier to fabricate and can be translated to production scale. All these make the ferrite-based metamaterials desirable candidates for future device applications such as tunable lenses, filters, phase shifters, waveguides, and broadband cloaks.

ACKNOWLEDGMENTS

This work is funded by a grant from the Office of Naval Research under the Program Director, then and now Dr. Ingham Mack and Dr. Dan Green, respectfully. Fruitful discussios with cite our group, Drs. Cite the NRL group, Profs. L. Brillson and J. Volakis of Ohio State and C. Patton of Colorado State are gratefully acknowledged.

References

[1] S. M. Sze and K. K. Ng, Physics of Semiconductor Devices, Third Edition, Wiley-Inerscience, A John Wiley & sons, Inc., Publication, 2006, p. 328.
[2] G. D. Wilk, R. M. Wallace, and J. M. Anthony, High-k gate dielectrics: Current status and materials properties considerations, J. Appl. Phys., 89, 5243-5275 (2001).
[3] R. M. C. de Almeida and I. J. R. Baumvol, Surface Science Reports, 49(1-3), 1-114 (2003).
[4] Robert M. Wallace and Glen D. Wilk, "High-κ Dielectric Materials for Microelectronics", Critical Reviews in Solid State and Materials Sciences, 28, 231 (2003).
[5]X.H. Zhu, J.M. Zhu, A.D. Li, Z.G. Liu, and N.B. Ming, Challenges in Atomic-Scale Characterization of High-k Dielectrics and Metal Gate Electrodes for Advanced CMOS Gate Stacks, J. Mater.Sci. Technol., 25, 289-313 (2009).
[6] D. G. Schlom, S. Guha,and S. Datta, Gate Oxides Beyond SiO_2, MRS BULLETIN, 33, 1017-1025 (2008).
[7] Mo Wu, Y. I. Alivov, and H. Morkoç, High-j dielectrics and advanced channel concepts for Si MOSFET, J. Mater. Sci.: Mater. Electron., 19, 915–951 (2008).
[8] Lee, S. C., Teowee, G.., Shrimpf, R. D.,Birnie, D. P., Uhlmann, D. R., and Galloway, K. F., "Total dose radiation effects on solgel derived PZT thin films", IEEE Transactions on Nuclear Science, 39, 2036, 1992.
[9] Scott, J. F., Araujo, C. A., Meadow, H. B., McMillan, L.D., Shawabkeh, A., "Radiation effects on ferroelectric thin-film memories: Retention failure mechanisms"", J. Appl. Phys. 66, 1444 ,1989.
[10] J. L. Snak, "Magnetic and electrical properties of the binary systems $MO{\cdot}Fe_2O_3$,Physica, vol. 3, p. 463, 1936.
[11] Ü. Özgür, Y. Alivov, and H. Morkoç, Microwave Ferrites, Part 1: Fundamental properties, be published in J. Mater. Sci.: Mater. Electron. (2009); Ü. Özgür, Y. Alivov, and H. Morkoç, Microwave Ferrites, Part 2: Passive components and electrical tuning, J be published in J. Mater. Sci.: Mater. Electron. (2009).
[12] J.G. Bednorz, K.A. Müller, Z. Phys. B:Condens. Matter 64, 189 (1986).
[13] J.B. Goodenough, G. Demazeau, M. Pouchard, P. Hagenmuller, J. Solid State Chem. 8, 325 (1973).
[14] R.J. Cava, B. Batlogg, R.B. van Dover, D.W. Murphy, S. Sunshine, T. Siegrist, J.P. Remeika, E.A. Rietman, S. Zahurak, G.P. Espinosa, Phys. Rev. Lett. 58, 408 (1987).
[15] M. Imada, A. Fujimori, Y. Tokura, Rev. Mod. Phys. 70, 1039 (1998).
[16] Jin S, Tiefel T H, Mc Cormack M, Fastnacht R A, Ramesh R, and Chen L H Thousandfold Change in Resistivity in Magnetoresistive La-Ca-Mn-O Films, Science 264, 413 (1994).
[17] R. Von Helmolt, J. Wecker, B. Holzapfel, L. Schultz, and K. Samwer, Giant negative magnetoresistance in perovskitelike $La_{2/3}Ba_{1/3}MnO_x$ ferromagnetic films, Phys. Rev. Lett. 71, 2331-2333 (1993).
[18] R. C. Sousa and I. L. Prejbeanu, Non-volatile magnetic random access memories (MRAM), C. R. Physique, 6, 1013–1021 (2005).
[19] D.D. Awschalom and M.E. Flatte, "Challenges for semiconductor spintronics," Nature Phys., 3, 153-159 (2007).

[20] R. M. Stroud, A. T. Hanbicki, Y. D. Park, G. Kioseoglou, A. G. Petukhov, B. T. Jonker, G. Itskos, and A. Petrou "Reduction of spin injection efficiency by interface defect spin scattering in ZnMnSe/AlGaAs-GaAs spin-polarized light-emitting diodes" Phys. Rev. Lett, 89, 166602-1 - 166602-4 (2002).
[21] M. V. Tsoi, A. G. M. Jansen, and J. Bass, "Search for point-contact giant magnetoresistance in Co/Cu multilayers," J. Appl. Phys., 81, Part 2B, 5530-5532 (1997).
[22] T. Dietl, H. Ohno, F. Matsukura, J. Cibert, and D. Ferrand, "Zener Model Description of Ferromagnetism in Zinc-Blende Magnetic Semiconductors," Science, 287, 5455, 1019-1022 (2000).
[23] K. Sato and H. Katayama-Yoshida, Material design for transparent ferromagnets with ZnO-based magnetic semiconductors, Jpn. J. Appl. Phys. 39, L555 (2000).
[24] Y. Matsumoto, M. Murakami, T. Shono, T. Hasegawa, T. Fukumura, M. Kawasaki, P. Ahmet, T. Chikyow, Shin-ya Koshihara, and H. Koinuma, Room-Temperature Ferromagnetism in Transparent Transition Metal-Doped Titanium Dioxide, Science 292, 854 (2001).
[25] H Bea, M Gajek, M Bibes, and A Barthelemy, Spintronics with multiferroics, J. Phys.: Condens. Matter, 20, 434221-1 - 434221-11 (2008).
[26] H. Schmid, Multiferroic Magnetoelectrics, Ferroelectrics 162, 317-338 (1994).
[27] W. Eerenstein, N. D. Mathur, and J. F. Scott, "Multiferroic and magnetoelectric materials" Nature 442, 759-765 (2006).
[28] M. Fiebig, "Revival of the magnetoelectric effect", J. Phys. D 38, R123-R152 (2005).
[29] Brown, W. F. Jr, Hornreich, R. M. & Shtrikman, S. Upper bound on the magnetoelectric susceptibility. Phys. Rev. 168, 574–-577 (1968).
[30] Wood, V. E.; Austin, A. E. In Magnetoelectric Interaction Phenomena in Crystals; Freeman, A. J., Schmid, H., Eds.; Gordon and Breach: Newark, NJ, 1975.
[31] M. Gajek, M. Bibes, S. Fusil, K. Bouzehouane, J. Fontcuberta, A. Barthe Lemy, and A. Fert, Tunnel junctions withmultiferroic barriers, Nature materials, 6, 296-302 (2007).
[32] Bibes M and Barthelemy B, Nat. Mater. 7, 425-426 (2008).
[33] N. A. Hill, Why Are There so Few Magnetic Ferroelectrics? J. Phys. Chem. B. 104, 6694-6709 (2000).
[34] Ce-Wen Nan, M. I. Bichurin, Shuxiang Dong, D. Viehland, G. Srinivasan, Multiferroic magnetoelectric composites: Historical perspective, status, and future directions, J. Appl. Phys. 103, 031101-1 – 031101-35 (2008).
[35] R. W. Ziolkowski and A. Kipple, IEEE Trans. Antennas Propag. 51, 2626 (2003).
[36] K. Buell, H. Mosallaei, and K. Sarabandi, IEEE Trans. Microw. Theory Tech. 54, 135 (2006).
[37] S. Hrabar, J. Bartolic, and Z. Sipus, IEEE Trans. Antennas Propag. 53, 110 (2005).
[38] B. Wu, W. Wang, J. Pacheco, X. Chen, J. Lu, T. M. Grzegorczyk, J. A. Kong, P. Kao, P. A. Theophelakes, and M. J. Hogan, Microw. Opt. Tech. Lett. 48, 680 (2006).
[39] N. Engheta, Science 317, 1698 (2007).
[40] M.G. Silveirinha and N. Engheta, Phys. Rev. B 76, 245109 (2007).
[41] Pendry J B Negative refraction makes a perfect lens, Phys. Rev. Lett. 85, 3966–9 (2000).
[42] Grbic, A., and Eleftheriades, G. V., Phys. Rev. Lett. (2004) 92, 117403

[43] R. V. Petrov, R. Pandey, G. Srinivasan, and M. I. Bichurin, A magnetic field controlled negative-index microwave lens, Microwave and Optical Technol. Lett., Vol. 50, No. 11, November 2008
[44] D. Schurig, J. J. Mock,B. J. Justice, S. A. Cummer, J. B. Pendry, A. F. Starr, D. R. Smith, Metamaterial Electromagnetic Cloak at Microwave Frequencies, Science 314, 977 (2006);
[45] A. Alu and N. Engheta, Plasmonic and metamaterial cloaking: physical mechanisms and potentials, J. Opt. A: Pure Appl. Opt., 10, 093002-1 – 093002-17 (2008).
[46] D. R. Smith, W. J. Padilla, D. C. Vier, S. C. Nemat-Nasser, S. Schultz, Composite Medium with Simultaneously Negative Permeability and Permittivity, Phys. Rev. Lett. 84, 4184 (2000).
[47] G. Dewar, Candidates for $\mu<0$, $\varepsilon<0$ nanostructures, Internat. J. Modern Phys. B, 15 (24-25), 3258-3265 (2001).
[48] G. E. Moore, "Cramming more components onto integrated circuits", Electronics 38, 114–116 (1965).
49 M. Czernohorsky, E. Bugiel, H. J. Osten, A. Fissel, and O. Kirfel, "Impact of oxygen supply during growth on the electrical properties of crystalline Gd2O3 thin films on Si(001)", Appl. Phys. Lett., 88, 152905 (2006).
50 L. Yan, C. M. Lopez, R. O. Shrestha, E. A. Irene, A. A. Suvorova, and M. Saunders, Magnesium oxide as a candidate for high-κ dielectric", Appl. Phys. Lett. 88, 142901 (2006).
51 S. Chen, Y. Zhu, R. Xu, Y. Q. Wu, X. J. Yang, Y. L.Fan, Z. M. Jiang, and J. Zou, "Superior electrical properties of crystalline Er_2O_3 films epitaxially grown on Si substrates", Appl. Phys. Lett. 88, 222902 (2006).
52 A. Fissel Z. Elassar, O. Kirfel, E. Bugiel, M. Czernohorsky, and H. J. Osten, "Interface formation during molecular beam epitaxial growth of neodymium oxide on silicon", J. Appl. Phys. 99, 074105-1 – 074105-6 (2006).
[53] A. A. Dakhel, Characterisation of Nd2O3 thick gate dielectric for silicon, phys. stat. sol. (a) 201, No. 4, 745–755 (2004).
[54] T. Busani and R. A. B. Devine, The importance of network structure in high-k dielectrics: LaAlO3, Pr2O3, and Ta2O5, J. Appl. Phys. 98, 044102 (2005).
[55] D. P. Brunco, A. Dimoulas, N. Boukos, M. Houssa, T. Conard, K. Martens, C. Zhao, F.Bellenger, M. Caymax, M. Meuris, and M. M. Heyns, Materials and electrical characterization of molecular beam deposited CeO_2 and CeO_2 /HfO_2 bilayers on germanium, J. Appl. Phys. 102, 024104-1 024104 -8 (2007).
[56] Y. Nishikawa, N. Fukushima, N. Yasuda, K. Nakayama, and S. Ikegawa, Electrical properties of single crystalline CeO_2 high-k gate dielectrics directly grown on Si (111), Jpn. J. Appl. Phys., Part 1 41, 2480 (2002).
57 Y. Nishikava, T. Yamaguchi, M. Yoshiki, H. Satake, and N. Fukushima, "Interfacial properties of single-crystalline CeO_2 high-k gate dielectrics directly grown on Si (111)", Appl. Phys. Lett. 81, 4386 (2002).
58 J. S. Suehle, E.M. Vogel, M.D. Edelstein, C.A. Richter, N.V. Nguyen, I. Levin, D.L.. Kaiser, H. Wu, J.B. Bemstein, "Challenges of High- K Gate Dielectrics for Future MOS Devices", 6th Intl. Symp. On Plasma Process-Induced Damage. pp. 90 (2001).
[59] Chiu FC, Chen SY, Chen CH, Chen HW, Huang HS, Hwang HL, Interfacial and

Electrical Characterization in Metal-Oxide-Semiconductor Field-Effect Transistors with CeO_2 Gate Dielectric, Jpn.J. Appl. Phys., 48, Part 2 Sp. Iss., 04C014 (2009).
[60] Juan PC, Liu CH, Lin CL, Ju SC, Chen MG, Chang IYK, Lu JH, Electrical Characterization and Dielectric Properties of Metal-Oxide-Semiconductor Structures Using High-kappa $CeZrO_4$ Ternary Oxide as Gate Dielectric, Jpn.J. Appl. Phys., 48, Part 2 Sp. Iss., 05DA02 (2009).
61 S. Guha, E. Cartier, Ma. A. M. Gribelyuk, N. A. Bojarczuk, and M. C. Copel, " Atomic Beam Deposition of Lanthanum and Yttrium based Oxide Thin Films for Gate Dielectrics", Appl. Phys. Lett. 77, 2710 (2000).
[62] V. V. Afanas'ev, A. Stesmans, C. Zhao, M. Caymax, T. Heeg, J. Schubert, Y. Jia, D. G. Schlom, and G. Lucovsky, Band alignment between (100)Si and complex rare earth/transition metal oxides, Appl. Phys. Lett. 85, 5917-5919 (2004).
63 Y. H. Wu, M. Y. Yang and C. M. Kwei, " Electrical Characteristics of High Quality La_2O_3 Gate Dielectrics with EOT of 5 angstroms", IEEE Electron Device Lett. 21, 7 (2000).
64 G. Aygun and R. Turan, Electrical and dielectrical properties of tantalum oxide films grown by Nd:YAG laser assisted oxidation, Thin Solid Films 517 994–999 (2008).
65 Dong GF, Qiu Y, Pentacene Thin-Film Transistors with Ta_2O_5 as the Gate Dielectric, JOURNAL OF THE KOREAN PHYSICAL SOCIETY 54, Part 2 Sp. Iss. SI, 493-497 (2009).
[66] V.A. Shvets, V.Sh. Aliev, D.V. Gritsenko, S.S. Shaimeev, E.V. Fedosenko, S.V. Rykhlitski, V.V. Atuchin, V.A. Gritsenko, V.M. Tapilin, and H. Wong, Electronic structure and charge transport properties of amorphous Ta_2O_5 films, J. Non-Crys. Sol. 354 3025–3033 (2008).
67 M.K. Bera, C. Mahata, and C.K. Maiti, Reliability of ultra-thin titanium dioxide (TiO2) films on strained-Si, Thin Solid Films 517, 27–30 (2008).
68 M. Copel, M. Giberyuk, and E. Gusev, Appl. Phys. Lett. 76, 436 (2000).
[69] M. Houssa, V. V. Afanas'ev, and A. Stesmans, Variation in the fixed charge density of SiOx ÕZrO2 gate dielectric stacks during postdeposition oxidation Appl. Phys. Lett. 77, 1885-1887 (2000).
[70] S. Sayan, N. V. Nguyen, and J. Ehrstein, T. Emge, E. Garfunkel, M. Croft, Xinyuan Zhao, David Vanderbilt, I. Levin, E. P. Gusev, Hyoungsub Kim, and P. J. McIntyre, Structural, electronic, and dielectric properties of ultrathin zirconia films on silicon, Appl. Phys. Lett. 86, 152902 (2005).
71 W. J. Qi, R. Neih, E. Dharmarajan, B. H. Lee, Y. Jeon, L. Kang, K. Onishi,and J. C. Lee, Ultrathin zirconium silicate film with good thermal stability for alternative gate dielectric application, Appl. Phys. Lett. 77, 1704 (2000) .
72 W. J. Zhu, T. Tamagawa, M. Gibson, T Furukawa, and T. P. Ma, IEEE Electron Device Lett. 23, 649 (2002).
73 B. H. Lee, L. Kang, R. Neeh, W. J. Qi, and J. C. Lee, Thermal stability and electrical characteristics of ultrathin hafnium oxide gate dielectric reoxidized with rapid thermal annealing Appl. Phys. Lett. 76, 1926-1928 (2000).
[74] A. Herrera-Gomez, F. S. Aguirre-Tostado, M. A. Quevedo-Lopez, P. D. Kirsch, M. J. Kim, and R. M. Wallace, T,hermal stability of nitrogen in nitrided HfSiO2 /SiO2/Si(001) ultrathin films, J. Appl. Phys. 104, 103520-1 - 103520-8 (2000).

[75] A. Hardy, C. Adelmann, S. Van Elshocht, H. Van den Rul, M.K. Van Bael, S. De Gendt, M. D'Olieslaeger, M. Heyns, J.A. Kittl, J. Mullens, Study of interfacial reactions and phase stabilization of mixed Sc, Dy, Hf high-k oxides by attenuated total reflectance infrared spectroscopy, Applied Surface Science 255, 7812–7817 (2009).
76 G. D. Wilk, R. M. Wallace and J. M. Anthony, Hafnium and zirconium silicates for advanced gate dielectrics, J. Appl. Phys. 87, 484-492 (2000).
[77] Reji Thomas, Peter Ehrhart, Martin Roeckerath, Sven van Elshocht, Eduard Rije, Martina Luysberg, Markus Boese, Juergen Schubert, Matty Caymax, and Rainer Waser, Liquid Injection MOCVD of Dysprosium Scandate Films Deposition Characteristics and High-k Applications, J. Electrochem. Soc. 154, G147-G154 (2007).
[78] S. Van Elshocht, C. Adelmann, P. Lehnen,b and S. De Gendt, Equivalent Oxide Thickness Reduction for High-k Gate Stacks by Optimized Rare-Earth Silicate Reactions, Electrochemical and Solid-State Letters, 12, G17-G19 (2009).
[79] Chun-Chieh Lin, Li-Wen Lai, Chih-Yang Lin, Tseung-Yuen Tseng, SrTiO3–SiO2 oxide films for possible high-k gate dielectric applications, Thin Solid Films 515 8005–8008 (2007).
[80] J.M.J. Lopes, M. Roeckerath, T. Heeg, E. Rije, J. Schubert, S. Mantl, V.V. Afanas'ev, S. Shamuilia, A. Stesmans, Y. Jia, D.G. Schlom, Amorphous lanthanum lutetium oxide thin films as an alternative high-gate dielectric, Appl. Phys. Lett. 89, 222902 (2006).
[81] Dina H. Triyoso, David C. Gilmera,1, Jack Jianga, Ravi Droopad, Characteristics of thin lanthanum lutetium oxide high-k dielectrics, Microelectronic Engineering 85, 1732–1735 (2008).
[82] R. Thomas, J.J. Saavedra-Arias, N.K. Karan, N.M. Murari, R.S. Katiyar, P. Ehrhart R. Waser, Thin films of high-k dysprosium scandate prepared by metal organic chemical vapor deposition for metal–insulator–metal capacitor applications, Solid State Communications 147 332–335 (2008).
[83] M. Roeckerath · J.M.J. Lopes · E. Dur˘gun Özben · C. Sandow · S. Lenk · T. Heeg · J. Schubert · S. Mantl, Gadolinium scandate as an alternative gate dielectric in field effect transistors on conventional and strained silicon, Appl Phys A 94, 521–524 (2009).
[84] E. Durğun Özben, J. M. J. Lopes, M. Roeckerath, St. Lenk, B. Holländer, Y. Jia, D. G. Schlom, J. Schubert, and S. Mantl, $SmScO_3$ thin films as an alternative gate dielectric, Appl. Phys. Lett. 93, 052902 (2008).
[85] C. Zhao, T. Witters, B. Brijs, H. Bender, O. Richard, M. Caymax, T. Heeg, J. Schubert, V. V. Afanas'ev, A. Stesmans, and D. G. Schlom, Ternary rare-earth metal oxide high-k layers on silicon oxide, Appl. Phys. Lett. 86, 132903 (2005).
[86] M. Wagner, T. Heeg, J. Schubert, St. Lenk, S. Mantl, C. Zhao, M. Caymax, and S. De Gent, Gadolinium scandate thin films as an alternative gate dielectric prepared by electron beam evaporation, Appl. Phys. Lett. 88, 172901 (2006).
[87] J. Robertson, B. Falabretti, Band offsets of high K gate oxides on high mobility semiconductors Mater. Sci. Eng. B 135, 267 (2006).
[88] V. V. Afanas'ev and A. Stesmans, Energy band alignment at the (100)Ge/HfO2 interface, Appl. Phys. Lett. 84, 2319-2321 (2004).
[89] V.S. Dharmadhikari and A. Goswami, Dielectric properties of electron-beam-evaporated Nd_2O_3 thin films, Thin Solid Films, 87 119-126 (1982).

[90] O. Seifarth,a_ J. Dabrowski, P. Zaumseil, S. Müller, D. Schmeißer, H.-J. Müssig and T. Schroeder, On the band gaps and electronic structure of thin single crystalline praseodymium oxide layers on Si,,111), J. Vac. Sci. Technol. B 27, 271-276 (2009).
[91] V. V. Afanas'ev, S. Shamuilia, A. Stesmans, A. Dimoulas, Y. Panayiotatos, and A. Sotiropoulos, M. Houssa, and D. P. Brunco, Electron energy band alignment at interfaces of (100)Ge with rare-earth oxide insulators, Appl. Phys. Lett. 88, 132111-1 – 132111-3 (2006).
[92] J. Robertson, Section 6. Theory and modelling of high-k dielectrics Band offsets of high dielectric constant gate oxides on silicon, Journal of Non-Crystalline Solids 303 (2002) 94–100
[93] Chang Liu, Eng Fong Chor, Leng Seow Tan, and Yufeng Dong, Band offset measurements of the pulsed-laser-deposition-grown Sc_2O_3 (111)/GaN (0001) heterostructure by X-ray photoelectron Spectroscopy, phys. stat. sol. (c) 4, No. 7, 2330–2333 (2007).
[94] G.-Y. Adachi and N. Imanaka, The binary rare earth oxides, Chem. Rev., 98, 1479–1514 (1998).
[95] Chung-Yuan Chang, Trevor Pi-chun Juan,a_ and Joseph Ya-min Lee, Fabrication and characterization of metal-ferroelectric ($PbZr_{0.53}Ti_{0.47}O_3$)-insulator (Dy_2O_3)-semiconductor capacitors for nonvolatile memory applications, Appl. Phys. Lett. 88, 072917 (2006).
[96] J. C. Wang, K. C. Chiang, T. F. Lei, and C. L. Lee, Electrochem. Solid-State Lett. 7, E55 _2004_.
[97] A. Dimoulas, G. Mavrou, G. Vellianitis, E. Evangelou, N. Boukos, M. Houssa, and M. Caymax, Appl. Phys. Lett. 86, 032908 (2005)
[98] Jaakko Niinisto¨*, Kaupo Kukli, Mikko Heikkila¨, Mikko Ritala and Markku Leskela, Atomic Layer Deposition of High-k Oxides of the Group 4 Metals for Memory Applications, ADVANCED ENGINEERING MATERIALS, 1, 223-234 (2009).
[99] A. Deshpande, R. Inman, G. Jursich, and C. G. Takoudis, J. Appl. Phys. 99, 094102 (2006)
[100] Hyoungsub Kim, Chi On Chui, Krishna C. Saraswat, and Paul C. McIntyre, Applied Physics Letters, Volume 83, Issue 13, pp. 2647-2649, September 29, 2003
[101] M. Ritala and M. Leskalä , Appl. Surf. Sci., 75, 333. (1994)
[102] K. Kukli, K. Forsgren, J. Aarik, A. Aidla, T. Uutare, M. Ritala, A. Niskanan, M. Leskalä and A. Härsta, J. Cryst. Growth, 231, 262 (2001)
[103] K. Kukli, M. Ritala, M. Leskela, T. Sajavaara, J. Keinonen, A. C. Jones and J. L. Roberts, "Atomic layer deposition of hafnium dioxide films from 1-methoxy-2-methyl-2-propanolate complex of hafnium", Chem. Mater., 15, 1722 (2003)
[104] K..Kukli, M. Ritala, T. Pilvi, T. Sajavaara, M. Leskela, A. C. Jones, H. C. Aspinall, D. C. Gilmer, P. J. Tobin, Chem. Mater., 16, 5162, (2004)
[105] Jani Päiväsaari, Matti Putkonen, Lauri Niinistö, Thin Solid Films, 472, 275 (2005)
[106] E. Rauwel, C. Dubourdieu, B. Holländer, N. Rochat, F. Ducroquet, M. D. Rossell, G. Van Tendeloo, and B. Pelissier, Appl. Phys. Lett. 89, 012902 (2006)
[107] S. Chakraborty, M. K. Bera, C. K. Maiti, and P. K. Bose, J. Appl. Phys. 100, 023706 (2006)
[108] Hang Hu, Chunxiang Zhu, Y. F. Lu, Y. H. Wu, T. Liew, M. F. Li, B. J. Cho, W. K. Choi, and N. Yakovlev, Journal of Applied Physics, 94, 551 (2003)

[109] S. Ferrari, S. Spiga, C. Wiemer, M. Fanciulli, and A. Dimoulas, Appl. Phys. Lett. 89, 122906 (2006)
[110] Z. J. Yan, R. Xu, Y. Y. Wang, S. Chen, Y. L. Fan, and Z. M. Jiang, Appl. Phys.Lett., 85, p.85 (2005)
[111] L. Niinistö, J. Päiväsaari, J, Niinistö, M. Putkonen, and M, Nieminen, phys. stat. sol. (a), 201, 1443 (2004)
[112] T. S. Suntola, A. J. Pakkala, and S. G. Lindfors, US Patent 4 413 022 (1983).
[113] K. Kukli, K. Forsgren, J. Aarik, A. Aidla, T. Uutare, M. Ritala, A. Niskanan, M. Leskalä and A. Härsta, J. Cryst. Growth, 231, 262 (2001)
[114] J. Aarik, A. Aidla, A.-A. Kiisler, T. Uustare and V. Sammelselg, Thin Solid Films, 340, 110 (1999)
[115] M. Ritala and M. Leskalä , Appl. Surf. Sci., 75, 333. (1994)
[116] K. Kukli, M. Ritala, M. Leskela, T. Sajavaara, J. Keinonen, A. C. Jones and J. L. Roberts, "Atomic layer deposition of hafnium dioxide films from 1-methoxy-2-methyl-2-propanolate complex of hafnium", Chem. Mater., 15, 1722 (2003)
[117] J.-H. Lee, J. P. Kim, J.-H. Lee, Y.-S. Kim, H.-S. Jung, N.-I. Lee, H.-K. Kang, K.-P. Suh, M.-M. Jeong, K.-T. Hyun, H.-S. Baik, Y. S. Chung, X. Liu, S. Ramanathan, T. Seidel, J. Winkler, A. Londergan, H. Y. Kim, J. M. Ha and N. K. Lee, "Mass production worthy HfO_2-Al_2O_3 laminate capacitor technology using Hf liquid precursor for sub-100 nm DRAMs", IEDM Tech. Digest, pp. 221–224 (2002)
[118] P. Myllym¨aki, M. Roeckerath, M. Putkonen, S. Lenk, J. Schubert, L. Niinist¨o, and S. Mantl, Characterization and electrical properties of high-k GdScO3 thin films grown by atomic layer deposition, Appl. Phys. A 88, 633–637 (2007).
[119] R.D. Shannon, J. Appl. Phys., 73, 348 (1993)
[120] T. Tsutsumi, Jpn. J. Appl. Phys. 9, 735 (1970)
[121] R. K. Sharma, A. Kumar and J. M. Anthony, JOM, 53, 53 (2001)
[122] Jani Päiväsaari, Matti Putkonen, Lauri Niinistö, Thin Solid Films, 472, 275 (2005)
[123] M. Nieminen, S. Lehto, and L. Niinistö, J. Mater. Chem. 11, 3148 (2001)
[124] Pia Myllyma¨ki, Minna Nieminen, Jaakko Niinisto, Matti Putkonen, Kaupo Kuklib and Lauri Niinisto, High-permittivity $YScO_3$ thin films by atomic layer deposition using two precursor approaches, J. Mater. Chem., 2006, 16, 563–569
[125] A B. Lee, K.J. Choi , A. Hande, M.J. Kim, R.M. Wallace, J. Kim, Y. Senzaki, D. Shenai, H. Li, M. Rousseau, J. Suydam," novel thermally-stable zirconium amidinate ALD precursor for ZrO_2 thin films", Microelectronic Engineering 86 (2009) 272–276
[126] R. L. Puurunen, Surface chemistry of atomic layer deposition: A case study for the trimethylaluminum/water process J. Appl. Phys. 2005, 97, 121301-1 121301-52 (2005).
[127] J. Kim and T.W. Kim, Initial surface reactions of atomic layer deposition, JOM (Journal of the Minerals, Metals and Materials Society), 61, 17-22 (2009).
[128] Y. Senzaki, A. K. Hochberg and J. T. Norman, "MOCVD of high-k dielectrics, tantalum nitride and copper from directly injected liquid precursors", Adv. Mater. Opt. Electron., 10, 93-103 (2000).
[129] Taylor, S.; Williams, P.A.; Roberts, J.L.; Jones, A.C.; Chalker, P.R., HfO_2 and ZrO_2 alternative gate dielectrics for silicon devices by liquid injection chemical vapour deposition, Electronics Letters, 38(21), 1285 – 1286 (2002).

[130] Paul A. Williams, John L. Roberts, Anthony C. Jones, Paul R. Chalker, Jamie F. Bickley, Alexander Steiner, Hywel O. Davies and Timothy J. Leedham, "Novel mononuclear zirconium and hafnium alkoxides; improved precursors for the MOCVD of ZrO_2 and HfO_2, J. Mater. Chem., 2002, 12, 165–167.
[131] P. A. Marshall, R. J. Potter, A. C. Jones, P. R. Chalker, S. Taylor, G. W. Critchlow and S. A. Rushworth, Growth of hafnium aluminate thin films by liquid injection MOCVD using alkoxide precursors, Chem. Vap. Deposition, 10, 275-279 (2004)

[132] A. Bastianini, G.A. Battiston, R. Gerbasi, M. Porchia, S. Daolio, "Chemical vapor deposition of ZrO_2 thin films using $Zr(NEt_2)_4$ as precursor", J. Phys. IV, 5(C5), 525-532, (1995).
[133] B. C. Hendrix, A. S. Borovik, C. Xu, J. F. Roeder, T. H. Baum, M. J. Bevan, M. R. Visokay, J. J. Chambers, A. L. P. Rotondaro, H. Bu and L. Colombo, Composition control of Hf1-xSixO2 films deposited on Si by chemical-vapor deposition using amide precursors, Appl. Phys. Lett., Vol. 80, p.2362-2364 (2002).
[134] Hang Hu, Chunxiang Zhu, Y. F. Lu, Y. H. Wu, T. Liew, M. F. Li, B. J. Cho, W. K. Choi, and N. Yakovlev, Journal of Applied Physics, 94, 551 (2003)
[135] M. Ratzke, M. Kappa, D. Wolfframm, S. Kouteva-Arguirova, J.Reif, Fifth International Symposium on Laser Precision Microfabrication. Edited by I. Miyamoto, H. Helvajian, I. Kazuyoshi, K. F. Kobayashi, A. Ostendorf, and K.Sugioka, Proceedings of the SPIE, Volume 5662, pp. 406-411 (2004).
[136] Satoshi Kitai, Osamu Maida, Takeshi Kanashima and Masanori Okuyama, Jpn. J. Appl. Phys. Vol. 42 (2003) pp. 247–253 Part 1, No. 1, January 2003.
[137] J. Zhu, Z.G. Liu, M. Zhu, G.L. Yuan, J.M. Liu, Thermal stability and electrical properties of Zr silicate films for high-k gate-dielectric applications, as prepared by pulsed laser deposition Applied Physics A: Materials Science & Processing, 80, 321-324, 2005.
[138] E. Desbiens and M. A. El Khakani, J. Appl. Phys. Vol 94, pp. 5969-5975 (2003).
[139] Zhu Yanyan, Fang Zebo, Liao Can, Chen Sheng, and Xu Run, Investigation on initial growth of Er2O3 films on Si(001), J. Rare Earth, 25 Sp. Iss. SI, 314-317 (2007).
[140] K. Y. Lee, W. C. Lee, L. K. Chu, M. L. Huang, Y. J. Lee, and M. Hong, Si metal-oxide-semiconductor devices with high HfO_2 fabricated using a novel MBE template approach followed by atomic layer deposition J. Vac. Sci. Technol. B Volume 26, Issue 3, pp. 1178-1181 (May 2008)

[141] J.W. Reiner, A. Posadas, M. Wang, T.P. Ma and C.H.Ahn, Growth and structural properties of crystalline $LaAlO_3$ on Si (0 0 1), Microelectronic Engineering Volume 85, Issue 1, January 2008, Pages 36-38

[142] Apurba Laha, A. Fissel, E. Bugiel, H.J. Osten, Epitaxial multi-component rare earth oxide for high-K application, Thin Solid Films 515 (2007) 6512–6517
[143] T.D. Lin, M.C. Hang, C.H. Hsu, J. Kwo and M. Hong, MBE grown high-quality Gd_2O_3/Si(1 1 1) hetero-structure, J. Cryst. Growth, Volumes 301-302, April 2007, Pages 386-389

[144] G. Vellianitis, G. Apostolopoulos, G. Mavrou, K. Argyropoulos, A. Dimoulas, J.C. Hooker, T. Conard, M. Butcher, MBE lanthanum-based high-k gate dielectrics as candidates for SiO2 gate oxide replacement, Mater. Science and Engineering B 109 pp.85–88 (2004).

[145] Lu, Y.K., Zhu, W., Zhang, Y., Lu, H.,Gopalkrishnan, R., Emerging Technologies - Nanoelectronics, 2006 IEEE Conference on 10-13 Jan. 2006 pp.273 – 277.
[146] Myoung-Seok Kim, Young-Don Ko, Minseong Yun, Jang-Hyuk Hong, Min-Chang Jeong, Jae-Min Myoung and Ilgu Yun, Characterization and process effects of HfO_2 thin films grown by metal-organic molecular beam epitaxy, Materials Science and Engineering: B, Volume 123, Issue 1, 15 November 2005, Pages 20-30

[147] Myoung-Seok Kim, Young-Don Ko, Jang-Hyuk Hong, Min-Chang Jeong, Jae-Min Myoung and Ilgu Yun, Characteristics and processing effects of ZrO_2 thin films grown by metal-organic molecular beam epitaxy, Applied Surface Science Volume 227, Issues 1-4, 15 April 2004, Pages 387-398

[148] C. H. Choi, S. J. Rhee, T. S. Jeon, N. Lu, J. H. Sim, R. Clark, M. Niwa, and D. L. Kwong, "Thermally stable CVD HfO_xN_y advanced gate dielectrics with poly-Si gate electrode", Tech. Dig. Int. Electron Devices Meeting, (IEEE Cat. No.02CH37358) p. 857-860 (2002).

[149] Jeon-Ho Kim, Kyu-Jeong Choi, Soon-Gil Yoon, "Effects of nitrogen in HFO_2 gate dielectric on the electrical and reliability characteristics by N_2 plasma", Electrochemical Society Proceedings, v 4, Dielectrics for Nanosystems: Materials Science, Processing, Reliability, and Manufacturing - proceedings of the First International Symposium, 2004, p 464-469

[150] K.J. Choi, J.H. Kim and S.G. Yoon, "Plasma nitration of HfO_2 gate dielectric in nitrogen ambient for improvement of TaN/HfO_2/Si performance", Electrochem. Solid-State Lett. 7 (10), p. F59-61, (2004).

[151] A.P. Huang, Ricky K.Y. Fu, Paul K. Chua, L. Wang, W.Y. Cheung, J.B. Xu and S.P. Wong, J. Crystal Growth, 277, 422 (2005)

[152] J.C. Wang, D.C. Shie, T.F. Lei and C.L. Lee, "Characterization of temperature dependence for HfO_2 gate dielectrics treated in NH_3 plasma", Electrochem. Solid-State Lett. 6 (10), p. F34-36. (2003)

[153] N. Umezawa, K. Shiraishi, T. Ohno, H. Watanabe, T. Chikyow, K. Torii, K. Yamabe, K. Yamada, H. Kitajima, and T. Arikado, Appl. Phys. Lett. 86, 143507 (2005)

[154] K. Tse and J. Robertson, "Defect passivation in HfO_2 gate oxide by fluorine", Appl. Phys. Lett. 89, 142914 (2006)

[155] M. Inoue, S. Tsujikawa, M. Mizutani, K. Nomura, T. Hayashi, K. Shiga, J. Yugami, J. Tsuchimoto, Y. Ohno, and M. Yoneda, "Fluorine incorporation into HfSiON dielectric for V_{th} control and its impact on reliability for poly-Si gate pFET", Tech. Dig. - Int. Electron Devices Meet, (IEEE Cat. No.05CH37703C), p. 413-416. (2005).

[156] K. I. Seo, R. Sreenivasan, P. C. McIntyre, and K. C. Saraswat, "Improvement in high-k (HfO_2/SiO_2) reliability by incorporation of fluorine" Tech. Dig.- Int. Electron Devices Meet., pp.417-420, (2005).

[157] H. H. Tseng, P. J. Tobin, E. A. Herbert, S. Kalpat, M. E. Ramon, L. Fonseca, Z. X. Jiang, J. K. Schaeffer, R. I. Hegde, D. H. Triyoso, D. C. Gilmer, W. J. Taylor, C. C. Capasso, O. Adetutu, D. Sing, J. Conner, E. Luckowski, B. W. Chan, A. Haggag, and B. E. White, "Microstructure modified HfO_2 using Zr addition with Ta $_xC_y$ gate for improved device performance and reliability", Tech. Dig. - Int. Electron Devices Meet., pp.35-38, (2005).

[158] S. H. Bae, C. H. Lee, R. Clark, and D. L. Kwong, IEEE Electron Devices Letters, 24, 9, 556 (2003).

[159] A. Toriumi, K. Tomida, H. Shimizu, K. Kita, and K. Kyuno, "Far- and Mid-Infrared Absorption Study of HfO2/SiO2/Si System," Silicon Nitride and Silicon Dioxide Thin Insulating Films and Other Emerging Dielectrics VIII, R. E. Sah, M. J. Deen, J. Zhang, J. Yota, and Y. Kamakura, Eds., PV 2005-01, Electrochemical Society, Piscataway, NJ, 2005, p. 471.

[160] Y.-H. Lin, C.-H. Chien, C.-T. Lin, C.-W. Chen, C.-Y. Chang, and T.-F. Lei, IEDM Tech. Digest, pp. 1080–1082 (2004).

[161] Akira Toriumi and Koji Kita, in chapter 7 "Material Engineering of High-k Gate Dielectrics" of "Dielectric Films for Advanced Microelectronics", ed. by Mihkail Baklanov, Karen Maex, Martin Green (Wiley, Chichester, UK, 2007), pp. 325

[162] Koji Kita, Kentaro Kyuno, and Akira Toriumi, Permittivity increase of yttrium-doped HfO2 through structural phase transformation, Appl. Phys. Lett. 86, 102906-1 – 102906-3 (2005).

[163] G. H. Chen, Z. F. Hou, X. G. Gong, and Quan Li, Effects of Y doping on the structural stability and defect properties of cubic HfO2, J. Appl. Phys. 104, 074101-1 – 074101-6 (2008).

[164] X.Y.Zhao and D. Vanderbilt, First-principles study of structural, vibrational, and lattice dielectric properties of hafnium oxide, Phys. Rev. B, 65, 233106-1 - 233106-4 (2002).

[165] D. A. Neumayer and E. Cartier, J. Appl. Phys., 90, 1801 (2001)

[166] S. Guha, E. P. Gusev, M. Copel, L.-Å . Ragnarsson, and D. A. Buchanan, Mater. Res. Soc. Bull. 27, 226 (2002).

[167] N. V. Nguyen, M. M. Frank, A. V. Davydov, and D. Chandler-Horowitz, Appl. Phys. Lett., 87, 192903 (2005).

[168] A. Chatterjee, R. A. Chapman, K. Joyner, M. Otobe, S. Hattangady, M. Bevan, G. A. Brown, H. Yang, Q. He, D. Rogers, D. Fang, S.J. Kraft, R. Rotondaro, A.L.P. Terry, M. Brennan, K. Aur, S.-W. Hu, J.C. Tsai, H.-L. Jones, P. Wilk, G. Aoki, M. Rodder, M. Chen, I.-C., "CMOS metal replacement gate transistors using tantalum pentoxide gate insulator", IEDM Tech. Digest, pp. 777-780, (1998).

[169] M. V. Fischetti, D. A. Neumayer, and E. A. Cartier, Effective electron mobility in Si inversion layers in metal–oxide–semiconductor systems with a high-k insulator: The role of remote phonon scattering J. Appl. Phys. 90, 4587-4608 (2001).

[170] L. Yang, J. R. Watling, J. R. Barker, and A. Asenov, The impact of soft-optical phonon scattering due to high-k dielectrics on the performance of sub-100nm conventional and strained Si n-MOSFETs, Physics of Semiconductors, eds. J. Menedez and C.G. Van de Walle, AIP Press, 27, 1497 (2005).

[171] Z. Ren, M. Fischetti, E. P. Gusev, E. Cartier, and M. Chudzik, "Inversion channel mobility in high-κ high performance MOSFETs", IEDM Tech. Digest, pp. 793-796, (2003)

[172] E. P. Gusev, D. A. Buchanan, P. Jamison, T. H. Zabel, and M. Copel, Microelectron. Eng., 48, 67 (1999)

[173] C. C. Hobbs, L. R. C. Fonseca, A. Knizhnik, V. Dhandapani, S. B. Samavedam, W. J. Taylor, J. M. Grant, L. G. Dip, D. H. Triyoso, R. I. Hegde, D. C. Gilmer, R. Garcia, D. Roan, M. L. Lovejoy, R. S. Rai, E. A. Hebert, H. H. Tseng, S. G. H. Anderson, B. E. White, and P. J. Tobin, Fermi-Level Pinning at the Polysilicon/Metal Oxide Interface—Part I, IEEE Trans. Electron Devices, 51, 971-977 (2004)

[174] C. C. Hobbs, L. R. C. Fonseca, A. Knizhnik, V. Dhandapani, S. B. Samavedam, W. J. Taylor, J. M. Grant, L. G. Dip, D. H. Triyoso, R. I. Hegde, D. C. Gilmer, R. Garcia, D. Roan, M. L. Lovejoy, R. S. Rai, E. A. Hebert, H. H. Tseng, S. G. H. Anderson, B. E. White, and P. J. Tobin, Fermi-Level Pinning at the Polysilicon/Metal–Oxide Interface—Part II, IEEE Trans. Electron Devices, 51, 978-984 (2004)

[175] W. S. Kim, S. Kamiyama, T. Aoyama, H. Itoh, T. Maeda, T. Kawahara, K. Torii, H. Kitajima, and T. Arikado, "Depletion-free poly-Si gate high-κ CMOSFETs", IEDM Tech. Digest, 833–836 (2004).

[176] M. M. Frank, V. K. Paruchuri, V. Narayanan, N. Bojarczuk, B. Linder, S. Zafar, E. A. Cartier, E. P. Gusev, P. C. Jamison, K.-L. Lee, M. L. Steen, M. Copel, S. A. Cohen, K. Maitra, X. Wang, P. M. Kozlowski, J. S. Newbury, D. R. Medeiros, P. Oldiges, S. Guha,

R. Jammy, M. Ieong, and G. Shahidi, “Poly-Si/high-κ gate stacks with near-ideal threshold voltage and mobility”, IEEE VLSI–TSA–Tech, International Symposium on VLSI Technology, pp. 97–98, (2005)

[177] H.N. Alshareef, H.R. Harris, H.C. Wen, C.S. Park, C. Huffman1, K. Choi, H.F. Luan, P. Majhi, B.H. Lee, and R. Jammy, D.J. Lichtenwalner, J.S. Jur, and A. I. Kingon, Digest of Technical Papers of Symposium on VLSI Technology, 2006, pp. 7-8.

[178] H. -J. Cho, H. Y. Yu, L.-A. Ragnarsson, V. S. Chang, T. Schram, B. J. O'Sullivan, S. Kubicek, R. Mitsuhashi, A. Akheyar, S. Van Elshocht, T. Witters, A. Delabie, C. Adelmann, E. Rohr, R. Singanamalla, S. -Z. Chang, J. Swerts, P. Lehnen, S. De Gendt, P. P. Absil, and S. Biesemans, Integrated Circuit Design and Technology, ICICDT '07. IEEE International Conference on, pp 1-3, (2007)

[179] P. Sivasubramani, T. H. Lee, M. J. Kim, J. Kim, B. E. Gnade, and R. M. Wallace, L. F. Edge, D. G. Schlom, F. A. Stevie, R. Garcia, Z. Zhu, and D. P. Griffis, Thermal stability of lanthanum scandate dielectrics on Si(100), Appl. Phys. Lett. 89, 242907-1 – 242907-3 (2006).

[180] J. M. J. Lopes,a_ U. Littmark, M. Roeckerath, St. Lenk, J. Schubert, and S. Mantl, and A. Besmehn, Effects of annealing on the electrical and interfacial properties of amorphous lanthanum scandate high-K films prepared by molecular beam deposition, J. Appl. Phys. 101, 104109-1 – 104109-5 (2007).

[181] J. Valasek, Piezo-Electric and Allied Phenomena in Rochelle Salt, Phys. Rev., 17, 475 (1921).

[182] I. V. Kurchatov, Segnetoelektriki, Moskva: Gosudarstvennoe Tekhniko-Teoreticheskoe Izdatel’stvo, 1933 (in Russian) Translation: I.V. Kurchatov, Ferroelectrics, Moscow, State Technical Theoretical Publishing House, 1933.

[183] G. Busch and P. Scherrer, “Eine neue seignette-elektrische Substanz (A new rocksalt-electric substance)”, Naturwissenschaften, 23, 737 (1935).

[184] B. Wul, and I. M. Goldman, Comptes Rendus URSS, 46, 139 (1945).

[185] V.M. Goldschmidt, “Geochemische Verteilungsgesetze VIII. Bau und Eigenschaften von Krystallen "(1927) Skrifter utgitt av det Norske Videnskaps-Akademi i Oslo 1: Matematisk-Naturvidenskapelig Klasse 1927, 1-156; von Hippel et al. (1946). Ind. Eng. Chem. 38, 1089. Internationale Tabellen zur Bestimmung yon Kristallstructuren (1935), Vol. 2. Berlin: Gebriider Borntraeger; Evans, H.T.Jr. The crystal structure of tetragonal barium titanate”,Acta Crystallographica 4, 377-377 (1951);Evans, H.T.Jr., “An X-ray diffraction study of tetragonal barium titanate”, Acta Crystallographica 14, 1019-1026(1961); H. D. Megaw, “Refinement of the structure of BaTiO3 and other ferroelectrics”, Acta Crystallographica 15, 972-973 (1962)

[186] V.L. Ginzburg, On the dielectric properties of ferroelectric (seignetteelectric) crystals and barium titanate, Zh. Eksp. Teor. Fiz. 15, 739 [J. Phys. (USSR) 10, 107 (1946)].

[187] G. A. Smolensky and A. I. Agranovskaya, A new group of ferroelectrics (with layered structure), Sov. Phys. Solid State, 1, 149-150 (1959).

[188] G. A. Smolensky, V. A. Isupov, and A. I. Agranovskaya, Ferroelectrics of the oxygen-octahedral type with layered structure, Sov. Phys. Solid State, 3, 651-655 (1961).

[189] E. C. Subbarao, A family of ferroelectric bismuth compounds, J. Phys. Chem. Solids, 23, 665, (1962).
[190] S. E. Cummins and L. E. Cross, Electrical and optical properties of ferroelectric $Bi_4Ti_3O_{12}$ single crystal, J. Appl. Phys. 39, 2268 (1968).
[191] K. Amanuma, T. Hase, and Y. Miyasaka, Appl. Phys. Lett. 66, 221 (1995).
[192] C.A. Paz de Araujo, J. D. Cuchiaro, L. D. McMillan, M. C. Scott, and J. F. Scott, Fatigue-free ferroelectric capacitors with platinum electrodes, Nature (London) 374, 627 (1995).
[193] J. F. Scott, F. M. Ross, C. A. Paz de Araujo, M. C. Scott, and M. Huffman, MRS Bull. 21, 33 (1996).
[194] O. Auciello, J. F. Scott, and R. Ramesh, Phys. Today 51, 22 (1998)
[195] Xu, Y., "Ferroelectric Materials and Their Applications", North Holland, 1991.
[196]Lines, M.E. and Glass, A.M., "Principles and Applications of ferroelectrics and related materials", Clarendon Press, Oxford 1977.
[197] Sonin, A.S. and Strukov, B.A., "Introduction in Ferroelectricity", Vysshaya Shkola, Moscow, 1970.
[198] D. Damjanovic and M. Demartin, Contribution of the irreversible displacement of domainwalls to the piezoelectric effect in barium titanate and lead zirconate titanate ceramics, J. Phys.—Condensed Matter 9, 4943 (1997).

[199] D. Damjanovic, Ferroelectric, dielectric and piezoelectric properties of ferroelectric thin films and ceramics, Rep. Prog. Phys. 61, 1267 (1998).

[200] Lupascu, D.C., "Fatigue in ferroelectric ceramics and related issues," (Springer Series in Materials Science, Volume 61), Springer press, 2004.

[201] Lupascu, D.C. and Roedel, J. "Fatigue in bulk lead zirconate titanate actuator materials," Adv Engr Mater, 7, 882, 2005.

[202] M. Grossmann, O. Lohse, T. Schneller, D. Bolten, U. Boettger, J. Contreras, Rodriguez, H. Kohlstedt, and R. Waser, Imprint in ferroelectric $Pb(Zr,Ti)O_3$ thin films with thin SrRuO3 layers at the electrodes, Int. Ferroelectrics 37, 205-214 (2001).
[203] Lee, J., Ramesh, R., Keramidas, V. G., Warren, W. L., Pike, G. E., and Evans, J. T., Jr., "Imprint and oxygen deficiency in $(Pb,La)(Zr,Ti)O_3$ thin-film capacitors with La-Sr-Co-O electrodes", Appl. Phys. Lett., 66, 1337, 1995.

[204] Pike, G. E., Warren, W. L., Dimos, D., Tuttle, B. A., Ramesh, R., Lee, J., Keramidas, V. G., and Evans, J. T., Jr., "Voltage offsets in $(Pb,La)(Zr,Ti)O_3$ thin films, Imprint and oxygen deficiency in $(Pb,La)(Zr,Ti)O_3$ thin-film capacitors with La-Sr-Co-O electrodes", Appl. Phys. Lett., 66, 484, 1995.

[205] Friessnegg, T., Aggarwal, S., Ramesh, R., Nielsen, B., Poindexter, E.H., and Keeble, D.J., "Vacancy formation in $(Pb,La)(Zr,Ti)O_3$ capacitors with oxygen deficiency and the effect on voltage offset", Applied Physics Letters, v 77, n 1, p 127-93 July 2000

[206] B. S. Kang, J.-G. Yoon, D. J. Kim, T. W. Noh, T. K. Song, Y. K. Lee, J. K. Lee, and Y. S. Park, Mechanisms for retention loss in ferroelectric Pt/Pb(Zr0.4Ti0.6)O3/Pt capacitors, Appl. Phys.Lett. 82, 2124-2126 (2003).
[207] Dawber, M., Rabe, K.M., and Scott, J.F., "Physics of thin-film ferroelectric oxides", Rev. Mod. Phys., 77, 1083, 2005.

[208] A. Dixit, S.B. Majumder, A. Savvinov, R.S. Katiyar, R. Guo,A.S. Bhalla, Mater. Lett. 56 (2002) 933.

[209] X.G. Tang, R.K. Zheng, Y.P. Jiang, H.L.W. Chan, J. Phys. D: Appl. Phys. 39 (2006) 3394.

[210] T.B. Wu, C.M. Wu, M.L. Chen, Appl. Phys. Lett. 69 (1996) 2659.

[211] B. A. Baumert, L.-H. Chang, A. T. Matsuda, T.-L. Tsai, C. J. Tracy, R. B. Gregory, P. L. Fejes, N. G. Cave, W. Chen, D. J. Taylor, T. Otsuki, E. Fujii, S. Hayashi, and K. Suu, Characterization of sputtered barium strontium titanate and strontium titanate-thin films, J. Appl. Phys. 82, 2558-2566 (1997).
[212] Sharmistha Lahiry and A. Mansingh, Dielectric properties of sol–gel derived barium strontium titanate thin films, Thin Solid Films 516 (2008) 1656–1662.

[213] C. Menoret, J. M. Kiat, B. Dkhil, M. Dunlop, H. Dammak, O. Hernandez, Structural evolution and polar order in $Sr_{1-x}Ba_xTiO_3$, Phys. Rev. B 65, 224104 (2002)

[214] D. Barb, E. Barbulescu and A. Barbulescu, Phys. Status Solidi A, 74, 79 (1982)
[215] V. V. Lemanov, E. P. Smirnova, P. P. Syrnikov, and E. A. Tarakanov, Phys. Rev. B 54, 3151 (1996)
[216] M. E. Guzhva, V. V. Lemanov, and P. A. Markovin, Fiz. Tverd. Tela S. Peterberg 39, 704 ~1997! @Phys. Solid State 39, 618, (1997).

[217] V. S. Tiwari, N. Singh and D. Pandey, J. Phys.: Condens. Matter 7, 1441 ~1995!.

[218] N. Singh and D. Pandey, J. Phys.: Condens.Matter 8, 4269 (1996). N. Singh, A. P. Singh, Ch. D. Prasad, and D. Pandey, J. Phys.: Condens. Matter 8, 7813 (1996).

[219] U. Syamaprasad, R. K. Galgali, and B. C. Mohanty, Mater. Lett. 7, 197–200 (1988).
[220] C. M. Carlson, T. V. Rivkin, P. A. Parilla, J. D. Perkins, D. S. Ginley,A. B. Kozyrev, V. N. Oshadchy, and A. S. Pavlov, Appl. Phys. Lett. 76, 1920 (2000)
[221] P. Bao, T. J. Jackson, X. Wang and M. J. Lancaster, Barium trontium titanate thin film varactors for room-temperature microwave device applications, J. Phys. D: Appl. Phys. 41, 063001 (2008)
[221] A. K. Tagantsev, V. O. Sherman, K. F. Astafiev, J. Venkatesh and N. Setter, J. Electroceram. 11, 5 (2003)

[222] D. Galt, J. Price, J.A. Beall, and R.H. Ono, Appl. Phys. Lett.63, 3078 (1992)
[223] V.N. Kesis, A.B. Kozyrew, M.L. Khazov, J. Sok, and J.S. Lee, Electron. Lett. 34, 107 (1998).
[224] Y. Liou, W.K. Chu, and C.W. Chu, Epitaxial ferroelectric $Ba_{0.5}Sr_{0.5}TiO_3$ thin films for room-temperature tunable element applications Appl. Phys. Lett. 75, 412 (1999).
[225] J. Im, O. Auciello, S. Streiffer, P. Baumann, D. Kaufman, and A.R. Krauss, Composition-control of magnetron-sputter-deposited $(Ba_xSr_{1-x})Ti_{1+y}O_{3+z}$ thin films for voltage tunable devices Appl. Phys. Lett. 76, 625 (2000).
[226] W.J. Kim, W. Chang, S.B. Qadri, J.M. Pond, S.W. Kirchoefer, D.B. Chrisey, and J.S. Howitz, Microwave properties of tetragonally distorted (Ba0.5Sr0.5)TiO3 thin films Appl. Phys. Lett. 76, 1185 (2000).
[227] Kwak, B.S., Erbil, A., Budai, J., Chisholm, M.F., Boatner, L.A., and Wilkents, B.J., "Domain formation and strain relaxation in epitaxial ferroelectric heterostructures", Phys. Rev. B. 49, 14865, 1994.
[228] Kong, L.B., Ma, J., Zhu, W., and Tan, O.K., "Preparation and characterization of lead zirconate ceramics from high-energy ball milled powder", Materials Letters, 49, 96, 2001.
[229] Woodward, D.I., Knudsen, J., and Reaney, I. M., "Review of crystal and domain structures in the $PbZr_xTi_{1-x}O_3$ solid solution", Phys. Rev. B. 72, 104110-1 – 104110-8, 2005.
[230] Noheda, B., Cox, D.E., Shirane, G.., Gonzalo, J.A., Cross, L.E., and Park, S-E., "A monoclinic ferroelectric phase in the $Pb(Zr_{1-x}Ti_x)O_3$ solid solution", Appl. Phys. Lett. 74, 2059, 1999.
[231] Noheda, B., Cox, D.E., Shirane, G., Guo, R., Jones, B., and Cross, L.E., "Stability of the monoclinic phase in the ferroelectric perovskite $PbZr_{1-x}Ti_xO_3$", Phys. Rev. B. 63, 014103, 2001.
[232] B. Noheda, and D. E. Cox, Bridging phases at the morphotropic boundaries of lead oxide solid solutions, Phase Transitions 79, 5
(2006).

[233] Smolenski, G.A., Isupov, V.A., Arganovskaya, A.A., and Popov, S.N., "Ferroelectrics with diffuse phase transition", Fiz. Tverd.Tela, 2, 2906, 1960.
[234]B. Aurivillius, Mixed bismuth oxides with layer lattices. I. Structure type of $CaCb_2Bi_2O_9$, Arkiv Kemi 1, 463 (1949); B. Aurivillius, Mixed bismuth oxides with layer lattices: II. Structure of $Bi_4Ti_3O_{12}$, Arkiv Kemi 1, 499 (1949).
[235] H. Amorín, V. V. Shvartsman, A. L. Kholkin, and M. E. V. Costa, Ferroelectric and dielectric anisotropy in high-quality $SrBi_2Ta_2O_9$ single crystals, Applied Physics Letters 85, 5667-5669 (2004).
[236] S. Kamba, J. Pokorny, V. Porokhonsky, J. Petzelt, M. P. Moret, A. Garg, Z. H. Barber, and R. Zallen, Appl. Phys. Lett. 81, 1056 (2002).
[237] A. Onodera, K. Yoshio, and H. Yamashita, Jpn. J. Appl. Phys., Part 1 42, 6218 (2003).
[238] J.-H. Ko, A. Hushur, S. Kojima, B. C. Sih, and Z.-G. Ye, Appl. Phys. Lett. 81, 4043 (2002).
[239] H. Irie and M. Miyayama, Appl. Phys. Lett. 79, 251 (2001).
[240] Y. Shimakawa, Y. Kubo, Y. Nakagawa, T. Kamiyama, H. Asano, and F. Izumi, Appl.

Phys. Lett. 74, 1904 (1999).
[241] B. H. Park, B. S. Kang, S. D. Bu, T. W. Noh, J. Lee, and W. Jo, Lanthanum-substituted bismuth titanate for use in non-volatile memories, Nature _London_ 401, 682 (1999)

[242] Shiosaki, T. and Shimizy, M., "Pb-based and Bi-based ferroelectric thin films", J. Korean Phys. Soc., 32, S1316, 1998.
[243] Funakubo, H., Watanabe, T, Morioka, H, Nagai, A, Oikawa, T, Suzuki, M, Uchida, H, Kouda, S, and Saito, K., "Polarization comparison of $Pb(Zr,Ti)O_3$ and $Bi_4Ti_3O_{12}$-based ferroelectrics", Mat. Sci.Engin. B, 118, 23, 2005.
[244] E.C. Subbarao, Ferroelectricity in $Bi_4Ti_3O_{12}$ and its solid solutions, Phys. Rev, 122, 804 (1961).
[245] Cummings, S.E., Cross, L.E., "Electrical and optical properties of ferroelectric $Bi_4Ti_3O_{12}$ single crystal", J. Appl. Phys., 39, 2268, 1968.
[246] P. C. Joshi and S. B. Krupanidhi, Rapid thermally processed ferroelectric Bi4Ti3012 thin films, J. Appl. Phys. 72, 5517 (1992).
[247] B. H. Park, S. J. Hyun, S. D. Bu, T. W. Noh, J. Lee, H.-D. Kim, T. H. Kim, and W. Jo, Differences in nature of defects between $SrBi_2Ta_2O_9$ and $Bi_4Ti_3O_{12}$ Appl. Phys. Lett. 74, 1907 (1999).

[248] B. H. Park, B. S. Kang, S. D. Bu, T. W. Noh, J. Lee, and W. Jo, Lanthanum-substituted bismuth titanate for use in non-volatile memories, Nature (London) 401, 682 (1999).

[249] Maeder, M. D., Damjanovic, D., and Setter, N., "Lead Free Piezoelectric Materials", J. Electroceram, 13, 385, 2004.
[250] Sinharoy, S. and Buhay, H., "Integration of ferroelectric thin films into nonvolatile memories", J. Vac. Sci. Technol. A, 10, 1554, 1992.

[251] Sun, H.-J., Choi, E. S., Kweon, S. Y., Kim, N. K., Yeom, S. J., Roh, J.-S., and Sohn, H.-C., "$Pb(Zr_xTi_{1-x})O_3$ Thin Film Fabricated on Heterogeneous Under-Layer of Pt and SiO_2 in High Density Ferroelectric Random Access Memory (FeRAM) Capacitor", Jpn. J. Appl. Phys., 42, L1504, 2003.

[252] K. Nashimoto, S. Nakamura, H. Moriyama, M. Watanabe,and E. Osakabe, Electro-optic beam deflector using epitaxialPb(Zr,Ti)O_3 waveguides on Nb-doped $SrTiO_3$, Appl. Phys. Lett.73, 303 (1998).
[253] S. H. Hu, X. J. Meng, G. J. Hu, J. H. Chu, N. Dai, L. Xu, L. Y.Liu, and D. X. Li, Preparation and optical waveguide property of metal alkoxide solution-derived Pb(Zr0.5Ti0.5)O3 thick films, Appl. Phys. Lett. 84, 3609 (2004).

[254] Sreenivas, K., Sayer, M., Baar, D. J., and Nishioka, M., "Surface acoustic wave propagation on lead zirconate titanate thin films", Appl. Phys. Lett., 52, 709, 1988.

[255] Lazarevic Z, Stojanovic BD, Varela JA, An approach to analyzing synthesis, structure and properties of bismuth titanate ceramics, SCIENCE OF SINTERING Volume: 37 Issue: 3 Pages: 199-216 2005

[256] Manoj Kumar, Ashish Garg, Ravi Kumar, M.C. Bhatnagar, Structural, dielectric and ferroelectric study of $Ba_{0.9}Sr_{0.1}Zr_xTi_{1-x}O_3$ ceramics prepared by the sol–gel method, Physica B 403 (2008) 1819–1823.

[257] Zhiqiang Wei,Huping Xu, Minoru Noda and Masanori Okuyama, Preparation of $Ba_xSr_{1-x}TiO_3$ thin films with seeding layer by a sol–gel method, Journal of Crystal Growth Volumes 237-239, Part 1, April 2002, Pages 443-447

[258] Reaney, I.M., Taylor, D.V., and Brooks, K.G., "Ferroelectric PZT Thin Films by sol-gel deposition", J. Sol-Gel Sci. Technol., 13, 813, 1998.

[259] Tsai SD, Suresh MB, Chou CC, Improvement in ferroelectric properties of PZT thick films prepared by a modified sol-gel technique using low temperature laser annealing, PHYSICA SCRIPTA Volume: T129 Pages: 175-179 Published: DEC 2007

[260] Pu, Zhaohui, Wu, Jiagang, Yu, Xudong, Xu, Peng, Cheng, Lifang, Xiao, Dingquan, Zhu, Hanguo, Enhanced electrical properties of Pb(Zr0.80Ti0.20)O-3 modified sol-gel technique, SURFACE & COATINGS TECHNOLOGY Volume: 202 Issue: 10 Pages: 2068-2071 Published: FEB 15 2008

[261] L.N. Gao, S.N. Song, J.W. Zhai, X. Yaoa, Z.K. Xu, Effects of buffer layers on the orientation and dielectric properties of $Ba(Zr_{0.20}Ti_{0.80})O_3$ thin films prepared by sol–gel method, Journal of Crystal Growth 310 (2008) 1245–1249.

[262] Graca MPF, da Silva MGF, Valente MA, Structural and electrical characteristics of $LiNbO_3$ embedded in a 34% SiO2 glass matrix, JOURNAL OF THE EUROPEAN CERAMIC SOCIETY Volume: 28 Issue: 6 Pages: 1197-1203 Published: 2008

[263] Qi, Yajun, Lu, Chaojing, Zhang, Qiaofeng, Wang, Lihua, Chen, Fang, Cheng, Chunsheng, Liu, Baoting, Improved ferroelectric and leakage properties in sol-gel derived $BiFeO_3/Bi_{3.15}Nd_{0.85}Ti_3O_{12}$ bi-layers deposited on $Pt/Ti/SiO_2/Si$, J. of Physics D-Applied Physics Volume: 41 Issue: 6 Article Number: 065407 Published: MAR 21 2008

[264] Ye, Wanneng, Lu, Chaojing, Qi, Yajun, Liu, Xiaolin, Senz, Stephan, Lee, Sung Kyun, Hesse, Dietrich, Sol-gel derived ferroelectric Bi3.15Nd0.85Ti3O12 thin films of predominant 100/010/119 orientation deposited both on Nb-doped (011)$SrTiO_3$ and on (011)$SrRuO_3$/(011)$SrTiO_3$, APPLIED PHYSICS A-MATERIALS SCIENCE & PROCESSING Volume: 91 Issue: 2 Pages: 323-326 Published: MAY 2008

[265] Schneller T, Waser R, Chemical solution deposition of ferroelectric thin films - State of the art and recent trends, FERROELECTRICS Volume: 267 Pages: 293-301 Published: 2002

[266] Waser, R., Schneller, T., Horrmann-Eifert, S., and Ehrhart, P., "Advanced chemical deposition techniques – from research to production", Integrated Ferroelectrics, 36, 3, 2001.

[267] Schwartz, R.W., Boyle, T.J., Lockwood, S.J., Sinclair, M.B., Dimos, D., and Buchheit, C.D., "Sol-gel processing of PZT thin films: A review of the state-of-the-art and process optimization strategies", Int. Ferroelectrics, 7, 259, 1995.

[268] Schwartz, R.W., Schneller, T., and Waser, R., "Chemical solution deposition of electrinic oxide films", Comptes Rendus Chimie, 7, 433, 2004.

[269] Majumder SB, Bhaskar S, Katiyar RS, Critical issues in sol-gel derived ferroelectric thin films: A review, INTEGRATED FERROELECTRICS, 42, 245-292, 2002

[270] Vorotilov KA, Yanovskaya MI, Turevskaya EP, Sigov AS, Sol-Gel Derived Ferroelectric Thin Films: Avenues for Control of Microstructural and Electric Properties, Journal of Sol-Gel Science and Technology 16, 109–118 (1999)

[271] Reaney, I.M., Taylor, D.V., and Brooks, K.G., "Ferroelectric PZT Thin Films by sol-gel deposition", J. Sol-Gel Sci. Technol., 13, 813, 1998.

[272] Brooks K. G., Reaney, I. M., Klissurska, R., Huang, Y., Buzsill, L., and Setter, N., "Orientation of rapid thermally annealed lead zirconate titanate thin films on (111) Pt substrates", J. Mater. Res. 9, 2540, 1994.

[273] Tiwari, V. S., Kumar, A., Wadhawan, V. K., "Kinetics of formation of the pyrochlore and perovskite phases in sol-gel derived lead zirconate titanate powder", J. Mater. Res., 13, 2170, 1998.

[274] Bursil, L.A. and Brooks, Keith G., "Crystallization of sol-gel derived lead-zirconate-titanate thin films in argon and oxygen atmospheres", J. Appl. Phys., 75, 4501, 1994.

[275] Klee, M., Eusemann, R., Waser, R., Brand, W., and Van Hal, H., "Processing and elelctrical properties of $Pb(Zr_xTi_{1-x})O_3$ (x=0.2-0.75) films: Comparison of metallo-organic decompostion and sol-gel processes", J. Appl. Phys., 72, 1566, 1992.

[276] Vorotilov, K.A., Yanovskaya, M.I., Turevskaya, E.P., and Sigov, A.S., "Sol-gel derived ferroelectric thin films: Avenues for control of microstructural an delectric properties". J. Sol-Gel Sci. Technol., 16, 109, 1999.

[277] Lefevre, M. J., Speck, J. S., Schwartz, R. W., Dimos, D., and Lockwood, S. J., "Microstructural development in sol-gel derived lead zirconate titanate thin films: The role of precursor stoichiometry and processing environment", J. Mater. Res, 11, 2076, 1996.

[278] Law, C. W., Tong, K.Y., Li, J. H., and Li, K., "Effect of pyrolysis temperature on the characteristics of PZT films deposited by the sol-gel method", Thin Solid Films, 335, 220, 1998.

[279] Gong, W., Li, J.-F., Chu, X., and Li, L., "Effect of pyrolysis temperature on preferential orientation and electrical properties of sol-gel derived lead zirconate titanate films", J. European Ceramic Soc., 24, 2977, 2004.

[280] Meng, X. J., Cheng, J. G., Li, B., Guo, S. L., Ye, H. J., and Chu, J. H., "Low-temperature preparation of highly (1 1 1) oriented PZT thin films by a modified sol–gel technique", J. Cryst. Growth, 208, 541, 2000.

[281] Shen, I.Y. (Steve)., Cao, G. Z., Wu, Chia-Che, and Lee, Cheng-Ghun, "PZT Thin-Film Meso- and Micro Devices", Ferroelectrics, 342, 15, 2006.

[282] Hwang, Jae-Seob., Kim, Woo Sik., Park, Hyung-Ho., Kim, Tae-Song, "The effect of intermediate anneal on the ferroelectric properties of direct-patternable PZT films", Sensors and Actuators A, 117, 137–142, 2005.

[283] Razak, K. A., Asadov, A., Yoo, J., Haemmerle, E.,Gao, W. Structural and dielectric properties of barium strontium titanate produced by high temperature hydrothermal method, JOURNAL OF ALLOYS AND COMPOUNDS, Volume: 449 Issue: 1-2 Pages: 19-23 2008

[284] Prabir K. Dutta, Reza Asiaie, Sheikh A. Akbar, and Weidong Zhug, Hydrothermal Synthesis and Dielectric Properties of Tetragonal BaTiO3, Chem. Mater. 1994, 6, 1542-1548

[285] Iain J. Clark, Tomanari Takeuchi, Noikazu Ohtoric and Derek C. Sinclaira, Hydrothermal synthesis and characterisation of BaTiO3 fine powders: precursors, polymorphism and properties, J. Mater. Chem., 1999, 9, 83–91

[286] Wada, H. Chikamori, T. Noma and T. Suzuki, Hydrothermal synthesis of barium titanate crystallites using new stable titanium chelated complex in aqueous solution, J. Mater. Sci. 19 (2000), p. 245.

[287] Weian Sun, Size effect in barium titanate powders synthesized by different hydrothermal methods, J. Appl. Phys. 100, 083503 _2006_

[288] Wei, Nian, Zhang, Duan-Ming, Han, Xiang-Yun, Yang, Feng-Xia, Zhong, Zhi-Cheng, Zheng, Ke-Yu, Synthesis and mechanism of ferroelectric potassium tantalate niobate nanoparticles by the solvothermal and hydrothermal processes, JOURNAL OF THE AMERICAN CERAMIC SOCIETY Volume: 90 Issue: 5 Pages: 1434-1437 Published: MAY 2007

[289] Anderson Dias and Roberto L. Moreira, Production of Sr-deficient bismuth tantalates frommicrowave–hydrothermal derived precursors: Structural and dielectric properties, Journal of Physics and Chemistry of Solids 68 (2007) 645–649

[290] Morita, T. and Cho, Y., "Epitaxial $PbTiO_3$ thin films on $SrTiO_3(100)$ and $SrRuO_3/SrTiO_3(100)$ substrates deposited by a hydrothermal method", Jpn. J. Appl. Phys., 43, 6535, 2004

[291] Kutty, T.R.N. and Balachandran, R., "Direct precipitation of lead zirconate titanate by the hydrothermal method", Mater. Res. Bull., 19, 1479, 1984.

[292] Trianidis, M., Courtois, C., Leriche, A., "Mechanism of PZT crystallization under hydrothermal conditions Development of a new synthesis route", J. Eur. Ceram. Soc., 20, 2713, 2000.

[293] Piticescu, R. M., Mitoseriu, L., Viviani, M., and Poladian, V. M., "Preparation and characterisation of $Pb(Zr_{0.52}Ti_{0.48})_{0.975}Nb_{0.025}O_3$ ceramics Modelling the device", J. Eur. Ceram. Soc., 25, 2491, 2005.

[294] Wendelbo, R., Akporiaye, D.E., Karlsson, A., Plassen, M., and Olafsen, A., "Combinatorial hydrothermal synthesis and characterisation of perovskites", J. Eur. Ceram. Soc., 26, 849, 2006.

[295] Han, S. H., Ahn, W. S., Lee, H. C., Choi, S. K., Ferroelectric properties of heteroepitaxial PbTiO3 and PbZr1-xTixO3 films on Nb-doped SrTiO3 fabricated by hydrothermal epitaxy below Curie temperature, JOURNAL OF MATERIALS RESEARCH Volume: 22 Issue: 4 Pages: 1037-1042 Published: APR 2007

[296] Naoyama, T., Sakioka, Y., Noda, M., Okuyama, M. Preparation of (Pb,Ba)TiO3 and BaTiO3 ferroelectric thin films at low temperatures less than 210 degree by sol-gel-hydrothermal treatment, FERROELECTRICS Volume: 335 Pages: 169-179 Published: 2006

[297] Gregory K.L. Goha,_, Carlos G. Levib, Joon Hwan Choib, Fred F. Lange, Hydrothermal epitaxy of KNbO3 thin films and nanostructures, Journal of Crystal Growth 286 (2006) 457–464.

[298] W. S. Ahn, W. W. Jung, and S. K. Choi, Ferroelectric properties and fatigue behavior of heteroepitaxial $PbZr_{1-x}Ti_xO_3$ thin film fabricated by hydrothermal epitaxy below Curie temperature, J. Appl. Phys. 99, 014103 (2006).

[299] Kawano T, Hashimoto K, Nishida A, Tsuchiya T, Preparation and electrical properties of Ba(Ti1-xZrx)O-3 thin films by hydrothermal method JOURNAL OF THE CERAMIC SOCIETY OF JAPAN Volume: 110 Issue: 6 Pages: 530-534 Published: JUN 2002

[300] Xu WP, Zheng LR, Lin CL, Okuyama M, Mild hydrothermal synthesis of titanate films: from polycrystalline $BaTiO_3$ to epitaxial $PbTiO_3$, PHILOSOPHICAL MAGAZINE

B-PHYSICS OF CONDENSED MATTER STATISTICAL MECHANICS ELECTRONIC OPTICAL AND MAGNETIC PROPERTIES Volume: 77 Issue: 1 Pages: 177-185 Published: JAN 1998

[301] Tho, Nguyen T.,Inoue, Akihiro, Noda, Minoru, Okuyama, Masanori, Low temperature preparation of bismuth-related ferroelectrics powder and thin films by hydrothermal synthesis, IEEE TRANSACTIONS ON ULTRASONICS FERROELECTRICS AND FREQUENCY CONTROL Volume: 54 Issue: 12 Pages: 2603-2607 Published: DEC 2007

[302] Shimomura K., Tsurumi T., Ohba Y., and Daimon M., "Preparation of lead zirconate titanate thin-film by hydrothermal method", Jpn. J. Appl. Phys., 30 Part 1, 2174, 1991.

[303] Morita, T., Wagatsuma, Y., Cho, Y., Morioka, H., and Funakubo, H., and Setter, N., "Ferroelectric properties of an epitaxial lead zirconate titanate thin film deposited by a hydrothermal method below the Curie temperature", Appl. Phys. Lett., 84, 5094, 2004.

[304] Suchanek, W.L., Lencka, M., McCandlish, L., Pfeffer, R.L., Oledzka, M., Mikulka-Bolen, K., Rossetti,G.A. Jr., and Riman, R.E., "Hydrothermal deposition of <001> oriented epitaxial Pb(Zr,Ti)O_3 films under varying hydrodynamic conditions", Crystal Growth and Design, 5, 1715, 2005.

[305] Ahn, W. S., Jung, W. W., and Choi, S. K., "Ferroelectric properties and fatigue behavior of heteroepitaxial $PbZr_{1-x}Ti_xO_3$ thin film fabricated by hydrothermal epitaxy below Curie temperature", Appl. Phys. Lett., 99, 014103, 2006.

[306] Fujiwara, N., Kusukawa, K., Razak, K.A., and Gao, W., "Piezoelectric properties and PZT films prepared by hydrothermal method", International Journal of Modern Physics B., 20, 3805, 2006.

[307] Ohba, Y., Miyauchi, M., Sakai, E., and Daimon, M., "Hydrothermal syntheses of lead zirconate titanate thin films fabricated by a continuous-supply autoclave", Jpn. J. Appl. Phys., 34 Part 1, 5162, 1995.

[308] Lee, Jae Shin, Lee, Hai Joon, Lee, Jae Young, Kang, Sun Hee, Kim, Ill Won, Ahn, Chang Won, Chung, Gwiy Sang, Preparation and evaluation of lead-free $Na_{0.5}K_{0.5}NbO_3$ ferroelectric thin films, JOURNAL OF THE KOREAN PHYSICAL OCIETY Volume: 52 Issue: 4 Pages: 1109-1113 Published: APR 2008 RF

[309] Ki Woong Kim,1 Tai Suk Kim,1 Min Ku Jeon,1 Kwang Seok Oh,1 Chang Hwa Jung,1 and Seong Ihl Woo, Ferroelectric properties of $Bi_{4-x}Ce_xTi_3O_{12}$ „0<x<4… thin film array fabricated from Bi2O3 /CeO_2 /TiO_2 multilayers using multitarget sputtering, Appl. Phys. Lett. 92, 052911 (2008)

[310] Suchaneck, Gunnar, Vidyarthi, Vinay S., Reibold, Marianne, Deyneka, Alexander, Jastrabik, Lubomir, Gerlach, Gerald, Hartung, Johannes, Large area deposition of Pb(Zr,Ti)O-3 thin films for piezoelectric MEMS devices, JOURNAL OF

ELECTROCERAMICS Volume: 20 Issue: 1 Pages: 17-20 Published: FEB 2008
[311] H.M. Duiker, P.D. Beale, J.F. Scott, C.A. Arayjo, B.M. Melnick, J.D. Cuchiaro, D. McMillan, J. Appl. Phys 68 (1990) 5783.
[312] G. Jhaa, A. Royb, A. Dharb, I. Mannaa, S.K. Ray, Effect of annealing temperature on the structural and electrical properties of $SrBi_2Ta_2O_9$ thin films for memory-based applications, Physica B 400 (2007) 33–37
[313] Yibin Li a, Sam Zhang a,□, Weidong Fei b, Thirumany Sritharan c, Cong Xu, Nd-substituted SrBi2Ta2O9 ferroelectric thin films prepared by radio frequency magnetron sputtering, Thin Solid Films 515 (2007) 8371–8375
[314] Li, Y. B., Zhang, S., Fei, W. D., Gan, Z. H., Mhaisalkar, S., Formation and stability of pyrochlore in sputtered SBT thin films, ADVANCES IN APPLIED CERAMICS Volume: 106 Issue: 4 Pages: 180-185 Published: AUG 2007
[315] Saravanan, K. Venkata, Sudheendran, K., Krishna, M. Ghanashyam, Raju, K. C. James, Broadband microwave dielectric properties of BST thin films on quartz substrates, FERROELECTRICS Volume: 356 Pages: 450-457 Published: 2007
[316] A. Petraru,a_ N. A. Pertsev,b_ H. Kohlstedt, U. Poppe, and R. Waser, A. Solbach and U. Klemradt, Polarization and lattice strains in epitaxial $BaTiO_3$ films grown by high-pressure sputtering, J. Appl. Phys. 101, 114106 (2007)
[317] Chen, Hongwei, Yang, Chuanren, Fu, Chunlin, Zhang, Jihua, Feng, Shucheng, Pei, Yafang, RF magnetron sputtering condition dependences of dielectric non-linearity of $Ba_{0.6}Sr_{0.4}TiO_3$ thin films, INTEGRATED FERROELECTRICS Volume: 91 Pages: 103-111 Published: 2007
[318] Kang, Heo-Soo and Lee, Won-Jong, "Effects of deposition temperature and seed layer on the optical properties of lead zirconate titanate films", J. Vac. Sci. Technol. A., 20, 1498, 2002.

[319] Vilquin, B., Bouregba, R., Poullain, G., Murray, H., Dogheche, E., and Remiens, D., "Crystallographic and optical properties of epitaxial $Pb(Zr_{0.6},Ti_{0.4})O_3$ thin films grown on $LaAlO_3$ substrates", J. Appl. Phys., 94, 5167, 2003.

[320] Cattan, E., Agius, B., Achard, H., Wong, J. C. Cheang, Ortega, C., and Siejka, J., "Physical properties of radio-frequency magnetron sputtered $Pb(Zr,Ti)O_3$ thin films: Direct determination of oxygen composition by Rutherford backscattering spectroscopy and nuclear reaction analysis", J.Vac. Sci.& Technol. A, 11, 2808, 1993

[321] Rhun, G. Le, Poullain, G., Bouregba, R., and Vilquin, B., "Influence of Orientation andOxygen Content on Electrical Properties of In Situ Deposited PZT Thin Films", Ferroelectrics, 288, 111,2003.

[322] Kalpat S., and Uchino K., "Highly oriented lead zirconium titanate thin films: Growth, control of texture, and its effect on dielectric properties". J. Appl. Phys., 90(6), 2703–2710, 2001.

[323] S.-S. Park, C.-H. Yang, S.-G. Yoon, J.-H. Ahn, H.-G. Kim, Characterization of Ferroelectric $SrBi_2Ta_2O_9$ Thin Films Deposited by a Radio Frequency Magnetron

Sputtering Technique, J. Electrochem. Soc. 144 (1997) 2855
[324] Okada, A., "Some electrical and optical properties of ferroelectric lead-zirconate–lead-titanate thin films", J. Appl. Phys., 48, 2905, 1977; Okada, A., "Electrical properties of lead-zirconate–lead-titanate ferroelectric thin films and their composition analysis by Auger electron spectroscopy", J. Appl. Phys., 49, 4495, 1978.

[325] Takayama, R. and Tomita, Y., "Preparation of epitaxial $Pb(Zr_xTi_{1-x})O_3$ thin films and their crystallographic, pyroelectric, and ferroelectric properties", J. Appl. Phys. 65, 1666, 1989.

[326] Zhong, Chaowei, Peng, Jiagen, Zhang, Shuren, and Zhang, Wangli, "Fabrication of PZT thin films with TiOx buffer layers by rf magnetron sputtering", Integrated Ferroelectrics, 80, 281, 2006.

[327] J. Schwarzkopf and R. Fornari, Epitaxial growth of ferroelectric oxide films, Progress in Crystal Growth and Characterization of Materials, 52 (2006) 159-212
[328] I. Aulika, J. Pokorny, V. Zauls, K. Kundzins, M. Rutkis, J. Petzelt, Structural and optical characterization of $Ba_{0.8}Sr_{0.2}TiO_3$ PLD deposited films, Optical Materials 30 (2008) 1017–1022
[329] Peng W (Peng, Wei), Bouquet V (Bouquet, Valerie), Deputier S (Deputier, Stephanie), Simon Q (Simon, Quentin), Guilloux-Viry M (Guilloux-Viry, Maryline), Perrin A (Perrin, Andre), Effect of thin KNbO3 seed layers on pulsed laser deposited ferroelectric KTa0.65Nb0.35O3 films for microwave tunable application INTEGRATED FERROELECTRICS Volume: 93 Pages: 126-132 Published: 2007
[330] Rasmi R. Das, P. Bhattacharya, W. Pérez, and Ram S. Katiyar, Seshu B. Desu, Ferroelectric properties of laser-ablated $Sr_{1-x}A_xBi_2Ta_2O_9$ thin films (where A = Ba, Ca), Appl. Phys. Lett. 80, 637 (2002);
[331] N. Scarisoreanu, M. Filipescu, A. Ioachim, M.I. Toacsan, M.G. Banciu, L. Nedelcu, A. Dutu, M. Buda, H.V. Alexandru, M. Dinescu, "BST thin films obtained by PLD for applications in electronics Applied Surface Science 253 (2007) 8254–8257
[332] Pingxiong Yang, Hongmei Deng, Meirong Shi, Ziyang Tong, Sumei Qin, Growth and properties of $SrBi_2TaNbO_9$ ferroelectric thin films using pulsed laser deposition, Materials Science and Engineering B 137 (2007) 99–102
[333] A. Rousseau, V. Laur, M. Guilloux-Viry, G. Tanné, F. Huret, S. Députier, A. Perrin, F. Lalu, P. Laurent, Pulsed laser deposited KNbO3 thin films for applications in high frequency range, Thin Solid Films 515 (2006) 2353–2360.
[334] H.N. Lee, A. Visinoiu, S. Senz, C. Harnagea, A. Pignolet, D. Hesse, U. Go¨sele, Structural and electrical anisotropy of (001)-, (116)-, and (103)-oriented epitaxial $SrBi_2Ta_2O_9$ thin films on $SrTiO_3$ substrates grown by pulsed laser deposition J. Appl. Phys. 88 (2000) 6658.
[335] H.N. Lee, D. Hesse, Anisotropic ferroelectric properties of epitaxially twinned $Bi_{3.25}La_{0.75}Ti_3O_{12}$ thin films grown with three different orientations, Appl. Phys. Lett. 80 (2002) 1040.
[336] Zhu, T.J., Lu, L., and Lai, M.O., "Pulsed laser deposition of lead-zirconate-titanate thin films and multilayered heterostructures", Appli. Phys. A., 81, 701, 2005.

[337] Lappalainen, J., Frantti, J., and Lantto, V., "Effect of laser-ablation process parameters and post-annealing treatment on ferroelectric PZT thin films", Appl. Surf. Sci., 142, 407, 1999.

[338] Lichtenwalner, D.J., Auciello, O., Dat, R. and Kingon, A.I., "Investigation of the ablated flux characteristics during pulsed laser ablation deposition of multicomponent oxides", J. Appl. Phys., 74, 7497, 1993

[339] Purice, A., Dinescu, G., Scarisoreanu, N., Verardi, P., Craciun, F., Galassi, C., Dinescu, M., "Ferroelectric thin films obtained by pulsed laser deposition", J. Eur. Ceram. Soc., 26, 2937, 2006.

[340] Kreutz, E.W. and Gottmann, J., "Dynamics in Pulsed Laser Deposition of Ceramics: Experimental, Theoretical and Numerical Studies ", phys. stat. sol. (a)., 166, 569, 1998.

[341] Giovanni A. Battiston,[1] Rosalba Gerbasi,[1] Giovanni Carta,[1] Fabio Marchetti,[2] Claudio Pettinari,[2] Agustin Rodriguez,[3] Davide Barreca,[4] Cinzia Maragno,[5] and Eugenio Tondello, Innovative Second-Generation Ba and Sr Precursors for Chemical Vapor Deposition of $Ba_{1-x}Sr_xTiO_3$ Thin Films, J. Electrochem. Soc., Volume 153, Issue 3, pp. F35-F38 (2006)

[342] Kim, H. R., Jeong, S., Jeon, C. B., Kwon, O. S., Hwang, C. S., Han, Y. K., Yang, D. Y., and Oh, K. Y., "Metalorganic chemical vapor deposition of very thin $Pb(Zr,Ti)O_3$ thin films at low temperatures for high-density ferroelectric memory applications", J. Mater. Res., 16, 3583, 2001.

[343] Shimizu, M., Okaniwa, M., Fujisawa, H., and Niu, H., "Ferroelectric properties of $Pb(Zr,Ti)O_3$ thin films prepared by low-temperature MOCVD using $PbTiO_3$ seeds", J. Europ. Ceramic Soc., 24, 1625, 2004.

[344] Funakubo, H., "Recent development in the preparation of ferroelectric thin films by MOCVD", Topics Appl. Phys., 93, 95-103 (2004).

[345] Rice, C. E., Cuchiaro, J. D., Sun, S., Provost, L G., Tompa, G. S., Beratan, H., Hanson, C., and Tanner, H., "Low temperature PZT film by MOCVD", Integr. Ferroelectr. 59, 1465, 2003.

[346] Funakubo, H., Tokita K., Oikawa T., Aratani M., and Saito K., "Comparison of crystal structure and electrical properties of tetragonal and rhombohedral $Pb(Zr,Ti)O_3$ films prepared at low temperature by pulsed-metalorganic chemical vapor deposition", J. Appl. Phys. 92, 5448, 2002.

[347] Shimizu, M., Fujisawa, H., Niu, H., and Honda, K., "Growth of ferroelectric $PbZr_xTi_{1-x}O_3$ thin films by metalorganic chemical vapor deposition (MOCVD)", J. Crystal Growth., 237-239, 448, 2002

[348] Zhao J. S., Park D.-Y., Seo M. J., Hwang C. S., Han Y. K., Yang C. H., and Oh K. Y., "Metallorganic CVD of high-quality PZT thin films at low temperature with new Zr and Ti precursors having MMP ligands", J. Electrochem. Soc., 151, C283, 2004.

[349] Asano, G., Oikawa, T., and Funakubo, H., "Highly-reproducible preparation of Pb(Zr, Ti)O_{-3} films at low deposition temperature by metal organic chemical vapor deposition", Jpn. J. Appl. Phys. Part 1., 42, 2801, 2003.

[350] Kim, D.-H., Yang, W.-Y., and Rhee, S.-W., "Low temperature CVD of Pb(Zr,Ti)O_{-3} using Pb(tmhd)(2), Zr(dmae)(4), and Ti(dmae)4", J. Electrochem. Soc., 150, C516, 2003.

[351] R. Ramesh, S. Aggarwal, and O. Auciello, Science and technology of ferroelectric films and heterostructures for non-volatile ferroelectric memories, Mater. Sci. Eng.: R 32, 191 (2001).

[352] Michael Mehring, From molecules to bismuth oxide-based materials: Potential homo- and heterometallic precursors and model compounds, Coordination Chemistry Reviews 251 (2007) 974–1006

[353] Battiston GA, Gerbasi R, Carta G, Marchetti F, Pettinari C, Rodriguez A, Barreca D, Maragno C, Tondello E, Innovative second-generation Ba and Sr precursors for chemical vapor deposition of Ba1-xSrxTiO3 thin films, JOURNAL OF THE ELECTROCHEMICAL SOCIETY Volume: 153 Issue: 3 Pages: F35-F38 Published: 2006

[354] Furukawa T (Furukawa, T.), Oshima N (Oshima, N.), Suzuki M (Suzuki, M.), Okaura S (Okaura, S.), Funakubo H (Funakubo, H.), Properties of a novel bismuth percursor for MOCVD, INTEGRATED FERROELECTRICS Volume: 84 Pages: 197-202 Published: 2006

[355] Condorelli GG, Favazza M, Bedoya C, Baeri A, Anastasi G, Lo Nigro R, Menou N, Muller C, Lisoni JG, Wouters D, Fragala IL, Metal-organic chemical vapor deposition of ferroelectric SrBi2Ta2O9 films from a fluorine-containing precursor system, CHEMISTRY OF MATERIALS Volume: 18 Issue: 4 Pages: 1016-1022 Published: FEB 21 2006

[356] Betts, R. A. and Pitt, C. W., "Growth of thin-film lithium niobate by molecular beam epitaxy", Electron Lett., 21, 960, 1985.

[357] Petrucci, M., Pitt, C. W., and Dobson, P. J., "RHEED studies on Z-cut $LiNbO_3$", Electron. Lett., 22, 954, 1986.

[358] F.Gitmans, Z.Sitar, and P.Gtinter, Structure and Properties of LiTaO3 Thin Films Grown by Modified Gas Source Molecular Beam Epitaxy, Microelectronic Engineering 29 (1995) 289-292

[359] Matthew J. Dicken_, Kenneth Diest, Young-Bae Park, Harry A. Atwater, Growth and optical property characterization of textured barium titanate thin films for photonic applications, Journal of Crystal Growth 300 (2007) 330–335

[360] McKee, R. A., Walker, F. J., Conner, J. R., Specht, E. D., and Zelmon, D. E.,

"Molecular beam epitaxy growth of epitaxial barium silicide, barium oxide, and barium titanate on silicon", Appl. Phys. Lett., 59, 782, 1991.

[361] Y. Yoneda a,*, K. Sakaue b, H. Terauchi, RHEED observation of BaTiO3 thin films grown by MBE, Surface Science 529 (2003) 283–287
[362] : Growth of perovskite type thin films by MBE Author(s): Yoneda Y, Okabe T, Sakaue K, et al. JOURNAL OF THE KOREAN PHYSICAL SOCIETY Volume: 29 Pages: S652-S655 Supplement: Suppl. S Published: NOV 1996
[363] H. Lia, J. Finder, Y. Liang, R. Gregory, and W. Qin, Dielectric properties of epitaxial $Ba_{0.5}Sr_{0.5}TiO_3$ films on amorphous SiO_2 on sapphire Appl. Phys. Lett. 87, 072905 (2005)
[364] Horiguchi A, Watanabe Y., Low temperature growth of epitaxial (Ba, Sr)TiO_2 thin film by sputter molecular beam epitaxy method", JAPANESE JOURNAL OF APPLIED PHYSICS PART 1-REGULAR PAPERS SHORT NOTES & REVIEW PAPERS Volume: 38 Issue: 9B Pages: 5314-5316 (SEP 1999)
[365] C.D. Theis, J. Yeh, D.G. Schlom, M.E. Hawley, G.W. Brown, The influence of vicinal $SrTiO_3$ surfaces on the growth and ferroelectric properties of epitaxial $Bi_4Ti_3O_{12}$ thin films, Materials Science and Engineering B56 (1998) 228–233
[366] G.W. BROWN, M.E. HAWLEY, C.D. THEIS, J. YEH and D.G. SCHLOM, Atomic Force Microscopy Examination of the Evolution of the Surface Morphology of Bi_4Ti_3O12 grown by Molecular Beam Epitaxy, Journal of Electroceramics 4:2/3, 351±356, 2000
[367] Gu, Xing., Izyumskaya, Natalia., Avrutin, Vitaly., Morkoç, Hadis., Kang, Tae Dong, and Lee, Hosun., "High quality epitaxial growth of $PbTiO_3$ by molecular beam epitaxy using H_2O_2 as the oxygen source", Appl. Phys. Lett., 89, 122912, 2006.

[368] Theis, C.D. and Schlom, D.G., "Epitaxial lead titanate grown by MBE", Journal of Crystal Growth, 174, 473, 1997.

[369] Theis, C. D., Yeh, J., Schlom, D. G., Hawley, M. E., and Brown, G. W., "Adsorption-controlled growth of $PbTiO_3$ by reactive molecular beam epitaxy", Thin Solid Films, 325, 107, 1998.

[370] N. Izyumskaya, V. Avrutin, X. Gu, B. Xiao, S. Chevtchenko, J.-G. Yoon, and H. Morkoç, Structural and electrical properties of $Pb(Zr,Ti)O_3$ films grown by molecular beam epitaxy, Appl. Phys. Lett. 91, 182906 (2007)

[371] Avrutin, V., Izyumskaya, N., Gu, Xing, Özgür, Ü., Xiao, B., Kang, Tae Dong, Lee, Hosun, and Morkoç, H., "Growth of high quality $Pb(Zr_xTi_{1-}x)O_3$ films by peroxide MBE and their optical and structural characteristics", Proceedings of Fall 2006 Materials Research Society Meeting, Nov 2006 Boston MA .

[372] K. Abe, S. Komatsu, J. Appl. Phys. 77 (1995) 6461.
[373] C. M. Foster, G.-R. Bai, R. Csencsits, J. Vetrone, R. Jammy,L. A. Wills, E. Carr, and J. Amano, Single-crystal $Pb(Zr_xTi_{1-x})O_3$ thin films prepared by metal-organic chemical

vapor deposition: Systematic compositional variation of electronic and optical properties, J. Appl. Phys. 81, 2349 (1997).
[374] M. De Keijser, J. F. M. Cillessen, R. B. F. Janssen, A. E. M. De Veirman, and D. M. de Leeuw, Structural and electrical characterization of heteroepitaxial lead zirconate titanate thin films, J. Appl. Phys. 79, 393 (1996).
[375] I. Kanno, H. Kotera, K. Wasa, T. Matsunaga, T. Kamada, and R. Takayama, Crystallographic characterization of epitaxial Pb(Zr,Ti)O_3 films with different Zr/Ti ratio grown by radio-frequency-magnetron sputtering, J. Appl. Phys. 93, 4091 (2003).
[376] R. Dittmann, R. Plonka, E. Vasco, N.A. Pertsev, J.Q. He, C.L. Jia, S. Hoffmann-Eifert, R. Waser, Appl. Phys. Lett. 83 (2003) 5011.
[377] N.J. Donnelly, G. Catalan, C. Morros, R.M. Bowman, J.M. Gregg, J. Appl. Phys. 93 (2003) 9924.
[378] D.-J. Kim, J.-P. Maria, A. I. Kingon, and S. K. Streiffer, Evaluationof intrinsic and extrinsic contributions to the piezoelectric properties of Pb(Zr1-xTix)O3 thin films as a function of composition, J. Appl. Phys. 93, 5568 (2003).
[379] N. Setter, D. Damjanovic, L. Eng, G. Fox, S. Gevorgian, S. Hong, A. Kingon, H. Kohlstedt, N. Y. Park, G. B. Stephenson, I. Stolitchnov, A. K. Taganstev, D. V. Taylor, T. Yamada, and S. Streiffer, Ferroelectric thin films: Review of materials, properties, and applications, JOURNAL OF APPLIED PHYSICS 100, 051606 (2006)]

[380] N. Izyumskaya, Y.-I. Alivov, S.-J. Cho, H. Morkoç, H. Lee, Y. -S. Kang, Processing, Structure, Properties, and Applications of PZT Thin Films, Critical Reviews in Solid State and Materials Sciences, 32,111 – 202 (2007).
[380] Looney, D. H., U.S. Patent No. 2791758 (1957); Brown, W. L., U.S. Patent No. 2791759 (1957); Ross, I. M., U.S. Patent No. 2791760 (1957); Morton, J. A., U.S. Patent No. 2791761 (1957).

[381] G. Suchaneck and G. Gerlach, Ferroelectri thin films: Deposition, Advanced film characterization and novel device concepts, Ferroelectrics, 335, 137-148 (2006).

[382] Sarin Kumar, A. K., Paruch, P., and Triscone, J.-M., Daniau, W., Ballandras, S., Pellegrino, L., Marré, D., and Tybell, T., "High-frequency surface acoustic wave device based on thin-film piezoelectric interdigital transducers", Appl. Phys. Lett. 85, 1757 (2004).

[383] Yamaguchi, M., Hashimoto, K., Nanjo, R., Hanazawa, N., Ttsutsumi, S., and Yonezawa, T., "Ultrasonic properties of PZT thin films in UHF-SHF ranges-preparedby sol gel method", Proc. IEEE, 544, 1997.

[384] Shih, W.-C. and Wu, M.-S., "Effect of a buffer layer on the surface acoustic wave characteristics of Pb(Zr,Ti)O_3 film/buffer layer/semiconductor substrate structures", Jpn. J. Appl. Phys., Part 1, 36, 203, 1997.

[385] Du, H., Johnson, D. W. Jr., Zhu, W., Graebner, J. E., Kammlott, G. W., Jin, S., Rogers, J., Willett, R., and Fleming, R. M., "Growth and measurements of ferroelectric lead

zirconate titanate on diamond by pulsed laser deposition", J. Appl. Phys., 86, 2220, 1999.

[386] Li, B., Lai, P.T., Li, G. Q., Zheng, S. H., and Huang, M. Q., "A new multi-function thin-film microsensor based on Ba1-xLaxTiO$_3$", Smart Mater. Struct., 9, 498-501 (2000).

[387] W. Qu, R. Green, and M. Austin, Development of multi-functional sensors in thick-film and thin-film technology, Meas. Sci. Technol., 11, 1111–1118 (2000).
[388] Xu, C. –N., Liu, Y., Akiyama, M., and Nonaka, K., "Multifunction study of PZT thin films on amorphous and polycrystalline substrates ", Ferroelectrics 263, 155, 2001.

[389] Uchino, K., "Ferroelectric devices", Marcel Dekker, New York, 2000.

[390] Thapliya, R., Okano, Y., and Nakamura, S., "Electrooptic Characteristics of Thin-Film PLZT Waveguide Using Ridge-Type Mach-Zehnder Modulator", J. Lightwave Technol., 21, 1820, 2003

[391] A. L. Glebov, M. G. Lee, L. Huang, S. Aoki, K. Yokouchi, M. Ishii, and M. Kato, "Electrooptic planar deflector switches with thin-film PLZT active elements", IEEE J. Selected Topics in Quantum Electronics, 11, 422-430, 2005.

[392] Y. Lu, G.-H. Jin, M. Cronin-Golombo, S.-W. Liu, H. Jiang, F.-L.Wang, J. Zhao, S.-Q.Wang, and A. J. Drehman, "Fabrication and optical characterization of $Pb(Mg_{1/3}Nb_{2/3})O_3$-$PbTiO_3$ planar thin film optical waveguides", Appl. Phys. Lett., 72, 2927, 1998.
[393] Tae Dong Kang, Bo Xiao, Vitaliy Avrutin, Ümit Özgür, Hadis Morkoç, Jun Woo Park, Ho Suk Lee, Hosun Lee, Xiaoyu Wang, and David. J. Smith "Large electro-optic effect in single-crystal $Pb(Zr,Ti)O_3$ (001) measured by spectroscopic ellipsometry", J. Appl. Phys. Vol. 104, n 9, p 093103 (5 pp.), 1 Nov. 2008.
[394] K. Nashimoto, S. Nakamura, H. Moriyama, M. Watanabe,and E. Osakabe, "Electro-optic beam deflector using epitaxial $Pb(Zr,Ti)O_3$ waveguides on Nb-doped $SrTiO_3$", Appl. Phys. Lett., 73, 303, 1998
[395] O. Eknoyan, V. P. Swenson, J. D. Quinn, and R. R. Neurgaonkar, "Low-voltage interferometric modulator in zinc-diffused strontium barium niobate (SBN:60)", Appl. Phys. Lett., 59, 28, 1991.

[396] L. Tian, D. A. Scrymgeour, A. Sharan, and V. Gopalan, "Anomalous electro-optic effect in $Sr_{0.6}Ba_{0.4}Nb_2O_6$ single crystals and its application in two-dimensional laser scanning", Appl. Phys. Lett., 83, 4375, 2003.

[397] A. Petraru, J. Schubert, M. Schmid, and Ch. Buchal, "Ferroelectric $BaTiO_3$ thin-film optical waveguide modulators", Appl. Phys. Lett., 81, 1375, 2002.

[398] A. K. Tagantsev, V. O. Sherman, K. F. Astafiev, J. Venkatesh and N. Setter, J. Electroceram. 11, 5 (2003)

[399] L. M. B. Alldredge, Wontae Chang, Steven W. Kirchoefer, and Jeffrey M. Pond, Phase transitions and the temperature dependence of the dielectric properties in tetragonally strained barium strontium titanate films, Appl. Phys. Lett. 94, 052904 (2009).
[400] Bo Xiao, Vitaliy Avrutin, Hongrui Liu, Emmanuel Rowe, Jacob Leach, Xing Gu, Ümit Özgür, and Hadis Morkoç, Effect of large strain on dielectric and ferroelectric properties of $Ba_{0.5}Sr_{0.5}TiO_3$ thin films, accepted for publication in Appl. Phys. Lett. (2009).

[401] W. Chang, L. M. B. Alldredge, S. W. Kirchoefer, and J. M. Pond, Microwave dielectric properties of strained Ba0.5Sr0.5TiO3 films with and without strain-induced permanent polarization at room temperature J. Appl. Phys. 102, 014105 (2007)
[402] N. A. Pertsev, V. G. Koukhar, R. Waser and S. Hoffmann, Appl. Phys. Lett. 77, 2596 (2000)
[403] M. W. Cole, E. Ngo, S. Hirsch, J. D. Demaree, S. Zhong, and S. P. Alpay, The fabrication and material properties of compositionally multilayered $Ba_{1-x}Sr_xTiO_3$ thin films for realization of temperature insensitive tunable phase shifter devices J. Appl. Phys. 102, 034104 (2007).
[404] M. Jain, S. B. Majumder, R. S. Katiyar, F. A. Miranda, and F. W. Van Keuls, Appl. Phys. Lett. 82, 1911 (2003).
[405] X.H. Zhu, N. Chong, H.L.W. Chan, C.L. Choy, Z.G. Liu, and N.B. Ming, Appl. Phys. Lett. 80, 3376 (2002).
[406] C. Wang, B. L. Cheng, S. Y. Wang, H. B. Lu, Y. L. Zhou, Z. H. Chen, and G. Z. Yang, Appl. Phys. Lett. 84, 765 (2004).
[407] R. Ramesh, A. Inam, W. K. Chan, F. Tillerot, B. Wilkens, C. C. Chang, T. Sands, J. M. Tarascon, and V. G. Keramidas, Topinterface- controlled fatigue of epitaxial $Pb(Zr_{0.52}Ti_{0.48})O_3$ ferroelectric thin films on $La_{0.7}Sr_{0.3}MnO_3$ electrodes, Appl. Phys. Lett. 59, 3542 (1991).

[408] R. Ramesh,W. K. Chan, B.Wilkens, H. Gilchrist, T. Sands, J. M.Tarascon, D. K. Fork, J. Lee, and A. Safari, Fatigue and retention in ferroelectric Y-Ba-Cu-O/Pb-Zr-Ti-O/Y-Ba-Cu-O heterostructures, Appl. Phys. Lett. 61, 1537 (1992).

[409] S. D. Bernstein, T. Y. Wang, Y. Kisler, and R. W. Tustison, Fatigue of ferroelectric PbZrxTiyO3 capacitors with Ru and RuO_X electrodes, J. Mater. Res. 8, 12 (1993).

[410] J. J. Lee, C. L. Thio, and S. B. Desu, Electrode contacts on ferroelectric $Pb(Zr_xTi_{1-x})O_3$ and $SrBi_2Ta_2O_9$ thin films and their influence on fatigue properties, J. Appl. Phys. 78, 5073, 1995.

[411] R. Dat, D. J. Lichtenwalner, O. Auciello, and A. I.Kingon, Polycrystalline $La_{0.5}Sr_{0.5}CoO_3/PbZr_{0.53}Ti_{0.47}O_3/ La_{0.5}Sr_{0.5}CoO_3$ ferroelectric capacitors on platinized silicon with no polarization fatigue, Appl. Phys. Lett. 64, 2673 (1994).

[412] I. Stolichnov, A. Tagantsev, N. Setter, J. S. Cross, and M. Tsukada,Top-interface-controlled switching and fatigue endurance of (Pb,La)(Zr,Ti)O_3 ferroelectric capacitors, Appl. Phys. Lett. 74,3552 (1999).

[413] www.engadget.com/2009/02/09/toshiba-makes-progress-on-feram-still-no-tangible-product-in-si

[414] Ishiwara, H., "Recent progress of FET-type ferroelectric memories", Integrated Ferroelectrics, v 34, n 1-4, pp. 11-20, (2001)

[415] Scott, J. F., "New developments on FRAMs: [3D] structures and all-perovskite FETs", Materials Science and Engineering B, 120, 6, 2005

[416] Kingon, A., Maria, J.-P., and Steffetr, S. K., "Alternative dielectrics to silicon dioxide for memory and logic devices" Nature, 406, 1032, 2000.

[417] Fox, G. R., Chu, F., and Davenpot, T., "Current and future ferroelectric nonvolatile memory technology", J. Vac. Sci. and Technol. B, 19, 1967, 2001

[418] Shaw, T. M., Trolier-McKinstry, S., and McIntyre, P. C., "The properties of ferroelectric films at small dimensions", Annu. Rev. Mater. Research, 30, 263, 2000.

[419] Haertling, G.. H., "Ferroelectric Ceramics: History and Technology", J. Am. Ceram. Soc. 82, 797, 1999.

[420] Ishwara, H., "Current status and prospects of FET-type ferroelectric memories", FED (Future Electron Devices) Journal, 11, 27, 2000.

[421] Scott, J. F., "New developments on FRAMs: [3D] structures and all-perovskite FETs", Mater. Sci. Eng. B, 120, 6, 2005.

422 P. G. Radaelli, Orbital ordering in transition-metal spinels, New Journal of Physics, 7, (2005) 53-1 – 53-22 (2005).

423 D Serrate, J M De Teresa, and M R Ibarra, Double perovskites with ferromagnetism above room Temperature, J. Phys.: Condens. Matter 19, 023201-023287 (2007).

[424] Matsumoto Y, Takahashi R, Murakami M, Koida T, Fan X-J, Hasegawa T, et al. Ferromagnetism in Co-doped TiO_2 rutile thin films grown by laser molecular beam epitaxy. Jpn J Appl Phys 2001;40:L1204–6.

[425] S. R. Shinde, S. B. Ogale, S. Das Sarma, J. R. Simpson, H. D. Drew, S. E. Lofland, C. Lanci, J. P. Buban, N. D. Browning, V. N. Kulkarni, J. Higgins, R. P. Sharma, R. L. Greene, and T. Venkatesan, Ferromagnetism in laser-deposited anatase Ti1-xCoxO2-δ films. Phys. Rev B 67, 115211 (2003).

[426] Hong NH, Sakai J, Prellier W, Hassini A, Ruyter A, Gervais F. Ferromagnetism in transition-metal-doped TiO2 thin films. Phys Rev B 2004;70:195204.

[427] R. Ramaneti, J. C. Lodder, and R. Jansen, Anomalous Hall effect in anatase Co:TiO2 ferromagnetic semiconductor, Appl. Phys. Lett. 91, 012502 (2007)
[428] Zhenjun Wang, Wendong Wang, and Jinke Tang, Le Duc Tung,b) Leonard Spinu, and Weilie Zhou, Extraordinary Hall effect and ferromagnetism in Fe-doped reduced rutile, Appl. Phys. Lett., 83, 518 (2003).
[429] Kelvin Y.S. Chan, Gregory K.L. Goh Hydrothermal growth of ferromagnetic Fe-doped TiO_2 films, Thin Solid Films 516 (2008) 5582–5585

[430] Hong, N.Y H., Sakai, J. & Hassini, A. Ferromagnetism at room temperature with a large magnetic moment in anatase V- doped TiO2 thin fi lms. Appl. Phys. Lett. 84, 2602–2604 (2004).
[431] T. C. Kaspar, T. Droubay, V. Shutthanandan, S. M. Heald, C. M. Wang, D. E. McCready, S. Thevuthasan, J. D. Bryan, D. R. Gamelin, A. J. Kellock, M. F. Toney, X. Hong, C. H. Ahn, and S. A. Chambers, Ferromagnetism and structure of epitaxial Cr-doped anatase TiO_2 thin films Phys. Rev. B 73, 155327 (2006)
[432] Jun Chen,Guang-Hong Lu, Honghong Cao, Tianmin Wang, and Yun Xu, Ferromagnetic mechanism in Ni-doped anatase TiO_2, Appl. Phys. Lett. 93, 172504 (2008)
[433] Kwang Joo Kima, Young Ran Parka, Jung Han Leea, Seung-Li Choia, Hee Jung Leea, Chul Sung Kimb, Jae Yun Park, Room-temperature ferromagnetic properties in Mn-doped rutile TiO_2 thin films, Journal of Magnetism and Magnetic Materials 316 (2007) e215–e218.
[434] S. Duhalde, M. F. Vignolo, F. Golmar, C. Chiliotte, C. E. R. Torres, L. A. Errico, A. F. Cabrera, M. Rentería, F. H. Sánchez, and M. Weissmann, Appearance of room-temperature ferromagnetism in Cu-doped TiO2−δ_ films
Phys. Rev. B 72, 161313 (2005).

[435] N. H. Hong, J. Sakai, N. T. Huong, N. Poirot, and A. Ruyter, Role of defects in tuning ferromagnetism in diluted magnetic oxide thin films, Phys. Rev. B 72, 045336 (2005).

[436] H. Liu, X. Zhang, L. Li, Y.X. Wang, K.H. Gao, Z.Q. Li, R.K. Zheng, S.P. Ringer, B. Zhang, X.X. Zhang, Role of point defects in room-temperature ferromagnetism of Cr-doped ZnO Appl. Phys. Lett. 91 (2007) 072511.

[437] Y. C. Yang,1 C. F. Zhong,2 X. H. Wang,2 B. He,3 S. Q. Wei,3 F. Zeng,1 and F. Pan, Room temperature multiferroic behavior of Cr-doped ZnO films, J. Appl. Phys. 104, 064102 (2008).
[438] H. Saeki, H. N. Tabata, and T. Kawai; “Magnetic and electric properties of vanadium doped ZnO films”; Solid State Commun.; 120, 439, (2001).
[439] V. Avrutin, Ü. Özgür, S. Chevtchenko, C. Litton, and H. Morkoç, “Optical and magnetic properties of ZnO:V prepared by ion implantation”, J. Electron. Mat. 36 483 (2007).
[440] M. Venkatesan, C. B. Fitzgerald, J.G. Lunney, and J.M. D. Coey, Anisotropic Ferromagnetism in Substituted Zinc Oxide, Phys. Rev. Lett. 93, 177206 (2004).
[441] N. Theodoropoulou, V. Misra, J. Philip, P. LeClair, G.P. Berera, J.S. Moodera, B.

Satpati, T. Som, High-temperature ferromagnetism in $Zn_{1\_x}Mn_xO$ semiconductor thin films, J. Magn. Magn. Mater. 300 (2006) 407.
[442] X.H. Xu, H.J. Blythe, M. Ziese, A.J. Behan, J.R. Neal, A. Mokhtari, R.M. Ibrahim, A.M. Fox, G.A. Gehring, Carrier-induced ferromagnetism in n-type ZnMnAlO and ZnCoAlO thin films at room temperature , New J. Phys. 8 (2006) 135.
[443] Y.B. Lin, J.P. Xu, W.Q. Zou, L.Y. Lv, Z.H. Lu, F.M. Zhang, Y.W. Du, Z.G. Huang, J.G.Zheng, Effects of annealing and hydrogenation on the properties of ZnMnO polycrystalline films synthesized by plasma enhanced chemical vapour deposition, J. Phys. D: Appl. Phys. 40 (2007) 3674.
[444] A. J. Behan, A. Mokhtari, H. J. Blythe, D. Score, X-H. Xu, J. R. Neal, A. M. Fox, and G. A. Gehring, Two Magnetic Regimes in Doped ZnO Corresponding to a Dilute Magnetic Semiconductor and a Dilute Magnetic Insulator, PRL 100, 047206 (2008).
[445] C. Song, K.W. Geng, F. Zeng, X.B. Wang, Y.X. Shen, F. Pan, Y.N. Xie, T. Liu, H.T. Zhou, Z. Fan, Giant magnetic moment in an anomalous ferromagnetic insulator: Co-doped ZnO Phys. Rev. B 73 (2006) 024405.
[446] C.B. Fitzgerald, M. Venkatesan, J.G. Lunney, L.S. Dorneles, J.M.D. Coey, Cobalt-doped ZnO – a room temperature dilute magnetic semiconductorAppl. Surf. Sci. 247 (2005) 493.
[447] Radovanovic PV, Gamelin DR. High temperature ferromagnetism in Ni^{2+}-doped ZnO aggregates prepared from colloidal diluted magnetic semiconductor quantum dots. Phys Rev Lett 2003; 91:157202.

[448] X. Liu, F. Lin, L. Sun, W. Cheng, X. Ma, W. Shi, Doping concentration dependence of room-temperature ferromagnetism for Ni-doped ZnO thin films prepared by pulsed-laser deposition, Appl. Phys. Lett. 88 (2006) 062508.
[449] X XWei1, C Song1, K W Geng1, F Zeng1, B He2 and F Pan, Local Fe structure and ferromagnetism in Fe-doped ZnO films, J. Phys.: Condens. Matter 18 (2006) 7471–7479
[450] D.L. Hou, X.J. Ye, H.J. Meng, H.J. Zhou, X.L. Li, C.M. Zhen, G.D. Tang, Magnetic properties of n-type Cu-doped ZnO thin films, Appl. Phys. Lett. 90 (2007) 142502.
[451] D. B. Buchholz and R. P. H. Chang, J. H. Song and J. B. Ketterson Room temperature ferromagnetism in Cu-doped ZnO films. Appl Phys Lett 2005;87:082504.

[452] S.-J. Han, J. W. Song, C.-H. Yang, S. H. Park, J.-H. Park, Y. H. Jeong, and K. W. Rhie, A key to room-temperature ferromagnetism in Fe-doped ZnO:Cu, Appl Phys Lett 2002;81:4212–4214.

[453] S. B. Ogale, R. J. Choudhary, J. P. Buban, S. E. Lofland, S. R. Shinde, S. N. Kale, V. N. Kulkarni, J. Higgins,C. Lanci, J. R. Simpson, N. D. Browning, S. Das Sarma, H. D. Drew, R. L. Greene, and T. Venkatesan High temperature ferromagnetism with a giant magnetic moment in transparent Co-doped SnO_2. Phys Rev Lett 2003;91:077205.

[454] C. B. Fitzgerald, M. Venkatesan, L. S. Dorneles, R. Gunning, P. Stamenov, and J. M. D. Coey, P. A. Stampe and R. J. Kennedy, E. C. Moreira, U. S. Sias, Magnetism in dilute magnetic oxide thin films based on SnO2. Phys. Rev. B 74, 115307 _2006_

[455] J. M. D. Coey, A. P. Douvalis, C. B. Fitzgerald, and M. Venkatesan, Ferromagnetism in Fe-doped SnO2 thin films, Appl. Phys. Lett. 84, 1332 (2004).
[456] A. Punnoose, J. Hays, A. Thurber, M. H. Engelhard, R. K. Kukkadapu, C. Wang, V. Shutthanandan, and S. Thevuthasan, Development of high-temperature ferromagnetism in SnO_2 and paramagnetism in SnO by Fe doping Phys. Rev. B 72, 054402 (2005).
[457] Nguyen Hoa Hong, Joe Sakai, W Prellier, and Awatef Hassini, Transparent Cr-doped SnO_2 thin films: ferromagnetism beyond room temperature with a giant magnetic moment, J. Phys.: Condens. Matter 17 (2005) 1697–1702.
[458] N. H. Hong, A. Ruyter, W. Prellier, J. Sakai, and N. T. Huong, Magnetism in Ni-doped SnO2 thin films J. Phys.: Condens. Matter. 17, 6533 (2005).

[459] N. H. Hong and J. Sakai, Ferromagnetic V-doped SnO2 thin films, Physica B 358, 265 (2005).

[460] G. Peleckis, X. Wang, and S. X. Dou, High temperature ferromagnetism in Ni-doped In2O3 and indium-tin oxide Appl. Phys. Lett. 89, 022501 (2006)
[461] J. PHILIP, A. PUNNOOSE, B. I. KIM, K. M. REDDY, S. LAYNE, J. O. HOLMES, B. SATPATI, P. R. LECLAIR, T. S. SANTOS AND J. S. MOODERA, Carrier-controlled ferromagnetismin transparent oxide semiconductors, Nature Materials 5, 298-304 (2006)
[462] G. Peleckis, X. L. Wang,a_ and S. X. Dou, Room-temperature ferromagnetism in Mn and Fe-codoped In_2O_3, Appl. Phys. Lett. 88, 132507 (2006)
[463] H W. Ho, B C Zhao, B Xia, S L Huang, YWu, J G Tao, A C H Huan and LWang, Magnetic and magnetotransport properties in Cu and Fe co-doped bulk In_2O_3 and ITO, J. Phys.: Condens. Matter 20 (2008) 475204
[464] N.H. Hong, J. Sakai, N.T. Huong, A. Ruyter, V. Brize´ , J. Phys.: Condens. Matter 18 (2006) 6897.
[465] T. Ohno, T. Kawahara, H. Tanaka, T. Kawai, M. Oku, K. Okada, S. Kohiki, Jpn J. Appl. Phys. 45 (2006) L957.

[466] J. He, S. Xu, Y. K. Yoo, Q. Xue, H. C. Lee, S. Cheng, X. D. Xiang, G. F. Dionne, and I. Takeuchi, Room temperature ferromagnetic n-type semiconductor in .$In_{1-x}Fe_{x.2}O_3{-}\sigma$Appl. Phys. Lett. 86, 052503 (2005).

[467] Y. K. Yoo, Q. Xue, H. C. Lee, S. Cheng, X. D. Xiang, G. F. Dionne, S. Xu, J. He, Y. S. Chu, S. D. Preite, S. E. Lofland, and I. Takeuchi, Bulk synthesis and high-temperature ferromagnetism of .$In_{1-x}Fe_{x.2}O_{3-\sigma}$ with Cu co-dopingAppl. Phys. Lett. 86, 042506 _2005_.

[468] G. Peleckis, X. L. Wang, R. S. Liu, and S. X. Dou, Magnetic and Transport Properties of Transition Metal Doped Polycrystalline In_2O_3 IEEE Trans. Magn. 42,2703 (2006).

[469] J. Philip, N. Theodoropoulou, G. Berara, and J. S. Moodera, High-temperature ferromagnetism in manganese-doped indium–tin oxide filmsAppl. Phys. Lett. 85, 777 (2004).

[470] H. S. Kim, S. H. Ji, H. Kim, S.-K. Hong, D. Kim, Y. E. Ihm, and W. K. Choo, Observation of ferromagnetism and anomalous Hall effect in laser-deposited chromium-doped indium tin oxide films Solid State Commun. 137, 41 _2006_.

[471] A.Tiwari, V. M. Bhosle, S. Ramachandran, N. Sudhakar, and J. Narayan, S. Budak and A. Gupta, Ferromagnetism in Co doped CeO2: Observation of a giant magnetic moment with a high Curie temperature, Appl. Phys. Lett. 88, 142511 (2006)
[472] H. Pan, J. B. Yi, L. Shen, R. Q. Wu, J. H. Yang, J.Y. Lin, Y. P. Feng, J. Ding,‡ L. H. Van, and J. H. Yin, Room-Temperature Ferromagnetism in Carbon-Doped ZnO, PRL 99, 127201 (2007)
[473] M.Venkatesan, C. B. Fitzgerald, J.M.D. Coey, Unexpected magnetism in a dielectric oxide, Nature 430, 630 (2004).
474 Coey JMD, Venkatesan M, Stamenov P, Fitzgerald CB, Dorneles LS, Magnetism in hafnium dioxide, Phys. Rev. B 72, 024450 (2005).
[475] N.H. Hong, J. Sakai, N. Poirot, and V. Briz´e, Room-temperature ferromagnetism observed in undoped semiconducting and insulating oxide thin films, 2006 Phys. Rev. B 73 132404

[476] Soack Dae Yoon, Yajie Chen, Aria Yang, Trevor L. Goodrich, Xu Zuo, Katherine Ziemer, Carmine Vittoria, Vincent G. Harris, Magnetic semiconducting anatase TiO2-δ grown on (1 0 0) $LaAlO_3$ having magnetic order up to 880K, 2007 J. Magn. Magn. Mater. 309 171.

[477] Soack Dae Yoon, Yajie Chen, Aria Yang, Trevor L Goodrich, Xu Zuo, Dario A Arena, Katherine Ziemer, Carmine Vittoria and Vincent G Harris, Oxygen-defect-induced magnetism to 880 K in semiconducting anatase $TiO_{2-\delta}$ films, J. Phys.: Condens. Matter 18 (2006) L355–L361
[478] J.C.A. Huang, H.S. Hsu, Appl. Phys. Lett. Inspection of magnetic semiconductor and clustering structure in CoFe-doped ZnO films by bias-dependent impedance spectroscopy, 87 (2005) 132503.
[479] K.P. Bhatti, S. Kundu, S. Chaudhary, S.C. Kashyap, D.K. Pandya, Observation of room temperature ferromagnetism in nanocrystalline ZnO:Co system , J. Phys. D: Appl. Phys. 39 (2006) 4909.

[480] S.J. Pearton, W.H. Heo, M. Ivill, D.P. Norton, T. Steiner, Dilute magnetic Semiconducting oxides, Semicond. Sci. Technol. 19 (2004) R59.

[481] X.X. Wei, C. Song, K.W. Geng, F. Zeng, B. He, F. Pan, Local Fe structure and ferromagnetism in Fe-doped ZnO films , J. Phys.: Condens. Matter 18 (2006) 7471.
[482] K. Potzger, Shengqiang Zhou, H. Reuther, A. Mücklich, F. Eichhorn, N. Schell, W. Skorupa, M. Helm, J. Fassbender, T. Herrmannsdörfer and T. P. Papageorgiou, “Fe

implanted ferromagnetic ZnO", Appl. Phys. Lett. Vol. 88, No.5, 052508-1 - 052508-3, Feb. 2006.

[483] Y. Belghazi, G. Schmerber, S. Colis, J.L. Rehspringer, A. Dinia, A. Berrada, Appl. Phys. Lett. 89 (2006) 122504.

[484] A. Che Mofor, A. El-Shaer, A. Bakin, A. Waag, H. Ahlers, U. Siegner, S. Sievers, M. Albrecht, W. Schoch, N. Izyumskaya, V. Avrutin, S. Sorokin, S. Ivanov, and J. Stoimenos, Magnetic property investigations on Mn-doped ZnO Layers on sapphire, Appl. Phys. Lett. 87, 062501 (2005).
[485] R. Seshadri, Zinc oxide-based diluted magnetic semiconductors, Current Opinion in Solid State and Materials Science 9 1–7(2005)

[486] D.W. Abraham, M.M. Frank, S. Guha, Absence of magnetism in hafnium oxide films , Appl. Phys. Lett. 87 (2005) 252502.

[487] J.-Y. Koo, J.-Y. Yi, C. Hwang, D.-H. Kim, S. Lee, and D. H. Shin, Phys. Rev. B 52, 17269 (1995).
[488] G. Lawes, A. S. Risbud, A. P. Ramirez, and R. Seshadri, Absence of ferromagnetism in Co and Mn substituted polycrystalline ZnOPhys. Rev. B 71, 045201 (2005).
[489] D. Be´rardan, E. Guilmeau, Magnetic properties of bulk Fe-doped indium oxide, J. Phys.: Condens. Matter 19 (2007)
236224.
[490] David Be´rardan, Emmanuel Guilmeau, Denis Pelloquin, Intrinsic magnetic properties of In_2O_3 and transition metal-doped-In_2O_3, Journal of Magnetism and Magnetic Materials 320 (2008) 983–989.
[491] T. C. Kaspar, S. M. Heald, C. M. Wang, J. D. Bryan, T. Droubay, V. Shutthanandan, S. Thevuthasan, D. E. McCready, A. J. Kellock, D. R.Gamelin, and S. A. Chambers, Negligible Magnetism in Excellent Structural Quality $Cr_xTi_{1-x}O_2$ Anatase: Contrast with High-T_C Ferromagnetism in Structurally Defective $Cr_xTi_{1-x}O_2$
Phys. Rev. Lett. 95, 217203 (2005).
[492] C. N. R. Rao and F. L. Deepak, Absence of ferromagnetism in Mn- and Co-doped ZnOJ. Mater. Chem. 15, 573 (2005).

[493]J.M.D. Coey, M. Venkatesan, C.B. Fitzgerald, Donor impurity band exchange in dilute ferromagnetic oxides, Nature Materials 4, 173 (2005)

[494] J. M. D. Coey and S.A. Chambers, Oxide dilute magnetic semiconductors – fact of fiction? MRS Bulletin 33, 1053 (2008).

[495] K. Sato and H. Katayama-Yoshida, K. Sato and H. Katayama-Yoshida, First principles materials design for semiconductor spintronics, Semicond. Sci. Technol. 17 (2002) 367–376.

[496] C. Zener; "Interaction Between the d Shells in the Transition Metals"; Phys. Rev.; 81,

440, (1951).
[497] C. Zener; "Interaction between the d-Shells in the Transition Metals. II. Ferromagnetic Compounds of Manganese with Perovskite Structure"; Phys. Rev.; 82, 403, (1951).

[498] J. M. D. Coey, Dilute magnetic oxides, Curr. Opin. Solid State Mater. Sci. 10, 83 (2006).

[499] A. Kaminski and S. Das Sarma, Polaron Percolation in Diluted Magnetic Semiconductors, Phys. Rev. Lett. 88, 247202 (2002).
[500] Durst, A. C., Bhatt, R. N. & Wolff, P. A. Bound magnetic polaron interactions in insulating doped diluted magnetic semiconductors. Phys. Rev. B 65, 235205 (2002).
[501] J.M.D. Coey, d^0 ferromagnetism, Solid State Sci. 7, 660 (2005).

[502] C.D. Pemmaraju and S. Sanvito, Ferromagnetism Driven by Intrinsic Point Defects in HfO2, Phys. Rev. Lett. 94, 217205 (2005).
[503] J. M. D. Coey and S.A. Chambers, Oxide dilute magnetic semiconductors – fact of fiction? MRS Bulletin 33, 1053 (2008).
[504] J M D Coey, KwanruthaiWongsaprom1, J Alaria and M Venkatesan, Charge-transfer ferromagnetism in oxide Nanoparticles, J. Phys. D: Appl. Phys. 41 (2008) 134012
[505] G. Cohen, V. Fleurov, and K. Kikoin, Vacancy mediated ferromagnetic interaction in TiO_2 doped with magnetic Ions, J. Appl. Phys. 101, 09H106 (2007)
[506] F. Ma, J. Kudrnovsky, V. Drchala and G. Bouzerar, Magnetism without magnetic impurities in oxides ZrO_2 and TiO_2, Philosophical Magazine, Vol. 88, Nos. 18–20, 2008, 2755–2764
[507] J. Osorio-Guillen, S. Lany, S.V. Barabash and A. Zunger, Magnetism without Magnetic Ions: Percolation, Exchange, and Formation Energies of Magnetism-Promoting Intrinsic Defects in CaO, Phys. Rev. Lett. 96 (2006) p.107203.

[508] Y.B. Zhang, Q. Liu, T. Sritharan, C.L. Gan, S. Li, Pulsed laser ablation of preferentially orientated ZnO:Co diluted magnetic semiconducting thin films on Si substrates Appl. Phys. Lett. 89 (2006) 042510.
[509] H.S. Hsu, J.C.A. Huang, Y.H. Huang, Y.F. Liao, M.Z. Lin, C.H. Lee, J.F. Lee, S.F. Chen, L.Y. Lai, C.P. Liu, Evidence of oxygen vacancy enhanced room-temperature ferromagnetism in Co-doped ZnO ,Appl. Phys. Lett. 88 (2006) 242507.
[510] Khare N, Kappers MJ, Wei M, Blamire MG, MacManus-Driscoll JL. Defect-induced ferromagnetism in Co-doped ZnO. Adv Mater 2006;18:449.
[511] Schwartz DA, Gamelin DR. Reversible 300 K ferromagnetic ordering in a diluted magnetic semiconductor. Adv Mater 2004;16: 2115–9.
[512] Sluiter MHF, Kawazoe Y, Sharma P, Inoue A, Raju AR, Rout C,et al. First principles based design and experimental evidence for a ZnO-based ferromagnet at room temperature. Phys Rev Lett 2005;94:187204.
[513] N. Khare, M.J. Kappers, M. Wei, M.G. Blamire, J.L. Macmanus-Driscoll, Defect-induced ferromagnetism in Co-doped ZnO, Adv. Mater.18 (2006) 1449.
[514] X.J. Liu, C. Song, F. Zeng, X.B. Wang, F. Pan, Influence of annealing on microstructure and magnetic properties of co-sputtered Co-doped ZnO thin films, J. Phys.

D: Appl. Phys. 40 (2007) 1608.
[515] M. Gacic, G. Jakob, C. Herbort, H. Adrian, T. Tietze, S. Bru¨ ck, E. Goering, Magnetism of Co-doped ZnO thin films, Phys. Rev. B 75 (2007) 205206.
[516] B. Huang, D. Zhu, X. Ma, Great influence of the oxygen vacancies on the ferromagnetism in the Co-doped ZnO films, Appl. Surf. Sci. 253 (2007) 6892.
[517] C. Song, S.N. Pan, X.J. Liu, X.W. Li, F. Zeng, W.S. Yan, B. He, F. Pan, Evidence of structural defect enhanced room-temperature ferromagnetism in Co-doped ZnOJ. Phys.: Condens. Matter 19 (2007) 176229.
[518] X.C. Liu, E.W. Shi, Z.Z. Chen, H.W. Zhang, B. Xiao, L.X. Song, High-temperature ferromagnetism in (Co, Al)-codoped ZnO powders, Appl. Phys. Lett. 88 (2006) 252503.

[519] X. H. Xu, H J Blythe, M Ziese, A J Behan, J R Neal,A Mokhtari, R M Ibrahim, A M Fox and G A Gehring, Carrier-induced ferromagnetism in n-type ZnMnAlO and ZnCoAlO thin films at room temperatureNew J. Phys. 8, 135 (2006).

[520] K.R. Kittilstved, D.A. Schwartz, A.C. Tuan, S.M. Heald, S.A. Chambers, D.R. Gamelin, Direct Kinetic Correlation of Carriers and Ferromagnetism in Co^{2+}: ZnO, Phys. Rev. Lett. 97 (2006) 037203.
[521] X.-L. Li, Z.-L. Wang, X.-F. Qin, H.-S. Wu, X.-H. Xu, G.A. Gehring, "Enhancement of magnetic moment of Co-doped ZnO films by postannealing in vacuum", J. Appl. Phys., vol. 103, No. 2, pp. 023911-1 – 023911-5, Jan. 2008.

[522] J. R. Neal, A. J. Behan, R. M. Ibrahim, H. J. Blythe, M. Ziese, A. M. Fox, and G. A. Gehring, "Room-Temperature Magneto-Optics of Ferromagnetic Transition-Metal-Doped ZnO Thin Films," Phys. Rev. B, vol. 96, no. 19, pp. 197208-1 – 197208-4, May 2006.

[523] A. J. Behan, A. Mokhtari, H. J. Blythe, D. Score, X-H. Xu, J. R. Neal, A. M. Fox, and G. A. Gehring, "Two Magnetic Regimes in Doped ZnO Corresponding to a Dilute Magnetic Semiconductor and a Dilute Magnetic Insulator," Phys. Rev. Lett., vol. 100, no. 4, pp. 047206-1 – 047206-4, Feb. 2008.

[524] A-M Haghiri-Gosnet and J-P Renard, CMR manganites: physics, thin films and Devices, J. Phys. D: Appl. Phys. 36 R127-R150 (2003)

[525] Y. Moritomo, A. Asamitsu, H. Kuwahara, and Y. Tokura, Giant magnetoresistance of manganese oxides with a layered perovskite structure Nature ~London! 380, 141 (1996).
[526] Y. Shimakawa, Y. Kubo, and T. Manako, Nature ~London! 379, 53 (1996).
[527] M. N. Baibich, J. M. Broto, A. Fert, F. Nguyen van Dau, F. Petroff, P. Etienne, G. Creuzet, A. Friederich, and J. Chazelas, Giant Magnetoresistance of (001)Fe/(001)Cr Magnetic Superlattices, Phys. Rev. Lett. 61, 2472 (1988)

[528] G. Binasch; P. Grünberg; F. Saurenbach; W. Zinn, Enhanced magnetoresistance in layered magnetic structures with antiferromagnetic interlayer exchange, Phys. Rev. B 39 (7): 4828–4830. (1989).

[529] A. E. Berkowitz, J. R. Mitchell, M. J. Carey, A. P. Young, S. Zhang, F. E. Spada, F. T. Parker, A. Hutten, and G. Thomas, Giant magnetoresistance in heterogeneous Cu-Co alloys, Phys. Rev. Lett. 68, 3745 - 3748 (1992)
[530] John Q. Xiao, J. Samuel Jiang, and C. L. Chien, Giant magnetoresistance in nonmultilayer magnetic systems, Phys. Rev. Lett. 68, 3749 - 3752 (1992)

[531] S. Tehrani, E. Chen, M. Durlam,M.D. Herrera, J.M. Slaughter, J. Shi, G. Kerszykowski, High density submicron magnetoresistive random access memory, J. Appl. Phys. 85 (1999) 5822.
[532] T. Miyazaki, and N. Tezuka, Giant magnetic tunneling effect in Fe/Al_2O_3/Fe junction J. Magn. Mater., 139, L231 (1995)

[533] J. S. Moodera, L. R. Kinder, T. M. Wong, and R. Meservey, Phys. Rev. Lett., 74, 3273 (1995)

[534] P K Siwach, H K Singh, and O N Srivastava, Low field magnetotransport in manganites, J. Phys.: Condens. Matter 20 (2008) 273201 (43pp).
535 H. Y. Hwang, S-W. Cheong, N. P. Ong, and B. Batlogg, Spin-Polarized Intergrain Tunneling in $La_{2-3}Sr_{1-3}MnO_3$, Phys. Rev. Lett. 77, 2041–2044 (1996)
[536] A. Gupta, G. Q. Gong, Gang Xiao, P. R. Duncombe, P. Lecoeur, P. Trouilloud, Y. Y. Wang, V. P. Dravid, and J. Z. Sun, Phys. Rev. B 54, R15629–R15632 (1996)

[537] L. I. Balcells, A. E. Carrillo, B. Martinez, and J. Fontcuberta, Appl. Phys. Lett. 74, 4014 (1999).
[538] S. A. Koster, V. Moshnyaga, K. Samwer, O. I. Lebedev, G. Van Tendeloo, O. Shapoval, and A. Belenchuk, Doping of interfaces in $(La_{0.7}Sr_{0.3}MnO_3)_{1-x}$ /(MgO)x composite film, Appl. Phys. Lett. 81, 1648-1650 (2002).
[539] D. Das, A. Saha, S. E. Russek, R. Raj, and D. Bahadur, J. Appl. Phys. 93, 8301 (2003).
[540] P. Kameli, H. Salamati, and M. Eshraghi, J. Appl. Phys. 98, 043908 (2005).
[541] J. H. Miao, S. L. Yuan, X. Xiao, G. M. Ren, G. Q. Yu, Y. Q. Wang, and S. Y. Yin, J. Appl. Phys. 101, 043904 (2007)

[542] S. R. Gupta , Ranjit, C. Mitra, P. Rayachaudhuri, and R. Pinto, Appl. Phys. Lett. 78, 362 (2001)

[543] L. E. Hueso, J. Rivas, F. Rivadulla, and M. A. Lopez-Quintela, J. Appl. Phys. 89, 1746 (2001).

[544] B. S. Kang, H. Wang, J. L. MacManus-Driscoll, Y. Li, Q. X. Jia, I. Mihut, and J. B. Betts, Appl. Phys. Lett. 88, 192514 (2006)

[545] D. K. Petrov, L. Krusin-Elbaun, J. Z. Sun, C. Field, and P. R. Duncombe, Appl. Phys. Lett. 75, 995 (1999)

[546] O. A. Shlyakhtin, K. H. Shin, and Y. J. Oh, J. Appl. Phys. 91, 7403 (2002)

[547] . C. Xia, S. L. Yuan, W. Feng, L. J. Zhang, G. H. Zhang, J. Tang, L. Liu, S. Liu, G. Peng, D. W. Niu, L. Chen, Q. H. Zheng, Z. H. Fang and C. Q. Tang, Solid State Commun. 128, 291 (2003)

[548] Q. Huang, J. Li, X. J. Huang, C. K. Ong, and X. S. Gao, J. Appl. Phys. 90, 2924 (2001).
[549] C. H. Yan, Z. G. Xu, T. Zhu, Z. M. Wang, F. X. Cheng, Y. H. Huang, and C. S. Liao, J. Appl. Phys. 87, 5588 (2000).
[550] Y. H. Huang, C. H. Yan, F. Luo, W. Song, Z. M. Wang, and C. S. Liao, Appl. Phys. Lett. 81, 76 (2002).
[551] C. H. Yan, F. Luo, Y. H. Huang, X. H. Li, Z. M. Wang, C. S. Liao, H. W. Zhao, and B. G. Shen, J. Appl. Phys. 91, 7406 (2002).
552 J.-M. Liu, J. Li, Q. Huang, L. P. You, S. J. Wang, C. K. Ong, Z. C. Wu, Z. G. Liu, and Y. W. Du, Appl. Phys. Lett. 76, 2286 (2000)
553 J. H. van Santen, and G. Jonker, 1950, Physica (Amsterdam) 16, 599
554 G. Jonker, and van Santen, 1950, Physica (Amsterdam) 16, 337
[555] Jonker, G. H., 1956, Physica, 22, 707
[556] Anderson, P. W., and Hasegawa, H., 1955, Phys. Rev., 100, 675.
[557] deGennes, P. G., 1960, Phys. Rev., 118, 141.
[558] Goodenough J B 1955 Phys. Rev. 100 564
[559] H. A. Kramers Physica 1, 182 (1934) L'interaction Entre les Atomes Magnétogènes dans un Cristal Paramagnétique

[560] P.W. Anderson, Phys. Rev. 79, 350 - 356 (1950)

[561] Elbio DAGOTTO, Takashi HOTTA, Adriana MOREO, COLOSSAL MAGNETORESISTANT MATERIALS: THE KEY ROLE OF PHASE SEPARATION, Physics Reports 344 (2001) 1-153
[562] Millis, A. J., Littlewood, P. B. & Shraiman, B. I. Double exchange alone does not explain the resistivity of La1-xSrxMnO3. Phys. Rev. Lett. 74, 5144–5147 (1995).

[563] Millis A J, Shraiman B I and Mueller R 1996 Phys. Rev. Lett. 77 175

[564] Millis A J, Mueller R and Shraiman B I 1996b Phys. Rev. B 54 5389

[565] Millis, A. J.,Mueller, R. & Shraiman, B. I. Fermi-liquid-to-polaron crossover. II. Double exchange and the physics of colossal magnetoresistance. Phys. Rev. B 54, 5405–5417 (1996).

[566] Millis A J Lattice effects in magnetoresistive manganese perovskites1998 Nature 392 147
[567] Y Tokura, Critical features of colossal magnetoresistive Manganites, Rep. Prog. Phys. 69 (2006) 797–851

[568] M.B. Salamon and M. Jaime, The physics of manganites: Structure and transport, Rev. Mod. Phys., 73, 583 (2001).
[569] L. Sudheendra, V. Moshnyaga, and K. Samwer, Metal-insulator transition and colossal magnetoresistance: relevance of electron-lattice coupling and electronic phase separation, Contemporary Physics, 48, 349 (2007).

[570] L. P. Gor'kov and V. Z. Kresin, Mixed-valence manganites: fundamentals and main properties, Physics Reports 400 149–208 (2004)
[571] M Ziese, Extrinsic magnetotransport phenomena in ferromagnetic oxides, Rep. Prog. Phys. 65 (2002) 143–249

[572] de Groot, R. A.,Muller, F. M., van Engen, P. G.&Buschow, K. H. J. Newclass of materials: half-metallic ferromagnets. Phys. Rev. Lett. 50, 2024–2027 (1983).
573 C. Phillips, Phys. Rev. 133, A1020-A1028 (1964)
574 P.M. Tedrow and R. Meservey, Phys. Rev. B 7, 318-326 (1973)
[575] Y. Okimoto, T. Katsufuji, T. Ishikawa, T. Arima, and Y. Tokura. Anomalous variation of optical spectra with spin polarization in double-exchange ferromagnet: $La_{1-x}Sr_xMnO_3$, Phys. Rev. Lett. 75, 109 (1995
[576] J.-H. Park., C. T. Chen,1 S-W. Cheong, W. Bao, G. Meigs,1 V. Chakarian, and Y. U. Idzerda, "Electronic aspects of the ferromagnetic transition in manganese perovskites". Phys. Rev. Lett. 76, 4215–4218 (1996).
[577] W.E. Pickett and D.J. Singh, Phys. Rev. B 53, 1146 (1996).

[578] Yu Lu, X. W. Li, G. Q. Gong, Gang Xiao, A. Gupta, P. Lecoeur, J.Z. Sun, Y.Y. Wang, and V.P. Dravid, Large magnetotunneling effect at low magnetic fields in micrometer-scale epitaxial La 0.67Sr 0.33MnO3 tunnel junctions, Phys. Rev. B 54, R8357 (1996).

[579] J.Z. Sun, L. Krusin-Elbaum, P.R. Duncombe, A. Gupta, and R.B. Laibowitz, Temperature dependent, non-ohmic magnetoresistance in doped perovskite manganate trilayer junctions, Appl. Phys. Lett. 70, 1769 (1997).

580 J.H. Park, E. Vescovo, H.J. Kim, C. Kwon, R. Ramesh, and T. Venkatesan, Direct evidence for a half-metallic ferromagnet, Nature 392, 794-796 (1998)
[581] D.C. Worlege and T.H. Geballe, Appl. Phys. Lett. 76, 900 (2000).

[582] Nadgorny B, Mazin I I, Osofsky M, Soulen J R J, Broussard P, Stroud R M, Singh D J, Harris V G, Arsenov A and Mukovskii Y 2001 Phys. Rev. B 63 184433

[583] M Bowen, J-LMaurice, A Barth´el´emy, M Bibes, D Imhoff,V Bellini, R Bertacco, D Wortmann, P Seneor, E Jacquet,A Vaur`es, J Humbert, J-P Contour, C Colliex, S Bl¨ugel and P H Dederichs, Using half-metallic manganite interfaces to reveal insights into spintronics, J. Phys.: Condens. Matter 19 (2007) 315208.

[584] J. O'Donnell, A. E. Andrus, S. Oh, E. V. Colla, and J. N. Eckstein, Appl. Phys. Lett. 76,

1914 (2000).
[585] Goldschmidt V M 1958 Goechemistry (Oxford: Oxford University Press);

[586] Goodenough J B 1997 J. Appl. Phys. 81 5330

[587] M. Imada, A. Fujimori, and Y. Tokura, Metal-insulator transitions, Rev. Mod. Phys., Vol. 70, 1039 (1998)

[588] J. M. D. Coey, Viret M and von Molnar S Mixed-valence manganites, Advances in Physics, 1999, Vol. 48, No. 2, 167 - 293
[589] Goodenough J B and Longo M 1970 Landolt–B¨ornstein Group III vol 4 126
[590] H. Y. Hwang, S. W. Cheong, P. G. Radaelli, M. Marezio, and B. Batlogg, B. Phys. Lattice Effects on the Magnetoresistance in Doped LaMnO3, Rev. Lett. 75, 914 (1995).
[591] Wollan E O and Koehler W C 1955 Phys. Rev. 100 545

[592] Jirak Z, Krupicka S, Sinsa Z, Dlouha M and Vratislav S 1985 J. Magn. Magn. Mater. 53 153

[593] C N R Rao, Anthony Arulraj, A K Cheetham, and Bernard Raveau, Charge ordering in the rare earth manganates: the experimental situation, J. Phys.: Condens. Matter 12 (2000) R83–R106.

[594] H.L. Ju, J. Gopalakrishnan, J.L. Peng, Q. Li, G.C. Xiong, T. Venkatesan, R.L. Greene, Dependence of giant magnetoresistance on oxygen stoichiometry and magnetization in polycrystalline La2/3Ba1/3MnOz, Phys. Rev. B 51 (1995) 6143–6146.

[595] D.J. Wang, C.M. Xiong, G.J. Liu, Y.W. Xie, B.G. Shen, J.R. Sun Effects of oxygen content on the transport property of $La_{0:7}Ce_{0:3}MnO_3$ film, Physica B 371 (2006) 187–191

[596] J. Sakai, N. Ito, and S. Imai, Oxygen content of La1−xSrxMnO3−y thin films and its relation to electric-magnetic properties J. Appl. Phys. 99, 08Q318 (2006)

[597] I.O. Troyanchuk, S.V. Trukanov, H. Szymezak, K. Baerner, Effect of oxygen content on the magnetic and transport properties of $Pr_{0:5}Ba_{0:5}$ $MnO_{3-\gamma}$ J. Phys. Condens. Matter 12 (2000) L155.
Effect of oxygen content on the magnetic and transport properties of $Pr_{0:5}Ba_{0:5}$ $MnO_{3-\gamma}$
[598] W. Prellier, M. Rajeswari, T. Venkatesan, R.L. Greene, Effects of annealing and strain on $La_{12x}Ca_xMnO_3$ thin films: A phase diagram in the ferromagnetic region Appl. Phys.Lett. 75 (1999) 1446.

[599] M. Salvato, A. Vecchione, A. De Santis, F. Bibba, A.M. Cucolo, Metal-insulator transition temperature enhancement in $La_{0.7}Ca_{0.3}MnO_3$ thin films J. Appl. Phys. 97 (2005) 103712.

600 G. L. Yuan, J. M. Liu, H. L. W. Chan, C. L. Choy, C. K. Ong, Z. G. Liu and Y. W. Du, Low-field magnetoresistance in oxygen-deficient La Sr MnO 0.5 0.5 3 thin films as approached by spin-polarized tunneling model Materials Letters 53, 76 (2002)
[601] Y. Yamada, O. Hino, S. Nohdo, and R. Kanao, T. Inami and S. Katano, Polaron Ordering in Low-Doping La12xSrxMnO3, Phys. Rev. Lett. 77, 904 (1996)

602 M. Paraskevopoulos, F. Mayr, C. Hartinger, A. Pimenov, J. Hemberger, P. Lunkenheimer, A. Loidl, A. A. Mukhin, V. Yu. Ivanov and A. M. Balbashov, Journal of Magnetism and Magnetic Materials 211, 118 (2000)
603 J. Hemberger, A. Krimmel, T. Kurz, H.-A. Krug von Nidda, V. Yu. Ivanov, A. A. Mukhin, A. M. Balbashov, and A. Loidl, Phys. Rev. B 66, 094410 (2002)
604 P. Schiffer, A. P. Ramirez, W. Bao, and S-W. Cheong, Phys. Rev. Lett. 75, 3336 (1995)
[605] Cheong S W and Hwang H Y 2000 Ferromagnetism versus charge/orbital ordering in mixed-valent manganites Colossal Magnetoresitance Oxides ed Y Tokura (London: Gordon and Breach)
[606] Wollan, E.O., Koehler, W.C., 1955. Phys. Rev. 100, 545.
[607] Matsumoto, G., 1970b. J. Phys. Soc. Japan 29, 615.
[608] 6Y. Tomioka, A. Asamitsu, Y. Moritomo, and Y. Tokura, J. Phys. Soc. Jpn. 64, 3626 ~1995!.
609 Y. Tomioka, A. Asamitsu, H. Kuwahara, Y. Moritomo, and Y. Tokura, Phys. Rev. B 53, R1689 (1996)
[610] C. Martin, A. Maignan, M. Hervieu, and B. Raveau, Phys. Rev. B 60, 12 191 ~1999!.
611 Y. Tomioka, A. Asamitsu, Y. Moritomo, H. Kuwahara, and Y. Tokura, Phys. Rev. Lett. 74, 5108 (1995)
[612] 30H. Kawano, R. Kajimoto, H. Yoshizawa, Y. Tomioka, H. Kuwahara, and Y. Tokura, Phys. Rev. Lett. 78, 4253 (1997).
[613] Kajimoto R, Yoshizawa H, Kawano H, Kuwahara H, Tokura Y, Ohoyama K and Ohashi M 1999 Phys. Rev. B 60 9506
[614] Tobe K, Kimura T and Tokura Y 2004 Phys. Rev. B 69 014407

[615] R. Kajimoto,1 H. Yoshizawa,2 Y. Tomioka,3 and Y. Tokura, Stripe-type charge ordering in the metallic A-type antiferromagnet $Pr_{0.5}Sr_{0.5}MnO_3$, PHYSICAL REVIEW B 66, 180402-R (2002)

[616] Y. Tokura and Y. Tomioka, Colossal magnetoresistive manganites,Journal of Magnetism and Magnetic Materials 200 (1999) 1-23

[617] R. Maezono, S. Ishihara, and N. Nagaosa, Phys. Rev. B Phase diagram of manganese oxides 58, 11 583 (1998),
[618] 9A. Urushibara, Y. Moritomo, T. Arima, A. Asamitsu, G. Kido, and Y. Tokura, Phys. Rev. B 51, 14 103 ~1995!.

[619] 10Y. Yamada, O. Hino, S. Nohdo, R. Kanao, T. Inami, and S. Katano, Phys. Rev. Lett. 77, 904 ~1996!.

[620] 11H. Kawano, R. Kajimoto, M. Kubota, and H. Yoshizawa, Phys. Rev. B 53, R14 709 ~1996!.

[621] 12 J.-S. Zhou, J.B. Goodenough, A. Asamitsu, and Y. Tokura, Phys. Rev. Lett. 79, 3234 ~1997!.

[622] Fujishiro, H, et al., 1998. J. Phys. Soc. Japan. 67 1799.

[623] Pal S, Bose E, Chaudhuri B K, Yang H D, Neeleshwar S and Chen Y Y Effect of Ni doping in rare-earth manganite $La_{0.7}Pb_{0.3}Mn_{1-x}Ni_xO_3$ (x=0.0–0.5) 2005 J. Magn. Magn. Mater. 293 872

[624] Zhi-Hong Wang, Bao-Gen Shen, Ning Tang, Jian-Wang Cai, Tian-Hao Ji, Jian-Gao Zhao, and Wan-Shan Zhan, Guang-Chan Che, J. Appl. Phys. 85, 5399 (1999)

[625] I. Kammouna, W. Cheikhrouhou-Koubaa a, W. Boujelben a, A. Cheikhrouhou Bi doping effects on the physical properties of$Pr_{0.6}Sr_{0.4}Mn_{1-x}Bi_xO_3$ ($0 \leq x \leq 0.2$) manganese oxides Journal of Alloys and Compounds 452 (2008) 195–199

[626] Ang R, Sun Y P, Yang J, Zhu X B and Song W H Transport mechanism and magnetothermoelectric power of electron-doped manganites $La_{0.85}Te_{0.15}Mn_{1-x}Cu_xO_3$ ($0 \leq x \leq 0.20$) 2006 J. Appl. Phys. 100 073706

[627] Yang J, Song W H, Ma Y Q, Zhang R L, Zhao B C, Sheng Z C, Zheng G H, Dai J M and Sun Y P Structural, magnetic, and transport properties of the Cu -doped manganite $La_{0.85}Te_{0.15}Mn_{1-x}Cu_xO_3$ ($0 \leq x \leq 0.20$) Phys. Rev. B 70, 092504 (2004)

[628] Wenger LE, Tsoi GM, Suryanarayanan R, Sudyoadsuk T. " Effect of Cr-doping on the magnetic and electrical properties of $La_{0.4}Ca_{0.6}MnO_3$ "' JOURNAL OF APPLIED PHYSICS Volume: 103 Issue: 7 Article Number: 07F723 : APR 1 2008

[629] Sotirova E, Wang X L, Horvat J, Silver T, Konstantinov K and Liu H K Study of structure, transport, paramagnetic and ferromagnetic properties of $La_{0.8}Sr_{0.2}Mn_{1-x}Zn_xO_3$ perovskite manganite 2002 Supercond. Sci. Technol. 15 346

[630] Sun Y, Xu X, Zheng L and Zhang Y Effects of Ga doping in the colossal magnetoresistance material $La_{0.67}Ca_{0.33}MnO_3$ Phys. Rev. B 60, 12317 - 12321 (1999)

[631] A. Nucara, P. Maselli, M. Del Bufalo, M. Cestelli Guidi, J. Garcia, P. Orgiani, L. Maritato, and P. Calvani, Effect of Ga substitution on the optical properties of La-Sr manganites, PHYSICAL REVIEW B 77, 064431 _2008_

[632] Blasco J, Garcia J, de Teresa J M, Ibarra M R, Perez J,

Algarabel P A and Ritter C Structural, magnetic, and transport properties of the giant magnetoresistive perovskites $La_{2/3}Ca_{1/3}Mn_{1-x}Al_xO_{3-\delta}$ Phys. Rev. B 55, 8905 - 8910 (1997)

[633] Nam, D. N. H, Dai, N. V., Hong, L. V., Phuc, N. X., Bau, L. V.), Nordblad, P., Newrock, R. S. " Effects of selective dilution on the magnetic properties of $La_{0.7}Sr_{0.3}Mn_{1-x}M'O_{-x}(3)$ (M ' = Al, Ti), JOURNAL OF THE KOREAN PHYSICAL SOCIETY Volume: 52 Issue: 5 Pages: 1460-1464 Published: MAY 2008

[634] Troyanchuk I O, Bushinsky M V, Szymazak H, Barner K,Maignan A Magnetic interaction in Mg, Ti, Nb doped manganites 2002 Eur. Phys. J. B 28 75

[635] Liu X, Xu X and Zhang Y Effect of Ti dopant on the carrier density collapse in colossal magnetoresistance material $La_{0.7}Ca_{0.3}Mn_{1-y}Ti_yO_3$ Phys. Rev. B 62, 15112 - 15119 (2000)

[636] Lakshmi L S, Dorr K, Nenkov K, Sridharan V, Sastry V S and Muller K-H Structure, transport and magnetism of $La_{0.67}Ca_{0.33}Mn_{1-x}Ta_xO_3$ 2005 J. Magn. Magn. Mater. 290–291 924

[637] S K Agarwal, Neeraj Panwar, Vikram Sen, and D K Pandya, Magneto-transport and thermal properties of $Pr_{2/3}Ba_{1/3}(Mn_{1-x}Sb_x)O_3$ system, J. Phys. D: Appl. Phys. 41 (2008) 105004

[638] Sen V, Panwar N, Bhalla G L and Agarwal S K Structural, electrical and magnetic properties of Sb-doped $Pr_{2/3}Ba_{1/3}MnO_3$ perovskite manganites 2007 J. Alloys Compounds 439 205

[639] Cai J W, Wang C, Shen B-G, Zhao J-G and Zhan W-S, "Colossal magnetoresistance of spin-glass perovskite $La_{0.67}Ca_{0.33}Mn_{0.9}Fe_{0.1}O_3$"Appl. Phys. Lett. 71, 1727 (1997);

[640] Ahn K H, Wu X W, Liu K and Chien C L Effects of Fe doping in the colossal magnetoresistive $La_{1-x}Ca_xMnO_3$ J. Appl. Phys. 81, 5505 (1997);

[641] Sridharan V, Lakshmi L S, Govindraj R, Nithya R, Natarajan D V and Radhakrishnan T S Transport and thermal properties of $La_{0.67}Ca_{0.33}Mn_{1-x}M_xO_3$ (M=Fe, Zr and Hf) 2001 J. Alloys Comp. 326 65

[642] Kim J S, Kim D C, McIntosh G C, Chu S W, Park Y W, Kim B J, Kim Y C, Maignan A and Raveau B Magnetothermoelectric power of $Pr_{0.5}Sr_{0.5}MnO_3$ with Ru substitution at the Mn site, 2002 Phys. Rev. B 66 224427

[643] Wang L M, Lai J-H, Wu J-I, Kuo Y-K and Chang C L Effects of Ru substitution for Mn on $La_{0.7}Sr_{0.3}MnO_3$ perovskites J. Appl. Phys. 102, 023915 (2007);

[644] Lorenzo Malavasi, Maria Cristina Mozzati, Cristina Tealdi, Carlo Bruno Azzoni, and Giorgio Flor, Influence of Ru Doping on the Structure, Defect Chemistry, Magnetic Interaction, and Carrier Motion of the La1-xNaxMnO3+ä Manganite J. Phys. Chem. B 2005, 109, 20707-20713

645 B. Raveau, A. Maignan, C. Martin, R. Mahendiran, and M. Hervieu, Ru-Induced Ferromagnetism and Metallicity in Mn(IV)-Rich Manganites Ln0.4Ca0.6MnO3 J. Solid State Chem. 151, 330 (2000).
646 A. Maignan, C. Martin, M. Hervieu, and B. Ravieu, Ru doping of the A-type antiferromagnet Pr0.5Sr0.5MnO3: Conversion to a metallic ferromagnet J. Appl. Phys. 89, 500 (2001)
647 H. Yamada, M. Kawasaki, and Y. Tokura, Ru-doped La0.6Sr0.4MnO3 thin films as a coercivity tunable electrode for magnetic tunnel junctions Appl. Phys. Lett. 86, 192505 (2005)
[648] S. Canulescu, Th. Lippert, A. Wokaun, M. Döbeli, A. Weidenkaff, R. Robert and D. Logvinovich, The effect of the fluence on the properties of La–Ca–Mn–O thin films prepared by pulsed laser deposition, Applied Surface Science Volume 253, Issue 19, 31 July 2007, Pages 8174-8178
[649] I. Bergenti, A. Riminucci, E. Arisi, L.E. Hueso, M. Cavallini, M. Solzi and V. Dediu, "Ultrathin manganite films grown by pulsed-plasma deposition", Journal of Magnetism and Magnetic Materials Volume 310, Issue 2, Part 3, March 2007, Pages e780-e782
650 M. Koubaa, A. M. Haghiri-Gosnet, R. Desfeux, Ph. Lecoeur, W. Prellier, and B. Mercey, Crystallinity, surface morphology, and magnetic properties of La0.7Sr0.3MnO3 thin films: An approach based on the laser ablation plume range models, J. Appl. Phys. 93, 5227 (2003)
651 S. Canulescu, Th. Lippert, A. Wokaun, M. Do¨beli, A. Weidenkaff , R. Robert, D. Logvinovich, The effect of the fluence on the properties of La–Ca–Mn–O thin films prepared by pulsed laser deposition, Applied Surface Science 253 (2007) 8174–8178.
652 R. Bertacco, J. P. Contour, A. Barthélemy and J. Olivier, Surface Science 511, 366 (2002)
[653] L. Signorini, M. Riva, M. Cantoni, R. Bertacco, F. Ciccacci, Epitaxial $La_{2/3}Sr_{1/3}MnO_3$ thin films with unconventional magnetic and electric properties near the Curie temperature, Thin Solid Films 515 (2006) 496–499
[654] J. Klein, C. HoK fener, L. Al, R. Gross, Laser ablation of manganite thin "lms monitored by in situ RHEED, Journal of Magnetism and Magnetic Materials 211 (2000) 9-15
[655] W. Prellier, Amlan Biswas, M. Rajeswari, T. Venkatesan, and R. L. Greene, Effect of substrate-induced strain on the charge-ordering transition in $Nd_{0.5}Sr_{0.5}MnO_3$ thin films, Appl. Phys. Lett., Vol. 75, 397 1999
[656] A. Abrutis, A. Bartasyte , G. Garciab, A. Teiserskisa, V. Kubiliusa, Z. Saltytea, V. Faucheux, "Metal-organic chemical vapour deposition of mixed-conducting perovskite oxide layers on monocrystalline and porous ceramic substrates", Thin Solid Films 449 (2004) 94–99

[657] J.J.Her emans, M. Carris, S.Y u, X.W atts, K.H.Dahmen, S. von Molnar, J.Appl. Phys.81 (1997) 4967.
[658] D.Studebaker , M.T odd, C.Seegel, T.H. Baum, Mater. Sci. Eng.B 56 (1998) 168.
[659] P.B. Tavares, V.S. Amaral, J.P. Araujo, J.B. Sousa, A.A.C.S Lourenco, J.M. Vieira, J.Appl.Phys.85 (1999) 5411.

[660] V.Moshnyaga, I.Khor oshun, A. Sidorenko, P.Petr enko, A. Weidinger, M.Zeitler , B. Rauschenbach, R. Tidecks, K. Samwer, Appl.Phys.Lett. 74 (1999) 2842.
661 C. Dubourdieu, M. Rosina, M. Audier, F. Weiss, J. P. Sénateur, E. Dooryhee and J. L. Hodeau, Application of pulsed liquid-injection MOCVD to the growth of ultrathin epitaxial oxides for magnetic heterostructures Thin Solid Films, 400, 81 (2001)
662 C. Dubourdieu, M. Rosina, H. Roussel, F. Weiss, J. P. Sénateur, and J. L. Hodeau, Pulsed liquid-injection metalorganic chemical vapor deposition of $La_{0.7}Sr_{0.3}MnO_3$ /$SrTiO_{3.15}$????superlatticesAppl. Phys. Lett. 79, 1246 (2001)
663 A. Abrutis, V. Plausinaitiene, V. Kubilius, A. Teiserskis, Z. Saltyte, R. Butkute and J. P. Senateur, Magnetoresistant La1yxSrxMnO3 films by pulsed injection metal organic chemical vapor deposition: effect of deposition conditions, substrate material and film thickness, Thin Solid Films 413, 32 (2002)
[664] O. Nilsen, E. Rauwel, H. Fjellva°ga and A. Kjekshusa, " Growth of $La_{12x}Ca_xMnO_3$ thin films by atomic layer deposition J. Mater. Chem., 2007, 17, 1466–1475
[665] M. Španková, Š. Chromik, I. Vávra, K. Sedláčková, P. Lobotka, S. Lucas and S. Stanček M. Španková' , Š. Chromik, I. Vávra, K. Sedláčková, P. Lobotka, S. Lucas and S. Stanček, Epitaxial LSMO films grown on MgO single crystalline substrates, Applied Surface Science 253 (2007) 7599–7603
[666] D.R. Sahu, D.K. Mishra, Jow-Lay Huang, and B.K. Roul, Annealing effect on the properties of $La_{0.7}S_{r0.3}MnO_3$ thin film grown on Si substrates by DC sputtering, Physica B 396 (2007) 75–80
667 M. J. Casanove, C. Roucau, P. Baulès, J. Majimel, J. -C. Ousset, D. Magnoux and J. F. Bobo, Growth and relaxation mechanisms in $La_{0.66}Sr_{0.33}MnO_3$ manganites deposited on $SrTiO_3$(001) and MgO(001) Applied Surface Science 188, 19 (2002)
668 L. M. Wang and Chih-Chian Guo, Anisotropic magnetoresistance and spin polarization of La0.7Sr0.3MnO3/SrTiO3 superlatticesAppl. Phys. Lett. 87, 172503 (2005)
669 L. M. Wang, H. H. Sung, B. T. Su, H. C. Yang, and H. E. Horng, J. Appl. Phys. 88, 4236 (2000)
670 T. Li, B. Wang, H. Dai, Y. Du, H. Yan, and Y. Liu, Annealing effect on the structural and magnetic properties of $La_{0.7}Sr_{0.3}MnO_3$ filmsJ. Appl. Phys. 98, 123505 (2005)
671 S. Y. Yang, W. L. Kuang, Y. Liou, W. S. Tse, S. F. Lee and Y. D. Yao, Growth and characterization of $La_{0.7}Sr_{0.3}MnO_3$ films on various substratesJ. Mag. and Mag. Mat., 268, 326 (2004)
[672] S.H. Seo, H.C. Kang, H.W. Jang, D.Y. Noh, Effects of oxygen incorporation in tensile $La_{0.84}Sr_{0.16}MnO_{3-d}$ thin films during ex situ annealing, Phys. Rev. B 71 (2005) 012412.

[673] J. J. Kavich, M. P. Warusawithana, J. W. Freeland, P. Ryan, X. Zhai, R. H. Kodama,1 and J. N. Eckstein, Nanoscale suppression of magnetization at atomically assembled manganite interfaces: XMCD and XRMS measurements, PHYSICAL REVIEW B 76, 014410 (2007)
[674] J. O'Donnell, M. Onellion, M. S. Rzchowski, J. N. Eckstein and I. Bozovic, Anisotropic properties of molecular beam epitaxy-grown colossal magnetoresistance manganite thin films, J. Appl. Phys. 81 (8), 4961 1997

675 S. Mercone, C. A. Perroni, V. Cataudella, C. Adamo, M. Angeloni, C. Aruta, G. De Filippis, F. Miletto,A. Oropallo, P. Perna, A. Yu. Petrov, U. Scotti di Uccio, and L. Maritato, Transport properties in manganite thin films, Phys. Rev. B 71, 064415 (2005)
676 J. O'Donnell, M. Onellion, M. S. Rzchowski, J. N. Eckstein and I. Bozovic, Phys. Rev. B 54, R6841 (1996)
677 J. O'Donnell, A. E. Andrus, S. Oh, E. V. Colla, and J. N. Eckstein, Colossal magnetoresistance magnetic tunnel junctions grown by molecular-beam epitaxy, Appl. Phys. Lett. 76, 1914 (2000).
678 S. Y. Bae and S. X. Wang, Sol–gel epitaxial growth of La12xCaxMnO3 with colossal magnetoresistance effect Appl. Phys. Lett. 69, 121 (1996)

679 Liu XD, Jiao ZK, Nakamura K, Hatano T, Zeng YW, The grain size dependence of the resistance behaviors in doped lanthanum manganite polycrystalline films, J. Appl. Phys., 87, 2431 2000
680 Wang SC, Hsu HZ, Wei WJ, Microstructure of porous Sr-doped lanthanum manganite fabricated by sol-gel process, ADVANCED CERAMICS AND COMPOSITES Volume: 247 Pages: 393-396 Published: 2003

681 In-Bo Shim, Key-Taeck Park, Chul-Sung Kim, Young-Jei Oh, Complex impedance analysis of granular La2/3Sr1/3MnO3 manganite thin films, Journal of Magnetism and Magnetic Materials 226}230 (2001) 733-735

682 Osami Yanagisawa, Mitsuru Izumi, Kai-Hua Huang, Wei-Zhi Hu, Yi Shen, Kenji Nakanishi", Yoshihiro Takahashi", Hideo Nojima, Comparative study of photo-induced e!ect on the charge-ordered state of $Pr_{0.65}Ca_{0.35}MnO_3$ in powder and thin "lms, Journal of Magnetism and Magnetic Materials 211 (2000) 133}138

683 . H. Yan, Y. H. Huang, Z. M. Wang, T. Zhu, C. S. Liao, F. X. Cheng, Z. L. Zhang and G. X. Xu, Microstructure and transport properties of sol-gel fabricated La0.7Sr0.3MnO3 nanocrystalline flms on Si(100) substrates, Thin Solid Films 366 (2000) 302-305

684 Shimizu Y, Murata T, Sol-gel synthesis of perovskite-type lanthanum manganite thin films and fine powders using metal acetylacetonate and poly(vinyl alcohol), JOURNAL OF THE AMERICAN CERAMIC SOCIETY Volume: 80 Issue: 10 Pages: 2702-2704 Published: OCT 1997

685 W Prellier, Ph Lecoeur and B Mercey, Colossal-magnetoresistive manganite thin films, J. Phys.: Condens. Matter 13 (2001) R915–R944 PII: S0953
685 L. B. Steren, M. Sirena, and J. Guimpel, J. Appl. Phys. 87, 6755, (2000).

686 G Van Tendeloo, O I Lebedev, M Hervieu and B Raveau, Structure and microstructure of colossal magnetoresistant materials, Rep. Prog. Phys. 67 (2004) 1315–1365
687 H. S. Kim and H. S. Kwok, Appl. Phys. Lett. 61, 2234 (1992).

[688] D. B. Geohegan, Appl. Phys. Lett. 60, 2732 (1992).
[689] M. Strikovski and J. H. Miller, Jr., Appl. Phys. Lett. 73, 1733 ~1998!.
[690] D. B. Geohegan, Thin Solid Films 220, 138 (1992).
691 G. C. Xiong, Q. Li, H. L. Ju, R. L. Greene, and T. Venkantesan, Appl. Phys. Lett. 66, 1690 (1995)
[692] J.P. Se´nateur, R.Madar , F.W eiss, O.Thomas, A. Abrutis, French patent FR 2707671 (1993), European patent EP 730671 (1994), US patent US 945162 (1999).
693 S. Matsuno, F. Uchikawa, S. Utsunomiya, and S. Nakabayashi, Metalorganic chemical vapor deposition using a single solution source for high J, $Y_1Ba_2Cu_3Q_{7-x}$ superconducting films Appl. Phys. Lett. 60, 2427 (1992)
694 J. Zhang, R. A. Gardiner, P. S. Kirlin, R. W. Boerstler, and J. Steinbeck, Single liquid source plasma-enhanced metalorganic chemical vapor deposition of high-quality YBa_2CuO_{7-x} thin films Appl. Phys. Lett. 61, 2884 (1992)
695 H. Xie and R. Raj, Epitaxial LiTaO, thin film by pulsed metalorganic chemical vapor deposition from a single precursor Appl. Phys. Lett. 63, 3146 (1993)
696 K. Dörr, T. Walter, M. Sahana, K.-H. Müller, K. Nenkov, K. Brand, and L. Schultz, Magnetotransport of $La_{0.7}Sr_{0.3}MnO_3$ /$SrTiO_3$ multilayers with ultrathin manganite layers J. Appl. Phys. 89, 6973 (2001)
[697] J. N. Eckstein and I. Bozovic, Annu. Rev. Mater. Sci. 25, 679 (1995).
[698] G.J. Snyder, R. Hiskes, S. DiCarolis, M.R. Beasley, T.H. Geballe, Phy. Rev. B 53 (1996) 14434.
[699] R. Shreekala, M. Rajeswari, K. Ghosh, A. Goyal, J. Y. Gu, C. Kwon, Z. Trajanovic, T. Boettcher, R. L. Greene, R. Ramesh, and T. Venkatesan, Effect of crystallinity on the magnetoresistance in perovskite manganese oxide thin films, Appl. Phys. Lett. 71 (2), 282 (1997)
[700] E. S. Vlakhov, R. A. Chakalov and R. I. Chakalova, and K. A. Nenkov, Influence of the substrate on growth and magnetoresistance of $La_{0.7}Ca_{0.3}$MnOz thin films deposited by magnetron sputteringJ. Appl. Phys. 83, 2152 (1998)

[701] Zhi-Hong Wang, H. Kronmu¨ller, O. I. Lebedev, G. M. Gross, F. S. Razavi, H. -U. Habermeier, and B. G. Shen, Phase transition and magnetic anisotropy of .La,Sr.MnO3 thin films, Phy. Rev. B 65 054411 (2002).
[702] Yuan-Chang Lianga,z and Yung-Ching Liangb. Quantifying Strain Effects on Physical Properties of $La_{0.68}Ba_{0.32}MnO_3$ Epilayers and Heterostructures, Journal of The Electrochemical Society, 154 ,12, P147-P151 (2007)
[703] P K Muduli, S K Bose and R C Budhani Stress-induced competing ferromagnetic and antiferromagnetic orders in epitaxial films of A-type antiferromagnet $La_{0.45}Sr_{0.55}MnO_3$ J. Phys.: Condens. Matter 19 (2007) 226204

[704] Ravikant Prasad, Anurag Gaur, P K Siwach, G D Varma,A Kaur4 and H K Singh, " Effect of large compressive strain on low field electrical transport in $La_{0.88}Sr_{0.12}MnO_3$ thin films J. Phys. D: Appl. Phys. 40 (2007)

[705] F. S. Razavi, G. V. Sudhakar Rao, H. Jalili and H.-U. Habermeier, Pressure induced phase transition in periodic microtwinned thin film of $La_{0.88}Sr_{0.1}MnO_3$, 2006 Appl. Phys.

Lett. 88 174103
[706] Q. Qian, T.A. Tyson, M. Deleon, C.-C. Kao, J. Bai and A.I. Frenkel, " Influence of strain on the atomic and electronic structure of manganite films", Journal of Physics and Chemistry of Solids Volume 68, Issue 3, March 2007, Pages 458-463
[707] Christen H M, Varela M, Kim D H, "The effect of strain and strain symmetry on the charge-order transition in $Bi_{0.4}Ca_{0.6}MnO_3$ films", PHASE TRANSITIONS Volume: 81 Issue: 7-8 Pages: 717-727 (2008)
[708] Abad, Llibertat, Laukhin, Vladimir , Valencia, Sergio , Gaup, Andreas, Gudat, Wolfgan, Balcells, Lluis, Martinez, Benjamin, " Interfacial strain: The driving force for selective orbital occupancy in manganite thin films", ADVANCED FUNCTIONAL MATERIALS Volume: 17 Issue: 18 Pages: 3918-3925 Published: DEC 17 2007
[709] C. Thiele, K. Dörr, O. Bilani, J. Rödel, and L. Schultz, Influence of strain on the magnetization and magnetoelectric effect in $La_{0.7}A_{0.3}MnO_3$/PMN-PT(001) (A=Sr,Ca), Phys. Rev. B 75, 054408 (2007)
[710] L. B. Steren, M. Sirena, and J. Guimpel, J. Appl. Phys. 87, 6755, (2000).

[711] X. W. Wu, M. S. Rzchowski, H. S. Wang, and Q. Li, Phys. Rev.B 61, 501 (2000).

[712] F. Tsui, M. C. Smoak, T. K. Nath, and C. B. Eom, Appl. Phys. Lett. 76, 2421 (2000).

[713] Y. Wu, Y. Suzuki, U. Ru¨diger, J. Yu, A. D. Kent, T. K. Nath, and C. B. Eom, Appl. Phys. Lett. 75, 2295 (1999!)

[714] H. W. Zandbergen, S. Freisem, T. Nojima, and J. Arts, Phys. Rev. B 60, 10 259 (1999).

[715] Ju H L, Krishnan K M and Lederman D 1998 J. Appl. Phys. 83 7073
[716] C. Kwon, M. C. Robson, K.-C. Kim, J. Y. Gu, S. E. Lofland, S. M. Bhagat, Z. Trajanovic, M. Rajeswari, T. Venkatesan, A. R. Kratz, R. D. Gomez, and R. Ramesh, J. Magn. Magn. Mater. 172, 229 (1997).

[717] Y. Suzuki, H. Y. Hwang, S.-W. Cheong, and R. B. van Dover, Appl. Phys. Lett. 71, 140 (1997).

[718] Amlan Biswas, M. Rajeswari, R. C. Srivastava, Y. H. Li, T. Venkatesan, and R. L. Greene, and A. J. Millis, Two-phase behavior in strained thin films of hole-doped manganites, Phys. Rev. B 61,9665 (2000).
[719] E.S. Vlakhova, K.A. Nenkova, T.I. Donchev, A.Y. Spasov, "Influence of misfit stress on the structure and magnetoresistive
properties of magnetron sputtered $La_{0.7}Sr_{0.3}MnO_3$ thin films on $LaAlO_3$(100) substrate", Vacuum 69 (2003) 255–259
[720] W. Zhang, X. Wang, M. Elliott, and I. Boyd, Stress effect and enhanced magnetoresistance in La0.67Ca0.33MnO32d filmsPhys. Rev. B 58, 14143 (1998).

[721] H. S. Wang,a) E. Wertz, Y. F. Hu, and Qi Li, D. G. Schlom, Role of strain in magnetotransport properties of Pr0.67Sr0.33MnO3 thin films, J. Appl. Phys., Vol. 87, 7409 (2000)

[722] A. J. Millis, T. Darling, and A. Migliori, Quantifying strain dependence in ‘‘colossal’’ magnetoresistance manganites J. Appl. Phys. 83, 1588, (1998).

[723] A. B. Shick, First-principles calculation of uniaxial magnetic anisotropy and magnetostriction in strained colossal magnetoresistance films Phys. Rev. B 60, 6254 (1999).

[724] D. P. Norton, Synthesis and properties of epitaxial electronic oxidethin-film materials, Mater. Sci. Eng. R. 43, 139 (2004).
[725] U. Ozgur, Ya. I. Alivov, C. Liu, A. Teke, M. A. Reshchikov, S.Dogan, V. Avrutin, S.-J. Cho, and H. Morkoc, A comprehensive review of ZnO materials and devices, J. Appl. Phys. 98, 041301 (2005).
[726] Z. Trajanovic, C. Kwon, M. C. Robson, K.C. Kim, M. Rajeswari, R. Ramesh, T. Venkatesan, S. E. Lofland, S. M. Bhagat, and D. Fork, Growth of colossal magnetoresistance thin films on silicon, Appl. Phys. Lett. 69, 1005 (1996)

727 E. S. Vlakhov, T. I. Donchev, A. Y. Spasov, K. Dörr, K. A. Nenkov, A. Handstein, S. Pignard and H. Vincent, Structural and magnetotransport properties of magnetron sputtered $La_{0.7}Sr_{0.3}MnO_3$ thin films Vacuum 69, 249 (2002)
[728] O.Yu. Gorbenko, I.E. Graboy, A.R. Kaul, H.W. Zandbergen" HREM and XRD characterization of epitaxial perovskite manganites J. Magn. Magn. Mater. 211 (2000) 97-104

[729] N. Okawa, H. Tanaka, R. Akiyama, T. Matsumoto and T. Kawai, Effects of film thickness on surface flatness and physical properties in $La_{12x}Sr_xMnO_3$ thin films investigated by scanning tunneling microscopy Solid State Communications 114, 601(2000)

[730] Yeh N C, Vasquez R P, Beam D A, Fu C C, Huynh J and Beach G 1997 J. Phys.: Condens. Matter 9 3713

[731] Ranno L, Llobet A, Hunt M B and Pierre J 1999 Appl. Surf. Sci. 138+139 228
[732] Trtik V, Sanchez F, Varela M, Bibes M, Martinez B and Fontcuberta J 1999 J. Magn. Magn. Mater. 203 256

[733] J. Gao and F.X. Hu, Rectifying behavior and magnetic tunability in heterojunctions composed of p-$La_{0.9}Ba_{0.1}MnO_3$/n-Si, Materials Science and Engineering: B Volume 144, Issues 1-3, 25 November 2007, Pages 100-103

[734] A. K. Pradhan,a_ J. B. Dadson, D. Hunter, K. Zhang, S. Mohanty, E. M. Jackson,

B. Lasley-Hunter, K. Lord, T. M. Williams, and R. R. Rakhimov, J. Zhang and D. J. Sellmyer, K. Inaba and T. Hasegawa, S. Mathews, B. Joseph, and B. R. Sekhar, U. N. Roy, Y. Cui, and A. Burger, Ferromagnetic properties of epitaxial manganite films on $SrTiO_3$ /Si heterostructures, J. Appl. Phys. 100, 033903 _2006_

735 J. Y. Gu, C. Kwon, M. C. Robson, Z. Trajanovic, K. Ghosh, R. P. Sharma, R. Shreekala, M. Rajeswari, T. Venkatesan, R. Ramesh, and T. W. Noh, Appl. Phys. Lett. 70, 1763 (1997).

[736] R. Ramesh, H. Gilchrist, T. Sands, V. G. Keramidas, R. Haakenaasen, and D. K. Fork, Appl. Phys. Lett. 63, 3592 (1993).

[737] J.Z. Sun, D.W. Abraham, R.A. Rao, and C.B. Eom, Appl. Phys.Lett. 74, 3017 ~1999!.

[738] R.A. Rao, D. Lavric, T.K. Nath, C.B. Eom, L. Wu, and F. Tsui, J. Appl. Phys. 85, 4794 ~1999!.

[739] J. Aarts, S. Freisem, R. Hendrikx, and H. Zandbergen, Disorder effects in epitaxial thin films of .La,Ca.MnO_3", Appl. Phys. Lett.
72, 2975 ~1998!.

740 M. Sahana, T. Walter, K. Dörr, K.-H. Müller, D. Eckert, and K. Brand, Magnetic properties of heteroepitaxial $La_{0.7}Sr_{0.3}MnO_3/SrTiO_3$ superlatticesJournal of Applied Physics 89, 6834 (2001)

741 K. Dörr, T. Walter, M. Sahana, K.-H. Müller, K. Nenkov, K. Brand, and L. Schultz, Magnetotransport of La0.7Sr0.3MnO3 ÕSrTiO3 multilayers with ultrathin manganite layersJournal of Applied Physics 89, 6973 (2001)

[742] H.S. Wang, Qi Li, Kai Liu, and C.L. Chien, Appl. Phys. Lett. 74,2212 (1999).

[743] Y. Z. Chen,1 J. R. Sun,1,a S. Liang,1 W. M. Lv,1 B. G. Shen,1 and W. B. Wu, Effect of anisotropic strain on the charge ordering transition in manganite Films, J. Appl. Phys. 103, 096105 (2008)

[744] G. Y. Gao, S. W. Jin, and W. B. Wu, Appl. Phys. Lett. 90, 012509 _2007_.

[745] Dai, Nguyen Van, Thuan, Nguyen Chi, Hong, Le Van, Phuc, Nguyen Xuan, Magnetoresistance effect in $La_{0.7}Sr_{0.3}MnO_3$ thin films fabricated by using pulsed laser deposition, JOURNAL OF THE KOREAN PHYSICAL SOCIETY Volume: 52 Issue: 5 Pages: 1452-1455 Published: MAY 2008

[746] I. C. Infante, F. Sánchez, and J. Fontcuberta, M. Wojcik and E. Jedryka, S. Estradé and F. Peiró, J. Arbiol, V. Laukhin, J. P. Espinós, Elastic and orbital effects on thickness-dependent properties of manganite thin films, PHYSICAL REVIEW B 76, 224415 (2007)

[747] Toshiyuki Taniuchi, Ryutaro Yasuhara, Hiroshi Kumigashira, Masato Kubota, Hiroyuki Okazaki, Takanori Wakita, Takanori Yokoya, Kanta Ono, Masaharu Oshima, Mikk Lippmaa, Masashi Kawasaki, and Hideomi Koinuma, "Thickness dependence of magnetic domain formation in $La_{0.6}Sr_{0.4}MnO_3$ epitaxial thin films studied by XMCD–PEEM Surface Science Volume 601, Issue 20, 15 October 2007, Pages 4690-4693

[748] Choudhary R J, Ogale S A, Shinde S R, Hullavarad S,Ogale S B, Bathe R N, Patil S I and Kumar R Evaluation of manganite films on silicon for uncooled bolometric applications 2004 Appl. Phys. Lett. 84 3846

[749] Lisauskas A, Khartsec S I and Grishin A Tailoring the colossal magnetoresistivity: $La_{0.7}(Pb_{0.63}Sr_{0.37})_{0.3}MnO_3$ thin-film uncooled bolometer 2000 Appl. Phys. Lett. 77 756-758

[750] Rajeswari M, Chen C, Goyal A, Kwon C, Robson M C, Ramesh R, Venkatesan T and Lakeou S Low-frequency optical response in epitaxial thin films of La0.67Ca0.33MnO3 exhibiting colossal magnetoresistance 1996 Appl. Phys. Lett. 68 3555

[751] Fu C C, Huang Z and Yeh N C Spin-polarized quasiparticle transport in cuprate superconductors 2002 Phys. Rev. B 65 224516-1 - 224516-14
[752] Chen Z Y, Biswas A, Zutic I, Wu T, Ogale S B, Greene R L and Venkatesan T 2001 Phys. Rev. B 63 212508

[753] Yeh N-C, Vasquez R P, Fu C C, Samoilov A V, Li Y and Vakili K 1999 Phys. Rev. B 60 10 522
[754] Dong Z W, Ramesh R, Venkatesan T, Johnson M, Chen Z, Pai S P, Shreekala R, Sharma R P, Lobb C J and Greene R L 1997 Appl. Phys. Lett. 71 1718

[755] Vas'ko V A, Larkin V A, Kraus P A, Nikolaev K R, Grupp D E, Nordman C A and Goldman A M 1997 Phys. Rev. Lett. 78 1134

756 Parkin SSP, Roche KP, Samant MG, et al. J Appl Phys 1999;85:5828.
757 M.G. Samant, S.S.P. Parkin, Magnetic tunnel junctions—principles and applications Vacuum 74 (2004) 705–709
758 P.K. Naji, M. Durlam, S. Tehrani, J. Calder, M.F. DeHerrera, A 256 kb 3.0 V 1T1MTJ nonvolatile magnetoresistive RAM, ISSCC Digest of Technical Papers (2001) 122–123.
759 M.-H. Jo, N. D. Mathur, J. E. Evetts, and M. G. Blamire, Coherent magnetic reversal in half-metallic manganite tunnel junctions, Appl. Phys. Lett. 77, 3803-3805 (2000).
[760] M.-H. Jo, N. D. Mathur, N. K. Todd, and M. G. Blamire, Very large magnetoresistance and coherent switching in half-metallic manganite tunnel junctions, Phys. Rev. B, 61, R14 905 - R14 908 (2000).
761 Z. Sefrioui, V. Cros, A. Barthelemy, V. Pena, C. Leon, J. Santamaria, M. Varela,and S. J. Pennycook, Tunnel magnetoresistance in $La_{0.7}Ca_{0.3}MnO_3/PrBa_2Cu_3O_7/La_{0.7}Ca_{0.3}MnO_3$ Appl. Phys. Lett. 88, 022512 (2006)
[762] M. Bowen, M. Bibes, A. Barthe lemy, J.-P. Contour, A. Anane, Y. Lemaıˆtre, and A. Fert, Nearly total spin polarization in La2/3Sr1/3MnO3 from tunneling experiments, Appl. Phys. Lett., Vol. 82, No. 2, 233-235 13 January 2003
763 L. Fratila, I. Mauria, C. Dubourdieu, and J. C. Villegier, Spin-polarized quasiparticles injection in $La_{0.7}Sr_{0.3}MnO_3$ /$SrTiO_3$/Nb heterostructure devices, App. Phys. Lett. 86, 122505 (2005)

[764] J. Salafranca, M. J. Calderón, and L. Brey, Phys. Rev. B 77, 014441 (2008).
765 Li X W, Lu Y, Gong G Q, Xiao G, Gupta A, Lecoeur P, Sun J, Wang Y Y and Dravid V P 1997 J. Appl. Phys.
81 5509
[766] S. Yunoki, E. Dagotto, S. Costamagna and J. A. Riera, Large magnetoresistance in a manganite spin tunnel junction using $LaMnO_3$as the insulating barrier, Phys. Rev. B, 78, 024405 (2008)
[767] J. Z. Sun, L. Krusin-Elbaum, P. R. Duncombe, A. Gupta, and R. B. Laibowitz, Temperature dependent, non-ohmic magnetoresistance in doped perovskite manganate trilayer junctions, Appl. Phys. Lett. 70 (13), 1769-1771 31 March 1997
[768] R. J. Soulen Jr., J. M. Byers,* M. S. Osofsky, B. Nadgorny, T. Ambrose, S. F. Cheng, P. R. Broussard, C. T. Tanaka, J. Nowak, J. S. Moodera, A. Barry, J. M. D. Coey, Measuring the Spin Polarization of a Metal with a uperconducting Point Contact, Science 282, 85-88 (1998).
[769] M. Viret, J. Nassar", M. Drouet", J.P. Contour", C. Fermon!, A. Fert, Spin polarised tunnelling as a probe of half metallic ferromagnetism in mixed-valence manganites, Journal of Magnetism and Magnetic Materials 198-199 (1999) 1-5
[770] V. Garcia, M. Bibes, A. Barthe´le´my, M. Bowen, E. Jacquet, J.-P. Contour, and A. Fert, Temperature dependence of the interfacial spin polarization of La2/3Sr1/3MnO3, PHYSICAL REVIEW B 69, 052403-1 – 052403-4 (2004).
[771] Yafeng Lu, Magnetotransport properties of manganite based magnetic tunnel junctions J. Appl. Phys. 102, 123906 _2007
[772] Jagadeesh S. Moodera, Elizabeth F. Gallagher, Keziah Robinson, and Janusz Nowak, Optimum tunnel barrier in ferromagnetic–insulator–ferromagnetic tunneling structures, Appl. Phys. Lett. 70 (22), 3050-3052 2 June 1997

[773] Hayakawa J, Ikeda S, Lee Y, Matsukura F and Ohno H 2006 Giant tunnel magnetoresistance and high annealing stability in CoFeB/MgO/CoFeB magnetic tunnel junctions with synthetic pinned layer, Appl. Phys. Lett. 89 232510
[774] Sakuraba Y, Hattori M, Oogane M, Ando Y, Kato H, Sakuma A, Miyazaki T and Kubota H 2006 Giant tunneling magnetoresistance in Co_2MnSi/Al–O/Co_2MnSi magnetic tunnel junctions, Appl. Phys.Lett. 88 192508
[775] M. Bibes, Ll. Balcells, S. Valencia, J. Fontcuberta, M. Wojcik, E. Jedryka, and S. Nadolski, Nanoscale Multiphase Separation at La2_3Ca1_3MnO3_SrTiO3 Interfaces Phys. Rev. Lett. 87, 067210 (2001)
[776] M. Bibes, S. Valencia, Ll. Balcells, B. Martı´nez, J. Fontcuberta, M. Wojcik, S. Nadolski, and E. Jedryka, Charge trapping in optimally doped epitaxial manganite thin films, Phys. Rev. B 66, 134416 (2002).
[777] J.-H. Park, E. Vescovo, H.-J. Kim, C. Kwon, R. Ramesh, and T. Venkatesan, Magnetic Properties at Surface Boundary of a Half-Metallic Ferromagnet $La_{0.7}Sr_{0.3}MnO_3$ Phys. Rev. Lett. 81, 1953 (1998)
[778] Calder´on M, Brey L and Guinea F, Surface electronic structure and magnetic properties of doped manganites 1999 Phys. Rev. B 60 6698
[779] M. Izumi, Y. Ogimoto, Y. Okimoto, T. Manako, P. Ahmet, K. Nakajima, T. Chikyow, M. Kawasaki, and Y. Tokura, Insulator-metal transition induced by interlayer coupling

in La0.6Sr0.4MnO3ÕSrTiO3 superlattices Phys. Rev. B 64, 064429 ~2001!.
780 I. E. Dzyaloshinskii, Sov. Phys. JETP 10, 628 (1960) Zh. Éksp. Teor. Fiz. 37, 881 _1959
781 D. N. Astrov, Sov. Phys. - JETP 11, 708 (1960). (J.Expt. Theoret. Phys. (USSR), 38 984 (1960) in Russian).
[782] V. J. Folen, G. T. Rado, and E. W. Stalder, "Anisotrophy of the magnetoelectric effect in Cr_2O_3", Phys. Rev. Lett. 6, 607-608 (1961).
[783] G. T. Rado and V. J. Folen, "Observation of the Magnetically Induced Magnetoelectric Effect and Evidence for Antiferromagnetic Domains", Phys. Rev. Lett. 7, 310-311 (1961).
[784] D. N. Astrov, Magnetoelectric effect in chromium oxide,Sov. Phys. JETP 13, 729–733 (1961) [Zh. Eksp. Teor. Fiz. 40, 1035–1041 (1961)]
[785] S.Foner and M. Hanabusa, Magnetoelectric effect in Cr_2O_3 and $(Cr_2O_3)_{0.8}\cdot(Al_2O_3)_{0.2}$, J. Appl. Phys. 34, 1246-1247 (1963).

[786] E. Ascher, H. Rieder, H. Schmid, and H. Stössel, "Some properties of ferromagnetic nickel-iodine boracite, $Ni_3B_7O_{13}$", J. Appl. Phys. 37, 1404 (1966).
[787] G.A. Smolenskii and I.E. Chupis, Sov. Phys. Usp. 25, 475 (1982).
[788] B. I. Al'shin and D. N. Astrov, Sov. Phys. JETP 17, 809 (1963).
[789] G. T. Rado, "Observation and Possible Mechanisms of Magnetoelectric Effects in a Ferromagnet", Phys. Rev. Lett 13, 335 (1964).
[790] R. P. Santoro, D. J. Segal, and R. E. Newnham, "Magnetic properties of $LiCoPO_4$ and $LiNiPO_4$", J. Phys. Chem. Solids 27, 1192 (1966).
[791] D. Vaknin, J. L. Zarestky, J. P Rivera, and H. Schmid, "Commensurate-Incommensurate Magnetic Phase Transition in Magnetoelectric Single Crystal $LiNiPO_4$", Phys. Rev. Lett. 92, 207201 (2004).

[792] T. H. O'Dell, "An induced magneto-electric effect in yttrium iron garnet", Phil. Mag. 16, 487 (1967).
[793] B. B. Krichevtsov, V. V. Pavlov, R. V. Pisarev, and A. G. Selitsky, "Linear magnetoelectric effect in magnetic garnet thin films", Ferroelectrics 161, 65 (1994).
[794] J. F. Scott, "Mechanisms of dielectric anomalies in $BaMnF_4$", Phys. Rev B 16, 2329-2331 (1977).
[795] G. A. Smolenskii, A. I. Agranovskaya, and V. A. Isupov, "Seignette-electrical properties of solid solutions in $PbNb_2O_6$-$BaNb_2O_6$-$SrNb_2O_6$ system", Sov. Phys. Solid State 1, 442 (1959).
[796] T. Watanabe and K. Kohn, "Magnetoelectric effect and low temperature transition of $PbFe_{0.5}Nb_{0.5}O_3$", Phase Trans. 15, 57 (1989).
[797] H. Tsujino and K. Kohn, "Magnetoelectric effect of $GdMn_2O_5$", Solid State Commun. 83, 639 (1992).
[798] B. Ponomarev, S. A. Ivanov, Yu F Popov, V. D. Negrii, and B. S. Redkin, "Magneto electric properties of some rare earth molydates", Ferroelectrics 161, 43 (1994).
[799] I. Kornev, M. Bichurin, J.-P. Rivera, S. Gentil, A. G. M. Jansen, H. Schmid, and P. Wyder, "Magnetoelectric properties of $LiCoPO_4$ and $LiNiPO_4$", Phys. Rev. B 62, 12247 (2000).

[800] M. Fiebig, Th. Lottermoser, D. Frohlich, A. V. Goltsev, and R. V. Pisarev, "Observation of coupled magnetic and electric domains", Nature 419, 818 (2002)
[801] A. Moreira dos Santos, S. Parashar, A. R. Raju, Y. S. Zhao, A. K. Cheetham, and C. N. R. Rao, "Evidence for the likely occurance of magnetoferroelectricity in the simple perovskite, $BiMnO_3$", Solid State Comm. 122, 49 (2002).
[802] T. Kimura, S. Kawamoto, I. Yamada, M. Azuma, M. Takano, and T. Yokura, "Magnetocapacitance effect in multiferroic $BiMnO_3$", Phys. Rev. B 67, 180401 (2003).
[803] Yu. F. Popov, A. M. Kadomtseva, S. S. Krotov, D. V. Belov, G. P. Vorob'ev, P. N. Makhov, and A. K. Zvezdin, "Features of the magnetoelectric properties of $BiFeO_3$ in high magnetic fields", Low. Temp. Phys. 27, 478 (2001).

[804] A.K. Zvezdin, A.M. Kadomtseva, S.S. Krotov, A.P. Pyatakov, Yu.F. Popov, G.P. Vorob'ev, "Magnetoelectric interaction and magnetic field control of electric polarization in multiferroics", J. Magnetism Magnetic Mater. 300, 224-228 (2006).

[805] N. Hur, S. Park, P. A. Sharma, J. S. Ahn, S. Guha, and S.-W. Cheong, "Electric polarization reversal in a multiferroic material induced by magnetic fields", Nature 429, 392 (2004).
[806] T. Kimura, G. Lawes, and A. P. Ramirez, "Electric Polarization Rotation in a Hexaferrite with Long-Wavelength Magnetic Structures", Phys. Rev. Lett. 94, 137201 (2005).
[807] J. Hemberger, P. Lunkenheimer, R. Fichtl, H.–A. Krug von Nidda, V. Tsurkan, and A. Loidl, "Relaxor ferroelectricity and colossal magnetocapacitive coupling in ferromagnetic $CdCr_2S_4$", Nature 434, 364 (2005).
[808] J. P. Rivera, "The linear magnetoelectric effect in $LiCoPO_4$ revisited", Ferroelectrics 161, 147 (1994).
[809] B. B. Krichevtsov, V. V. Pavlov, and R. V. Pisarev, "Giant linear magnetoelectric effect in garnet ferrite films", JETP Lett. 49, 535 (1989).
[810] G. T. Rado, J. M. Ferrari, and W. G. Maisch, "Magnetoelectric susceptibility and magnetic symmetry of magnetoelectrically annealed $TbPO_4$", Phys. Rev. B 29, 4041 (1984).
[811] Smolensky G. A., Isupov V. A., Krainik N. N., Agranovskaya A. I. Izvestia Akad. Nauk SSSR Ser. Fiz.–Mat. Nauk 25, 1333 (1961) (In Russian)
[812] E. Wendling, R. von Hodenberg, and R. Kuhn, "Congolit, der trigonale Eisenboracit. Kali und Steinsalz", (in German). Vol. 6, pp. 1–3 (1972) Amer. Mineral., 57, 1315 (abs. ref. 1). ??????

[813] P.C. Burns and M.A. Carpenter "Phase transitions in the series boracite – trembathite – congolite: phase relations", Can. Mineral., 34, 881–892, (1996).

[814] R.M. Honea, and F.R. Beck "Chambersite, a new mineral", Amer. Mineral., Vol. 47, pp. 665–671(1962).685*?

815 G.A. Smolenskii and I.E. Chupis, Ferroelectric magnetic materials, Usp. Fiz. Nauk 137, 415-448 (1982) (in Russian).

[816] A. Munoz, J. A. Alonso, M. J. Martınez-Lope, M. T. Casais, and J. L. Martınez, M. T. Fernandez-Dıaz, Magnetic structure of hexagonal RMnO3 (R=Y, Sc), Thermal evolution from neutron powder diffraction data, Phys. Rev. B, 62, 9498 (2000).

[817] Z. J. Huang, Y. Cao, Y. Y. Sun, Y. Y. Xue, and C. W. Chu, Coupling between the ferroelectric and antiferromagnetic orders in YMnO3, Phys. Rev. B 56, 2623 (1997).

[818] Th. Lonkai, D.G. Tomuta, U. Amann, J. Ihringer, R.W.A.Hendrikx, D.M. To¨ bbens, J.A. Mydosh, Development of the high-temperature phase of hexagonal manganites, Phys. Rev. B 69 (2004) 134108 and references therein.

[819] T. Kimura, S. Ishihara, H. Shintani, T. Arima, K. T. Takahashi, K.Ishizaka, and Y. Tokura, Distorted perovskite with eg 1 configuration as a frustrated spin system Phys. Rev. B 68, 060403(R) (2003).

[820] O.P.Vajk, M.Kanzelmann, J.W.Lynn, S.B.Kim, and S.-W. Cheong, Neutron-scattering studies of magnetism in multiferroic HoMnO3 (invited) J. Appl. Phys. 99, 08E301 (2006).

[821] L. J. Wang, S. M. Feng, J. L. Zhu, R. C. Yu, and C. Q. Jin, W. Yu, X. H. Wang and L. T. Li, Ferroelectricity of multiferroic hexagonal TmMnO3 ceramics synthesized under high pressure, Appl. Phys. Lett. 91, 172502 (2007).

[822] M. Kenzelmann, A. B. Harris, S. Jonas, C. Broholm, J. Schefer, S. B. Kim, C. L. Zhang, S.-W. Cheong, O. P. Vajk, and J.W. Lynn, Magnetic Inversion Symmetry Breaking and Ferroelectricity in TbMnO3, Phys. Rev. Lett. 95, 087206 (2005).

[823] T. Goto, T. Kimura, G. Lawes, A. P. Ramirez, and Y. Tokura, Ferroelectricity and Giant Magnetocapacitance in Perovskite Rare-Earth Manganites, Phys. Rev. Lett. 92, 257201-1 – 257201-4 (2004).

[824] Tadahiro Yokosawa, Alexei A. Belik, Toru Asaka, Koji Kimoto, Eiji Takayama-Muromachi, and Yoshio Matsui, Crystal symmetry of BiMnO3: Electron diffraction study, Phys. Rev. B 77, 024111 (2008).

[825] Shishidou, T.; Mikamo, N.; Uratani, Y.; Ishii, F.; Oguchi, T. J. Phys.:Condens. Matter 2004, 16, S5677-S5683.

[826] S. V. Kiselev, R. P. Ozerov, and G. S. Zhdanov, Sov. Phys. Dokl.7, 742 (1963).

[827] C. Michel, J.-M. Moreau, G. D. Achenbach, R. Gerson, and W. J. James, Solid State Commun. 7, 701 _1969_

[828] Teague JR, Gerson R, James WJ. Dielectric hysteresis in single crystal BiFeO3. Solid State Commun, 8, 1073–4 (1970).

[829] Alexei A. Belik, Satoshi Iikubo, Katsuaki Kodama, Naoki Igawa, Shinichi Shamoto,

and Eiji Takayama-Muromachi, Neutron Powder Diffraction Study on the Crystal and Magnetic Structures of $BiCrO_3$ Chem. Mater., 20, 3765–3769 (2008).

[830] Dae Ho Kim, Ho Nyung Lee, Maria Varela, and Hans M. Christen, Antiferroelectricity in multiferroic BiCrO3 epitaxial films, Appl. Phys. Lett. 89, 162904 (2006).

[831] T. Kimura, Y. Kamada, Y. Noda, S. Wakimoto, K. Kaneko, N. Metoki, K. Kakurai, and K. Kohn, Field-Indu7ced Dielectric and Magnetic Phase Transitions in multiferroic compounds of RMn2O5 (R=Er, Ho), J. Korean Phys. Soc., 51, 870 (2007).

[832] J. A. Alonso, M. T. Casais, M. J. Martínez-Lope, and I. Rasines, High Oxygen Pressure Preparation, Structural Refinement, and Thermal Behavior of RMn2O5 (R=La, Pr, Nd, Sm, Eu), J. Solid State Chem. 129, 105-112 (1997).

[833] T. Kimura, S. Kobayashi, S. Wakimoto, Y. Noda, and K. Kohn, Magnetically induced ferroelectricity in multiferroic compounds of RMn2O5, Ferroelectrics, 354, 77 (2007).

[834] Hur N, Park S, Sharma P A, Guha S and Cheong S W P,Colossal Magnetodielectric Effects in DyMn2O5, Phys. Rev. Lett. 93, 107207 (2004).

[835] Munoz, J. A. Alonso, M. T. Casais, M. J. Martınez-Lope, J. L. Martınez, and M. T. Fernandez-Dıaz, Magnetic structure and properties of BiMn2O5 oxide: A neutron diffraction study, Phys. Rev. B, 65, 144423 (2002).

[836] W. von Wartburg, The magnetic structure of magnetoelectric nickel-iodine boracite $Ni_3B_7O_{13}I$, Phys. Stat. Solidi (a)-Applied Research, 21, 557-568 (1974).

[837] K. Knizek, P. Novák, and M. Küpferling, Electronic structure and conductivity of ferroelectric hexaferrite: Ab initio calculationsPhys. Rev. B 73, 153103 (2006).

[838] P. Baettig and N. A. Spaldin, Ab initio prediction of a multiferroic with large polarization and magnetization, Appl. Phys. Lett. 86, 012505 _2005_.

[839] P. Baettig, C. Ederer, and N. A. Spaldin, First principles study of the multiferroics BiFeO3, Bi2FeCrO6, and BiCrO3: Structure, polarization, and magnetic ordering temperature, Phys. Rev. B 72, 214105 _2005_.

[840] S. Kamba, D. Nuzhnyy, R. Nechache, K. Závěta, D. Nižňanský, E. Šantavá, C. Harnagea, and A. Pignolet, Infrared and magnetic characterization of multiferroic Bi2FeCrO6 thin films over a broad temperature range, Phys. Rev. B 77, 104111 (2008)._

[841] T. Kimura, T. Goto, H. Shintani, K. Ishizaka, T. Arima, and Y. Tokura Nature 426, 55 (2003).

842 Nicola A. Hill and Alessio Filippetti , Journal of Magnetism and Magnetic Materials,

242, 976 (2002)
843 Alessio Filippetti and Nicola A. Hill, Coexistence of magnetism and ferroelectricity in perovskites. Phys. Rev. B 65, 195120 (2002)
[844] Hill NA. Density functional studies of multiferroic magnetoelectrics.
Annu Rev Mater Res 2002;32:1–37.
[845] C. Ederer, N.A. Spaldin, Recent progress in first-principles studies of magnetoelectric Multiferroics, Current Opinion in Solid State and Materials Science 9 (2005) 128–139
[846] Bas B. Van Aken, T. T. M. Palstra, A. Filippetti, and N. A. Spaldin, The origin of ferroelectricity in magnetoelectric $YMnO_3$, Nat. Mater. 3, 164 _2004_.
[847] T. Katsufuji, M. Masaki, A. Machida, M. Moritomo, K. Kato, E. Nishibori, M. Takata, M. Sakata, K. Ohoyama, K. Kitazawa, and H. Takagi, Crystal structure and magnetic properties of hexagonal $RMnO_3$ (R=Y, Lu, and Sc) and the effect of doping, Phys. Rev. B 66, 134434 (2002)
[848] Seshadri R, Hill NA. Visualizing the role of Bi 6s ‘‘lone pairs’’ in the
off-center distortion in ferromagnetic BiMnO3. Chem Mater 2001;13:
2892–9.
[849] Neaton JB, Ederer C, Waghmare UV, Spaldin NA, Rabe KM. Firstprinciples
study of spontaneous polarization in multiferroic BiFeO3.
Phys Rev B 2005;71:014113.
[850] Kubel, F., and Schmid, H., STRUCTURE OF A FERROELECTRIC AND FERROELASTIC MONODOMAIN CRYSTAL OF THE PEROVSKITE BIFEO3 Acta Crystallogr., Sect. B: Struct. Sci. (1990) B46, 698
[851] Neaton, J. B., Ederer, C., Waghmare, U. V., Spaldin, N. A. & Rabe, K. M. First-principles study of spontaneous polarization in multiferroic BiFeO3. Phys. Rev. B 71, 014113 (2005).
[852] I. Sosnowska, W. Schäfer, W. Kockelmann, K. H. Andersen, and I. O. Troyanchuk, Crystal structure and spiral magnetic ordering of $BiFeO_3$ doped with manganese Appl. Phys. A: Mater. Sci. Process. 74, S1040 (2002).
[853] SOSNOWSKA I, PETERLINNEUMAIER T, STEICHELE E, SPIRAL MAGNETIC-ORDERING IN BISMUTH FERRITE, JOURNAL OF PHYSICS C-SOLID STATE PHYSICS Volume: 15 Issue: 23 Pages: 4835-4846 Published: ~1982
[854] Y. P. Wang, L. Zhou, M. F. Zhang, X. Y. Chen, J. M. Liu, and Z. G. Liu, Room-temperature saturated ferroelectric polarization in $BiFeO_3$ ceramics synthesized by rapid liquid phase sinteringAppl. Phys. Lett. 84, 1731 (2004).
[855] V. R. Palkar and R. Pinto, Pramana, J. Phys. 58, 1003 (2002).
[856] V. R. Palkar, J. John, and R. Pinto, Observation of saturated polarization and dielectric anomaly in magnetoelectric BiFeO3 thin filmsAppl. Phys. Lett. 80, 1628 ~2002!.

[857] W. M. Zhu and Z.-G. Ye, Ceram. Int. 30, 1435 _2004_.
[858] M. Mahesh Kumar!, S. Srinath", G.S. Kumar!, S.V. Suryanarayana, Spontaneous magnetic moment in BiFeO3 -BaTiO3 solid solutions at low temperatures, Journal of Magnetism and Magnetic Materials 188 (1998) 203-212
[859] J. S. Kim, C. I. Cheon, C. H. Lee, and P. W. Jang, Weak ferromagnetism in the ferroelectric BiFeO3-ReFeO3-BaTiO3 solid solutions (Re=Dy,La)J. Appl. Phys. 96, 468 _2004_.

[860] N. Wang, J. Cheng, A. Pyatakov, A. K. Zvezdin, J. F. Li, L. E. Cross, and D. Viehland,
Multiferroic properties of modified BiFeO3-PbTiO3-based ceramics: Random-field induced release of latent magnetization and polarization
Phys. Rev. B 72, 104434 _2005_.

[861] Hanjong Paik,a_ Hosung Hwang, and Kwangsoo No, Seunghwa Kwon and David P. Cann, Room temperature multiferroic properties of single-phase „Bi0.9La0.1…FeO3–Ba„Fe0.5Nb0.5…O3 solid solution ceramics, Appl. Phys. Lett. 90, 042908 _2007).
[862] 13B. Ruette, S. Zvyagin, A. P. Pyatakov, A. A. Bush, J. F. Li, V. I. Belotelov, A. K. Zvezdin, and D. Viehland, Magnetic-field-induced phase transition in BiFeO3 observed by high-field electron spin resonance: Cycloidal to homogeneous spin orderPhys. Rev. B 69, 064114 _2004_.

[863] J. Wang, J. B. Neaton, H. Zheng, V. Nagarajan, S. B. Ogale, B. Liu, D. Viehland, V. Vaithyanathan, D. G. Schlom, U. V. Waghmare, N. A. Spaldin, K. M. Rabe, M. Wuttig, and R. Ramesh, Epitaxial $BiFeO_3$ Multiferroic Thin Film Heterostructures, Science 299, 1719 (2003).

[864] F. Bai, J. Wang, M. Wuttig, J. Li, N. Wang, A. P. Pyatakov, A. K. Zvezdin, L. E. Cross, and D. Viehland, Destruction of spin cycloid in (111)c-oriented BiFeO3 thin fi lms by epitaxial constraint: enhanced polarization and release of latent magnetization. Appl. Phys. Lett. 86, 032511 (2005).
865 K. Y. Yun, M. Noda, and M. Okuyama, Prominent ferroelectricity of BiFeO3 thin films prepared by pulsed-laser deposition Appl. Phys. Lett. 83, 3981 (2003).
866 K. Y. Yun, D. Ricinschi, T. Kanashima, M. Noda, and M. Okuyama, Giant ferroelectric polarization beyond 150 mu C/cm(2) in BiFeO3 thin film Jpn. J. Appl. Phys., Part 2 43, L647 (2004).
[867] Kwi Young Yun, Minoru Noda, Masanori Okuyama, Hiromasa Saeki, Hitoshi Tabata, and Keisuke Saito, Structural and multiferroic properties of BiFeO3 thin films at room Temperature, J. Appl. Phys., 96, 3399 2004
[868] Kwi Young Yun,a_ Dan Ricinschi, Takeshi Kanashima, and Masanori Okuyama, Enhancement of electrical properties in polycrystalline BiFeO3 thin films, Appl. Phys. Lett. 89, 192902 _2006_
[869] Ricinschi D, Yun KY, Okuyama M, First-principles study of BiFeO3 films with giant polarization and its dependence on structural parameters, FERROELECTRICS Volume: 335 Pages: 181-190 Published: ~2006
[870] Jiefang Li, Junling Wang, M. Wuttig, R. Ramesh, Naigang Wang, B. Ruette, A. P. Pyatakov, A. K. Zvezdin, and D. Viehland, Dramatically enhanced polarization in .001., .101., and .111. BiFeO3 thin
films due to epitiaxial-induced transitionsAppl. Phys. Lett. 84, 5261 (2004)

[871] W. Eerenstein, F. D. Morrison, J. Dho, M. G. Blamire, J. F. Scott, and N. D. Mathur Comment on "Epitaxial BiFeO3 Multiferroic Thin Film Heterostructures (2005) Science 307, 1203a

[872] J. Wang, A. Scholl, H. Zheng, S. B. Ogale, D. Viehland, D. G. Schlom, N. A. Spaldin, K. M. Rabe, M. Wuttig, L. Mohaddes, J. Neaton, U. Waghmare, T. Zhao, and R. Ramesh, Response to Comment on "Epitaxial BiFeO3 Multiferroic Thin Film Heterostructures. (2005) Science 307, 1203b

873K. Y. Yun, D. Ricinschi, T. Kanashima, M. Noda, and M. Okuyama, Giant ferroelectric polarization beyond 150 mu C/cm(2) in BiFeO3 thin film Jpn. J. Appl. Phys., Part 2 43, L647 (2004).
874 S. Y. Yang, F. Zavaliche, L. M. Ardabili, V. Vaithyanathan, D. G. Schlom, Y. J. Lee, Y. H. Chu, M. P. Cruz, Q. Zhan, T. Zhao, and R. Ramesh, Appl. Phys. Lett. 87, 102903 (2005).
875 R. Ueno, S. Okaura, H. Funakubo, and K. Saito, Jpn. J. Appl. Phys., Part 2 44, L1231 (2005).
876 S. K. Singh and H. Ishiwara, Jpn. J. Appl. Phys., Part 2 44, L734 (2005).
[877] Chin-Feng Chung, Jen-Po Lin, and Jenn-Ming Wu, Influence of Mn and Nb dopants on electric properties of chemical-solution-deposited BiFeO3 filmsAppl. Phys. Lett. 88, 242909 (2006)

[878] Chia-Ching Lee and Jenn-Ming Wu, Applied Surface Science 253, 7069 (2007)
[879] C. Ternon, J. Thery, T. Baron, C. Ducros, F. Sanchette, J. Kreisel, Thin Solid Films 515 pp. 481–484 (2006)
[880] Jong Kuk Kim, Sang Su Kim, and Won-Jeong Kim, Materials Letters 59, 4006 (2005)

[881] Seung Wha Lee and Chul Sung Kim, Journal of Magnetism and Magnetic Materials 304, 772 (2006)

[882] R. D. King-Smith and D. Vanderbilt, Phys. Rev. B 47, 1651 s1993d.

[883] D. Vanderbilt and R. D. King-Smith, Phys. Rev. B 48, 4442 s1994d
[884] R. Resta, Rev. Mod. Phys. 66, 899 s1994d

[885] S. Fujino, M. Murakami, S.-H. Lim, M. Wuttig, L.G. Salamanca-Riba and I. Takeuchi, Ferroelectric properties of multiphase Bi–Fe–O thin films Solid State Ionics 178, 1257-1261 (2007)

886 X. Qi, J. Dho, R. Tomov, M. G. Blamire, and J. L. MacManus-Driscoll, Greatly reduced leakage current and conduction mechanism
in aliovalent-ion-doped BiFeO3, Appl. Phys. Lett. 86, 062903 (2005).

887 Youn-Ki Jun, Won-Taek Moon, Chae-Myung Chang, Hyun-Su Kim, Hyun Sam Ryu, Jae Wook Kim, Kee Hoon Kim and Seong-Hyeon Hong, Solid State Communications, 135, 133 (2005)
888 S. K. Singh and H. Ishiwara, Room temperature ferroelectric properties of Mn-substituted BiFeO3 thin
films deposited on Pt electrodes using chemical solution depositionAppl. Phys. Lett. 88, 262908 (2006)
889 Jong Kuk Kim, Sang Su Kim, and Won-Jeong Kim, Amar S. Bhalla and Ruyan Guo, Appl. Phys. Lett. 88, 132901 (2006)
[890] D. H. Wang, W. C. Goh, M. Ning, and C. K. Effect of Ba doping on magnetic, ferroelectric, and magnetoelectric properties in mutiferroic BiFeO3 at room temperatureO, Appl. Phys. Lett. 88, 212907 (2006)

[891] A. Scholl, J. Stohr, J. Luning, J.W. Seo, J. Fompeyrine, H. Siegwart, J.P. Locquet, F. Nolting, S. Anders, E.E. Fullerton, M.R. Scheinfein and H.A. Padmore. Observation of antiferromagnetic domains in epitaxial thin films Science 287 (2000), p. 1014
[892] Zalesskii AV, Frolov AA, Khimich TA, Bush AA, Composition-induced transition of spin-modulated structure into a uniform antiferromagnetic state in a Bi1-xLaxFeO3 system studied using Fe-57 NMR, PHYSICS OF THE SOLID STATE Volume: 45 Issue: 1 Pages: 141-145 Published: ~2003
[893] Yi-Hsien Lee, Jenn-Ming Wu, and Chih-Huang Lai, Influence of La doping in multiferroic properties of BiFeO3 thin films, Appl. Phys. Lett. 88, 042903 (2006)
[894] Dongeun Lee, Min G. Kim, Sangwoo Ryu, and Hyun M. Jang, Epitaxially grown La-modified $BiFeO_3$ magnetoferroelectric thin films, Appl. Phys. Lett. 86, 222903 (2005).
[895] Shan-Tao Zhang, Yi Zhang, Ming-Hui Lu, Chao-Ling Du, Yan-Feng Chen, Zhi-Guo Liu, Yong-Yuan Zhu, and Nai-Ben Ming, Substitution-induced phase transition and enhanced multiferroic properties of $Bi_{1-x}La_xFeO_3$ ceramics, Appl. Phys. Lett. 88, 162901 (2006)
[896] Hiroshi Uchida, Risako Ueno, Hiroshi Funakubo, and Seiichiro Koda, J. Appl. Phys. 100, 014106 (2006)
897 V.A. Bokov, I.E. Myl'nikova, S.A. Kizhaev, M.F. Bryzhina, and
N.A. Grigoryan, Fiz. Tverd. Tela ~Leningrad! 7, 2993 ~1966!
@Sov. Phys. Solid State 7, 2993 ~1966!#.
898 F. Sugawara, S. Ihda, Y. Syono and S. Akimoto J. Phys. Soc. Jpn 25 (1968), p. 1553
899 E. Ohshima, Y. Saya, M. Nantoh and M. Kawai Solid State Commun. 116 (2000), p. 73.
900 A. M. dos Santos, A. K. Cheetham,T. Atou, Y. Syono, Y. Yamaguchi, K. Ohoyama, H. Chiba and C. N. R. Rao, Orbital ordering as the determinant for ferromagnetism in biferroic BiMnO3 Phys. Rev. B, 2002, 66, 064425.
[901] T. Kimura, S. Kawamoto, I. Yamada, M. Azuma, M. Takano, and Y. Tokura, Magnetocapacitance effect in multiferroic BiMnO3, Phys. Rev. B 67, 180401 (2003)

[902] T. Kimura, S. Kawamoto, I. Yamada, M. Azuma, M. Takano, and Y. Tokura, Magnetocapacitance effect in multiferroic BiMnO3Phys. Rev. B 67, 180401 (2003)

903 T. Atou, H. Chiba, K. Ohoyama, Y. Yamaguchi, and Y. Syono, J. Solid State Chem. 145, 639 (1999).
[904] Belik AA, Iikubo S, Yokosawa T, Kodama K, Igawa N, Shamoto S, Azuma M, Takano M, Kimoto K, Matsui Y, Takayama-Muromachi E Origin of the monoclinic-to-monoclinic phase transition and evidence for the centrosymmetric crystal structure of BiMnO3 (2007) J Am Chem Soc 129:971
[905] H. Yang Æ Z. H. Chi Æ J. L. Jiang Æ W. J. Feng Æ J. F. Dai Æ C. Q. Jin Æ R. C. Yu, Is ferroelectricity in BiMnO3 induced by superlattice? J Mater Sci (2008) 43:3604–3607

[906] P. Baettig, R. Seshadri, and N. A. Spaldin, Anti-Polarity in Ideal BiMnO3J. Am. Chem. Soc.
129, 9854 _2007_.
[907] E. Montanari, G. Calestani, L. Righi, E. Gilioli, F. Bolzoni, K. S. Knight, and P. G. Radaelli, Structural anomalies at the magnetic transition in centrosymmetric BiMnO3Phys. Rev. B 75, 220101(R)_ _2007_.
[908] C. N. R. Rao and C.R. Serrao, New routes to multiferroics, J. Mater. Chem., 2007, 17, 4931–4938
[909] Chan-Ho Yang, Sung-Ho Lee, Tae Yeong Koo, and Yoon Hee Jeon, Dynamically enhanced magnetodielectric effect and magnetic-field-controlled electric relaxations in La-doped BiMnO3 Phys.Rev. B 75, 140104(R) (2007)
[910] N. A. Hill, P. Battig, and C. Daul, First Principles Search for Multiferroism in BiCrO3 , J. Phys. Chem. B 106, 3383-3388 (2002).
[911] S. Niitaka, M. Azuma, M. Takano, E. Nishibori, M. Takata and M. Sakata, Crystal structure and dielectric and magnetic properties of BiCrO3
as a ferroelectromagnet
Solid State Ionics, 2004, 172, 557.
[912] Belik, A. A.; Tsujii, N.; Suzuki, H.; Takayama-Muromachi, E. Inorg. Chem. 2007, 46, 8746.
[913] F. Sugawara, S. Iiida, Y. Syono, and S. Akimoto, J. Phys. Soc. Jpn. 25, 1553 (1968)
[914]M. R. Suchomel, C. I. Thomas, M. Allix, M. J. Rosseinsky, A. M. Fogg, and M. F. Thomas, “High pressure bulk synthesis and characterization of the predicted multiferroic Bi(Fe1/2Cr1/2)O3,” Appl. Phys. Lett. 90, 112909 _2007_.

[915] Dae Ho Kima_ and Ho Nyung Lee, Michael D. Biegalski, and Hans M. Christen, Large ferroelectric polarization in antiferromagnetic BiFe0.5Cr0.5O3 epitaxial films, Appl. Phys. Lett. 91, 042906 _2007_

[916] R. Nechache, C. Harnagea, L.-P. Carignan, D. Ménard, and A. Pignolet, Philos. Mag. Lett. 87, 231 _2007
[917] R. Nechache, C. Harnagea, A. Pignolet, F. Normandin, T. Veres, L.-P. Carignan, and D. M´enard, “Growth, structure, and properties of epitaxial thin films of first-principle predicted multiferroic

Bi2FeCrO6," Appl. Phys. Lett., vol. 89, art. no. 102902, 2006.
[918] R. Nechache, L.-P. Carignan, L. Gunawan, C. Harnagea, G. A. Botton, D. M´enard, and A. Pignolet, "Epitaxial thin films of multiferroic Bi2FeCrO6 with B-site cationic order," J. Mater. Res., vol. 22, pp. 2102–2110, 2007.
[919] Riad Nechache, Catalin Harnagea, Lina Gunawan, Louis-Philipe Carignan, Christian Maunders, David M´enard, Gianluigi A. Botton, and Alain Pignolet, Growth, Structure, and Properties of BiFeO3-BiCrO3 Films Obtained by Dual Cross Beam PLD, ieee transactions on ultrasonics, ferroelectrics, and frequency control, vol. 54, no. 12, december 2007
[920] H. L. Yakel, W. D. Koehler, E. F. Bertaut, and F. Forrat, Acta Crystallogr. 16, 957 _1963_.
[921] 3W. C. Koehler, H. L. Yakel, E. O. Wollan, and J. W. Cable, Phys. Lett. 9, 93 ~1964!;
[922] R. Pauthenet and C. Veyret, J. Phys. ~France! 31, 65 ~1970!;
[923] V. E. Wood, A. E. Austin, E. W. Collings, and K. C. Brog, J. Phys. Chem. Solids 34, 857 ~1973!.

[924] Makoto Tachibana,1 Tomotaka Shimoyama,2 Hitoshi Kawaji,2 Tooru Atake,2 and Eiji Takayama-Muromachi, Jahn-Teller distortion and magnetic transitions in perovskite $RMnO_3$ (R=Ho, Er, Tm, Yb, and Lu), PHYSICAL REVIEW B 75, 144425 (2007)

[925] M. Fiebiga, Th. Lottermosera, Th. Lonkaib, A.V. Goltsevc, R.V. Pisarev, Magnetoelectric effects in multiferroic manganites, Journal of Magnetism and Magnetic Materials 290–291 (2005) 883–890, and references therein

[926] T. Lottermoser, T. Lonkai, U. Amann, D. Hohlwein, J. Ihringer, and M. Fiebig, Magnetic phase control by an electric field Nature _London_ 430, 541 _2004_.
[927] M. Fiebig, Th. Lottermoser, R.V. Pisarev, Spin-rotation phenomena and magnetic phase diagrams of hexagonal RMnO3, J. Appl. Phys. 93 (2003) 8194
[928] J.-H. Lee, P. Murugavel, D. Lee, T. W. Noh, Y. Jo and M.-H. Jung, K. H. Jang, and J.-G. Park, Multiferroic properties of epitaxially stabilized hexagonal DyMnO3 thin films, Appl. Phys. Lett. 90, 012903 (2007)

[929] J.-S. Zhou,1 J. B. Goodenough,1 J. M. Gallardo-Amores,2 E. Morán,2 M. A. Alario-Franco,2 and R. Caudillo, Hexagonal versus perovskite phase of manganite RMnO3 (R=Y, Ho, Er, Tm, Yb, Lu), PHYSICAL REVIEW B 74, 014422 _2006_

[930] J. A. Alonso, M. J. Martínez-Lope, and M. T. Casais, M. T. Fernández-Díaz, Evolution of the Jahn-Teller Distortion of MnO_6 Octahedra in $RMnO_3$ Perovskites (R = Pr, Nd, Dy, Tb, Ho, Er, Y): A Neutron Diffraction Study, Inorg. Chem., 39 (5), 917 -923, 2000.
[931] A. A. Bosak, A. A. Kamenev, I. E. Graboy, S. V. Antonov, O. Y. Gorbenko, A. R. Kaul, C. Dubourdieu, J. P. Senateur, V. L. Svechnkikov, H. W. Zandbergen, and B. Holländer, Thin Solid Films 400, 149 (2001)

[932] Brinks, H.W., FjellvaÊ g, H. & Kjekshus, A. (1997). J. Solid State Chem. 129, 334.
[933] Waintal, A. & Chevanas, J. (1967). Mater. Res. Bull. 2, 819.
[934] J.-S. Zhou and J. B. Goodenough, Phys. Rev. Lett. 96, 247202 (2006).
[935] J.-H. Lee, P. Murugavel, D. Lee, T. W. Noh, Y. Jo and M.-H. Jung, K. H. Jang, and J.-G. Park, Multiferroic properties of epitaxially stabilized hexagonal DyMnO3 thin filmsAppl. Phys. Lett. 90, 012903 (2007)

[936] K. R. Balasubramanian, A. A. Bagal, O. Castillo, A. J. Francis, and P. A. Salvador, Ceram. Trans. 162, 59 (2004)
[937] D. Lee, J. H. Lee, P. Murugavel, S. Y. Jang, T. W. Noh, Y. Jo, M. H. Jung, Y. D. Ko, and J. S. Chung, Epitaxial stabilization of artificial hexagonal $GdMnO_3$ thin films and their magnetic properties Appl. Phys. Lett. 90, 182504 (2007)
[938] A. A. Bosak, C. Dubourdieu, J. P. Senateur, O. Y. Gorbenko, and A. R. Kaul, J. Mater. Chem. 12, 800 (2002)
[939] K. R. Balasubramaniam, S. Havelia, P. A. Salvador, H. Zheng and J. F. Mitchell, Appl. Phys. Lett. 91, 232901 (2007)
[940] Graboy I E, Bosak A A, Gorbenko OY, Kaul A R, Dubourdieu C, Senateur J P, Svetchnikov VL, Zandbergen HW, HREM study of epitaxially stabilized hexagonal rare earth manganites, CHEMISTRY OF MATERIALS Volume: 15 Issue: 13 Pages: 2632-2637 Published: JUL 1 2003
[941] Seongsu Leea, Misun Kanga, Changhee Leeb, A. Hoshikawac, M. Yonemurac, T. Kamiyamac, J.-G. Park, Multiferroic behavior and two-dimensional magnetism of hexagonal manganites, Physica B 385–386 (2006) 405–407
[942] B. B. van Aken, A. Meetsma, and T. T. M. Palstra, Hexagonal YMnO3 Acta Crystallogr., Sect. C: Cryst. Struct. Commun. 57, 230 (2001).

[943] Salvador, P. A., Doan, T.-D., Mercey, B. & Raveau, B. (1998). Chem. Mater. 10, 2595.
[944] Marti X , Skumryev V, Laukhin V, Sanchez F, Garcia-Cuenca MV, Ferrater C, Varela M, Fontcuberta J, Dielectric anomaly and magnetic response of epitaxial orthorhombic $YMnO_3$ thin films, J. Mater. Res., 22, 2096-2101 (2007).

[945] X. Martí, F. Sánchez, and J. Fontcuberta, M. V. García-Cuenca, C. Ferrater, and M. Varela Exchange bias between magnetoelectric $YMnO_3$ and ferromagnetic $SrRuO_3$ epitaxial films, J. Appl. Phys. 99, 08P302 (2006).
[946] S.L. Samal[a], W. Green[b], S.E. Lofland[c], K.V. Ramanujachary[b], D. Das[d] and A.K. Ganguli, Study on the solid solution of $YMn_{1-x}Fe_xO_3$: Structural, magnetic and dielectric properties, Journal of Solid State Chemistry
Volume 181, Issue 1, January 2008, Pages 61-66

[947] A. Veres, J.G. Noudem, S. Fourrez and G. Bailleul, The influence of iron substitution to manganese on the physical properties of $YMnO_3$Solid State Sci. 8 (2006), pp. 137–141

[948] Mori, S., Tokunaga, J., Horibe, Y., Asada, T., Koyama, Y., Katsufuji, T., "Doping

effect on ferroelectric microstructure in $YMn_{1-x}Ti_xO_3$ “,FERROELECTRICS Volume: 348 Pages: 572-578 (2007)

[949] H. D. Zhou, J. C. Denyszyn, and J. B. Goodenough, Effect of Ga doping on the multiferroic properties of $RMn_{1-x}Ga_xO_3$ (R=Ho,Y) PHYSICAL REVIEW B 72, 224401 (2005)

[950] M. Chandra Sekhar, Seongsu Lee, Gwangho Choi, Changhee Lee, and J.-G. Park, Doping effects of hexagonal manganites $Er_{1-x}Y_xMnO_3$ with triangular spin structure, PHYSICAL REVIEW B 72, 014402 (2005)

[951] Iliev MN, Lorenz B, Litvinchuk AP, Wang YQ, Sun YY, Chu CW Structural, transport, magnetic properties and Raman spectroscopy of orthorhombic $Y_{1-x}Ca_xMnO_3$ (0 <= x <= 0.5) JOURNAL OF PHYSICS-CONDENSED MATTER Volume: 17 Issue: 21 Pages: 3333-3341 : JUN 1 2005

[952] Bas B. Van Aken, Jan-Willem G. Bos, Robert A. de Groot, and Thomas T. M. Palstra, Asymmetry of electron and hole doping in $YMnO_3$ PHYSICAL REVIEW B, VOLUME 63, 125127

[953] Taekjib Choi and Jaichan Lee, Bi modification for low-temperature processing of $YMnO_3$ thin films, Appl. Phys. Lett., Vol. 84, No. 24, 14 June 2004

[954] S. Imada, S. Shouriki, E. Tokumitsu, and H. Ishiwara, Jpn. J. Appl. Phys., Part 1 37, 6497 (1998)

[955] S. Imada, T. Kuraoka, E. Tokumitsu, and H. Ishiwara, Jpn. J. Appl. Phys., Part 1 40, 666 (2001)

[956] Daisuke Ito, Norifumi Fujimura, Takeshi Yoshimura, and Taichiro Ito, J. Appl. Phys. 93, 5563 (2003)

[957] T. Yoshimura, N. Fujimura, and T. Ito, Appl. Phys. Lett. 73, 414 (1998)

[958] E. Rokuta, Y. Hotta, H. Tabata, H. Kobayashi, and T. Kawai, J. Appl. Phys. 88, 6598 (2000)

[959] N. Fujimura, S. Azuma, N. Aoki, and T. Yoshimura, J. Appl. Phys. 94, 4036 (2003)

[960] J. Dho and M. G. Blamire, Competing functionality in multiferroic YMnO3, Appl. Phys. Lett. 87, 252504 (2005)

[961] K.R. Balasubramanian, Kai-Chieh Chang , Feroz A. Mohammad , Lisa M. Porter, Paul A. Salvador, Jeffrey DiMaio, Robert F. Davis, Growth and structural investigations of epitaxial hexagonal $YMnO_3$ thin films deposited on wurtzite GaN(001) substrates, Thin Solid Films 515 (2006) 1807–1813

[962] N. Fujimura a; N. Shigemitsu a; T. Takahashi a; A. Ashida a; T. Yoshimura a; H. Fukumura b; H. Harima, Multiferroic behaviour of YMnO3 and YbMnO3 epitaxial Films, Philosophical Magazine Letters, Vol. 87, Nos. 3–4, March–April 2007, 193–201

[963] Norifumi Fujimura, Shu-ichiro Azuma, Nobuaki Aoki, Takeshi Yoshimura, and Taichiro Ito, J. Appl. Phys. 80, 7084 (1996)

[964] Y. T. Kim, I. S. Kim, S. I. Kim, D. C. Yoo, and J. Y. Lee, J. Appl. Phys. 94, 4859 (2003)

[965] H. N. Lee, Y. T. Kim, and Y. K. Park, Appl. Phys. Lett. 74, 3887 (1999)

[966] H. Kitahata, K. Tadanaga, T. Minami, N. Fujimura, and T. Ito, Appl. Phys. Lett. 75, 719 (1999)

[967] W.-C. Yi, C.-S. Seo, S.-I. Kwun, and J.-G. Yoon, Appl. Phys. Lett. 77, 1044 (2000)

[968] K.-J. Choi, W.-C. Shin, J.-W. Yang, and S.-G. Yoon, Appl. Phys. Lett. 75, 722 (1999)

[969] Norifumi Fujimura, Tadashi Ishida, Takeshi Yoshimura, and Taichiro Ito, Norifumi Fujimura, Tadashi Ishida, Takeshi Yoshimura, and Taichiro Ito, Appl. Phys. Lett. 69, 1011 (1996)

[970] Dho J, Leung C W, MacManus-Driscoll J L and Blamire M G, Epitaxial and oriented YMnO3 film growth by pulsed laser deposition J. Cryst. Growth 267, 548 (2004).
[971] X. Martí, F. Sánchez, D. Hrabovsky, L. Fàbrega, A. Ruyter, and J. Fontcuberta, V. Laukhin, V. Laukhin, M. V. García-Cuenca, C. Ferrater, and M. Varela, A. Vilà, U. Lüders and J. F. Bobo, Exchange biasing and electric polarization with $YMnO_3$, Appl. Phys. Lett. 89, 032510 (2006)
[972] Maeda K, Yoshimura T, Fujimura N, Influence of antiferromagnetic ordering on ferroelectric polarization switching of YMnO3 epitaxial thin films, IEEE TRANSACTIONS ON ULTRASONICS FERROELECTRICS AND FREQUENCY CONTROL Volume: 54 Issue: 12 Pages: 2641-2644 Published: DEC 2007
[973] 1R.M. Kusters, J. Singleton, D.A. Keen, R. McGreevy, and W. Hayes, Physica B 155, 362 ~1989!.
974 E.F. Bertaut, G. Buisson, A. Durif, A. Mareschal, M.C. Montmory, and S. Quezel-Ambrunaz, Bull. Soc. Chim. Fr. 1965, 1132.
[975] J.A. Alonso, M.T. Casais, M.J. Martínez-Lope, J.L. Martínez, M.T. Fernández-Díaz, A structural study from neutron diffraction data and magnetic properties of RMn2O5 (R = La, rare earth) J. Phys. Condens. Matter 9 (1997) 8515.
[976] G. Buisson, HELIOMAGNETIC ORDER OF MANGANESE IN TMN2O5 SERIES (Ordre hélimagnétique du manganèse dans la série TMn_2O_5), Phys. Status Solidi A APPLIED RESEARCH, 16 533-543 (1973).
[977] 7G. Buisson, Phys. SINUSOID AND HELICOID MAGNETIC STRUCTURES OF RARE-EARTHS IN TMNO5 Status Solidi A 17, 191 ~1973!.

[978] C. Wilkinson, F. Sinclair, P. Gardner, J.B. Forsyth, B. Wanklyn, J. Phys. C Solid State Phys. 14 (1981) 1671.
[979] 9G. P. Blake, L. C. Chapon, P. G. Radaelli, S. Park, N. Hur, S-W. Cheong, and J. Rodríguez-Carvajal, Spin structure and magnetic frustration in multiferroic RMn2O5 .R=Tb,Ho,Dy. Phys. Rev. B 71, 214402 (2005).
[980] W. Ratcliff, V. Kiryukhin, M. Kenzelmann, S.-H. Lee, R. Erwin, J. Schefer, N. Hur, S. Park, and S.-W. Cheong, Phys. Rev. B 72, 060407_R_ _2005_.
[981] C.R. dela Cruz, F. Yen, B. Lorenz, M.M. Gospodinov, C.W. Chu, W. Ratcliff, J.W. Lynn, S. Park, S.-W. Cheong, Structural anomalies at the magnetic and ferroelectric transitions in RMn_2O_5R=Tb,Dy,Ho", Phys. Rev. B 73, (2006) 100406(R).

[982] M. Mostovoy, Ferroelectricity in Spiral Magnets, Phys. Rev. Lett. 96 (2006), p. 067601.
[983] C. R. dela Cruz,1 B. Lorenz,1 Y. Y. Sun,1 Y. Wang,1 S. Park,2 S-W. Cheong,2 M. M. Gospodinov,3 and C. W. Chu, Pressure-induced enhancement of ferroelectricity in multiferroic RMn_2O_5 R=Tb,Dy,Ho", PHYSICAL REVIEW B 76, 174106 _2007_

[984] D. Higashiyama, S. Miyasaka, N. Kida, T. Arima, and Y. Tokura, Control of the ferroelectric properties of DyMn2O5 by magnetic fields, Phys. Rev. B 70, 174405 (2004).

[985] A. B Sushkov, R. V. Aguilar, S. Park, S.-W. Cheong, and H. D. Drew, Phys. Rev. Lett. 98, 027202 (2007).
[986] C. R. dela Cruz, B. Lorenz, Y. Y. Sun, C. W. Chu, S. Park, and S.-W. Cheong, Magnetoelastic effects and the magnetic phase diagram of multiferroic DyMn2O5, PHYSICAL REVIEW B 74, 180402_R_ (2006)
[987] C.R. dela Cruz, B. Lorenz, C.W. Chu, Tuning ferroelectricity in $DyMn_2O_5$ by pressure and magnetic fields, Physica B: Condensed Matter, 403, 1331-1335 (2008)
[988] Hemberger J, Lunkenheimer P, Fichtl R, Krug von Nidda H A, Tsurkan V and Loidl A Relaxor ferroelectricity and colossal magnetocapacitive coupling in ferromagnetic $CdCr_2S_4$, Nature 434 364-367 (2005).
[989] C. Vecchini, L. C. Chapon, P. J. Brown, T. Chatterji, S. Park, S-W. Cheong, and P. G. Radaelli, Commensurate magnetic structures of RMn2O5 (R=Y,Ho,Bi) determined by single-crystal neutron diffraction, Phys. Rev. B 77, 134434 (2008)
[990] E. Granado, M. S. Eleotério, A. F. García-Flores, J. A. Souza, E. I. Golovenchits,4 and V. A. Sanina, Magnetoelastic and thermal effects in the $BiMn_2O_5$ lattice: A high-resolution x-ray diffraction Study, Phys. Rev. B 77, 134101 (2008)
[991] R.D. Shannon, Acta Crystallogr., Sect. A: Cryst. Phys., Diffr.,Theor. Gen. Crystallogr. A32, 751 (1976).
[992] P.P. Gardner, C. Wilkinson, J.B. Forsyth, and B.M. Wanklyn, J.Phys. C 21, 5653 (1988).

[993] Munoz A, Alonso JA, Martinez-Lope MJ, Martinez JL Synthesis, structural, and magnetic characterization of a new ferrimagnetic oxide: YFeMnO5 CHEMISTRY OF MATERIALS Volume: 16 Issue: 21 Pages: 4087-4094 Published: OCT 19 2004

[994] Alonso J A, Martinez-Lope M J, Casais M T, Martinez J L, Pomjakushin V, Synthesis, structural, and magnetic characterization of $YCrMnO_5$ EUROPEAN JOURNAL OF INORGANIC CHEMISTRY Issue: 13 Pages: 2600-2606 JUL 4 2005

[995] Z. H. Sun, B. L. Cheng, S. Dai, K. J. Jin, Y. L. Zhou, H. B. Lu, Z. H. Chen, and G. Z. Yang, Effect of Ce substitution on magnetic and dielectric properties of $BiMn_2O_5$, J. Appl. Phys. 99, 084105 (2006)

[996] C. de la Calle, J.A. Alonso , M.J. Martínez-Lope,M. García-Hernández, G. André, Synthesis under high-oxygen pressure, magnetic and structural characterization from neutron powder diffraction data of $YGa_{1-x}Mn_{1+x}O_5$ (x = 0.23): A comparison with YMn_2O_5, Materials Research Bulletin 43 (2008) 197–206

[997] Shim I-B, Yeom J H, Choi K R, Kim C S, Shin H J and An S Y Magnetic properties of

helimagnetic $YMn_{2-x}(Fe,Co)(_x)O_5$-delta(0.0 <= x <= 1.0) for the room temperature ferroism 2004 J. Appl. Phys. 95 7070

[998] V. A. Sanina, E. I. Golovenchits, and V. G. Zalesskii, Phase Separation with Charge Self-Organization in the $Tb_{0.95}Bi_{0.05}MnO_3$, $Gd_{0.75}Ce_{0.25}Mn_2O_5$, and $Eu_{0.8}Ce_{0.2}Mn_2O_5$ Manganite Multiferroics, Physics of the Solid State, 2008, Vol. 50, No. 5, pp. 913–921.

[999] C. Thiele, K. Dörr, O. Bilani, J. Rödel, and L. Schultz, "Influence of strain on the magnetization and magnetoelectric effect in $La_{0.7}A_{0.3}MnO_3$ /PMN-PT(001) (A=Sr,Ca)", Phys. Rev. B 75, 054408 (2007).

[1000] G. Srinivasan, E. T. Rasmussen, J. Gallegos, R. Srinivasan, Yu. I. Bokhan and V. M. Laletin, "Magnetoelectric bilayer and multilayer structures of magnetostrictive and piezoelectric oxides", Phys. Rev. B 64, 214408 (2001).

[1001] G. Srinivasan, E. T. Rasmussen, J. Gallegos, R. Srinivasan, Yu. I. Bokhan, and V. M. Laletin, Magnetoelectric bilayer and multilayer structures of magnetostrictive and piezoelectric oxides, Phys. Rev. B 64, 214408-1 - 214408-6 (2001).

[1002] G. Srinivasan, E. T. Rasmussen, B. J. Levin, and R. Hayes, "Magnetoelectric effects in bilayers and multilayers of magnetostrictive and piezoelectric perovskite oxides", Phys. Rev. B 65, 134402-1 – 134402-7 (2002).

[1003] Q. H. Jiang, Z. J. Shen, J. P. Zhou, Z. Shi, and C. W. Nan, Magnetoelectric composites of nickel ferrite and lead zirconnate titanate prepared by spark plasma sintering J. Eur. Ceram. Soc. 27, 279-284 (2007).

[1004] S. Q. Ren, L. Q. Weng, and S. H. Song, $BaTiO_3/CoFe_2O_4$ particulate composites with large high frequency magnetoelectric resp, J. Mater. Sci. 40, 4375-4378 (2005).

[1005] Veselago, V.G.: 'The electrodynamics of substances with simultaneously negative values of e and m', Sov. Phys. Uspekhi, 1968, 10, (4), pp. 509–514 (originally in: Usp. Fiz. Nauk, 1967, 92, p. 517)

[1006] J. B. Pendry, A. J. Holden, W. J. Stewart, I. Youngs, "Extremely

low frequency plasmons in metallic meso structures Phys. Rev. Lett. 76, 4773 (1996).

[1007] J. B. Pendry, A. J. Holden, D. J. Robbins, W. J. Stewart, Magnetism from Conductors and Enhanced Nonlinear Phenomena, IEEE Trans. Microwave Theory Tech. 47, 2075 (1999).

[1008] D. R. Smith and N. Kroll, Negative Refractive Index in Left-Handed Materials, Phys. Rev. Lett, 85 (14), 2933 (2000).

[1009] R. Shelby, D. R. Smith, S. Schultz, Experimental Veriication of a Negative Index of Refraction Science 292, 77 (2001).

[1010] J. B. Pendry, Negative refraction, Contemporary Physics, 45(3), 191 – 202 (2004).

[1011] T. A. Klar, A.V. Kildishev, V. P. Drachev, and V.M. Shalaev, Negative-Index Metamaterials: Going Optical, IEEE JOURNAL OF SELECTED TOPICS IN QUANTUM ELECTRONICS, VOL. 12, NO. 6, 1106 (2006).

[1012] Al`u A and Engheta N Achieving transparency with plasmonic and metamaterial coatings Phys. Rev. E 72 016623(2005).

[1013] W.J. Padilla, D. N. Basov, and D. R. Smith, Negative refractive index metamaterials, Materials Today, JULY-AUGUST 2006 | VOLUME 9 | NUMBER 7-8, 28 (2006).

[1014] Focus Issue on Metamaterials, J. Opt. Soc. Am. B (2006) 23, 386

[1015] V. M. Shalaev, "Optical negative index metamaterials," Nature Photon. 1, 41- 48 (2007).

[1016] B. Wood, Structure and properties of electromagnetic metamaterials, Laser & Photon. Rev. 1, No. 3, 249–259 (2007)

[1017] C.M. Soukoulis, Jiangfeng Zhou, T. Koschny, M. Kafesaki, and E.N. Economou, The science of negative index materials, J. Phys.: Condens. Matter 20 (2008) 304217.

[1018] V.G.Harris, A. Geiler, Y. Chen, S.D. Yoon, M. Wu, A. Yang, Z. Chen, P. He, P.V. Parimi, X. Zuo, C.E. Patton, M. Abe, O. Acher, C. Vittoria, Recent advances in processing and applications of microwave ferrites, J. Mag. Mag. Mater., 321 2035–2047 (2009).

[1019] G. Dewar, "A thin wire array and magnetic host structure with n < 0,"J. Appl. Phys., vol. 97, p. 10Q101, 2005.

[1020] S. T. Chui and L. B. Hu, Theoretical investigation on the possibility of preparing left-handed materials in metallic magnetic granular composites, Phys. Rev. B 65, 144407 _2002_.

[1021] R.X. Wu, Effective negative refraction index in periodic metal–ferrite–metal film composite, J. Appl. Phys. 97 (2005) 076105.

[1022] Yongxue He, Peng He, V.G. Harris, and C.Vittoria, Role of Ferrites in Negative Index Metamaterials, IEEE TRANSACTIONS ON MAGNETICS, VOL. 42, NO. 10, 2852, 2006

[1023] D. R. Fredkin and A. Ron, Effectively left-handed "negative index" composite material ,Appl. Phys. Lett. 81, 1753 (2002).

[1024] S. O'Brien and J. B. Pendry, Photonic band-gap effects and magnetic activity in dielectric composites, J. Phys.: Condens. Matter 14, 4035 (2002)

[1024] Kerwyn Casey Huang, M. L. Povinelli, and John D. Joannopoulos, Appl. Phys. Lett. 85, 543 (2004).

[1025] V. Yannopapas and A. Moroz, Negative refractive index metamaterials from inherently non-magnetic materials for deep infrared to terahertz frequency ranges, J. Phys.: Condens. Matter 17, 3717–3734 (2005).

[1026] M. S. Wheeler, J. S. Aitchison, and M. Mojahedi, Coated nonmagnetic spheres with a

negative index of refraction at infrared frequencies, Phys. Rev. B 73, 045105 (2006).

[1027] A. Pimenov, A. Loidl, P. Przyslupski, B. Dabrowski, Negative Refraction in Ferromagnet-Superconductor Superlattices, Phys. Rev. Lett.95 (2005) 247009.

[1028] F. J. Rachford, D. N. Armstead, V. G. Harris and C. Vittoria, "Simulations of ferrite-dielectric-wire composite negative index materials," Phys. Rev. Lett. 99, 057202 (2007).

[1029] H. J. Zhao, J. Zhou, Q. Zhao, B. Li, L. Kang, and Y. Bai, "Magnetotunable left-handed material consisting of yttrium iron garnet slab and metallic wires," Appl. Phys. Lett. 91, 131107 (2007).

[1030] Yongxue Hea, Peng Hea, Soack Dae Yoona, P.V. Parimic, F.J. Rachfordd, V.G. Harrisa, and C. Vittoriaa, Tunable negative index metamaterial using yttrium iron garnet, Journal of Magnetism and Magnetic Materials 313 (2007) 187–191

[1031] C. L. Holloway, E. F. Kuester, J. Baker-Jarvis, and P. Kabos, A double negative (DNG) composite medium composed of magnetodielectric spherical particles embedded in a matrix IEEE Trans. Antennas Propag. 51, 2596 (2003).

[1032] A. Pimenov, A. Loidl, K. Gehrke, V. Moshnyaga, and K. Samwer, Negative Refraction Observed in a Metallic Ferromagnet in the Gigahertz Frequency Range, Phys. Rev. Let., PRL 98, 197401-1 – 197401-4 (2007)

[1033] N. Koga and T. Tsutaoka, Preparation of substituted barium ferrite $BaFe_{12-x}(Ti0.5Co0.5)_xO_{19}$ by citrate precursor method and compositional dependence of their magnetic properties, Journal of Magnetism and Magnetic Materials 313 (2007) 168–175

[1034] G.P. Rodrigue, A Generation of Microwave Ferrite Devices, Proc. IEEE 76 (1988) 121-137

[1035] S. Geller and M. A. Gilleo, THE CRYSTAL STRUCTURE AND FERRIMAGNETISM OF YTTRIUM-IRON GARNET, Y,Fe, (FeO,) 3J. Phys. Chem. Solids 3, 30-36 (1957).

[1036] R.C. Lecraw, E.G. Spencer, C.S. Porter, Phys. Rev. 110 (1958) 1311–1313.

[1037] J. J. Went, G. W. Ratheneau, E. W. Gorter, and G. W. Van Oosterhout, Philips Tech. Rev. 13, 194 (1952).

[1038] J. A. Weiss, N. G. Watson, and G. F. Dionne, "New uniaxial-ferrite millimeter-wave junction circulators," in IEEE MTT-S Int. Microwave Symp. Dig., 1989, pp. 145–148.

[1039] Yang Bai, Hongsheng Chen, Jingjing Zhang, Yu Luo, Bo Li, Lixin Ran, Jin Au Kong, and Ji Zhou, Left-handed material based on ferroelectric Medium, Optics Express, 15, 8284-8289 (2007).

[1040] M.I. Bichurin, A.S. Tatarenko, G. Srinivasan, and J.V. Mantese, Left-handed materials

based on ferromagnetic-ferroelectroc composites, in Magnetoelectric Interaction Phenomena in Crystals, NATO Science Series, 2003, Physics and Chemistry, V. 164, Edited by M. Fiebig, V.V. Eremenko, and I.E. Chupis, pp.81-86, Kluwer Academic Publishers 2004.

[1041] Wiltshire, M. C. K., et al., Science (2001) 291, 849

[1042] Yen, T. J., et al., Science (2004) 303, 1494

[1043] Linden, S., et al., Science (2004) 306, 1351

[1044] Zhang, S., et al., Phys. Rev. Lett. (2005) 95, 137404

[1045] Enkrich, C., et al., Phys. Rev. Lett. (2005) 95, 203901

[1046] F. Magnus, B. Wood, J. Moore, K. Morrison, G. Perkins, J. Fyson, M. C. K. Wiltshire, D. Caplin, L. F. Cohen, and J. B. Pendry, "A d.c magnetic metamaterial," Nature Materials 7, 295 - 297 (2008).

[1047] B. Wood and J. B. Pendry, Metamaterials at zero frequency, J. Phys.: Condens. Matter 19, 076208-1 - 076208-9 (2007).

[1048] www.intel.com/technology/45nm/index.htm?iid=tech_as+silicon_45nm